Ink-jet printed carbon nanotube based transistors as water quality sensors

Gookbin Cho

INSTITUT POLYTECHNIQUE DE PARIS

NNT : 2021IPPAX122

Thèse de doctorat

Ink-jet printed carbon nanotube-based transistors as water quality sensors

Thèse de doctorat de l'Institut Polytechnique de Paris

préparée à l' École Polytechnique

École doctorale n°626 École doctorale de l'Institut Polytechnique de Paris (ED IP Paris)

Spécialité de doctorat: Physique

Thèse présentée et soutenue à Palaiseau, le 15 Decembre 2021, par

Gookbin CHO

Composition du Jury :

Jean-christophe GABRIEL CEA- NIMBE (UMR CEA-CNRS), Paris-Saclay, France	Rapporteur
Paolo BONDAVALLI Prof., Unité mixte de Physique CNRS/Thales (UMR 137), France	Président
Yamin LEPRINCE-WANG Prof., Laboratoire ESYCOM, Université Gustave Eiffel (UMR 9007), France	Examinateur
Henri HAPPY Prof., Laboratoire IEMN, Université Lille 1 (UMR 8520), France	Examinateur
Bérengère LEBENTAL Dr., Université Gustave Eiffel, COSYS, LISIS, Marne-La-Vallée, France	Directeur de thèse
Gaël ZUCCHI Dr., Ecole Polytechnique, IP Paris (UMR 7647), Paris-Saclay, France	Co-Directeur de thèse

ECOLE DOCTORALE

Table of contents

Throughout the writing of this dissertation, I have received a great deal of support and assistance.

Foremost, I would first like to thank my supervisor, Dr. Bérengère Lebental, whose insightful feedback and direction pushed me to sharpen my thinking and brought my work to a higher level. Her guidance and advice made this work possible. I would also like to thank co-supervisor, Dr. Gaël Zucchi, for his valuable guidance throughout my studies. I also thank Professor Yvan Bonnassieux, who gave me a chance to study in France and organized our laboratory in a proper way. I thank Professor Jungho Kim as well, for his insightful guidance during my study in Korea.

I would like to acknowledge all of colleagues during my studies at Ecole Polytechnique. I would particularly thank Robert Benda, who provided valuable support and help since I came to France.

I would also like to thank my friends, Hyeonseok Sim, Sangjun Park and Junha Park who came to France together, for all the fun we have had in the last five years.

Finally, I would like to thank my family as well. Words can not express how grateful I am to my parents and my brother for helping me a lot.

1 Introduction

While fresh water represents 3% of the total water on Earth, only 0.01% is available for human consumption [1]. Rapid population growth, unsustainable water use in agriculture and industry and climate changes are bringing about hydric stress worldwide. While drink water availability decreases, its quality also degrades: World Health Organization (WHO) reports that, in developing countries, 80% of human diseases, are water borne [2]. Drinking water quality in numerous countries does not meet WHO standards [3], [4]. The presence of water contaminants critically impacts human beings and ecosystem. It is thus of vital importance to be able to analyze fresh water, whether it is groundwater, irrigation water or tap water.

Concerning drinking water networks, water quality monitoring and control mainly takes place at the water supply intake or at the water treatment plant. However, this seems inadequate given the important variations in water quality observed throughout drinking water distribution systems [5]. Online sensing – also called on-site sensing – is currently seen as the best solution to provide continuous, early warning systems for chemical contamination throughout the water network (from drink water production to waste water treatment). It designates the capability to monitor water quality accurately and in real time, and it is expected to yield public health improvements *via* improved water safety [6]. To cover recent advances in the field, Kruse recently reviewed chemical sensors for water quality evaluation [7]. After detailing the parameters and contaminants that are currently relevant to water monitoring, the authors present exhaustively transduction methods for water quality sensors. The review shows that, despite worldwide efforts, there are still plenty of challenges to be met by online water quality sensors: reduction of costs and calibration frequency, increase in sensitivity and selectivity, reduction of power consumption and size, and enhancement of lifetime [8].

These challenges have motivated a wide range of studies toward water quality sensors based on nanomaterials, for instance as described in references [9]–[11], as nanomaterials-based sensors are well-known to meet those specific challenges across all fields of research on sensors [12], [13]. Among sensors fabricated with nanomaterials, those comprising carbon nanotubes (CNT) have been continuously proposed for chemical sensing since the early days of CNT research [14] taking advantage of their excellent chemical stability and their large surface area. Most recently, Schroeder *et al* [15] reviewed CNT-based chemical sensors, with applications covering gas sensors, biosensors, food sensors or aqueous sensors.

Many researchers have introduced nanomaterials-based water quality sensors with the goal to reduce cost and to increase sensitivity and selectivity [8]–[11], [13], [16]. Among various nanomaterials, carbon nanotube (CNT) sensors have been widely proposed for chemical sensing in water due to their excellent mechanical and chemical stability, their large surface area and their chemical tunability which enables selective sensing [17], [18]. One of the key parameters in this field is pH (concentration of H^+ ions) since monitoring and control of pH are essential to manage chemical, biological and environmental conditions of water. Among CNT-based water quality sensors, pH is the most studied parameter before lead [19].The fabrication of CNT electronic devices has been widely studied and discussed by many researchers [20]. One of the most challenging parts is

to organize CNTs on a substrate (between electrodes). Two main strategies can be suggested, devices using either as-grown CNT films or prefabricated CNTs. Devices can be either based on a single CNT or a CNT network. In turn, this network may be either random or organized (for instance aligned).

Among many fabrication methods for CNT electronic devices, ink-jet printing is a direct fabrication technique based on solution process, which provides moderate control over the architecture, localization and thickness of patterns on a variety of substrates. Contrary to lithography or other conventional printing techniques, ink-jet printing process has great potential due to its simple, low cost and non-contact deposition method, which is suitable for mass production and large-scale production [21]. For the last decade, solution processed or ink-jet printed SWCNTs have achieved remarkable progress on their ideal semiconducting behaviors [22]. Furthermore, development of high-purity SWCNTs has also led to significantly improved electrical performance. Ink-jet printing process has been widely used for the fabrication of conductive patterns or electrodes, and also thin film transistors [22], solar cells [23], sensors [24]–[28], electrochemical energy storage devices [29], light-emitting devices [30], memory and magnetic devices [31], etc.

However, ink-jet printed CNT-FETs have been scarcely studied for water quality sensors whereas other solution-based fabrication methods as spin coating [32], [33], dip coating [34]–[36], spray deposition [37], aerosol jetting [38] and drop casting [39] are widely used for CNT-FET chemical sensors.

In this dissertation, we first review and present the highlights of reported CNT-based electronic devices – chemistors, chemFET and electrochemical sensors - for chemical sensing. We propose a quantitative comparison of their performances based on limit of detection, sensitivity, detection range and relevant target analytes for water quality monitoring. Based on this review, chemFETs appear particularly promising and less studied. Thus we discuss the state of the art of CNT-FETs, introducing their architecture, the morphology of carbon nanotubes, length of semiconducting channel, fabrication process and their current injection properties.

Using this state of the art, a design is then developed: we demonstrate fabrication and characterization of ink-jet printed CNT-FETs. An unique design of bottom-gate field effect transistor with double insulating layer consisting of Si_3N_4 and SiO_2 layer is proposed since Si_3N_4 is a significantly better diffusion barrier against water molecules and sodium ions than SiO_2 [40]–[42]. We also optimize the thickness of each dielectric layer to obtain an optimal oxide capacitance. Detailed ink-formulation, ink-jet printing process and post-processing steps optimized in this work are also introduced. Particularly, passivation of CNT-FETs by poly(methyl methacrylate)(PMMA) after ink-jet printing process is introduced in details since the passivation of printed CNT random network is essential to avoid any physical degradation in aqueous solution.

We fabricate two different types of CNT-FETs based on non-functionalized CNTs (pristine CNTs) and functionalized CNTs by an in-house developed conjugated polymer. We compare both pristine CNT-FETs (p-CNT FETs) and functionalized CNT-FETs (f- CNT FETs) in air and water (for the latter, after optimization of

the characterization process to ensure stability of measurements). Effect of PMMA passivation is quantitively studied in air (under ambient conditions) by comparing their electrical characteristics before and after PMMA passivation.

When we consider chemical sensing in water, one of the key parameters is H^+ (pH) since monitoring and control of pH are essential to manage chemical, biological and environmental conditions of water. Among CNT-based water quality sensors, it is the most studied parameters before lead concentrations [19]. Hence, the pH sensitivity and linearity of both types of CNT-FETs are studied and compared in phosphate buffer solution (PBS) and in borate buffer solution (BBS). Study on the response to phosphate ions for f-CNT FETs is particularly studied to investigate possible interferences in PBS. Device reversibility and lifetime study are monitored. Lastly, a preliminary study on the detection of other analytes ($MgCl_2$, Na_4Cl, KNO_3 and HNO_3) is introduced.

2 Review on state of the art CNT chemical sensors

This section is adapted from the review paper by Cho, Azzouzi, Zucchi and Lebental presently undergoing peer-review, with various extensions relevant to the topic of the present dissertation. First, we provide generalities on CNTs, following fabrication of CNT-based electronic devices and functionalization strategies. Then we review state of the art CNT chemical sensors by presenting their operating principles, including a description of the three electrical transduction modes, a description of the different fabrication strategies. Finally, we present exhaustively the various electrical sensors presently reported in the literature from 2000 to mid-2021. We sort them by types of analytes and the various reports are analyzed in terms of sensing performances. Selected papers are highlighted in view of understanding the sensing mechanisms.

2.1 Definition and general property of CNTs

2.1.1 Carbon, graphene and carbon nanotubes

Carbon is a non-metallic element with the atomic configuration $(1s)^2\ (2s)^2\ (2p)^2$. It possesses four valence electrons which are distributed into the $2s$, $2p_x$, $2p_y$ and $2p_z$ atomic orbitals. Since the energy difference between the $2p$ and $2s$ energy levels is relatively small, wave functions of these valence electrons can easily mix with each other, leading to hybridization of the orbitals [43]. There are three possible atomic configurations when $2s$ and $2p$ orbitals hybridize, named sp, sp^2 and sp^3: each carbon atom has (n+1) sigma (σ) bonds in the sp^n hybridization. Sigma bonds are formed by an axial overlapping between atomic orbitals and are known as the strongest type of covalent chemical bond. A sp hybridization results in an one-dimensional (1D) chain structure with two σ bonds per carbon atom, an sp^2 orbital is a planar structure such as graphene or graphite with strong in-plane trigonal σ bonds and an sp^3 orbital leads to a tetrahedral three-dimensional (3D) structure called diamonds with four σ bonds [44].

2.1.2 From graphene to carbon nanotubes

Let us focus only on sp^2 hybridized carbon atoms: they form a planar and hexagonal structure like a honeycomb lattice, of which graphene is the most well-known example. Graphene is a carbon allotrope consisting of a two-dimensional single sheet of carbon atoms arranged in the honeycomb lattice nanostructure [45]. Carbon nanotubes (CNTs) can be described as a rolled sheet of a graphene layer with axial symmetry [43]. Their diameter ranges from 0.4 to 40 nm, and their length between 0.14 nm and 55.5 cm [46], [47], leading to extremely high aspect ratio (length-to-diameter ratio, up to 10^8). As such, they are regarded as 1D nanostructures [48].

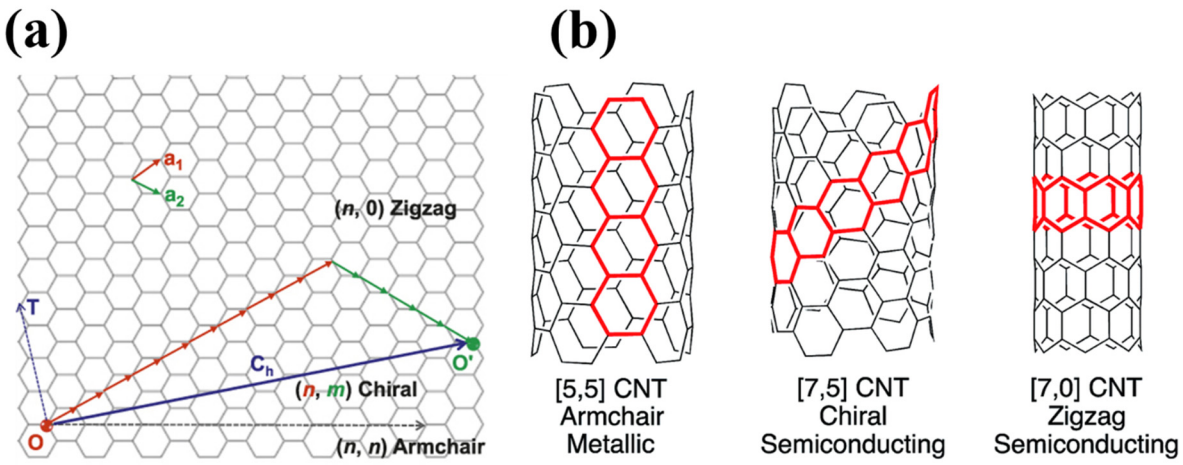

Figure 1. (a) Graphene honeycomb lattice with the lattice vectors a1 and a2, and three types of chiral vectors defining how CNTs are formed by rolling up graphene. (b) Three types of CNTs corresponding to different chirality. Images taken from [49], [50] with permission from the Royal Society of Chemistry.

CNTs are usually described using graphene lattice vectors $\boldsymbol{a_1}$ and $\boldsymbol{a_2}$, and most specifically using the chiral vector $\boldsymbol{c} = n_1\boldsymbol{a_1} + n_2\boldsymbol{a_2}$, where the chiral numbers $[n_1, n_2]$ $(n_1 \geq n_2 \geq 0)$ are two integers that describe the way graphene is folded to form a given tube (Figure 1). There are two remarkable types of CNT chirality, armchair CNTs (when $n - m = 3i$, *i as an integer*) and zigzag CNTs (when $m = 0$). Other CNTs are simply called chiral. The electronic properties of CNTs are determined by their chirality. Armchair CNTs are metallic, all the other types are semiconducting [51]–[53].

2.1.3 Single- and Multi-walled CNTs

CNTs are classified into Single-Walled Carbon Nanotubes (SWCNTs) and Multi-Walled Carbon Nanotubes (MWCNTs) depending on the number of graphene layers rolled into a coaxial array (Figure 2). A CNT formed of a single sheet of graphene is called a Single-Walled Carbon Nanotube (SWCNT). SWCNTs have typical diameters in the range 0.5 to 1.5 nm and typical lengths from 100 nm to several µm depending on their synthesis methods [54]. They have high tensile strength in the range 50 ~ 150 GPa and high elasticity up to 1 TPa [55].

MWCNTs consist of a coaxial array of SWCNTs, where each CNT is separated from one another by 0.34 to 0.39 nm [56]. In MWCNTs, each tube is separated from the next by 0.34 to 0.36 nm. MWCNTs may have diameter between 1 nm (double-walled carbon nanotubes (DWCNTs)) to 300 nm (about 100 coaxial tubes) and typical length from 1 µm to 550 mm [46]. MWCNTs have lower tensile strength and elastic modulus than SWCNTs [55], and are mostly conductive (except for certain types of DWCNTs). MWCNTs are generally bulk-produced in larger volume and at lower cost than SWCNTs.

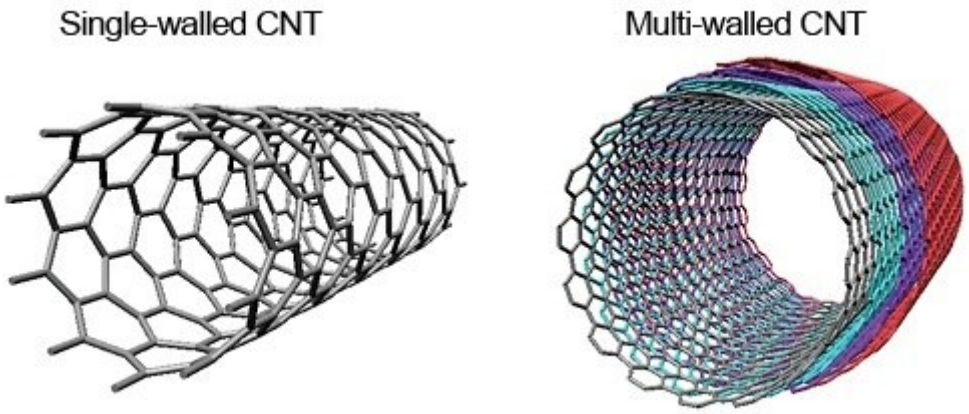

Figure 2. Basic structure of a single walled carbon nanotube (left) and of a multi-walled carbon nanotube (right). Image taken from [57].

2.1.4 Synthesis of CNTs

CNTs can be synthesized by several different methods such as chemical vapor deposition (CVD) [58], [59], laser ablation [56], [60] or arc-discharge technique [61]–[63]. All of these synthesis methods generally require catalysts such as Fe, Co, Ni or Mo since the use of these transition metals favors the nucleation and the growth of SWCNTs and also increases the process yield [64]. These metals may be applied as a mixture with carbonaceous solid electrodes (arc-discharge) or targets (laser ablation), or may be deposited and processed (for instance annealing) on the target substrate before CNT synthesis to form nanoclusters on a substrate. Temperature, pressure, density and chemical environment determine the different types and structures of synthesized CNTs.

CVD methods are often preferred because of the high potential for upscaling, relatively simple operating procedures at relatively low cost and because of their suitability to grow high crystalline quality CNTs for future power and electronic devices. Figure 3 shows a schematic diagram of CVD system.

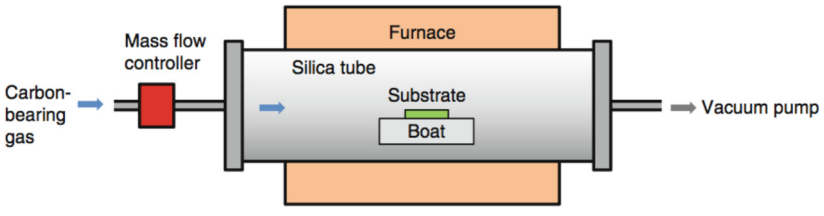

Figure 3. Schematic diagram of chemical vapor deposition system to synthesize the CNTs. Image taken from [65].

The synthesis of CNTs by CVD involves substrate temperatures between 750 and 1200 ºC and the use of hydrocarbon gases or liquids such as methane, acetylene, carbon monoxide or alcohols [64]. The general growth mechanism CNT by CVD methods involves the dissociation of hydrocarbons, then dissolution and saturation of the resulting carbon atoms over the highly saturated catalysts. During the process, the diameter and chirality of synthesized CNT is thought to depends on the characteristics of metal catalyst nanoparticles. First-row transition metals such as Ni, Fe or Co selectively produce SWCNTs rather than MWCNTs. The formation of individual or bundled nanotubes may also be controlled. These as-synthesized SWCNTs contain a mixture of metallic and semiconducting carbon nanotubes. In contrast, metal catalysts in large particles generally produce MWCNTs. The size of the particles should however not be too large since the growth may then result in carbon filaments or fibers instead of nanotubes. There are several conventional CVD production processes for SWCNTs such as nano agglomerate fluidized (NAF) process, high pressure carbon monoxide (HiPco) process, CoMoCAT process and floating catalyst CVD method.

Using the laser ablation method, high quality SWCNTs may be synthesized with yield of more than 70 % nanotubes. Figure 4 shows a schematic diagram of laser ablation system.

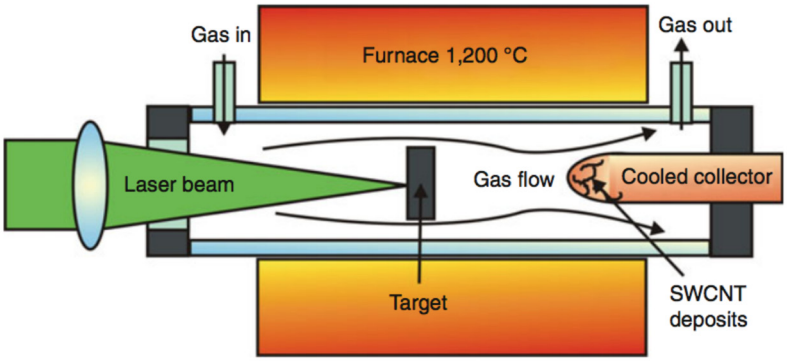

Figure 4. Schematic diagram of laser ablation system to synthesize the SWCNTs. Image taken from [65].

The method relies on an intense laser beam ablating a carbon target loaded with about 0.5 at.% of nickel and cobalt [63]. During this process, the carbon target is heated up to 1200 ºC in a furnace. The vaporized carbon atoms are transported away from the target by an inert gas flow to form condensates such as SWCNTs or metal catalysts at a cold finger. SWCNTs synthesized during this process organize each other to form ropes with 100 ~ 500 SWCNTs due to the vans der Waals force [66]. Approximately 45g/hour of SWCNTs is synthesized with ultrafast laser pulses at maximum power of a free electron laser. This makes a high production rate for SWCNTs compared to other synthesizing methods.

The electric arc discharge method operates as follows: an electric arc is generated by a DC current (50 ~ 100 A) applied between a carbon anode and cathode in an inert atmosphere such as helium or argon. This high temperature discharge makes the carbon atoms of the electrodes vaporize. Then they condensate to form CNTs.

Straight MWCNTs are generally synthesized during this process. They tend to have high crystallinity. Transition metal catalysts are needed in the arc discharge for the growth of SWCNTs, instead of MWCNTs. High yield of SWCNTs of 70 ~ 90 % nanotubes was reported by using a carbon anode with 1 at.% yttrium and 4.2 at.% of nickel as catalysts [67].

Using commercial versions of these processes, CNTs are nowadays available in bulk quantities (from gram to metric ton). Several CNT manufacturers have more than 100 tons per year production capacity for MWCNT. In 2006, the global capacity of MWCNTs productionwas approximately 300 tons. In 2010, a facility of the German company Bayer opened the biggest carbon nanotube facility in the world.

2.1.5 Fabrication of CNT electronic devices

The fabrication of CNT electronic devices has been extensively discussed in the literature (see for instance the review by Anantram *et al.* (2006) [20]). One of the most challenging parts is usually to organize CNTs on a substrate (with electrodes). One differentiates two main strategies, using as-grown CNTs or prefabricated CNTs. Devices can be either based on a single CNT or a CNT network. In turn, this network may be either random or organized (for instance aligned).

In devices based on as-grown CNT, CNTs are usually synthesized via chemical vapor deposition (CVD) directly onto pre-patterned electrodes within a temperature range from 750 to 950°C [68]–[70]. It leads to robust electrode/CNT contacts and high CNT crystalline quality while avoiding bundling. However, the high temperature CVD growth conditions usually prevents the use of flexible substrates. The need for metallic growth catalysts is often incompatible with the architecture of electronic devices (as they require well-defined insulating surfaces). For those reasons, as-grown CNT films are often transferred as a whole from the synthesis substrate onto more appropriate substrates via lift-off [71]. Another drawback, in-place synthesis does not allow for perfect control of CNT alignment, nor of their diameter, chirality or crystallinity, while these parameters have key impacts on device features. There are several purification and sorting techniques available to tune these parameters for CNTs on solid substrates. The most frequently reported post-growth processes are removal of the metallic CNTs by electrical breakdown [72] (application of a high current to a CNT network while the semiconducting CNTs are polarized in their OFF-state, which burns out metallic CNTs only) or degradation of the CNT crystalline quality by plasma etching [73], irradiation [74], or thermal oxidation [75].

By contrast, in devices relying on pre-fabricated CNTs, CNTs available in powder form are dispersed in a solvent and deposited onto the appropriate substrate *via* wet process. It is the most frequently reported approach to fabricate CNT-based sensors. It is advantageous because it features little constraints regarding to substrates and because it allows the use of a large panel of solution-based CNT pre-treatment protocols, such as purification, acidification, functionalization [76], sorting by chirality or by diameter [77]. A large variety of

techniques is available to deposit CNTs from a liquid suspension onto a substrate: drop-casting [78], [79], spin coating [32], [33], dip-coating [80]–[82], inkjet printing [83], [84], spray-coating [37], [85]–[87] or aerosol jet printing [88]. Dielectrophoresis may also be used when specific CNT orientation is desired [89]–[91].

Table 1 details and compare those methods. Let us note that, despite the advantages of using prefabricated CNTs compared to in-place growth CNTs, it also has a few drawbacks, such as: CNT placement on the substrate may not be as accurate; low network density is more difficult to achieve; CNT-substrate interaction may be less strong; CNT crystallinity may be degraded (by the liquid phase processing). Moreover, all solution-based process are crucially dependent on the quality of the CNT dispersion. The CNT dispersion should remain agglomerate-free, bundle-free for a long time [92], e.g. contain only individual nanotubes. Bundles can degrade the repeatability between different devices and the performances of chemFET by short-circuiting the source and drain.

Table 1. Comparison between liquid-based deposition methods for CNT

CNT deposition method	Concept	Ease of implementation	Controllability	Comments
Drop casting	CNT dispersion deposited drop by drop onto a substrate	++	-	Lack of precision in CNT positioning
Spray casting	A fine mist of CNTs dispersion from a humidifier is sprayed onto substrate	+	++	Needs mask to have precise deposition area
Spin coating	CNT dispersion is dripped onto a substrate rotating at high speed. Uniform distribution is ensured by centrifuge effect.	+	+	Layer thickness can be controlled accurately, but a lot of CNT dispersion is wasted
Dip coating	Substrate is dipped vertically into a dispersion of CNT with tension-active additives and withdrawn at controlled speed.	+	+	Thin CNT layer thickness can be achieved but difficult to deposit CNT in predefined locations.
Ink-jet printing	CNT ink is printed onto a substrate via droplet ejection	+	+++	No prefabrication of mask needed, allowing for a rapid printing process at low cost; precise method of patterning
Aerosol jet printing	Ultrasonic atomization is used to generate droplets of the active ink.	+	+	The morphology of the lines depends on the speed of the furnace gas, the printing process of the gas atomization
Dielectrophoresis	Deposition of CNT under AC electrical field	-	+++	Allows for CNT alignment. Tends to overconcentrate CNT around the electrode and to foster deposition of metallic CNT. Requires solvent optimization as well as a more complex setup for deposition

Among these techniques, Dielectrophoresis (DEP) should be discussed further as it is often used for CNTFET fabrication. It is a room-temperature technique for CNT deposition using a non-uniform AC (alternating current) electric field on patterned electrodes (Figure 5) [92].

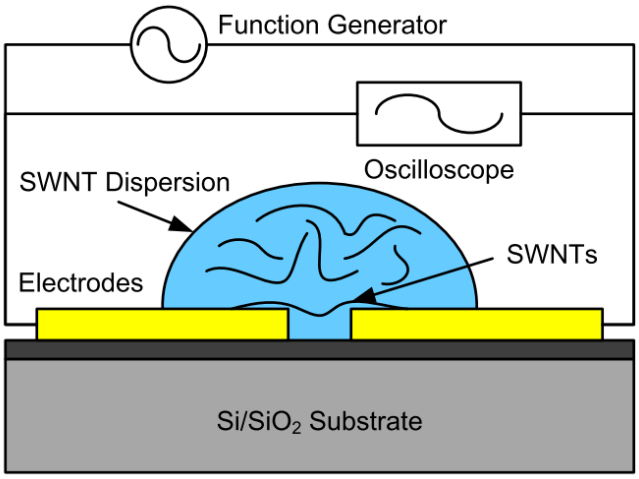

Figure 5. Experimental setup for the SWCNT deposition by using dielectrophoresis [93].

DEP controls the motion of polarizable particles (i.e CNTs) dispersed in liquid media. This method does not require the particles to be charged but only depends on the size, geometry and the dielectric properties of the particle. Unlike other random network deposition methods such as ink-jet printing and spray methods, DEP allows at the same time large area production and precise positioning of CNTs at certain coordinates on a substrate by application of an AC electric field. Detailed theory of dielectrophoresis is introduced in [94]. DEP method can be applied to either short channel [95] or long channel CNTFET (Figure 6) [92], [93], [96], [97] (see section 3.2.3.3).

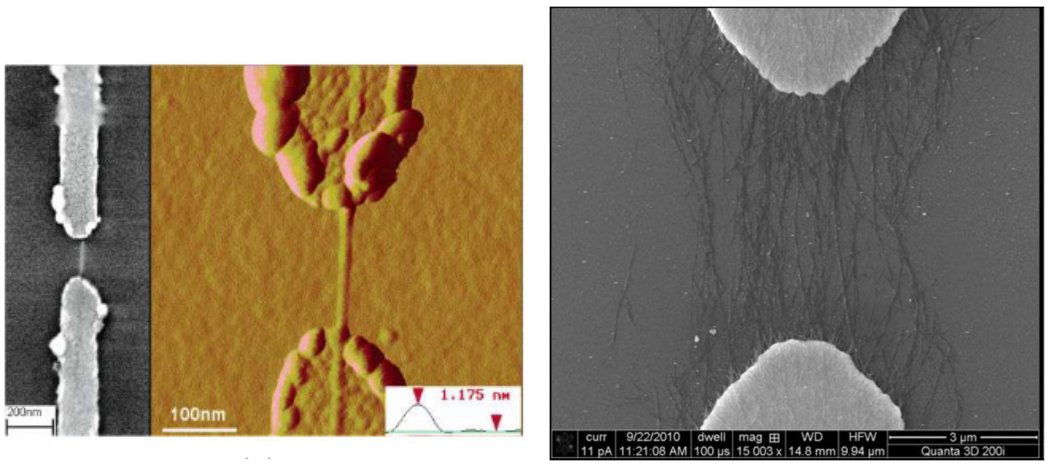

Figure 6. (left) SEM and AFM image of an individual SWCNT between metal electrodes deposited by dielectrophoresis (DEP) (right) SEM image of sparsely deposited SWCNTs between metal electrodes by dieelectrophoresis. Image copyright [93], [95]

2.1.6 Functionalization of CNTs for selective sensing

CNTs are very attractive as active materials in chemical sensors as they have high adsorption capability to most analytes. However, various results show the limited selectivity of pristine CNT-based chemical sensors (for both gas-phase and liquid-phase sensing): they are often sensitive to different analytes with the same range of magnitude of sensitivity and response time [98], [99].

Functionalizing CNT consists in hybridizing them with other molecules either by covalent [100] or non-covalent bonds [101]. Functionalization is advantageous for selective sensing because the functionalizing molecules can be selected for their affinity to the target analyte. It has become the most popular approach to enhance the selectivity of CNT-based chemical sensors, though some studies report on modulating electrode material instead of functionalizing CNT as a mean to achieve selectivity [102].

One of the main challenges in using functionalization for selective sensing lies in ensuring that the changes occurring in the functionalizing molecules in the presence of the target analyte can be detected through the CNTs in the selected electronic device configuration. At the same time, the functionalization itself should not degrade dramatically the properties of the electronic device itself.

For instance, covalent functionalization is usually expected to allow for stronger charge transfer between CNT and functionalizing molecules, thus providing stronger sensitivity to the target analytes. However, covalent bonds degrade the crystalline structure of the CNTs, thus degrading their conduction properties and subsequently the transduction quality. As a consequence, the density of covalent functionalization that can be achieved in practice remains limited, which in turn may limit the gain in sensitivity and selectivity [103].

By contrast, using non-covalent functionalization, full coverage of the CNT surface may be achieved without degrading the intrinsic electronic properties of the CNTs; however, selecting functionalizing molecules that strongly impact the electronic properties of CNTs is challenging [104]. Usually, molecules that can functionalize CNTs by strong π-stacking are selected among aromatic molecules such as derivatives of benzene, fluorene, carbazole, or porphyrin, or conjugated polymers [105], [106].

CNTs often carry some carboxyl groups (-COOH functions) on their sidewalls as a result of the synthesis process or of the post-synthesis purification – see section 2.2.2.3. The density of these groups may for instance be evaluated by Raman spectroscopy [107], [108], but is not systematically studied in the literature on CNT sensors. Hence CNTs reported on as non-functionalized CNTs may actually carry COOH groups. The COOH density may also be increased on purpose to enhance sensitivity, for instance by strong oxidative acidic treatments [109]. In this thesis, CNTs oxidized on purpose are labelled CNT-COOH.

2.2 CNT-based chemical sensors

2.2.1 Generalities on chemical nanosensors

In general, a chemical sensor transforms a chemical information (typically the presence or concentration of a target analyte in water) into an exploitable electrical signal. It consists of a chemical recognition layer (receptor) and a physicochemical transducer. The receptor interacts with target analytes, which induces an effect in the transducer, which then turns it into an exploitable signal [110]. When either of the transducer or the recognition layer contains a nanomaterial or is nanostructured, the device is said to be a nano-sensor.

The performance of a chemical sensor is characterized by its response curve, namely the relationship linking the sensor signal to the analyte concentration. The response is preferably linear, though exponential and logarithmic responses are also reported. The sensitivity of a sensor is defined as the slope of the response curve in its linear range. A chemical sensor is said to be selective if it can discriminate between a selected analyte and other analytes (said to be "interfering") within a sample. Increasing sensitivity and selectivity is the main goal driving the use of nanomaterials in chemical sensors. Because of their high surface over volume ratio, nanomaterials are expected to have higher sensitivity. The capability to engineer their composition and crystalline structure at the atomic scale opens up the possibility to design more selective recognition layers. Among various nanomaterials, CNTs are very attractive as active materials in chemical sensors as they have high adsorption capability to most analytes.

2.2.2 CNT-based electrochemical sensors

2.2.2.1 Electrochemical cells

An electrochemical sensor is a device that detects an electron exchange between sensor and analyte. It is usually composed of two basic components, a chemical recognition layer and a physicochemical transducer, the latter comprising several metal electrodes, the working electrode, the reference electrode and in most cases a counter electrode. Immersed into an electrolyte solution, they make up the electrochemical cell (or voltaic or galvanic cell) [111].

A two-electrode cell consists of only working and reference electrodes. It is used for low current operation (small-sized working electrodes, very low analyte concentrations) because at higher current, the potential of the working electrode becomes unstable. In most applications, a three-electrode cell is used; the reference electrode is maintained at stable potential, while the current passes through working and counter electrodes.

Two types of processes occur at the electrolyte-electrode interfaces. The first type is called faradaic. It comprises reactions in which charges are transferred across the electrode-electrolyte interface. Charge transfer enables reduction or oxidation to occur. The amount of reactions is directly linked to the current passing through the cell while the potential drop between the electrodes depends on the half-reactions taking place at the electrolyte-electrode interfaces according to Nernst's law.

The second type of processes are called non-faradaic. They include processes of desorption and adsorption occurring at the electrode-electrolyte interface which may impact the electrolyte composition or the electrical

response of the cell. Processes of ionic transport within the electrolyte are also determining, as they enable the movement of charges between the electrodes required for faradaic processes to occur.

2.2.2.2 Electrochemical transduction

There are various types of electrochemical transducers depending on how the electrochemical cell is operated. The most popular ones are briefly described in the following paragraphs.

In potentiometric sensors, the measured signal is the potential difference between the working electrode and the reference electrode in the absence of current. The working electrode potential depends on the concentration of the target analyte. A reference electrode is needed to provide a defined reference potential. The response of a potentiometric sensor is interpreted using Nernst equation, which states that the activity of the species of interest is in a logarithmic relationship with the potential difference [112]. This approach works well when the activity of a given species can be approximated to the molar concentration, namely at low concentration.

In voltametric sensors, the current response is measured as a function of the applied potential. It is directly correlated to the rate of electron transfer occurring *via* electrochemical reactions [113]. This approach differentiates well species with different redox potential (separated by more than ± 0.04-0.05 V). In turn, there are significant interfering effects if two or more species in the sample solution have similar redox potentials. There are different types of voltammetry depending on the way the voltage is applied, notably linear sweep or pulse-wise increase. The latter, called differential pulse voltammetry, is reported to be well suited for solid electrodes based on organic compound and more sensitive than the former.

Electrochemical impedance spectroscopy (EIS) is a derivative of voltammetry where the voltage is alternating (AC) and applied at different frequency. The current is measured and from that, one derives the impedance Z, which is then studied as a function of the frequency. It provides information on the rate of the electrochemical reactions as well as on the ionic transport in the electrolyte [114].

Stripping voltammetry consists of two steps. First, target chemical species are electrolytically deposited on the surface of one of the electrodes using a constant potential, for instance by reduction of metal ions on the cathode. Second, a voltage scan is applied to the electrode, which progressively strips the target analytes from the electrode depending on their redox potential. At a given voltage, the resulting faradic current is proportional to the concentration of the target chemical ionic species [115]. If the different species are stripped at different voltages, selectivity is possible. The electrode deposition step has a pre-concentration effect on the target analyte, which yields this technique its considerable sensitivity (sub-nanomolar range for metal ions).

Figure 7 shows example of measured responses by these three transduction methods.

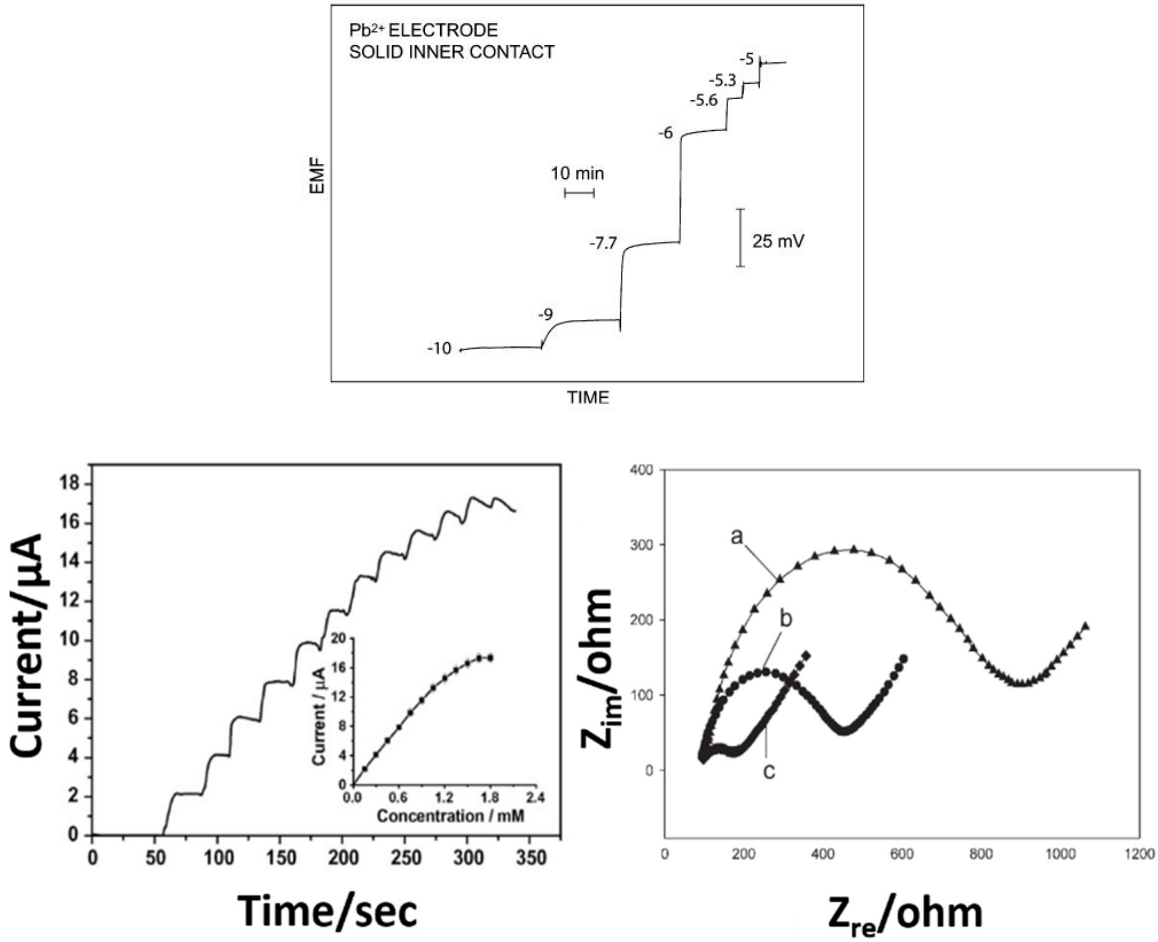

Figure 7. Measured response by three different transduction methods of electrochemical sensors: (Top) Potentiometry (Potential at zero current – EMF electromotive force - vs time under increasing volume of analyte - the numbers shown are logarithmic molar sample concentrations. Reproduced from [112] (Left) Voltammetry (Current versus time under increasing volume of analyte) Reproduced from [116] (Right) Electrochemical impedancemetry (Nyquist plot: real impedance vs imaginary impedance for different of electrodes). Reproduced from [117].

2.2.2.3 Use of CNTs in electrochemical sensors

Because the performances of electrochemical sensors are driven by the specificities of the electrodes and of the electrolyte/electrode interfaces, improvements in sensor performances can be achieved by tuning either the electrode bulk material or the electrode surfaces, the latter using either dedicated coatings or by surface engineering (for instance, roughness increase). CNTs are used both as coatings and as electrode material to leverage their high specific surface area. It allows for a large dynamic range and for a high loading in

electrocatalysts (defined as the catalysts that participate in electrochemical reactions by increasing the rate of chemical reactions without being consumed in the process). Moreover, CNTs display resistance to fouling [118].

In the literature review which follow, 66 reports deal with electrochemical sensing. Among these, 31 (47%) reports address CNTs coated on glassy carbon electrodes, 10 (15%) electrodes directly made out of CNTs or CNT paste, the rest electrodes made of miscellaneous metallic materials (gold, steel…). For coating electrodes with CNTs, the most frequently reported method (28 references – 42%) is drop casting: CNTs are first purified, then chemically activated (either oxidized or functionalized) and dispersed in a solvent with sonication. The dispersion is then dropped on the electrode surfaces and the solvent is evaporated rapidly. The prevalence of drop-casting methods is due to their simple implementation. They are often used as a stepping stone on the path toward more reproducible, but often less straightforward, fabrication processes. One of the main shortcomings of techniques based on CNT dispersion (drop and spray casting, dip coating, dielectrophoresis, printing…) is that most solvents have low exfoliation efficiency for CNTs and the resulting solutions have low stability due to the rather weak interactions between these solvents and CNTs [119]. As a consequence, CNT-paste-based electrodes are a popular alternative to CNT-coated electrodes (13 references – 20%). The reported binders are often mineral oils, often mixed with graphite powder and/or ionic liquids (for instance [120], [121])

Regarding electrochemical sensing mechanisms, the carbon atoms at the CNT ends have been shown to behave like the edge planes of highly orientated pyrolytic graphite (HOPG) and to feature rapid electron transfer kinetics: they contribute to the Faradaic processes and provide quick response time. By contrast, the carbon atoms of the sidewalls resemble the basal plane of HOPG and show slower electron transfer kinetics than end atoms [122] (though still higher than HOPG due to curvature [123]). In other words, they are much less involved in oxidoreduction reactions with the electrolyte. However, they contribute to non-Faradaic processes driven by adsoption and desorption mechanisms.

The processes used to remove from CNTs the impurities left by the synthesis process (carbon nanoparticles, nanocrystal metal catalysts, amorphous carbon…) play a strong role in the electrochemical properties of the CNTs. Raw CNTs are usually purified before use by thermal treatment at around 400°C or by chemical oxidation via acid treatment. It leads to shortened and partially oxidized CNT. In particular, the resulting CNTs feature functional oxygenated groups at the open ends and increased defect density along the sidewalls [124]. In addition to CNT curvature, those defects also explain that CNT sidewalls contribute to Faradaic process in electrochemical sensors. Luo *et al.* for instance detailed the oxidation-reduction reactions for carboxylic CNT sidewall defects in [125] (Figure 8).

(A)

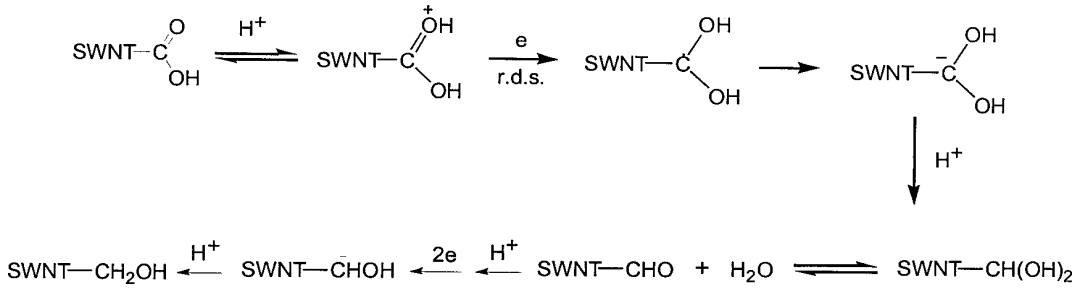

(B)

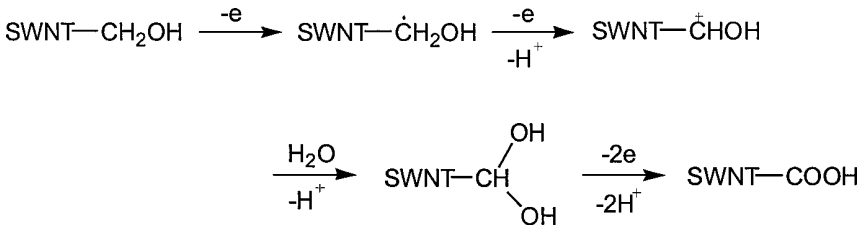

Figure 8. (A) Oxidation and (B) reduction reactions for carboxylic CNT sidewall defects. Reproduced from [125]

2.2.3 CNT-based electrical sensors

2.2.3.1 CNT Chemistors

Chemi-resistors, or chemistors, are sensors operating by measuring the variation in the electrical resistance or the electrical resistivity of a sensing (also called active) material due to its interaction with the target analyte. The target analyte has to be in direct contact or close proximity to the active material. The possible interactions are highly diversified: bulk or catalytic reactions, reversible or irreversible reactions, chemi- or physisorption, surface or volume reactions or reactions at grain boundaries.

In most chemistors, resistance changes are measured in a two-terminal configuration (Figure 9-left). A small constant current is applied between two electrodes separated by a short distance (µm to mm) and the resulting voltage is measured. Alternately, four-terminal configurations may also be used to reduce the influence of contact resistance on the sensitivity, especially in the case of high resistance devices (MΩ range and higher). Four parallel electrodes are often used in those cases; the current is applied on the external electrodes and the voltage drop is measured across the two internal electrodes. In the case of arbitrary electrode disposition (for instance, anisotropic surface), the Van der Pauw method can be used to measure the bulk resistivity (ρ) and the Hall coefficient of the surface by using four different contact point [126].

The use of CNT as active layer and/or electrode material in chemistor is prominent across various sensing

applications (Gas sensing, biological sensing)[127], as it is the most straightforward device structure available to assess sensitivity of CNTs to chemicals (in terms of design, fabrication, electronics, signal processing…). The high surface area results in high adsorption rates for analytes leading to a rapid response time. Typically, only a fraction of µg or less of CNT material is needed for a single chemistor, so the raw material cost is not a limiting factor [128]. Moreover, a small (1 cm^2) chip-based device can hold hundreds of sensor elements. Such miniaturization leads to a reduction in size and weight of the assembled systems.

Most reports on chemistors in our review (10 out of 13) use SWCNTs rather than MWCNTs. CNT chemistors are mostly often fabricated using electrode materials made of noble metals (platinum and gold), though occasionally (here 4 reports out of 12) the CNTs make up both electrode material and active layer. The electrode metal is usually thermally evaporated on the substrate and patterned with photolithography. After purification (eliminating synthesis residues), sorting (for instance by diameter) and dispersion in a solvent, the CNTs are deposited across the gap, bridging the electrodes or electrode fingers (Figure 9-left), then the solvent is evaporated. Various methods can be used for this deposition step, either wet-processing techniques (such as drop-casting, inkjet printing, spraying… - 11 references) or dry-processing techniques (such as direct (in-place) chemical vapor deposition (CVD) growth or CVD-growth followed by solid-state transfer or by nanoimprint as nano-scale patterning process – 2 references). The CNT networks are in most cases random (except in 3 references where there are aligned through dielectrophoresis [93] or threading of CVD-aligned CNTs [129]).

The baseline resistance level of a device and its sensitivity depend on the geometry of the electrodes, on the type and quality of CNTs as well as on their surface density. The latter actually depends on both the CNT concentration in the dispersion and the selected deposition process. The geometry of the electrodes is characterized primarily by their spacing – often called the gap – and the length of the gap. The gap ranges between 1µm and 100µm, the gap length between 10µm and several mm. To optimize space occupation, the electrodes are often interdigitated (Figure 9-right): instead of a straight gap, the gap is formed by a series of parallel fingers. The effective gap length is thus roughly equal to twice the finger length multiplied by the number of fingers. Finger widths are typically in the 1 to 10µm range, lengths in the 10 to 100µm range [130].

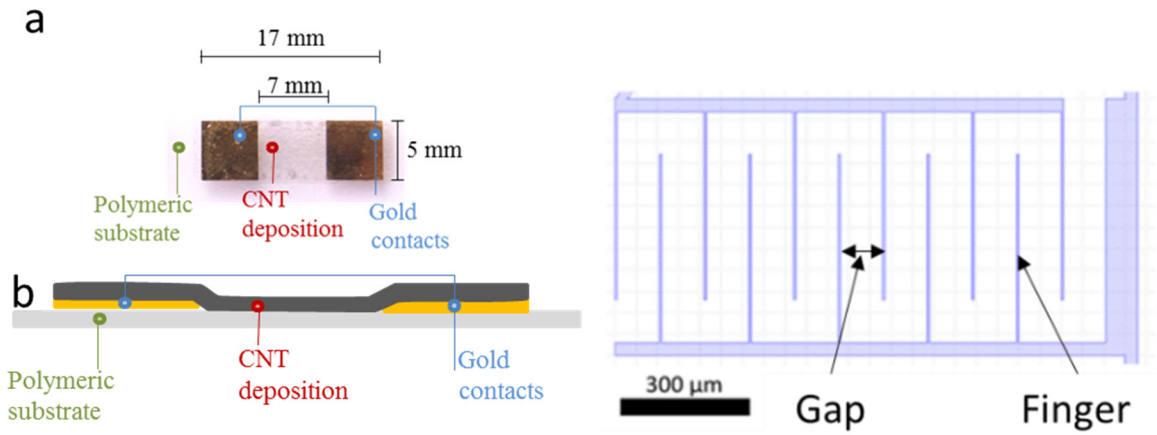

Figure 9. Left) Example of two terminal resistive CNT sensor on ETFE: a) top view; b) cross section.

Reproduced from [25]. Right) Schematic of interdigitated electrodes.

2.2.3.2 CNT ChemFET

A field-effect transistor (FET) is an electronic device consisting of a semiconducting layer, called channel, linking a source and a drain electrode; the density of electronic carriers flowing in the channel between source and drain electrodes is modulated by the potential of a third electrode, called gate electrode, insulated from the active layer by a dielectric material. A chemical FET is a FET whose conduction characteristics are modulated by the presence and concentration of electrolytes around the device. The chemically sensitive layer is usually the semiconducting channel, though the electrodes and the dielectric layer may also contribute to sensitivity. The device design allows for the semiconducting layer to be exposed to the target liquid. In electrolyte-gated chemFET, the target liquid itself is used as gate and dielectric layer (there may not be solid-state dielectric layer and gate electrode)

Similarly to chemistors, chemical detection is enabled by short-range interactions between the target analyte and the active layer. However, while in chemistors only the resistance (and sometimes the resistivity and contact resistance) of the active layer may be exploited to derive the analyte concentration, in chemFET there are many more parameters to exploit: the current or resistance between source and drain Ids for a given gate Vg and drain Vd voltage (thus operating the chemFET as a chemistor with gate-controlled baseline resistance), or one may further explore the ON and OFF current levels (values of Ids when the semiconducting channel is respectively in its most conducting and most insulating state) for different ranges of Vd, the transconductance (the maximum value of the first derivative of Ids(Vg), which is related to the mobility of the semiconducting channel), the threshold voltage (the gate voltage for which the semiconducting channel transitions from conducting to insulating), or even the hysteresis observed between threshold voltage values or transconductance values during upward and downward sweep of the gate voltage [131]–[133]. Because of this, for the same active layer, chemFETs are usually considered to be more sensitive and more selective than chemistors. In turn, they usually require significantly more complex fabrication procedure and operating electronics.

CNT-FET is a chemFET with CNT layer as channel. Because a semiconducting channel is required, only single-walled carbon nanotubes (SWCNTs) are used [134]. As SWCNTs may be either semi-conducting or metallic depending on their chiral structure, either pre-processing of the SWCNT (for instance, sorting of semiconducting SWCNT before deposition) or post-processing (for instance, electrical breakdown of metallic SWCNT after deposition or in-place growth) is needed so that the channel is semi-conducting [135]–[139].

The CNT-FET channel may be formed by a single SWCNT or a percolating network of SWCNTs. While devices based on single SWCNT have remarkable electrical performances [20]. Devices based on random-network of SWCNTs are more popular for sensing applications due to their higher effective sensing area, their

usually simpler fabrication procedure as well as their better up-scalability (for mass production), even though their electrical performances are not as good as these of single SWCNT devices. In the field of water quality monitoring, only devices based on random network of CNT-FET have been reported so far.

There are four main types of device architecture for CNT-FET chemical sensors: top gate, bottom gate, liquid gate and hybrid structures (Figure 10). The original architecture is the bottom gate one, where the gate is embedded below the semiconducting layer with a separating dielectric layer. In the context of water quality monitoring, it has the significant drawback of requiring a high gate voltage (usually several tens of Volts) for good electrical performances, which leads to hydrolysis of water (beyond 1V). In top gate structures, the gate layer is located on top of the semiconducting channel instead, which makes it more straightforward to fabricate. It requires a lower operating gate voltage, but it is relatively little used for sensing applications as well because the top gate insulates the sensitive channel from the environment. A variation on the top gate structure, the liquid gate structure, consists in applying the gate voltage through the electrolyte surrounding the device. It is particularly interesting for chemical sensing in water because it allows much lower-voltage operation (in the sub-volt range) compared to the usual bottom-gate structure (Figure 10 (a)). It is also more straightforward to fabricate considering that it requires one less electrode by an embedded gate structure compared to the top gate structure. Hybrid CNT-FET architectures consist in coupling in the same architecture several gating strategies. The extended gate concept consists on placing an ion-sensitive membrane on top of the top gate of the double-gated CNT-FET (Figure 10 (c)). SiO_2 is the most frequently used dielectric material used for the layer between the semiconducting channel and the substrate or gate electrode (Figure 10 (b)). However, oxides with a higher dielectric constant such as Al_2O_3 or Si_3N_4 may also be used in order to have a thinner insulating layer with better homogeneity and durability compared to SiO_2.

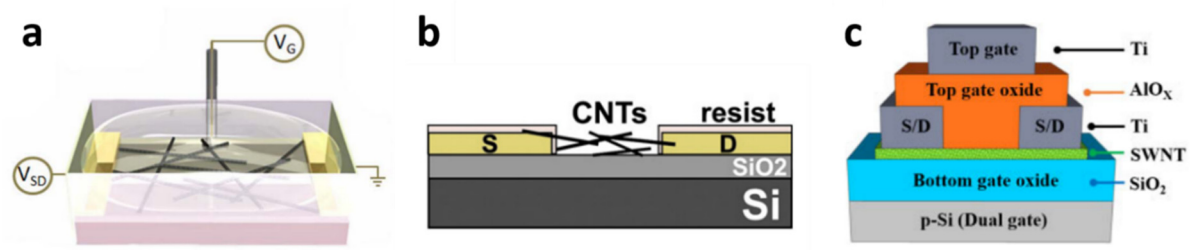

Figure 10. Topology of (a) liquid top gate (b) bottom gate (c) extended-dual gate CNT-FET. Reproduced from [32], [33], [91]. Reprinted with permission. Copyright (2014) from Biochimica et Biophysica Acta (BBA) – General subjects.

Table 2 shows all examples of reported CNT-FET designs for water quality monitoring applications. Random network deposition of CNTs is the most widely used (10 papers out of 11).

Table 2. CNT-based chemFET for water quality monitoring.

Geometrical layout	CNT morphology	CNT deposition method	Dielectric layer	Substrate	Contact electrodes	References
Top gate	Random network	Selective deposition on chemically modified APS	500 nm APS	SiO_2	Cr/Au (30/50 nm) source & drain electrodes, Ag/AgCl for reference electrode	[140]
Hybrid top gate	Random network	Dip coating	100 nm SiO_2	SiO_2	Ti/Au (10/30 nm) contacts	[82]
Bottom gate	Random network	Spin coating	65 nm SiO_2	Silicon	Cr/Au (5/40 nm) contacts	[32]
Bottom gate	Random network	Drop casting	160 nm SiO_2	Silicon	Cr/Au (10/90 nm) contacts	[39]
Double gate	Random network	Spin coating	10 nm AlO_x (Top), 500 nm SiO_2 (Bottom)	p-Si (Bottom gate)	100 nm Ti contacts for source, drain and gate, Ti (100 nm) for top gate	[33]
Liquid gate	Random network	Spray deposition	Aqueous electrolyte	Flexible polyimide (Kapton®)	Cr/Au (5/50 nm) contacts	[37]
Liquid gate	Random network	Dielectrophoresis	300 nm SiO_2	Silicon	Au contacts, Pt wire (Auxillary), Ag/AgCl electrode (Reference)	[91]
Liquid gate	Random network	CVD*	200 nm SiO_2	Silicon	300 nm Au contacts, Pt wire (Counter), Ag/AgCl electrode (Reference)	[70]
Liquid gate	Random network	Dip coating	300 nm SiO_2	SiO_2	Pd/Au (10/30 nm) contacts, selective alignment by electro potential	[35]
Liquid gate	Random network	Dip coating on a self-assembled monolayer	300 nm SiO_2	Flexible poly(ethyleneterephtalate)	Pd/Au (10/30 nm) contacts	[36]

Geometrical layout	CNT morphology	CNT deposition method	Dielectric layer	Substrate	Contact electrodes	References
Bottom gate	Vertically aligned	CVD	120 nm SiO_2	PDMS film	Gold foil contacts	[141]

**CVD: chemical vapor deposition*

APS: 3-aminopropyltriethoxysilane

PDMS : Polydimethylsiloxane

2.2.4 Sensing mechanisms in CNT-based chemistors and chemFET

The mechanisms of sensitivity of CNT-based chemistors and chemFET are usually extrapolated from their mechanisms of sensitivity to gas [142], mechanisms that still remain somewhat debated. Overall, the response to analytes is attributed to a change in the conduction properties of either, or all, of the three following components of the devices, as shown in Figure 11 [15]: the conduction along the tube length ("intra-CNT"), the contact points between tubes behaving as tunnel junctions ("inter-CNT"), and the contact points between the tubes and the metal electrodes behaving as Schottky barriers. Sensitivity is attributed either to direct adsorption of the analytes on these sites, or to analytes not adsorbed, but at a distance small enough to these sites to perturb their electrical behavior.

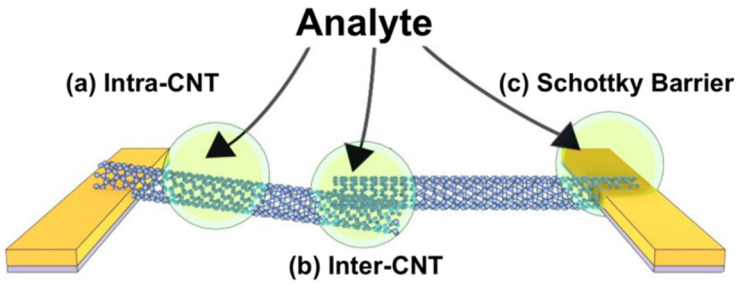

Figure 11. Schematic of possible sensitivity sites which affect the conductivity: (a) at the sidewall or along the length of the CNT itself, (b) interface between CNT-CNT (inter-CNT), and (c) at the interface between the metal electrodes and the CNT (Schottky barrier). Reprinted with permission from [15]. Copyright (2018) from American Chemical Society.

Modulation of the Schottky barrier is caused by a change in the work function of either the electrode metal or the CNTs in the presence of the target analytes. The inter-CNT modulation corresponds to a change in the transmission coefficient of the inter-tube tunneling junction, which in turn can be attributed to either a change in the inter-tube distance, or a change in the work functions of the tubes. The intra-CNT conduction modulation is caused by a change either in the density of charge along the sidewalls (resulting in a doping effect) or in the scattering properties of the sidewalls (impacting mobility).

Each of these three modulations may impact the global device response, with specificities depending on the type of transduction (chemFET or chemistor) and on the device morphology (particularly on the network density).

Regarding to chemFET, Figure 12 provides an insight into the impact of Schottky-barrier modulation and intra-CNT modulation (doping or mobility variation) on the typical I-V characteristics of a chemFET [15]. Inter-CNT effects (contact resistance modulation) are usually neglected when analyzing sensing performances of chemFET as their electric performances are mostly driven by intra-CNT effects and Schottky barrier modulation.

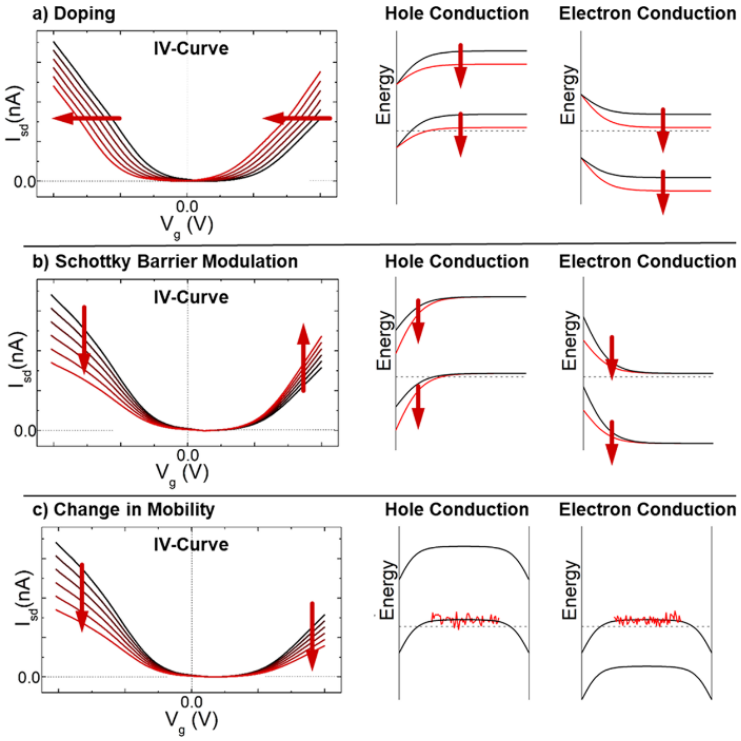

Figure 12. Theoretical I-V curves of a chemFET depending on the doping. Reprinted with permission from [15]. Copyright (2018) from American Chemical Society.

By contrast, in chemistors, the inter-CNT modulation is generally accepted to have the strongest impact on the device response, as the global baseline resistance of the network is mostly controlled by inter-CNT contacts. This is confirmed by modelling results for high density networks. In low density networks, modelling suggests that the variations of the electrode-CNT resistance and of the intra-CNT resistance may also contribute to the global relative resistance variation occurring upon exposure to chemicals [143].

2.3 Performance comparison of CNT-based chemical sensors in water from review

2.3.1 General summary of reported CNT-based chemical sensors in water.

We review here CNT-based chemical sensors in water. The review includes references on all the water-quality relevant analytes discussed until April 2021 except for pesticides, this specific and very large topic having been reviewed very recently [144]. The most investigated analytes are H^+ (pH) and lead (with 18% of references each), then cadmium (14%) and nitrite (11%). Altogether, micronutrients and toxic metals cover 37 papers, so 40% of references, a lot of these references covering several analytes at the same time.

The large majority of reports addresses MWCNTs (71%) instead of SWCNTs, functionalized CNTs (82%) instead of pristine or COOH-CNT, and electrochemical transduction (73%) instead of chemistor (14%) or chemFET (12%).

Table 3. Summary of reported CNT-based water quality monitoring sensors.

Type of Analytes		**Numbers of refs**	**Ref SWCNT**	**Ref MWCNT**	**Ref CNTFET**	**Ref chemistors**	**Ref EC**	**Ref functionalized (COOH excluded)**
All analytes		**90**	**26 (29%)**	**64 (71%)**	**11 (12%)**	**13 (14%)**	**66 (73%)**	**74 (82%)**
pH		16 (18%)	12	4	6	7	5 (2 with CNTFET)	8
Micronutrients and toxic metals (total)	All included	36 (40%)	5	32	2	2	33	31
	Lead(II)	16 (18%)	0	16	0	0	16	12
	Cadmium (II)	13 (14%)	0	13	0	0	13	11
	Copper(II)	9 (10%)	1	9	1	0	8	8
	Mercury (II)	8 (9%)	3	5	1	1	6	6
	Arsenic(III)	5 (6%)	0	5	0	0	5	5
	Zinc (II)	4 (4%)	0	4	0	0	4	2
	Miscellaneous	2 (2%)	2	0	1	1	0	2
Nitrite		10 (11%)	1	9	0	0	10	10
Water hardness		2 (2%)	1	1	1	0	1	2
DO		2 (2%)	0	2	0	0	2	2
Disinfectants	Free chlorine	3 (3%)	1	2	0	2	1	2
	Hydrogen peroxide	6 (7%)	1	5	0	1	5	6
Sulfur	Sulfide	4 (4%)	0	4	0	0	4	4
	Sulfite	2 (2%)	0	2	0	0	2	2
Miscellaneous		9 (10%)	4	5	2	1	5	8

The following sections provide for each analyte a table with all the relevant references. The tables include the following information for each reference:

- Materials: type of CNT (MWCNT or SWCNT), functional probe, type of functionalization (covalent or not),
- Device strategy: type of transduction (including type of electrochemical measurement and type of FET, gating), CNT deposition process, electrode material and configuration, choice of substrate
- Performances: limit of detection (LOD) (converted in the most used unit for the target analyte), sensitivity in the measured range of concentration (converted whenever possible in a common unit), and the results of interference study

For each analyte, the best results are then singled out for discussions on the choice of functionalization and of the transduction strategies. Whenever possible, the impact of the fabrication strategy is discussed.

2.3.2 Sensitivity analysis & comparison by analytes

2.3.2.1 pH

pH is the physicochemical quantity defined as $pH=-\log[H_3O^+]$ that is used to quantify the hydrogen ion concentration in water [145]. Recommended level of pH are 6.5 to 8.5 according to World Health Organization [146].

Table 4 shows the 16 reported CNT-based pH sensors in water: 7 are chemistors, 6 chemFETs and 5 electrochemical sensors (among which 2 are CNT-FET operated as EC sensors). Only 4 reports out of 16 use MWCNTs; 8 reports out of 16 address non-functionalized CNTs (including COOH functionalization). This is in contrast with other analytes (as summarized in Table 3), where functionalization is quasi-systematic and the use of chemistors is rare.

By contrast to other analytes also, the use of detection limits (LOD) expressed in M of H^+ as a mean of comparison between references is challenging because, due to the logarithmic pH scale, these LOD do not translate directly into pH detection limits. Moreover, it is only rarely provided (here 7 papers only out of 16). Because of the variety of reported response types (current, voltage, resistance, conductance, impedance, percentages) the absolute sensitivities (e.g. variation of the response by pH unit) cannot be compared either. As an alternative, we elected here to compare the relative sensitivity at pH 7 (e.g. the variation of the response by pH unit divided by the response at pH 7) which allows for comparison across transduction methods.

Using this indicator, we observe that the 3 non-functionalized and the 1 COOH-based chemistors have considerably better performances than functionalized ones, the best performance being achieved at 18%/pH unit (63Ω/pH unit) with MWCNTs sucked by vacuum force on filter paper [89].

For FET as well, the best performance (23%/pH unit) is achieved with spin coated non-functionalized SWCNT

in a dual gate chemFET structure [33], the authors showing that double-gated operation performs better than single-gated.

The same performance (23%/pH unit) is achieved with impedance spectroscopy of COOH-functionalized MWCNT spin-coated on Kapton® with gold electrodes [80]. With Aluminum electrode, the performance falls down to 14% only.

These results underline the very good sensitivity to pH of pristine CNTs and CNT-COOH for all three types of transductions, while the use of other functional probes degrades performances. This confirms the widespread theory mentioned in section that the sensitivity of pristine CNT and CNT-COOH to pH is due to the presence of carboxyl groups on the CNT sidewalls.

It is worth mentioning that the five references on potentiometry yield sensitivities in mV/pH unit very close to Nernst law irrespective of the functionalization (58mV/pH unit) [33], [47], [85], [91], [147].

Finally, one observes that, while there are several reports with the same transduction mode (particularly resistive) and the same functionalization (pristine) [78], [86], [88], [89], it is not possible to draw conclusions regarding to optimal design and fabrication of pH sensors as there is still too much variability in the choice of substrates, electrode materials and deposition method.

Table 4. CNT-based pH sensors in water, sorted by transduction type then by relative sensitivity

Type of CNT	Functional probe	Functionalization	Analyte	Detection range	Detection limit	Sensitivity Relative Sensitivity*	Transduction method	CNT Deposition method	Electrode material Contact configuration	Substrate	Comments	Ref.
SWCNT	Polyaniline	Non covalent	pH	pH 2.1~12.8	2.74 nM	N/A	Chemistor	Drop-casting	Ti/Au	Si/SiO_2		[78]
SWCNT	Nafion	Non covalent	pH	pH 1~12	N.P.	3.5 %/pH	Chemistor	Screen printing	SWCNT	Polymide		[148]
MWCNT	Ni NP*	Non covalent	pH	pH 2~10	N.P.	5.0%/pH	Chemistor	Continuous pulling of super-aligned, CVD grown MWCNTs	MWCNT	PDMS		[149]
SWCNT	Pristine	Non functionalized	pH	pH 1~11	<10 pM	34nS/pH 3.4 %/pH (pH 1~6) 163nS/pH 9.3%/pH (pH 7~11)	Chemistor	Spray-casting	Cr	Si/SiO_2		[86]
SWCNT	COOH	Covalent	pH	pH 5~9	N.P.	75Ω/pH 11%/pH	Chemistor	Dielectrophoresis (aligned CNTs)	Cr/Au	Si/SiO_2	Response time: 2s at pH 5, 24s at pH 9	[93]
SWCNT	Pristine	Non functionalized	pH	pH 4~10	N.P.	5.2kΩ/pH 14%/pH	Chemistor	Aerosol jet printing	Ag	Kapton		[88]
MWCNT	Pristine	Non functionalized	pH	pH 5~9	N.P.	63Ω/pH 18%/pH	Chemistor	Sucked by vacuum force	MWCNT	Filter paper		[89]
SWCNT	Malt extract agar	Non covalent	pH	pH 3~5	100 mM	N/A	FET (hybrid top gate)	Dip coating	Ti/Au (10/30 nm) contacts	Si/SiO_2(100nm)	Multiplexed detection of Fungus (A. niger, A. versicolor) and Yeast (S. cerevisiae)*	[82]
SWCNT	ETH500*, MDDA-Cl	Non covalent	pH	pH 2~7.5	10 mM	71nA/pH 7.5%/pH	FET (liquid gate)	Spray deposition	Aqueous electrolyte (gate) Cr/Au (5/50 nm)	Polymide (Kapton®)	Change from p-type to n-type transistor with the membrane layer	[37]
SWCNT	COOH	Covalent	pH	pH 3~8	N.P.	17nA/pH 8.2%/pH	FET (top gate)	N.P.	Cr/Au (30/50 nm) source & drain electrodes, Ag/AgCl for reference electrode	Glass/APS(50-200nm)/SWCNT /APS(500nm)/TopGate	CNT placement controlled by location of APS (modified to immobilize the CNTs)	[140]
SWCNT	Pristine	Non functionalized	pH	pH 3.4~7.8	10 mM	3.9μA/pH 13%/pH	FET (bottom gate)	Spin coating	Cr/Au (5/40 nm)	Si/SiO2(65nm)		[32]

Type of CNT	Functional probe	Functionalization	Analyte	Detection range	Detection limit	Sensitivity Relative Sensitivity*	Transduction method	CNT Deposition method	Electrode material Contact configuration	Substrate	Comments	Ref.
SWCNT	Poly(1-aminoanthracene)	Non covalent	pH	pH 3~11	1 µM	FET 19µS/pH 14 %/pH potentiometry 55 mV/pH	FET, potentiometry (liquid gate)	Dielectrophoresis (aligned CNTs)	Au contacts, Pt wire (Auxillary), Ag/AgCl electrode (Reference)	Si/SiO_2(300nm)	Multiplexed detection of Ca^{2+} and Na^+	[91]
SWCNT	Pristine	Non functionalized	pH	pH 3~10	1 mM	7600mV/pH 23%/pH (Dual-gate mode) 59.5 mV/pH (single-gate mode potentiometry)	FET (double gate)	Spin coating	100 nm Ti contacts for source, drain and top gate	p-Si (substrate acting as bottom gate)		[33]
SWCNT	Polyaniline	Non covalent	pH	pH 1~13	N.P.	56 mV/pH	potentiometry	Spray casting	Polyvinyl chloride-coated steel wire	PVC	Highly selective against Li^+, Na^+, K^+	[85]
MWCNT	$COF_{THi\text{-}TFPB}$ *	Covalent	pH	pH 1~12	N.P.	54 mV/pH	Differential pulse voltammetry	Drop casting	Glassy carbon electrode	Glassy carbon	multiplexed detection of Ascorbic acid.	[147]
MWCNT	COOH	Covalent	pH	pH 4~9	N.P.	17Ω/pH 23%/pH (Au), 16Ω/pH 14 %/pH (Al)	Impedance spectroscopy	Dip coating	Au and Al interdigitated electrodes	Kapton®		[80]

The relative sensitivity is calculated using the formula $Relative\ Sensitivity = (x/x_0) * 100\ (\%)$ *, with* x *the absolute sensitivity expressed (depending on the transduction) in units of resistance, voltage or current per pH unit and* x_0 *the baseline parameter (resistance, voltage or current) at pH 7. The relative sensitivity is not calculated for potentiometry-based transduction as it depends on the choice of reference voltages and the three references can be easily compared by their absolute sensitivity.*

N.P. : not provided

Ni NP: Nickel nanoparticle, PDMS: Polydimethylsiloxane, APS: 3-aminopropyltriethoxysilane, ETH500: tetradodecylammonium tetrakis(4-chlorophenyl)borate, MDDA-Cl: methyltridodecylammonium chloride, A. niger: Aspergillus niger; A. versicolor: Aspergillus versicolor, S. cerevisiae: Saccharomyces cerevisiae, PVC: poly vinyl chloride, COF: Covalent organic framework, Thi: Thionine; TFPB: 1,3,5-tris(p-formylphenyl)benzene

2.3.2.2 Micronutrients and heavy metals

Micronutrients (Iron, manganese, cobalt, copper, molybdenum, zinc, selenium, cadmium, iodine, boron, fluorine …) are mineral materials that play an important role in metabolic activities and tissue function maintenance in living beings. Subsequently, a suitable intake of micronutrients is necessary, often in trace amount, and they should not be entirely removed from the water supply. However, they usually become harmful at large doses and constitute a water quality concern.

Even though various heavy metals, notably cadmium, lead and mercury, are not micronutrients as they are very toxic even in trace amount, a lot of micronutrients actually are heavy metals (notably iron, copper, cobalt, zinc). Hence, micronutrients and heavy metals are often classified jointly in the water quality literature. We proceed in the same manner here.

Metal ions detection in water by CNT-based sensors has been heavily studied since 2005 with 37 papers reported out of 90 papers in total in this review, the large majority of this dealing with electrochemical transduction (33 papers) and with functionalized CNTs (31 papers). In the following subsections, we summarize the results on the following ions by order of frequency of occurrence in the literature: Pb(II), Cd(II), Zn(II), Cu(II), Hg(II), As(III), Ni(II) and Co(II). We then discuss the multiplexing performances and the interference studies. The performances of the reported sensors are compared in terms of limit of detection which is the most frequently provided indicator.

2.3.2.2.1 Detection of Lead II:

Table 5 summarizes the different CNT-based lead(II) sensors used for water quality monitoring. All references but three are based on functionalized MWCNTs sensors using stripping voltammetry, the others one using stripping voltammetry with pristine MWCNTs [28], [150]or potentiometry with functionalized MWCNTs [151], [152]. Interestingly for comparison purposes, 6 out of 16 references discuss functionalized MWCNTs drop cast onto glassy carbon electrodes and operated through stripping voltammetry.

The reported ranges of detection cover a large scale, from 0.1 ppt to 100 ppb. By comparison, the maximum acceptable concentration (MAC) of lead worldwide ranges from 10 to 15ppb [7]. The lowest limits of detection are 0.3 ppb, 0.04 ppb and 0.02ppt with pristine[150], non-covalently functionalized (Nafion/Bismuth [153] and covalently functionalized (Dithizone [154]) MWCNTs.

Refs [150] and [28] on pristine CNTs show that while the limits (0.3ppb and 1ppb respectively) of detection of a pristine CNT electrode are theoretically sufficient for lead detection in the context of water quality monitoring, the ranges of detection are not compatible (lowest limit at respectively 210ppb and 15ppb). While ref [150] demonstrates that joint detection of several metal ions is possible (as expected from the principles of

stripping voltammetry) both references remark on interferents (dissolved oxygen for [150] and cadmium and copper for [28]), as is expected from pristine nanotubes (non-selective sensing).

Concerning covalent functionalization, the three references [155], [156] and [154] are based on the same architecture (drop casting on glassy carbon and stripping voltammetry), so the major differences in limits of detection can easily be linked to the functionalization strategy. Refs [155] and [156] rely on grafting respectively cysteine and thiacalixarene (TCA) on MWCNT by exploiting their sidewall carboxyl groups as reaction sites. The major difference in performances show that TCA is much more favorable for lead complexation than cysteine. Notably, ref [156] shows by computational method that Pb^{2+} ions can stably adsorb onto the TCA molecules and that there is significant electron delocalization between Pb^{2+} and the sulfur atoms in the TCA molecule. To move beyond the performances of TCA-functionalized CNTs, ref [154] relies not only on complexation of MWCNTs by dithizone (as thiols have strong interaction with metal ions) but also on the processing of MWCNTs into a bucky-gel, a porous MWCNT-based structure filled with ionic gel (here 1-butyl-3-methylimidazolium hexafluorophosphate). While the functionalization provides reactivity to the target metal ion, the bucky gel is thought to provide strong specific surface area enhancement[158].

For non-covalent functionalization strategies, bismuth or its derivatives are used in the majority of reports (8 out of 10), the other references citing mercury [151] and antimony oxide [159]. Bismuth is an environmentally friendly material often used as a replacement to mercury in electrochemical applications [160]. Its sensitivity to lead is attributed to its ability to form “fusible” alloys with heavy metals in general. It tends to facilitate their nucleation and subsequent reduction. However, this nucleation process of lead ions around bismuth could in theory limit the reusability of the sensing devices. In practice, Xu *et al.* (the reference with the best limit of detection among this category) report that the relative standard deviation (RSD) on sensitivity was lower than 5 % for Pb(II) detection after 50 repetitive measurements [153].

It is worth noting that the three references on covalent functionalization do not identify any interferent materials, while among the 7 references on non-covalent functionalization discussing interferent, only one features no interferent[153], the others mentioning reduced or strong interferents. It suggests that, in the context of lead(II) monitoring, covalent functionalization yields not only better limits of detection but also better selectivity than non-covalent functionalization.

Refs [161] and [162] also give the opportunity to discuss the specificity of the stripping voltammetry protocol. Indeed, both references using the exact same materials and process (plating of Bismuth on screen printed CNT electrodes), Injang et al. (2010) [161] achieve almost one order of magnitude improvement on lead(II) LOD and sensitivity compared to Hwang et al. (2008) [162]by complementing anodic stripping voltammetry (ASV) with sequential injection analysis [163]. It is a technique known to enhance sensitivity and selectivity in stripping voltammetry by better controlling reagent and sample volumes. In these two papers, the benefit for this technique occurs only for Pb(II), the two papers reporting similar LOD and sensitivity for Cd(II) and Zn(II)

detection (see next sections). This suggests that the optimization of the electrochemical transduction scheme may have very strong impact on sensitivity and selectivity, possibly stronger than the functionalization choice. However, this impact can rarely be assessed in the literature as it is seldom discussed in the individual papers and reliable comparison between protocols requires references with very strong similarities in electrode design, fabrication process and material choices.

Table 5. CNT-based sensors for detecting Pb^{2+} ions in water, sorted by type of functionalization then detection limit.

Type of CNT	Functional probe	Functionalization	Analyte (Add. Analytes)	Detection limit	Sensitivity (Detection range)	Transduction method	Deposition method	Electrode material Contact configuration	Substrate	Interference study	Ref.
MWCNT	Pristine	Non functionalized	Pb^{2+} (Cd^{2+}, Zn^{2+}, Cu^{2+})	0.3 ppb	2.2 nA/ppb (210~830 ppb)	Stripping voltammetry	CNT thread	Metal wire and silver conductive epoxy	Glass capillary	-Simultaneous determination of Cd(II), Cu(II), Pb(II) and Zn(II) demonstrated -The presence of Dissolved Oxygen changes the calibration law for Cd(II)	[150]
MWCNT	Pristine	Non functionalized	Pb^{2+}	1.0 ppb	1.5 nA/ppb (15 ~ 40 ppb) 3.5 nA/ppb (40 ~ 70 ppb)	Stripping voltammetry	Inkjet printing	Inkjet-printed silver ink	PEN	Effects of copper and cadmium are reported.	[28]
MWCNT	Ionic liquid - dithizone based bucky-gel	Covalent	Pb^{2+}	0.02 ppt	0.024 µA/ppb (0.1ppt~210 ppb)	Stripping voltammetry	Drop-casting	Glassy carbon electrode	Glassy carbon	-No interference of Cd^{2+} and Cu^{2+} ions with the detection of Pb^{2+} ion.	[154]
MWCNT	Thiacalixarene	Covalent	Pb^{2+}	8 ppt	3.8 µA/ppb (0.04 -2.07 ppb)	Differential pulse anodic stripping voltammetry	Drop casting	Glassy carbon electrode	Glassy carbon	Detection of Pb^{2+} was clearly not affected by Zn^{2+}, Cd^{2+}, Ni^{2+} (100-fold excess)	[156]
MWCNT	Cysteine	Covalent	Pb^{2+} (Cu^{2+})	1 ppb	0.23* µA/ppb (25~750 ppb)	Differential pulse anodic stripping voltammetry	Drop casting	Glassy carbon electrode	Glassy carbon.	40-fold Cl^{-}, 30-fold SO^{2-}_{4} and four fold CO^{2-}_{3} did not have any significant effect on the stripping peak current of Pb^{2+} and Cu^{2+}	[155]
MWCNT	Poly(o-toluidine) Ce(III)tungstate	Covalent	Pb^{2+}	210 ppb	27 mV/decade (21ppb – 2.1%)	Potentiometry	Liquid mixing and membrane formation through drying	Calomel electrode	Glass tube (araldite)	Strong selectivity (from 50 to 500 times) against Zn(II), Sr(II), Hg(II), Ca(II), Pd(II), Cu(II), Mg(II)	[152]

Type of CNT	Functional probe	Functionalization	Analyte (Add. Analytes)	Detection limit	Sensitivity (Detection range)	Transduction method	Deposition method	Electrode material Contact configuration	Substrate	Interference study	Ref.
MWCNT	Nafion/Bismuth	Non covalent	Pb^{2+}, (Cd^{2+})	25 ppt	0.22 µA/ppb (0.05 to 5 ppb) 0.27 µA/ppb (5~100 ppb)	Stripping voltammetry	Drop casting	Glassy carbon electrode	Glassy carbon	500-fold of SCN^-, Cl^-, F^-, PO^{3-}_4, SO_4^{2-}, NO_3^-, and various cations such as Na^+, Ca^{2+}, Mg^{2+}, Al^{3+}, K^+, Zn^{2+}, Co^{2+} and Ni^{2+} had no influences on the signals of Pb(II) and Cd(II).	[153]
MWCNT	PSS-Bi	Non covalent	Pb^{2+} (Cd^{2+})	0.04 ppb	0.079 µA/ppb (0.5 ~ 90 ppb)	Stripping voltammetry	Drop casting	Glassy carbon electrode	Glassy carbon	- 20-fold amounts of Zn^{2+}, 5-fold amounts of Sn^{2+} and 1-fold amounts of Cu^{2+} have influence on the determination of Cd^{2+} and Pb^{2+} with deviation of 10%.	[164]
MWCNT	Bismuth	Non covalent	Pb^{2+} (Cd^{2+})	~0.04 ppb	N/A	Stripping voltammetry	Plasma-enhanced CVD (vertically aligned MWCNTs in epoxy matrix)	Cr	Silicon	N.P.	[165]
MWCNT	Fe_3O_4-LSG-CS-Bi	Non covalent	Pb^{2+} (Cd^{2+})	0.07 ppb	0.21 µA/ppb (1 ~ 20 ppb) 0.24 µA/ppb (20 ~ 200 ppb)	Stripping voltammetry	Drop casting	Glassy carbon electrode	Glassy carbon	- Slight changes in peak currents of Pb^{2+} and Cd^{2+} were observed in presence of interfering ions Na^+, Cl^-, SO_4^{2-}, PO_4^{3-}, Fe^{2+}, Fe^{3+}, Zn^{2+}, As^{3+}. -Significant increase in response signals of Hg^{2+} was probably due to the formation of amalgam -Dramatically decreased response signals of Cu^{2+} was ascribed to the formation of Pb-Cu inter-metallic compounds.	[166]

Type of CNT	Functional probe	Functionalization	Analyte (Add. Analytes)	Detection limit	Sensitivity (Detection range)	Transduction method	Deposition method	Electrode material Contact configuration	Substrate	Interference study	Ref.
MWCNT	PPy-Bi NPs	Non covalent	Pb^{2+} (Cd^{2+})	0.1 ppb	1.1 µA/ppb (0.11~ 120 ppb)	Stripping voltammetry	Paste mixture with MWCNT, parrafin oil and graphite powder	Stainless steel rod	Teflon (PTFE) tube	-Good selectivity towards Fe^{2+}, Al^{3+}, Zn^{2+}, Mg^{2+}, SO_4^{2-}, CO_3^{2-}, Ca^{2+}, K^+, Na^+. The absolute relative change of signal varied from 0.40 to 4.88%). -High interference from Cu^{2+} (1-fold mass ratio was found as the tolerance ratios for the detection of Pb and Cd ions)	[167]
MWCNT	rGO-Bi	Non covalent	Pb^{2+} (Cd^{2+})	0.2 ppb	930 nA/ppb cm^2 (20 ~ 200 ppb)	Stripping voltammetry	Spray coating	Cr(30nm)/Au(200nm)	Polymide (VTEC 1388)	-100-fold K^+, Na^+, Ca^{2+}, Cl^-, NO^{3-}, and a 30-fold Fe^{3+} increase had no significant effect on the signals of Cd and Pb ions. - Cu ions were found to reduce the response of target metal ions due to the competition between electroplating Bi and Cu on the electrode surface (close reduction potential of Cu and Bi.)	[168]
MWCNT	Bismuth	Non covalent	Pb^{2+} (Cd^{2+},Zn^{2+})	0.2 ppb	0.39 µA/ppb (2~18 ppb) 0.67 µA/ppb (20~100 ppb)	Stripping voltammetry	Screen printing	Screen printed MWCNT based electrode	Ceramic substrates	N.P.	[161]
MWCNT	Bismuth	Non covalent	Pb^{2+} (Cd^{2+},Zn^{2+})	1.3 ppb	1.2 µA/ppb (2~100 ppb)	Stripping voltammetry	Screen printing	Screen printed MWCNT based electrode	Alumina plates	- The addition of copper ions strongly influenced the stripping responses. Decrease of lead and cadmium pics by 65.5%.	c
MWCNT	Pristine	Non covalent	Pb^{2+} (Cd^{2+}, Zn^{2+})	6.6 ppb	0.47* sec/V/ppb (58~650 ppb)	Stripping potentiometry	Paste mixture of MWCNT and mineral oil	MWCNT paste electrode	Glass tube	Al (III), Mg (II), Fe (III), Ni (II), Co (II), Cr (III), Cu (II) and Sb (III) were investigated in the ratio analyte : Interferent 1:1 and 1:10. the interference was observed for the ratios analyte : interferent 1:1 and 1:10 for Co (II), 1:10 for Cr (III) and Cu (II).	[151]

Type of CNT	Functional probe	Functionalization	Analyte (Add. Analytes)	Detection limit	Sensitivity (Detection range)	Transduction method	Deposition method	Electrode material Contact configuration	Substrate	Interference study	Ref.
MWCNT	Sb_2O_3	Non covalent	Pb^{2+} (Cd^{2+})	24 ppb	2.7 µA/ppb (5-35 ppb)	Stripping voltammetry	Paste mixture of MWCNT, silicon oil , Sb_2O_3 powder and ionic liquid	Copper wire	PTFE tube	N.P.	[159]

N.P.: Not provided
PSS-Bi: Poly(sodium 4-styrenesulfonate)-Bismuth
rGO-Bi: Reduced graphene oxide-Bismuth
PPy-Bi NPs: Polypurrole-Bismuth NanoParticles
PTFE: poly tetra fluoro ethylene
LSG-Cs-Bi: laser-scribed graphene-chitosan-Bismuth
Sb_2O_3 : antimony oxide

PEN: polyethylene naphtalate

1µM Pb^{2+} = 210 ppb Pb^{2+}

2.3.2.2.2 Detection of Cadmium(II):

Table 6 presents the 13 CNT sensors reported for Cadmium(II) detection in water. Similarly to lead(II) references, all references but one are based on functionalized MWCNTs sensors using stripping voltammetry, the other ones using stripping voltammetry with pristine MWCNTs [150] or stripping potentiometry with functionalized MWCNTs[151]. All but one paper [169] are common with the previous able reporting on lead(II) sensors. By contrast with Lead, there is no reference on covalently functionalized CNT for Cadmium.

The reported detection limits lie between 0.02 ppb and 17 ppb to be compared to the MAC of Cadmium(II) in water between 3 and 5ppb. Similarly to the case of lead, ref [150]on pristine CNTs shows an acceptable detection limit (0.23ppb) but a range of detection not compatible with water quality monitoring (lowest limit at 170ppb).

For the same reason as for lead(II) sensing (Bismuth forming alloys with heavy metals), all but five papers out of 13 use functionalization compounds integrating Bismuth. The best result in term of LOD (0.02 ppb) is achieved with non-covalent functionalization with Poly(sodium4-styrenesulfonate)-Bismuth (PSS-Bi) [164]. The remarkable LOD is attributed to the wrapping of the PSS polymer around the CNTs, providing high density of adsorbing sites for metal binding without affecting the electronic property of the CNTs.

From these references, and those on lead as well, one may note that paste-based approaches do not perform very well overall in terms of limits of detection compared to more traditional processing of MWCNTs.

Table 6. CNT-based sensors for detecting Cd^{2+} ions in water, sorted by type of functionalization then by detection limit.

Type of CNT	Functional probe	Functionalization	Analyte (Add. Analytes)	Detection limit	Sensitivity (Linear range)	Transduction method	Deposition method	Electrode material Contact configuration	Substrate	Interference study	Ref.
MWCNT	Pristine	Non functionalized	Cd^{2+} (Pb^{2+} Zn^{2+}, Cu^{2+})	0.23 ppb	3.9 nA/ppb (170~500 ppb)	Stripping voltammetry	CNT thread	Metal wire and silver conductive epoxy	Glass capillary	-Simultaneous determination of Cd(II), Cu(II), Pb(II) and Zn(II) demonstrated -The presence of Dissolved Oxygen changes the calibration law for Cd(II)	[150]
MWCNT	PSS-Bi	Non covalent	Cd^{2+} (Pb^{2+})	0.02 ppb	0.23 µA/ppb (0.5 ~50 ppb)	Stripping voltammetry	Drop casting	Glassy carbon electrode	Glassy carbon	- 20-fold amounts of Zn^{2+}, 5-fold amounts of Sn^{2+} and 1-fold amounts of Cu^{2+} have influence on the determination of Cd^{2+} and Pb^{2+} with deviation of 10%.	(Jia, Li, & Wang, 2010) [164]
MWCNT	Nafion/Bismuth	Non covalent	Cd^{2+} (Pb^{2+})	0.04 ppb	0.18 µA/ppb (0.08~5 ppb) 0.16 µA/ppb (5~100 ppb)	Stripping voltammetry	Drop casting	Glassy carbon electrode	Glassy carbon	500-fold of SCN^-, Cl^-, F^-, PO^{3-}_4, SO_4^{2-}, NO_3^-, and various cations such as Na^+, Ca^{2+}, Mg^{2+}, Al^{3+}, K^+, Zn^{2+}, Co^{2+} and Ni^{2+} had no influences on the signals of Pb(II) and Cd(II).	[153]
MWCNT	Bismuth	Non covalent	Cd^{2+} (Pb^{2+})	0.04 ppb	0.037 µA/ppb (0.5~8 ppb)	Stripping voltammetry	Plasma-enhanced CVD (vertically aligned MWCNTs in epoxy matrix)	Cr	Silicon	N.P.	[165]
MWCNT	Fe_3O_4-LSG-CS-Bi	Non covalent	Cd^{2+} (Pb^{2+})	0.1 ppb	0.097 µA/ppb	Stripping voltammetry	Drop casting	Glassy carbon electrode	Glassy carbon	- Slight changes in peak currents of Pb^{2+} and Cd^{2+} were observed in presence of interfering ions Na^+, Cl^-, SO_4^{2-}, PO_4^{3-},	[166]

Type of CNT	Functional probe	Functionalization	Analyte (Add. Analytes)	Detection limit	Sensitivity (Linear range)	Transduction method	Deposition method	Electrode material Contact configuration	Substrate	Interference study	Ref.
					(1 ~ 20 ppb) 0.32 µA/ppb (20 ~ 200 ppb)					Fe^{2+}, Fe^{3+}, Zn^{2+}, As^{3+}. -Significant increase in response signals of Hg^{2+} was probably due to the formation of amalgam -Dramatically decreased response signals of Cu^{2+} was ascribed to the formation of Pb-Cu inter-metallic compounds.	
MWCNT	PPy-Bi	Non covalent	Cd^{2+} (Pb^{2+})	0.16 ppb	0.47 µA/ppb (0.16~120 ppb)	Stripping voltammetry	Paste mixture with MWCNT, parrafin oil and graphite powder	Stainless steel rod	Teflon (PTFE) tube	-Good selectivity towards Fe^{2+}, Al^{3+}, Zn^{2+}, Mg^{2+}, SO_4^{2-}, CO_3^{2-}, Ca^{2+}, K^+, Na^+. The absolute relative change of signal varied from 0.40 to 4.88%). -High interference from Cu^{2+} (1-fold mass ratio was found as the tolerance ratios for the detection of Pb and Cd ions)	[167]
MWCNT	Poly(1,2-diaminobenzene)	Non covalent	Cd^{2+}, (Cu^{2+})	0.25 ppb	0.14 µA/ppb (5~100 ppb)	Stripping voltammetry	Multipulse potentiostatic method	Glassy carbon electrode	Glassy carbon	N.P.	[117]
MWCNT	rGO-Bi	Non covalent	Cd^{2+} (Pb^{2+})	0.6 ppb	26 nA/ppb cm^2 (20~200 ppb)	Stripping voltammetry	Spray coating	Cr(30nm)/Au(200nm)	Polymide (VTEC 1388)	-100-fold K^+, Na^+, Ca^{2+}, Cl^-, NO^{3-}, and a 30-fold Fe^{3+} increase had no significant effect on the signals of Cd and Pb ions. - Cu ions were found to reduce the response of target metal ions due to the competition between electroplating Bi and Cu on the electrode surface (close reduction potential of Cu and Bi.)	[168]

Type of CNT	Functional probe	Functionalization	Analyte (Add. Analytes)	Detection limit	Sensitivity (Linear range)	Transduction method	Deposition method	Electrode material Contact configuration	Substrate	Interference study	Ref.
MWCNT	Bismuth	Non covalent	Cd^{2+} (Pb^{2+},Zn^{2+})	0.7 ppb	0.22 µA/ppb (2~18 ppb) 1.5 µA/ppb (20~100 ppb)	Stripping voltammetry	Screen printing	Screen printed MWCNT based electrode	Alumina plates	- The addition of copper ions strongly influenced the stripping responses. Decrease of lead and cadmium pics by 65.5%.	[167]
MWCNT	Bismuth	Non Covalent	Cd^{2+} (Pb^{2+},Zn^{2+})	0.8 ppb	0.59 µA/ppb (2~18 ppb) 0.80 µA/ppb (20~100 ppb)	Stripping voltammetry	Screen printing	Screen printed MWCNT based electrode	Ceramic substrates	N.P.	[161]
MWCNT	Fe_3O_4/ eggshell	Non covalent	Cd^{2+}	2.4 ppb	19 µA/ppb (0.5~210 ppb)	Stripping voltammetry	Paste mixture of MWCNT, graphite powder, paraffin oil and Fe3O4-eggshell	Copper wire	Glass tube	-500-fold amounts of the following ions: Na^{+}, Ca^{2+}, Mg^{2+}, Fe^{3+}, Mn^{2+}, Cr^{3+}, Ba^{2+}, Co^{2+}, Hg^{2+}, K^{+}, NH^{4+}, NO_3^{-}, SO_4^{2-}, PO_4^{3-} made no alteration of the peak currents of Cd(II). -100-fold amounts of Sn^{2+} and Cu^{2+} with deviation of 9%, 50 fold amounts of Ni^{2+} and Zn^{2+} with deviations of 8% and 6% respectively had influence on the determination of Cd(II).	[169]

Type of CNT	Functional probe	Functionalization	Analyte (Add. Analytes)	Detection limit	Sensitivity (Linear range)	Transduction method	Deposition method	Electrode material Contact configuration	Substrate	Interference study	Ref.
MWCNT	Pristine	Non covalent	Cd^{2+} (Pb^{2+},Zn^{2+})	8.4 ppb	0.36* sec/V/ppb (58~646 ppb)	Stripping potentiometry	Paste mixture of MWCNT and mineral oil	MWCNT paste electrode	Glass tube	Al (III), Mg (II), Fe (III), Ni (II), Co (II), Cr (III), Cu (II) and Sb (III) were investigated in the ratio analyte : Interferent 1:1 and 1:10. the interference was observed for the ratios analyte : interferent 1:1 and 1:10 for Co (II), 1:10 for Cr (III) and Cu (II).	[151]
MWCNT	Sb_2O_3	Non covalent	Cd^{2+} (Pb^{2+})	17 ppb	1.9 µA/ppb (80~150 ppb)	Stripping voltammetry	Paste mixture of MWCNT, silicon oil , Sb_2O_3 powder and ionic liquid	Copper wire	PTFE tube	N.P.	[159]

PSS-Bi: Poly(sodium 4-styrenesulfonate)-Bismuth
rGO-Bi: Reduced graphene oxide-Bismuth
PPy-BiNPs: Polypurrole-Bismuth
LSG-Cs-Bi: laser scribed graphene-chitosan-Bismuth
Sb_2O_3 : antimony oxide
MWCNT/MES/CPE : Multi walled carbon nanotube/ magnetic eggshell/Carbon paste electrode
1µM Cd^{2+} = 112 ppb Cd^{2+}

2.3.2.2.3 Detection of Zinc(II):

The detection of the Zn^{2+} ion in water using CNT sensors has only been investigated with electrochemical, MWCNT-based sensors (Table 7). The four references have been listed in the previous tables as they address also lead and cadmium. Unlike results on lead and cadmium, one observes that pristine MWCNTs in [150] have a remarkably better limit of detection (0.09ppb – two orders of magnitude lower) than the two references with bismuth non covalent functionalization, with a range of detection between 200 and 590ppb. This is to be compared to the maximum acceptable range of Zn(II) in water at 5ppm. It suggests a strong natural affinity of MWCNT to Zn(II), which the functionalization with Bismuth may hide (by promoting first complexation with lead and cadmium).

Table 7. CNT-based sensors for detecting Zn^{2+} ions in water, sorted by detection limit.

Type of CNT	Functional probe	Functionalization	Analyte (Add. Analytes)	Detection limit	Sensitivity (Linear range)	Transduction method	Deposition method	Electrode material Contact configuration	Substrate	Interference study	Ref.
MWCNT	Pristine	Non functionalized	Zn^{2+} (Cd^{2+}, Pb^{2+}, Cu^{2+})	0.08 ppb	3.4 pA/ppb (200~590 ppb)	Stripping voltammetry	CNT thread	Metal wire and silver conductive epoxy	Glass capillary	-Simultaneous determination of Cd(II), Cu(II), Pb(II) and Zn(II) demonstrated -The presence of Dissolved Oxygen changes the calibration law for Cd(II)	[150]
MWCNT	Bismuth	Non covalent	Zn^{2+} (Pb^{2+}, Cd^{2+})	11 ppb	0.18 µA/ppb (12~18 ppb) 0.24 µA/ppb (20~100 ppb)	Stripping voltammetry	Screen printing	Screen printed MWCNT based electrode	Ceramic substrates	N.P.	[161]
MWCNT	Bismuth	Non covalent	Zn^{2+} (Pb^{2+}, Cd^{2+})	12 ppb	0.38 µA/ppb (20~100 ppb)	Stripping voltammetry	Screen printing	Screen printed MWCNT based electrode	Alumina plates	- The addition of copper ions strongly influenced the stripping responses. Decrease of lead and cadmium pics by 65.5%.	[167]
MWCNT	Pristine	Non covalent	Zn^{2+} (Pb^{2+}, Cd^{2+})	28 ppb	0.11* sec/V/ppb (58~646 ppb)	Stripping potentiometry	Paste mixture of MWCNT and mineral oil	MWCNT paste electrode	Glass tube	Al (III), Mg (II), Fe (III), Ni (II), Co (II), Cr (III), Cu (II) and Sb (III) were investigated in the ratio analyte : Interferent 1:1 and 1:10. the interference was observed for the ratios analyte : interferent 1:1 and 1:10 for Co (II), 1:10 for Cr (III) and Cu (II).	[151]

**1µM Zn^{2+} = 65 ppb Zn^{2+}*

2.3.2.2.4 Detection of mercury(II):

Table 8 presents the CNT-based Hg(II) sensors that were reported to date. The literature is more varied in terms of transduction methods than for lead, cadmium and zinc: 1 chemFET and 1 chemistor based approaches (with pristine SWCNT) are proposed in addition to 4 references on stripping voltammetry and 2 on potentiometry (all 6 with functionalized MWCNT).

The only report about chemistor (with pristine SWCNTs) addresses the ppm range (LOD 0.6ppm; range 1 to 30 ppm) which is not truly relevant for drink water monitoring as the maximum acceptable concentration (MAC) of mercury in water is 1 ppb [69]. By comparison, the pristine SWCNT-based chemFET structure provides widely improved performances (LOD of 2 ppb, range 0.2 ppb to 200 ppm – still a bit high for drink water application). While an improvement on performances is expected when switching from chemistor to CNTFET, such a magnitude (2 orders of magnitude of improvement) is usually not. It may be linked to the use of an octadecyl-trichlorosilane (OTS) self-assembled monolayer (SAM) in [35] to favor the adsorption of SWCNT on the SiO_2 substrate. This type of SAM is reported to improve FET electronic transport performances [170]. Interestingly, both references report very good selectivity despite the absence of functionalization, which suggests a strong natural affinity of pristine CNT to mercury. This is actually confirmed by studies on water purification using CNTs showing remarkable adsorption capability of mercury without functionalization (beside native functional probes such as COOH or OH) [171].

The LOD drops significantly and the range of detection shifts towards lower (and more relevant) detection limits when functionalization and electrochemical transduction are used. Covalent functionalization with thiophenol brings the LOD down to 0.6 ppb (range from 1 to 18 ppb)[172]. The lowest LOD is 2ppt (range 2ppt to 1000 ppm)[173]. It is reached (with differential pulse voltammetry) by functionalizing a 3D structure made of MWCNTs randomly arranged around graphene oxide sheets with Bismuth-doped polyaniline chains (PANI). Once again, Bismuth is used successfully for its ability to complex heavy metals, while the 3D scaffold is thought to enhance specific surface area.

Table 8. CNT-based sensors for detecting Hg^{2+} ions in water, sorted by type of functionalization, then detection limit.

Type of CNT	Functional probe	Functionalization	Analyte (Add. Analytes)	Detection limit	Sensitivity (Linear range)	Transduction method	Deposition method	Electrode material Contact configuration	Substrate	Interference study	Ref.
SWCNT	Pristine	Non functionalized	Hg^{2+}	0.6 ppm	12 mV/ ppm (1~30 ppm)	Chemistor	CVD	SWCNT	Glass	1000 fold excess of Fe(II), Fe(III), Ni(II), Cu(II),Zn(II), Cr(III) and 500 folds of As(III), Sb(III), Se(IV) and Pb(II) had no interfering effect in the analysis of mercury solution.	[69]
SWCNT	Pristine	Non functionalized	Hg^{2+}	2 ppb	0.22/decade 0.2 ppb ~ 201 ppm	FET (Liquid gate)	Dip coating with selective CNT placement	Pd/Au (10/30 nm)	Glass	Good selectivity towards interferent ions (only Hg^{2+} causes conductance increase.)	[35]
SWCNT	Thiophenol	Covalent	Hg^{2+}	0.6 ppb	0.14 µA/ppb (1 ~18 ppb)	Stripping voltammetry	Dip coating	Au	Au	The presence of 100-fold concentration of Cr(II), Mn(II), Co(II), Ni(II), Zn(II), 50-fold concentration of Fe(II),and 20-fold Cu(II), have no influence on the signals of 50 nM Hg(II) with deviation below 5%.	[172]
MWCNT	PANi-Bi NPs@GO	Non covalent	Hg^{2+} (Cu^{2+})	2 ppt	1.3 µA/ppb (2 ppt ~ 1000 ppm)	Differential pulse voltammetry	Screen printing	(commercial) Carbon ink	PET	Not provided	[173]
MWCNT	Au NPs	Non covalent	Hg^{2+}	0.06 ppb	0.59 µA/ppb (0.1 ~ 1 ppb) 0.045 µA/ppb (1 ~ 250 ppb)	Stripping voltammetry	Drop casting	Glassy carbon electrode	Glassy carbon	Not provided	[174]
MWCNT	ENTZ	Non covalent	Hg^{2+}	0.5 ppb	29.3 mV/decade	Potentiometry	Paste mixture of MWCNT,	Copper wire	Polypropylene syringe	The interfering ions (Ag^{+}, Zn^{2+}, Pb^{2+}, Ni^{2+}, $Cd^{2+}$and Cu^{2+}) do not have	[121]

Type of CNT	Functional probe	Functionalization	Analyte (Add. Analytes)	Detection limit	Sensitivity (Linear range)	Transduction method	Deposition method	Electrode material Contact configuration	Substrate	Interference study	Ref.
					(1 ppb ~20 ppm)		graphite powder, ENTZ ionophore and ionic liquid			any effect on the response of proposed electrodes to Hg^{2+}	
MWCNT	Thiol-functionalized chitosan	Non covalent	Hg^{2+}	0.6 ppb	1060 µA/ppb (2~28 ppb)	Stripping voltammetry	Drop casting	Glassy carbon electrode	Glassy carbon	100-fold $Cd^{2+,}$ 100-fold Pb^{2+}, 50-fold Zn^{2+}, 25-fold Cu^{2+}, 10-fold Ag^{2+} , 10-fold Fe^{2+}, and 10-fold Mn^{2+} caused within ±5% changes of voltammetric signals for Hg(II).	[175]
MWCNT	Triazene (BEPT)	Non covalent	Hg^{2+}	0.62 ppb	29 mV/decade (0.8 ppb~440 ppm)	Potentiometry	Paste mixture of MWCNT, graphite powder, Triazene (BEPT) ionophore and paraffin oil	Copper wire	Polyethylene tube	The proposed electrode has a high performance to selective potentiometric assay of Hg(II) in aqueous samples containing some interfering ions (Cu^{2+}, Ag^{2+}, Cd^{2+}, Co^{2+}, Al^{3+}, Pb^{2+},K^{+}.	[176]

ENTZ: 1-(2-ethoxyphenyl)-3-(3-nitrophenyl)triazene.

PANI: polyaniline

GO: graphene oxide

NP: nanoparticles

1µM Hg^{2+} = 200 ppb Hg^{2+}

2.3.2.2.5 Detection of Arsenic(III):

Table 9 presents the five stripping voltammetry sensors reported for the detection of As^{3+} in water using functionalized MWCNTs. No report was found on As^{5+} detection even though it is a relevant species for water quality monitoring. The maximum acceptable concentration of Arsenic in drink water is 10 ppb.

COOH functionalized CNTs [177]are sensitive to As(III) in the proper range of concentration (0.3 to 50ppb), though the LOD is not provided. It suggests that pristine CNT (which naturally carry COOH groups on their sidewalls) are sensitive to As(III) as well, though the reference reports on interference with antimony.

Among the 4 references on non-covalent functionalization, all but one [178]use metal nanoparticles (NP) as functional probes, as they have been reported to provide good performances for Arsenic detection in water [179]. More specifically, the best LOD here is achieved with Au-NP at 0.1ppb [180]. The enhanced performances of Gold NPs compared to others metal NPs for heavy metal detection are usually attributed to their high electrical conductivity, high surface area and catalytic activity. A comparable LOD (0.13ppb) is achieved with a Leucine/Nafion functionalization [178]. The Leucine peptide is known for its capability to coordinate metal ions though hydrogen bonds through its $–NH_3^+$ and –COOH group.

Table 9. CNT-based sensors for detecting As^{3+} ions in water, sorted by detection limit.

Type of CNT	Functional probe	Functionalization	Analyte (Add. Analytes)	Detection limit	Sensitivity (Linear range)	Transduction method	Deposition method	Electrode material Contact configuration	Substrate	Interference study	Ref.
MWCNT	COOH	Covalent	As^{3+}	N.A	0.24 µA/ppb (0.3~50 ppb)	Stripping voltammetry	Dip coating	Au	Au electrode	- Interference was significant when the Sb/As ratio is higher than 1.	[177]
MWCNT	Au-NP	Non covalent	As^{3+}	0.1 ppb	26 µA/ppb (75 ppt - 5.3 ppm)	Stripping voltammetry	Drop casting	Glassy carbon	Glassy carbon	Not provided	[180]
MWCNT	Leucine/ Nafion	Non covalent	As^{3+}	0.13 ppb	0.27 µA/ppb (0.37~ 150 ppb)	Stripping voltammetry	Drop casting	Pt	Pt electrode	- Zn^{2+} and Fe^{2+} could be tolerated up to at least 0.05 mM whereas commonly encountered matrix components such as Cd^{2+}, Co^{2+}, Mg^{2+}, Ni^{2+} and Cu^{+} did not show high percentage of interference.	[178]
MWCNT	Pt-Fe NP	Non covalent	As^{3+}	0.75 ppb	64 nA/ppb (0.75~22 ppb)	Stripping voltammetry	Drop casting	Glassy carbon	Glassy carbon	-No interference from copper ion	[181]
MWCNT	Au NPs	Non covalent	As^{3+}	0.75 ppb	2.6 Q/mL/ppb (0.75 ~750 ppb)	Stripping voltammetry	Vaccuum filtration	MWCNT membrane	A chercher	-The presence of copper at 10 µM strongly affects the analytical response of As (III); - The presence of Pb (II) caused a minor broadening of the peak of As(III) resulting in a slight reduction of the peak current;	[182]

NP: nanoparticles

Q/mL: charge at the peak current by mL of solution passing through (the conversion to A/ppb was not possible with provided information)

1µM As^{3+} = 75 ppb As^{3}

2.3.2.2.6 Detection of Copper(II):

***Table** 10* shows the results of the 7 reported papers for Cu(II) ions detection. All but one [150] (mentioned before regarding Zn(II), Cd(II) and Pb(II) detection) address functionalized CNTs-based sensors. All but one paper address stripping voltammetry with MWCNTs. The remaining one [70]achieves with a peptide-functionalized-SWCNT-FET structure the best LOD of the literature, 3 ppt, over the range 0.6-600 ppt. The authors actually test different combinations of peptides (of which there are in theory unlimited numbers) to identify the one with optimal sensitivity. The approach is also tested successfully for Ni^{2+} detection (see next section).

It should be noted that the MAC of Cu(II) in drink water is 1 ppm, so the other references targeting the ppb to ppm range with LOD in the ppb range are more relevant to drink water applications. Comparable LOD of 0.01 ppb, 0.02ppb and 0.03ppb are achieved respectively with Schiff base [183], pristine [150] and 2-amino-4-thiazoleacetic acid [184]functionalization and stripping voltammetry. While it suggests again a strong natural affinity of CNTs to Copper, both functional probes are found interesting as they carry amine groups which are well known to easily complex copper ions [185].

Table 10. CNT-based sensors for detecting Cu^{2+} ions in water, sorted by detection limit.

Type of CNT	Functional probe	Functionalization	Analyte (Add. Analytes)	Detection limit	Sensitivity	Transduction method	Deposition method	Electrode material Contact configuration	Substrate	Interference study	Ref.
SWCNT	PANI-GGHH	Non covalent	Cu^{2+}	3 ppt	N/A (3 ~ 29 ppt)	FET (liquid gate)	CVD	300 nm Au	Si/SiO2 (120nm)	-His_6 shows higher chelation power for Ni^{2+} than to Cu^{2+}.	[70]
MWCNT	$C_{24}H_{30}N_6$ Schiff base	Non covalent	Cu^{2+}	10 ppt	N/A (0.09~340 ppb)	Stripping voltammetry	Paste of MWCNT, Schiff base and mineral oil	Copper wire	Filter membrane	Not provided	[183]
MWCNT	Pristine	Non functionalized	Cu^{2+} (Cd^{2+}, Zn^{2+}, Pb^{2+})	17 ppt	9.4 pA/ppb (32~220 ppb)	Stripping voltammetry	CNT thread aspirated into a glass capillary	Metal wire and silver conductive epoxy	Glass capillary	-Simultaneous determination of Cd(II), Cu(II), Pb(II) and Zn(II) demonstrated - Dissolved Oxygen changes the calibration law for Cd(II)	[150]
MWCNT	2-amino-4-thiazoleacetic acid	Non covalent	Cu^{2+}	30 ppt	0.02 µA/ppb* (44 ppb ~ 3.2 ppm)	Stripping voltammetry	Drop casting	Glassy carbon electrode	Glassy carbon	-At a concentration ratio below 10, the presence of Zn^{2+}, Mn^{2+}, Ni^{2+}, Co^{2+} has led to lower than 6% decreasing of DPSV currents of Cu^{2+}.	[184]
MWCNT	PANi-BiNPs@GO	Non covalent	Cu^{2+} (Hg^{2+})	32 ppt	0.23 uA/ppb (32 ppt ~ 320 ppm)	Differential pulse voltammetry	Screen printing	(commercial) Carbon ink	PET	Not provided	[173]

Type of CNT	Functional probe	Functionalization	Analyte (Add. Analytes)	Detection limit	Sensitivity	Transduction method	Deposition method	Electrode material Contact configuration	Substrate	Interference study	Ref.
MWCNT	N-doped carbon spheres	Non covalent	Cu^{2+}	92 ppt	0.28 µA/ppb (0.5~200 ppb)	Stripping voltammetry	Drop casting	Glassy carbon electrode	Glassy carbon	EDTA can seriously affect the stripping peak current of Cu(II) with a decrease of 79%.	[186]
MWCNT	Poly(1,2-diaminobenzene)	Non covalent	Cu^{2+} (Cd^{2+})	0.33 ppb	0.11 µA/ppb (5~100 ppb)	Stripping voltammetry	Multipulse potentiostatic method	Glassy carbon electrode	Glassy carbon	Not provided	[117]
MWCNT	SSA/MoS_2	Non covalent	Cu^{2+}	3.6 ppb	0.13 µA/ppb (6.4~-700 ppb)	Stripping voltammetry	Drop casting	Glassy carbon electrode	Glassy carbon	10-fold concentration of the metal ions (K^{+}, Ca^{2+}, Na^{+}, Mg^{2+}, Zn^{2+}, Pb^{2+}, Cd^{2+}, Fe^{3+}, Mn^{2+}, Co^{2+}, Cr^{3+}, Cr^{6+}, Ni^{2+} and Hg^{2+}, no effect on the Cu^{2+} peak current.	[187]
MWCNT	Cysteine	Covalent	Cu^{2+} (Pb^{2+})	15 ppb	0.13* µA/ppb (250~1500 ppb)	Differential pulse anodic stripping voltammetry	Drop casting	Glassy carbon electrode	Glassy carbon	40-fold Cl^{-}, 30-fold SO^{2-}_{4} and four fold CO^{2-}_{3} no effect on the stripping peak current of $Pb2^{+}$ and $Cu2^{+}$	[155]

SSA/MoS_2: 5-sulfosalicylic acid/MoS_2
PANI-GGHH: polyaniline functionalized with peptide chain glycine-glycine-histidine-histidine
PANI: polyaniline
GO: graphene oxide
NP: nanoparticles
1µM Cu^{2+} = 64 ppb Cu^{2}

2.3.2.2.7 Detection of other metal ions:

As listed in Table 11, the detection of two additional metal ions, Ni^{2+} and Co^{2+}, has been reported in the literature using respectively SWCNT-FET and chemistor transduction.

The peptide-functionalized SWCNT-FET mentioned in the previous section for copper detection [70], was also applied to Ni^{2+} detection with a different peptide sequence. As for Cu(II), a remarkably low LOD was achieved (2.8 ppt) within the range 0.58 to 587 ppt. Such a low LOD is interesting for drink water monitoring as the MAC for Ni (II) is low (20 ppb).

Gou et al. [87] compared flexible polyazomethine-PAM-polymer and rigid (shape persistent macrocycle) functional probes on SWCNTs for chemiresistive Co^{2+} sensing. They indicate that the flexibility of the PAM allows for better performances as it rearranges over the SWCNT network when binding the metal ions, enabling strong electronic interaction with the SWCNT. They report 0.04 ppt of LOD over an extremely large range (0.04 ppt ~ 440 ppm), which is remarkable not only for chemistors (usually less sensitive than FET and electrochemical sensors) but also for electrochemical detection of heavy metals as discussed in the previous sections. It raises the question whether even better LOD could be achieved with alternative transduction modes.

Table 11. CNT-based sensors for detecting Ni(II) and Co(II) ions in water.

Type of CNT	Functional probe	Functionalization	Analyte (Add. Analytes)	Detection limit	Sensitivity	Transduction method	Deposition method	Electrode material Contact configuration	Substrate	Interference study	Ref.
SWCNT	Polypyrrole-His_n	Non covalent	Ni^{2+}	2.8 ppt	1.5 µS/decade (5% / decade) (0.59 ppt~59 ppb)	FET (liquid gate)	CVD	300 nm Au Pt wire (Counter electrode), Ag/AgCl (Reference electrode)	Si/SiO2(120nm)	-His_6 shows higher chelation power for Ni^{2+} than to Cu^{2+}.	[70]
SWCNT	PAM	Non covalent	Co^{2+}	0.04 ppt	0.014* /decade (0.04 ppt ~ 440 ppm)	Chemistor	Spay-casting	Al tape Ag paint	Si/SiO2	Selectivity to Co^{2+} was investigated in presence of Cu^{2+}. The electrical response was higher with Co^{2+}.	[87]

His: peptide histidine

PAM : polyazomethine

2.3.2.2.8 Multiplexed detection of metal ions.

As reported above, studies on metal ions detection rely heavily on electrochemical transduction (32 papers out of 36 in total). Electrochemical detection, and more specifically stripping voltammetry, is particularly interesting for the simultaneous detection of different metals in water, as the current peaks for each metal appear at different voltage range, as can be shown for example in Figure 13 reproduced from [150] (obtained with MWCNTs threads electrodes).

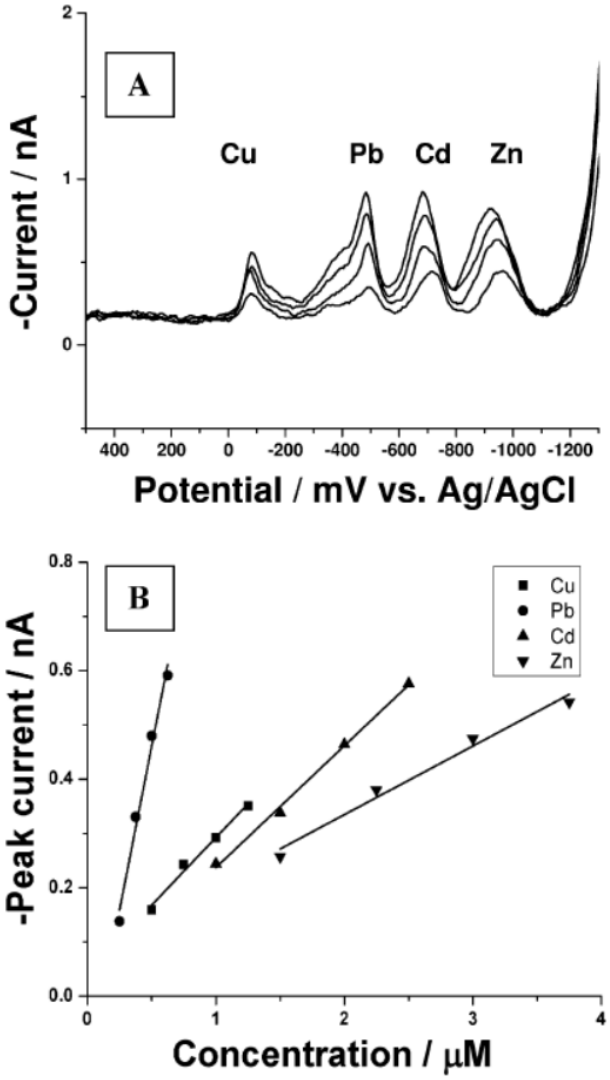

Figure 13. (A) Simultaneous detection of Cu^{2+}, Pb^{2+}, Cd^{2+} and Zn^{2+}, ion concentrations 0.5, 0.25, 1.0, 1.5 µM for Cu^{2+}, Pb^{2+}, Cd^{2+}, Zn^{2+}, respectively; and 1.5, 2, 2.5 times of above concentrations for these metals ions. (B) Calibration Curve for Cu^{2+}, Pb^{2+}, Cd^{2+}, Zn^{2+}. Accumulation time: 120 s, deposit potential: -1.5 V. Reproduced from [150].

Naturally, among these 32 references on electrochemical transduction, 14 report on multiplexed detection with stripping voltammetry (while none of the 4 papers based on electrical transduction does). Investigated groups of metal ions are Cd(II)/Pb(II) (7), Cd(II)/Zn(II)/Pb(II) (3), Cd(II)/Zn(II)/Pb(II)/Cu(II) (1), Cd(II)/Cu(II) (1), Cu(II)/Pb(II) (1) and Hg(II)/Cu(II) (1). The simultaneous detection of lead and cadmium is particularly focused on (10 papers out of the 14), as these two heavy metals are commonly found together in soil and water supplies and are both severe environmental contaminants even at trace levels. Table 12 provides a comparison of the performances of the devices reported in these 14 papers as a function of the target species, with conversion from ppb to M unit to allow comparison across analytes.

Overall, one observes that devices are slightly better detection limit to Pb(II) than to Cd(II) irrespective of the functionalization (Bismuth-based compounds - 0.3 to 1 - or Sb_2O_3 - 0.7 - or pristine - 0.4 to 0.5), except for the Bismuth-reduced graphene oxide functionalization reported in [168]with sensitivity to Pb(II) enhanced by a factor of 50 compared to Cadmium.

By contrast, the limit of detection to Cd(II) is much lower than to Zn(II) (by a factor 6 to 30), except in [150]with non-functionalized MWCNT threads where it is 1.6 times higher. Finally, the limit of detection to Cu(II) is much higher than for other species by about 1 order of magnitude.

Table 12. Comparison of the performances of sensors based on multiplexed detection as a function of the target species

Type of CNT	Functional probe	Functionalization	Cd(II) LOD	Pb(II) LOD (LOD Pb/ Cd)	Zn(II) LOD (LOD Zn/Cd)	Cu(II) LOD (LOD Cu/Cd)	Hg(II) LOD	Ref.
MWCNT	Nafion/Bismuth	Non covalent	0.04 ppb – 0.4nM	0.025 ppb – 0.12nM 0.3				[153]
MWCNT	Bismuth	Non covalent	0.04 ppb – 0.4nM	~0.04 ppb – 0.2nM 0.5				[165]
MWCNT	PSS-Bi	Non covalent	0.02 ppb – 0.2nM	0.04 ppb – 0.2nM 1				[164]
MWCNT	rGO-Bi	Non covalent	0.6 ppb – 50nM	0.2 ppb – 1nM 0.02				[168]
MWCNT	PPy-Bi	Non covalent	0.16 ppb – 1.4nM	0.1 ppb – 0.5nM 0.4				[167]
MWCNT	Fe_3O_4-LSG-CS-Bi	Non covalent	0.1 ppb – 0.9nM	0.07 ppb – 0.3nM 0.3				[166]
MWCNT	Sb_2O_3	Non covalent	17 ppb – 0.15µM	24 ppb – 110nM 0.7				[159]
MWCNT	Pristine	Non functionalized	8.4ppb – 75nM	6.6 ppb – 31nM 0.4	28 ppb – 0.43µM 6			[151]
MWCNT	Bismuth	Non covalent	0.8ppb – 7nM	0.2 ppb – 1nM 0.14	11ppb – 0.17µM 24			[161]
MWCNT	Bismuth	Non covalent	0.7ppb – 6nM	1.3 ppb – 6.2nM 1	12 ppb – 0.18µM 30			[162]
MWCNT	Pristine	Non functionalized	0.23 ppb – 2nM	0.3 ppb – 1nM 0.5	0.08 ppb – 1.2 nM 0.6	17 ppt – 0.26nM 0.13		[150]
MWCNT	Poly(1,2-diaminobenzene)	Non covalent	0.25 ppb – 0.22nM			0.33 ppb – 5nM 22		[117]
MWCNT	Cysteine	Covalent		1 ppb – 4nM		15 ppb – 0.23µM		[155]

Type of CNT	Functional probe	Functionalization	Cd(II) LOD	Pb(II) LOD (LOD Pb/ Cd)	Zn(II) LOD (LOD Zn/Cd)	Cu(II) LOD (LOD Cu/Cd)	Hg(II) LOD	Ref.
MWCNT	PANi-Bi NPs@GO	Non covalent				32 ppt – 0.5nM	2 ppt – 0.01nM	[173]

PSS-Bi: Poly(sodium 4-styrenesulfonate)-Bismuth
rGO-Bi: Reduced graphene oxide-Bismuth
PPy-BiNPs: Polypyrrole-Bismuth
LSG-Cs-Bi: laser scribed graphene-chitosan-Bismuth
Sb_2O_3 : antimony oxide
PANI: polyaniline
GO: graphene oxide
NP: nanoparticles
1µM Cd^{2+} = 112 ppb Cd^{2+}
1µM Zn^{2+} = 65 ppb Zn^{2+}
1µM Pb^{2+} = 210 ppb Pb^{2+}
1µM Cu^{2+} = 64 ppb Cu^{2+}
1µM Hg^{2+} = 200 ppb Hg^{2+}

2.3.2.2.9 Interference studies

Interferent studies are particularly significant regarding to toxic metal ions detection because in most water matrices, a wide range of ions are present at the same time, some of these at concentrations orders of magnitude larger than the target trace metals. For these reasons, most studies include interfering studies (30 out of 36 papers).

Among these, most papers study interferences by other toxic ions typically present in the ppb range in water, such as Cu(II), Fe(II), Fe(III), Ni(II), Zn(II), Cr(III), As(III), Sb(III), Se(IV), Pb(II), Al (III), Fe (III), Ni (II), Co (II), F^- , and SCN^-. Among these, Cu(II) is the one reported most consistently as being an interferent for bismuth functionalized CNT sensors due to the competition between bismuth ions and copper ions. It notably impacts performances for Zn(II), Cd(II), Pb(II) and As(III) detection [154], [162], [166]–[168], [182].

Other papers rather focus on more ubiquitous ions usually present in the ppm range in water, such as Cl^-, PO_4^{3-} , SO_4^{2-} , NO_3^-, Na^+, Ca^{2+}, Mg^{2+}, K^+ or CO_3^{2-} [153], [169]. For these ions, no interference to Pb(II), Cu(II) and Cd(II) detection was found.

These two types of interferents are mentioned in the literature on Hg(II) sensors. Out of 8 papers, 7 report on interferent studies. All these studies conclude toward a strong selectivity toward Hg(II) against the various interferent ions (see Table 12), irrespective of the types of functionalization (pristine, covalent, non-covalent) and of transduction (electrochemical, ChemFET, chemistor). It suggests a strong selectivity of the CNTs themselves toward Hg(II).

Among other chemicals tested for interference, EDTA was found to particularly affect the detection of Cu(II) because EDTA forms complexes with every cation through its two amine and four carboxylate groups [186]. Benzene, xylene and some surfactants also interfere with metal ions detection by preventing the stripping of trace metals during stripping voltammetry measurements.

2.3.2.3 Nitrogen (Ammonia, nitrite, nitrate)

Ammonia (NH_3) is highly soluble in water and found under the form of dissolved gas or as the ammonium ion (NH_4^+) depending on pH. Though it may be present in water as a result of normal biological degradations of proteins it may also be brought by industrial water discharge. It is also sometimes used for drink water treatment (notably in the USA).

Nitrite ions (NO_2^-) are widely used as fertilizing agents and food preservatives. They are in consequence among the pollutants most often identified in natural waters. They are highly toxic for human beings (fatal dose of nitrite ingestion is between 8.7 and 28.3 µM) [188]. Nitrate ions (NO_3^-) are also widely found in groundwater and subsequently in drinking water. They primarily result from fertilizers, septic systems, and manure storage or spreading operations. Although nitrite, nitrate and ammonia all have strong health and environmental impacts, only nitrite sensing has been reported with CNTs so far. Table 13 summarizes the reported performances. All the papers rely on electrochemical transduction with non-covalently functionalized CNTs, only one paper using SWCNT.

The reported LODs vary from 0.016 µM to 25 µM (1 mM Nitrite = 46 ppm), and the ranges of detection cover the scale from 0.1 µM to 10 mM. The MAC for nitrite in drinking water is around 1ppm/20 µM, so 9 papers out of 10 show acceptable limit of detection for nitrite monitoring in drink water with 7 papers out of 10 reporting negligible interferences.

The best result is reported with a LOD of 0.016 µM with a functional probe based on a nanocomposite made of Co_3O_4 and rGO (reduced graphene oxide) [189]. With the same electrode and deposition process (drop casting on glassy carbon, using only rGO only as functional probe leads to a considerably higher LOD of 25 µM [190], underlying the role of the cobalt oxide functionalization in the sensitivity. Consistently, cobalt oxide on its own has been reported to be promising for nitrite sensing by its reduction process upon exposure to nitrite [191].

Table 13. CNT-based nitrogen sensors for water quality monitoring, sorted by detection limit.

Type of CNT	Functional probe	Functionalization	Analyte	Detection limit	Sensitivity (Detection range)	Transduction method	Deposition method	Electrode material Contact configuration	Substrate	Interference study	Ref.
MWCNT	Co_3O_4-rGO	Non covalent	Nitrite	0.016 μM	0.408 μA/μM/ cm^2 (0.1 ~ 8000 µM)	Voltammetry	Drop casting	Glassy carbon electrode	Glassy carbon	100-fold of alcohol, Na^+, K^+, Cl^-, NO_3^-, N_2H_4, SO_3^{2-},SO_4^{2-}, has no effect on sensor response.	[189]
MWCNT	PCMA*	Non covalent	Nitrite	0.067 µM	-0.023 µA/µM (1 ~ 10 µM) -0.022 µA/µM (10 ~ 100 µM) -0.034 µA/µM\ (100 ~ 1000 µM) -0.026 µA/µM (1000 ~ 4000 µM)	Differential pulse voltammetry, Chronoamperometry	Drop cast of PCMA/ MWCNT, then electrochemical crosslinking	Au	Au	Not provided	[192]
MWCNT	AuNPs/ PEI/ MWCNT-COOH	Non covalent	Nitrite	0.2 µM	-0.500 µA/µM* (1 ~ 2000 µM) -58 µA/mM (1 ~ 1400 µM)	Voltammetry	Drop casting	Au	Au	Na^+, Mg^{2+}, Ca^{2+}, Zn^{2+}, Fe^{2+}, Cl^-, I^-, and SO_4^{2-} did not have significant interference in the detection of nitrite.	[193]
SWCNT	Pd	Non covalent	Nitrite	0.25 µM	420 µA mM^{-1} cm^{-2} (2 ~ 240 µM) 190 µA mM^{-1} cm^{-2} (280~1230 µM)	Differential pulse voltammetry	Vacuum filtration	SWCNT	PET	Negligible effect of K^+, Na^+, Cl^-, PO_4^{3-}, NH_4^+, CH_3COO^-, and Zn^{2+} in concentration above500 mM and concentrations of Mg^{2+}, Ca^{2+}, Cd^{2+}, CO_3^{2-}, NO_3^-,and SO_4^{2-} above 200 mM	[194]

Type of CNT	Functional probe	Functionalization	Analyte	Detection limit	Sensitivity (Detection range)	Transduction method	Deposition method	Electrode material Contact configuration	Substrate	Interference study	Ref.
MWCNT	Ni_7S_6	Non covalent	Nitrite	0.3 µM	0.185 µA/µM (1 ~ 4200 µM)	Voltammetry	Drop casting	Glassy carbon electrode	Glassy carbon	Results comparable to high-performance liquid chromatography for lake water, tap water and pickle water	[195]
MWCNT	GO-MWCNT-PMA-Au	Non covalent	Nitrite	0.67 µM	0.484 µA/µM (2 ~ 10,000 µM)	Differential pulse voltammetry	Drop casting	Glassy carbon electrode	Glassy carbon	No obvious response was observed when injection of 0.4 Mm of Na^+, Ca^{2+}, NO_3^-, CO_3^{2-}, K^+, Cl^-, SO_4^{2-}, IO_3^-	[196]
MWCNT	Au/TiO2	Non covalent	Nitrite	3 µM	N/A (4 ~ 225 µM)	Differential pulse voltammetry	Pulsed electrodeposition	Glassy carbon electrode	Glassy carbon	The presence of arginine, serine, tyrosine, cysteine, glucose, alanine (each of 0.1 mM) causes less than 5% variation on sensor response.	[188]
MWCNT	Thionine	Non covalent	Nitrite	4 µM	0.002 µA/µM (6 µM ~ 15, 000 µM)	Voltammetry	Transfer via abrasion from filter paper to heated GC electrode	Glassy carbon electrode	Glassy carbon	Not provided	[197]
MWCNT	PANI	Non covalent	Nitrite	6.1 µM	0.684 µA/µM/ cm^2 (N/A)	Voltammetry	Electrodeposition	Glassy carbon electrode	Glassy carbon	Not provided	[198]
MWCNT	rGO	Non covalent	Nitrite	25 µM	0.01 µA/µM (75 ~ 6060 µM)	Differential pulse voltammetry	Drop casting	Glassy carbon electrode	Glassy carbon	0.6 M Ca^{2+}, Cu2+, K^+, Na^+, Zn^{2+},$SO4^{2-}$, l-cysteine, NO_3^- and Cl^- did not interfere with the pick signals of 0.15 mM HQ, 0.15 mM CC, 0.15 mM PC and 0.15 mM NO_2^- .	[190]

In case of Nitrite ion (NO_2^-), 1 mM = 46 ppm.

PEI: polyethyleneimine

NP: nanoparticles

PCMA: poly(VMc-co-VCz-coAA ; VMc: 7-(4-vinylbenzyloxy)-4-methyl coumarin, VCz: 9-Vinylcarbazole, AA: Acrylic acid),

GO: Graphene oxide; rGO: Reduced graphene oxide,

GCE: Glassy carbon electrode,

CTAB: hexadecyl trimethyl ammonium bromide,

Mb: Myoglobin,

PANI: Polyaniline.

2.3.2.4 Water hardness (Ca2+, Mg2+, total)

In general, the total hardness of water is defined as the sum of the concentrations of calcium (Ca^{2+}), magnesium (Mg^{2+}) and of all the other alkaline earth ions in the water matrix such as strontium (Sr^{2+}) and Barium (Ba^{2+}). The concentration of calcium and magnesium ions is dominant to the other alkaline-earth metals, therefore water hardness is generally estimated from the concentration of these two ions [199]. Determination of water hardness is important as hard water can precipitate inside a water pipe and cause limescale. The sum of recommended Ca^{2+} and Mg^{2+} concentration in water is between 2 to 4 mM.

There has been relatively few studies on CNT sensors for Ca^{2+} and Mg^{2+} ions measurement, as reported in Table 14, both addressing functionalized CNT. To be noted, both sensors are tested to measure either Ca^{2+} or Mg^{2+} concentration in water, not the total water hardness (which is the sum of the concentrations of both ions). The best reported limit of detection is achieved with a chemFET approach, reaching down to 100 pM of Ca^{2+} (4 ppt). It is based on the functionalization of SWCNT by Fluo-4 AM (Fluorescent acetoxymethyl ester). It is a fluorescein derivative comprising amino carboxylate coordinating groups that has been widely used for calcium detection [200].

Table 14. CNT-based water hardness sensors in water.

Type of CNT	Functional probe	Functionalization	Analyte	Detection limit	Sensitivity (Detection range)	Transduction method	Deposition method	Electrode material Contact configuration	Substrate	Comments	Ref.
SWCNT	Fluo-4 AM	Non-covalent	Ca^{2+}	100 pM	69 nA/decade (100 nM ~ 1 mM)	CNT-FET	Dip coating	Ti (10nm)/Au (30nm) (liquid, floating gate)	Glass (borosilicate glass capillary)	-FET at the end of a nanoneedle for intracell monitoring	[201]
MWCNT	PDMS	Non-covalent	Ca^{2+} (Mg^{2+})	25 µM	N/A (25 µM ~ 5 mM (Not linear))	Capacitive measurement	Mold injection and thermal curing	MWCNT	PDMS	Measured at 2.4kHz frequency	[202]

Fluo-4 AM: Fluorescent acetoxymethyl ester

PDMS: Polydimethylsiloxane

1 ppm Ca2+ = 0.025 mM Ca^{2+}

2.3.2.5 Dissolved oxygen

Dissolved oxygen (DO) refers to the amount of free oxygen present in water in gaseous form. It is measured in mg/L or in ppm. Algal biomass, dissolved organic matter, ammonia, volatile suspended solids and sediment oxygen demand can affect the variation of DO in water. Hence DO is used widely used as indicator of the metabolism and pollution levels of waterbodies [203], [204].

Several groups reported that molecular oxygen acts as dopant for CNTs and thus limit the selectivity and sensitivity of CNT-based sensors to other gas (in air) or chemicals (in water) [205], [206]. In turn, this suggested the feasibility of CNT-based DO sensors. Table 15 shows the two instances of DO sensors based on CNT reported so far. Both are based on cyclic voltammetry with non-covalently functionalized MWCNT coated on glassy carbon electrodes.

Regarding the first reported CNT-based dissolved oxygen sensor in 2004 [207], the functional probe is hemin. Hemin is an iron-containing porphyrin that can be found in red blood cells, and that efficiently binds dioxygen [208]. Hemin-functionalized MWCNTs show a better sensitivity to O_2 than non-functionalized ones in O_2-saturated phosphate buffer solution.

More recently, Tsai *et al* (2013 [209]) used gold nanoparticles as functional probe, gold being selected as an effective catalyst for oxygen reduction. The electrodes showed a quasi-linear response to dissolved oxygen with a detection limit at 0.1 ppm (~ 3 µM). Such resolution is suitable to determine the spatial variation of DO concentration for oxygen profiling in water bodies [210].

Table 15. CNT-based dissolved oxygen sensors in water.

Type of CNT	Functional probe	Functionalization	Analyte	Detection limit	Sensitivity (Linear range)	Transduction method	Deposition method	Electrode	Ref.
MWCNT	Hemin	Non-covalent	O_2	N/A	N/A (N/A)	Cyclic voltammetry, Amperometry	In-place CVD (densely-packed, vertically aligned CNTs)	Glassy carbon electrode	[207]
MWCNT	Au NP*	Non-covalent	O_2	0.1 ppm	N/A (0~ 50 ppm)	Cyclic voltammetry	Not provided	Glassy carbon electrode	[209]

**NP: nanoparticles*

2.3.2.6 Disinfectants (Hypoclorite, hydrogen peroxide, chloroamine, peratic acid)

Free chlorine, hydrogen peroxide, peracetic acid, potassium permanganate and chloramine, are chemicals with an outstanding oxidation capacity. They are used either in the initial disinfection process of water or to keep the drinking water disinfected during distribution.

One of the most widely used drink water disinfectants is free chlorine. Its concentration in water should be in the range from 0.5 to 2 mg/L after disinfection (in which case it is called residual free chlorine). At lower concentrations, bacterial contamination may occur; at higher concentrations it is hazardous to human health.

Table 16 shows the reported CNT-based sensors for detecting disinfectants in water.

The detection of hydrogen peroxide is reported in 6 articles, all but one by the means of electrochemical measurements with non-covalently functionalized CNT. The detection limit is about 3ppm for the chemistor device (which is acceptable for the applicative range: conventional hydrogen peroxide sensors have a range from 0 to 2000 ppm and EPA (US) recommended levels in drink water are from 25 to 50ppm). The use of electrochemical transduction with CNT functionalized by metallic materials lowers this threshold by several orders of magnitude, reaching down to 3.4ppb with a 3D structure based on nitrogen doped Co-CNTs over graphene sheets [211]. An approach based on petal-like chromium hexacyanoferrate (Cr-hcf) crystallites yields 17ppb in detection limit, this later material being specifically studied because of its electrocatalytic activity in the reduction of H_2O_2 [212]. As in the previous sections, the use of these two types of 3D structuration appears to lead to large improvement (more than one order of magnitude) of performances compared to more traditional 2D architecture such as [213]and [214](also metal based).

Regarding free chlorine (or hypochlorite detection for detection at pH higher than 7), the non-functionalized, aligned MWCNT-based chemistor device shows the lowest LOD below 5ppb. The sensitivity in this reference is attributed to the oxidative properties of NaOCl leading to doping effect of the CNTs [215].

Table 16. CNT-based sensors for detecting disinfectants in water. References are sorted by type of analyte (hydrogen peroxide, free chlorine) then by limit of detection.

Type of CNT	Functional probe	Functionalization	Analyte	Detection limit	Sensitivity (Detection range)	Transduction	Deposition method	Electrode material Contact configuration	Substrate	Interference	Ref.
MWCNT	PVC, DBE	Non covalent	Hydrogen peroxide	N/A	Not Provided	Amperometry, voltammetry	Screen Printing	CNT electrodes	Alumina	Not provided	[216]
MWCNT	nitrogen doped Co-CNTs over graphene sheets	Non covalent	Hydrogen peroxide	100nM 3.4ppb	-0.85µA/ppm	Voltammetry, amperometry	Coating	Glassy carbon electrode	Glassy carbon electrode	No interference with uric acid, ascorbic acid and glucose	[211]
SWCNT	Cr-hcf*	Non covalent	Hydrogen peroxide	0.5µM 17ppb	1 µA/ppm (17 ppb ~ 340 ppm)*	Amperometry, voltammetry	Drop casting	Glassy carbon electrode	Glassy carbon	No interference from ascorbic acid and uric acid	[212]
CNT (probably Multi-walled)	Fe - Ni	Non covalent	Hydrogen peroxide	16µM 540ppb	1.2µA/ppm (34ppm ~ 510ppm)	Voltammetry	Paste poured into electrode	Glassy carbon electrode	Glassy carbon electrode	Not provided	[213]
MWCNT	Chitosan/Cu/MWCNT -COOH	Non covalent	Hydrogen peroxide (pH)	<25µM <850ppb	0.97 nA/ppb (500µM ~ 10 mM)	Amperometry	Potentiostatic polarization	Glassy carbon electrode	Chitosan-coated glassy carbon	No interference from ascorbic acid and uric acid	[214]
SWCNT	Phenyl capped aniline tetramer	Non covalent	Hydrogen peroxide	<3ppm	1%/ppm (3ppm ~ 8 ppm) Nonlinear <1%/100ppm (48ppm ~ 1200 ppm)	Chemistor	Drop casting	Carbon ink	Glass	Not provided	[217]

Type of CNT	Functional probe	Functionalization	Analyte	Detection limit	Sensitivity (Detection range)	Transduction	Deposition method	Electrode material Contact configuration	Substrate	Interference	Ref.
MWCNT	Pristine	Non functionalized	Free chlorine in its hypochlorite ion form	<5ppb	Logarithmic 39% /decade* (0.03~8 ppm)	Chemistor	Dielectrophoresis (aligned MWCNT)	Cr/Au	Glass	No information about selectivity, pH information not provided	[215]
MWCNT	Epoxy EpoTek H77A	Non covalent	Free chlorine under hypochlorous acid form (At pH 5.5)	20 ppb	0.15 µA/ppb (0.02~4 ppm)	Voltammetry	Paste poured into tube and thermally cured	Epoxy /MWCNT composite	Not provided (tube)	Validated in real water matrices (tap water and swimming pool)	[218]
SWCNT	Phenyl capped aniline tetramer	Covalent	Free chlorine	<60ppb	92 nA/decade (0.06~60 ppm (linear up to 6ppm))	Chemistor	Drop casting	Au	Glass	Non selective to different oxidants – list of oxidants not provided Regeneration possible	[79]

Cr hcf: Chromium hexacyanoferrate
PVC: Polyvinyl chloride

DBE: dibasic ester

1mM = 34ppm H_2O_2

2.3.2.7 Sulfur (Sulfide, sulfite, sulfate)

Sulfur can be found in aqueous environments in oxidized form as sulfite (SO_3^{2-}), sulfate (SO_4^{2-}), or in reduced form as sulfide (S^{2-}). The oxidized forms of sulfur play an important role within environmental systems [219]. In fact, they are detected in natural waters, waste waters and in boiler waters (those treated with sulfur for dissolved oxygen control). High concentrations of sulfite in boiler waters is harmful, since it decreases pH and subsequently, stimulates corrosion.

Table 17 compares the different CNT-based sulfur (sulfite (SO_3^{2-}) and sulfide (S^{2-})) sensors used for water quality monitoring. No sulfate (SO_4^{2-}) sensor has been reported yet. All of these studies address electrochemical sensing with non-covalently functionalized CNTs.

Regarding sulfite detection, both reports [116], [120], use a functional probe based on ferrocene. Zhou *et al*. (2008) used ferrocene-branched chitosan composites, while Hassan *et al*. (2011) used only ferrocene for GCE modification. Indeed, ferrocene and its derivatives have been reported as strong electrocatalysts for sulfite detection [220]. The LOD and sensitivity of the probe using ferrocene being directly in contact with MWCNTs are better by a factor of more than 20 than those of the probe using ferrocene-branched chitosan.

Regarding the detection of sulfide, all reports address electrochemical sensing with MWCNTs. Best LODs are in the range 0.2 to 0.3 µM (1 mM sulfide = 34 ppm). These LOD are too high compared to drink water quality requirements as sensitivity to sulfide in the ppt to sub-ppm range is needed. The best limit of detection at 0.2µM is reported with Hematoxylin [221], a compound reported to foster electrocatalyic oxidation of sulfide. Platinum [68] nanoparticles (also expected to oxidize sulfide) electrodeposited on vertically aligned CNT arrays perfom also very well, comparably to non-functionalized CVD-grown MWCNTs [222].

Table 17. CNT- based sulfur sensors for water quality monitoring. References are sorted by analyte (sulfite and sulfide), then by limit of detection.

Type of CNTs	Functional probe	Functionalization	Analyte	Detection Limit	Sensitivity (Detection range)	Transduction method	Deposition method	Electrode material Contact configuration	Substrate	Interference study	Ref.
MWCNT	Ferrocene-branched chitosan	Non covalent	Sulfite	2.8 µM	0.013 µA/µM (5 μM~1500 µM)	Amperometry	Drop casting	Glassy carbon electrode	Glassy carbon	600-fold excess of Ca^{2+}, Mg^{2+}, Ba^{2+}, PO_4^{3-}, NO_3^-, CO_3^{2-} and Cl− did not interfere in the determination of sulfite.	[116]
MWCNT	Ferrocene	Non covalent (Physical immobilization)	Sulfite	0.1 µM	3.3 µA/µM (0.4 μM ~ 4 µM) 0.18 µA/µM (4 µM ~ 120 μM)	Differential Pulse Voltammetry	Paste mixture with graphite powder blended with paraffin oil	MWCNT paste, Copper wire	Glass tube	Not provided	[120]
MWCNT	Hematoxylin	Non covalent	Sulfide	0.2 µM	103 nA/ µM (0.5 µM ~ 150 µM)	Amperometry	Paste mixture of MWCNT, mineral oil and graphite powder	Carbon paste	Teflon tube	No interference with Sn2+, Co2+, Pb2+, Zn2+, Cu2+, Ni2+, Mn2+, Fe2+ and Fe3+	[221]
MWCNT	Platinum	Non covalent (plating)	Sulfide	0.26 µM	0.63 µA/µM (0.26 µM ~ 40 µM and 40 µM ~ 100 µM)	Amperometry Differential pulse voltammetry	Thermal CVD (vertically aligned CNTs)	Stainless steel	Stainless steel	Not provided	[68]
MWCNT	Pristine	Not functionalized	Sulfide	0.3 µM (CVD), 12.5 µM (ARC)	0.12 µA/µM (1.3 µM ~ 113 µM) (CVD), 0.005 µA/µM (12.5 µM ~ 87.5 µM) (ARC)	Hydrodynamic voltammetry	Drop casting	Glassy carbon electrode	Glassy carbon	Not provided	[222]

Type of CNTs	Functional probe	Functionalization	Analyte	Detection Limit	Sensitivity (Detection range)	Transduction method	Deposition method	Electrode material Contact configuration	Substrate	Interference study	Ref.
MWCNT	Copper phenanthroline	Non covalent (Physical immobilization)	Sulfide	1.2 µM	34 nA/µM (5 µM ~ 400 μM)	Amperometry	Drop casting	Glassy carbon electrode	Glassy carbon	No interference with SO3 2-, SO4 2-, S2 O3 2-, S4 O6 2-, Cysteine. [223]	[223]

**ARC: Arc discharge method, CVD: Chemical vapor deposition method.*

2.3.2.8 Other contaminants

The detection of various additional analytes is also reported in the literature, as detailed in Table 18.

Zhao *et al (2012)* reported that the threshold voltage of a CNT-FET with interdigitated electrodes using pristine, in-place grown SWCNT showed a response to glycerol in water [90]. This response is attributed to polar glycerol molecules adsorbing on the SWCNT sidewalls and acting as dopant for SWCNT. Glycerol is relevant to monitor in water as it is widely used in the food, beverage and e-cigarettes industry, and is also used in the formulation of numerous solvents. Thus, it ends up in the water cycle from human and industrial waste and may feature ecotoxicity [224].

Regarding to security applications (detection of explosive materials at extremely low concentration in water), Wei *et al* (2014) demonstrated that a SWCNT-based chemistor functionalized with 1-pyrenemethylamine (PMA) could detect 2,4,6-trinitrotoluene in water, with a detection limit of 10 ppt and less than 1 minute of response time [81]. The sensor showed high selectivity to several interfering molecules, for example, 2,6-dinitrotoluene (DNT) and 2,4-dinitrotoluene (2,4-DNT). The amino substituent in PMA was reported to interact selectively with TNT by forming negatively-charged complexes on the SWCNT sidewalls.

Regarding to the identification of dangerous toxins, Lee *et al* (2018) reported that CNT-FET showed a response to botulinum neurotoxin (BoNT) in water with a detection limit up to 60 pM in case of peptide-modified CNT ((A)), and 52 fM in case of CNT modified with the anti-botulineum neurotoxin (B)) [141].

The detection of coliforms (notably Escherichia coli, but also other bacterial pathogens) is of major impact to drink water quality monitoring. However, standard assays take 24h to 48h to determine presence or absence of coliforms, so reducing this detection time is of major interest. It relies on indirect detection of chemicals released by the bacteria, often upon addition of reagents. In [225], p-aminophenol is used as an indicator of coliform presence and detected through a glassy carbon electrode coated with Nafion/MWCNT. Coliform detection down to 10cfu/mL is possible with 5h response time.

Finally, references [190], [226]–[228] address with electrochemical sensors based on CNT modified carbon electrodes the topic of emerging contaminants, through the angle of drugs and hormones [190], [226] and of bisphenol A [227]–[229]. Emerging contaminants are compounds derived from manufactured chemicals and that despite being present only in µg/L concentrations (or below) in water bodies are known to have strong impact on health and environment [230]. Among these, bisphenol A is notably acknowledged as endocrine disruptor and as toxic to reproduction. It is worth mentioning that regarding drug and health-care related chemicals, there are more references available beyond the field of drink water monitoring which are not included here, as detailed recently in [231].

Table 18. Reported chemical CNT sensors for water quality monitoring with different probes and analytes.

Type of CNT	Functional probe	Functionalization	Analyte	Detection limit	Sensitivity (Detection range)	Transduction method	Deposition method	Electrode material Contact configuration	Substrate	Interference study	Ref.
SWCNT	Pristine	Not functionalized	Glycerol	N/A	~ 10 Ω/Glycerol by weight % in water (10~50 %)	CNT-FET	Dielectrophoresis	Cr/Au	Si/SiO_2	Not provided	[90]
SWCNT	1-phyrenemethylamine	Non-covalent	Trinitrotoluene	~ ppt	N/A (> 0.01 ppb)	Chemistor with interdigitated electrodes (IDEs)	Dip coating	Cr/Au	Si/SiO2	Relatively selective to 2,6-DNT, 2,4-DNT, 1,3-DNB, 1-NB*, Response time ~ 30s	[81]
SWCNT	Peptides, anti-BoNT/E-Lc*	Non-covalent	BoNT*	60 pM (Peptide probe), 52 fM (Anti-BoNT/E-Lc probe)	27.95 nS/nM (Peptide), 313 nS/pM (Anti-BoNT)	CNT-FET	CVD (vertically aligned SWCNTs)	Au foils Bottom gate	120 nm SiO2 on PDMS film	Not provided	[141]
MWCNT	Nafion	Non covalent	p-aminophenol (Coliforms)	10cfu/mL	10 to 10^4 cfu/mL	Cyclic voltammetry, amperometry	Drop casting	Glassy carbon electrode	Glassy carbon	Not provided	[225]

Type of CNT	Functional probe	Functionalization	Analyte	Detection limit	Sensitivity (Detection range)	Transduction method	Deposition method	Electrode material Contact configuration	Substrate	Interference study	Ref.
MWCNT	rGO	Non covalent	Hydroquinone Catechol p-cresol (nitrite)	2.6 µM 1.8 µM 1.6 µM	0.19 µA/µM (8~391 µM) 0.07 µA/µM (5.5~540 µM) 0.04 µA/µM (5~430 µM)	Differential pulse voltammetry	Drop casting	Glassy carbon electrode	Glassy carbon	0.6 M Ca^{2+}, Cu2+, K^{+}, Na^{+}, Zn^{2+},$SO4^{2-}$, l-cysteine, NO_3^{-} and Cl^{-} did not interfere with the pic signals of 0.15 mM HQ, 0.15 mM CC, 0.15 mM PC	[190]
MWCNT	Fe-Co doped TNTs	Non-covalent	Sulpiride	87 nM	58.8 mV/decade (100 nM ~ 10 mM)	Potentiometry	Paste mixture of graphite powder, MWCNT, Fe-CO-TNT, βCD ionophore, NaTPB anionic additive, DBP plasticizer	Carbon paste electrode	Syringe	No interference observed with K^{+}, Na^{+}, Ca^{2+}, Mg^{2+}, Cd^{2+}, Co^{2+}, Mn^{2+}, Fe^{2+}	[226]
SWCNT	βCD	Covalent	Bisphenol A	1.0 nM	1.3mA/mM 11nM – 19µM	Cyclic voltammetry	Drop casting	Glassy carbon electrode	Glassy carbon	No interference study, but tested on real plastic samples	[229]
MWCNT	βCD	Covalent	Bisphenol A	14 nM	7.2 µA/µM (125 nM ~ 2 µM) 2.2 µA/µM (2 µM ~ 30 µM)	Linear sweep voltammetry	Drop casting	Screen printed carbon electrode	Not provided	Selective to APAP, BPA, BPS	[227]

Type of CNT	Functional probe	Functionalization	Analyte	Detection limit	Sensitivity (Detection range)	Transduction method	Deposition method	Electrode material Contact configuration	Substrate	Interference study	Ref.
MWCNT	ZIF-67	Covalent	TBBPA	4.2 nM	21.08 µA/µM (0.01~1.5 µM)	Differential pulse voltammetry, cyclic voltametry	Paste mixture of paraffin oil, AB, and CNTs	Carbon paste electrode	Syringe	TBBME, TBBDE, BPAF, BPA, TCBPA, TBBPS did not show remarkable interference.	[228]

DNT: Dinitrotoluene DNB: Dinitrobenzene NB: Nitrobenzene BoNT: Botulinum neurotoxin rGO: reduced graphene oxide TNT: titanate nanotube E-Lc: E light chain

ZIF-67: Zeolitic imidazole framework-67 βCD: β-cyclodextrin TBBPA: Tetrabromobisphenol A AB: acetylene black DBP: dibutyl phthalate NaTPB: sodium tetraphenylborate

BPA: bisphenol A TBBME: tetrabromobisphenol A-bis(dibromopropyl ether) TCBPA: tetrachlorobisphenol A BPAF: hexa-fluorobisphenol A (BPAF, 98%),

TBBPS: 4,4- sulphonyl-bis-(2,6-dibromophenol) TBBDE: tetrabromobisphenol A diallyl ether BPS: bisphenol S APAP: acetaminophen

2.3.3 Performance comparison & overview

To get an overview on the best device strategy to achieve best performances, Table 19 summarizes the best references for each type of functionalization and transduction for the 15 analytes that are addressed by more than one reference: pH, lead(II), cadmium(II), zinc(II), mercury(II), arsenic(III), copper(II), nitrite, calcium(II), dissolved oxygen, hydrogen peroxide, free chlorine, sulfite, sulfide.

Across all analytes, while electrochemical sensing with MWCNTs is the most frequently reported approach and allows to reach remarkable limit of detection (down to the ppt level), FET and chemistor approaches – which are much less frequently used - may also reach detection limits in the ppt range. In the rare instances where they are tested for the same analyte, FETs may perform as well or better than MWCNT electrodes, while chemistors usually perform worse than both of these. Overall, a more extensive evaluation of FET and chemistors for various analytes would be valuable.

Table 19. Summary of best performances for all analytes addressed by more than one reference. When several transduction types or functionalization strategies are available for a given analyte, the table includes the best performing reference for each type.

Analyte (Add. Analytes)	Type of CNT	Functional probe	Functionalization	Detection limit	Sensitivity (Detection range)	Transduction method	Deposition method	Electrode material Contact configuration	Substrate	Interference study	Ref.
pH	MWCNT	Pristine	Non functionalized	N.P.	63 /pH 18%/pH pH 5~9	Chemistor	Sucked by vacuum force	MWCNT	Filter paper	Not provided	[89]
	SWCNT	**Pristine**	**Non functionalized**	**1 mM**	**7600mV/pH 23%/pH (Dual-gate mode) pH 3~10**	**FET, potentiometry (double gate)**	**Spin coating**	**100 nm Ti contacts for source, drain and top gate**	**p-Si (substrate acting as bottom gate)**	**Not provided**	[33]
	SWCNT	Poly(1-aminoanthracene)	Non covalent	1 µM	FET 19µS/pH 14 %/pH	FET, potentiometry (liquid gate)	Dielectrophoresis (aligned CNTs)	Au contacts, Pt wire (Auxillary), Ag/AgCl electrode (Reference)	Si/SiO_2 (300nm)	Multiplexed detection of Ca^{2+} and Na^{+}	[91]
	MWCNT	**COOH**	**Covalent**	**N.P.**	**17 /pH 23%/pH (Au) pH 4~9**	**Impedance spectroscopy**	**Dip coating**	**Au and Al interdigitated electrodes**	**Kapton®**	**Not provided**	[80]
Pb^{2+}	MWCNT	Pristine	Non functionalized	0.3 ppb	2.2 nA/ppb (210~830 ppb)	Stripping voltammetry	CNT thread	Metal wire and silver conductive epoxy	Glass capillary	-Simultaneous determination of Cd(II), Cu(II), Pb(II) and Zn(II) demonstrated -The presence of Dissolved Oxygen changes the calibration law for Cd(II)	[150]
	MWCNT	**Ionic liquid - dithizone based bucky-gel**	**Covalent**	**0.02 ppt**	**0.024 µA/ppb (0.1ppt~210 ppb)**	**Stripping voltammetry**	**Drop-casting**	**Glassy carbon electrode**	**Glassy carbon**	**-No interference of Cd^{2+} and Cu^{2+} ions with the detection of Pb^{2+} ion.**	[154]

Analyte (Add. Analytes)	Type of CNT	Functional probe	Functionalization	Detection limit	Sensitivity (Detection range)	Transduction method	Deposition method	Electrode material Contact configuration	Substrate	Interference study	Ref.
	MWCNT	Nafion/Bismuth	Non covalent	25 ppt	0.22 µA/ppb (0.05 to 5 ppb) 0.27 µA/ppb (5~100 ppb)	Stripping voltammetry	Drop casting	Glassy carbon electrode	Glassy carbon	500-fold of SCN^-, Cl^-, F^-, PO^{3-}_4, SO_4^{2-}, NO_3^-, and various cations such as Na^+, Ca^{2+}, Mg^{2+}, Al^{3+}, K^+, Zn^{2+}, Co^{2+} and Ni^{2+} had no influences on the signals of Pb(II) and Cd(II).	[153]
	MWCNT	PSS-Bi	Non covalent	0.04 ppb	0.079 µA/ppb (0.5 ~ 90 ppb)	Stripping voltammetry	Drop casting	Glassy carbon electrode	Glassy carbon	- 20-fold amounts of Zn^{2+}, 5-fold amounts of Sn^{2+} and 1-fold amounts of Cu^{2+} have influence on the determination of Cd^{2+} and Pb^{2+} with deviation of 10%.	[164]
Cd^{2+}	MWCNT	Pristine	Non functionalized	0.23 ppb	3.9 nA/ppb (170~500 ppb)	Stripping voltammetry	CNT thread	Metal wire and silver conductive epoxy	Glass capillary	-Simultaneous determination of Cd(II), Cu(II), Pb(II) and Zn(II) demonstrated -The presence of Dissolved Oxygen changes the calibration law for Cd(II)	[150]
	MWCNT	**PSS-Bi**	**Non covalent**	**0.02 ppb**	**0.23 µA/ppb (0.5 ~50 ppb)**	**Stripping voltammetry**	**Drop casting**	**Glassy carbon electrode**	**Glassy carbon**	**- 20-fold amounts of Zn^{2+}, 5-fold amounts of Sn^{2+} and 1-fold amounts of Cu^{2+} have influence on the determination of Cd^{2+} and Pb^{2+} with deviation of 10%.**	[164]
Zn^{2+}	**MWCNT**	**Pristine**	**Non functionalized**	**0.08 ppb**	**3.4 pA/ppb (200~590 ppb)**	**Stripping voltammetry**	**CNT thread**	**Metal wire and silver conductive epoxy**	**Glass capillary**	**Simultaneous determination of Cd(II), Cu(II), Pb(II) and Zn(II) demonstrated The presence of Dissolved Oxygen changes the calibration law for Cd(II)**	[150]
	MWCNT	Bismuth	Non covalent	11 ppb	0.18 µA/ppb (12~18 ppb) 0.24 µA/ppb (20~100 ppb)	Stripping voltammetry	Screen printing	Screen printed MWCNT based electrode	Ceramic substrates	N.P.	[161]
Hg^{2+}	SWCNT	Pristine	Non functionalized	0.6 ppm	12 mV/ ppm (1~30 ppm)	Chemistor	CVD	SWCNT	Glass	1000 fold excess of Fe(II), Fe(III), Ni(II), Cu(II),Zn(II), Cr(III) and 500 folds of As(III), Sb(III), Se(IV) and Pb(II) had no interfering effect in the analysis of mercury solution.	[69]
	SWCNT	Pristine	Non functionalized	2 ppb	0.22/decade 0.2 ppb ~ 201 ppm	FET (Liquid gate)	Dip coating with	Pd/Au (10/30 nm)	Glass	Good selectivity towards interferent ions	[35]

Analyte (Add. Analytes)	Type of CNT	Functional probe	Functionalization	Detection limit	Sensitivity (Detection range)	Transduction method	Deposition method	Electrode material Contact configuration	Substrate	Interference study	Ref.
							selective CNT placement				
	SWCNT	Thiophenol	Covalent	0.6 ppb	0.14 µA/ppb (1 ~18 ppb)	Stripping voltammetry	Dip coating	Au	Au	The presence of 100-fold concentration of Cr(II), Mn(II), Co(II), Ni(II), Zn(II), 50-fold concentration of Fe(II),and 20-fold Cu(II), have no influence on the signals of 50 nM Hg(II) with deviation below 5%.	[172]
	MWCNT	**PANi-Bi NPs@GO**	**Non covalent**	**2 ppt**	**1.3 µA/ppb (2 ppt ~ 1000 ppm)**	**Differential pulse voltammetry**	**Screen printing**	**(commercial) Carbon ink**	**PET**	**Not provided**	[173]
As^{3+}	MWCNT	COOH	Covalent	N.A	0.24 µA/ppb (0.3~50 ppb)	Stripping voltammetry	Dip coating	Au	Au electrode	- Interference was significant when the Sb/As ratio is higher than 1.	[177]
	MWCNT	**Au-NP**	**Non covalent**	**0.1 ppb**	**26 µA/ppb (75 ppt - 5.3 ppm)**	**Stripping voltammetry**	**Drop casting**	**Glassy carbon**	**Glassy carbon**	**Not provided**	[180]
Cu^{2+}	**SWCNT**	**PANI-GGHH**	**Non covalent**	**3 ppt**	**N/A (3 ~ 29 ppt)**	**FET (liquid gate)**	**CVD**	**300 nm Au**	**Si/SiO2 (120nm)**	**-His_6 shows higher chelation power for Ni^{2+} than to Cu^{2+}.**	[70]
	MWCNT	$C_{24}H_{30}N_6$ Schiff base	Non covalent	10 ppt	N/A (0.09~340 ppb)	Stripping voltammetry	Paste of MWCNT, Schiff base and mineral oil	Copper wire	Filter membrane	Not provided	[183]
	MWCNT	Pristine	Non functionalized	17 ppt	9.4 pA/ppb (32~220 ppb)	Stripping voltammetry	CNT thread aspirated into a glass capillary	Metal wire and silver conductive epoxy	Glass capillary	-Simultaneous determination of Cd(II), Cu(II), Pb(II) and Zn(II) demonstrated -The presence of Dissolved Oxygen changes the calibration law for Cd(II)	[150]
Nitrite	**MWCNT**	**Co_3O_4-rGO**	**Non covalent**	**0.016 μM**	**0.408 μA/μM/ cm^2 (0.1 ~ 8000 µM)**	**Voltammetry**	**Drop casting**	**Glassy carbon electrode**	**Glassy carbon**	**100-fold of alcohol, Na^+, K^+, Cl^-, NO_3^-, N_2H_4, SO_3^{2-},SO_4^{2-}, has no effect on sensor response.**	[189]
Ca^{2+}	**SWCNT**	**Fluo-4 AM**	**Non-covalent**	**100 pM**	**69 nA/decade**	**FET**	**Dip coating**	**Ti (10nm)/Au**	**Glass**	**-FET at the end of a nanoneedle for intracell**	[201]

Analyte (Add. Analytes)	Type of CNT	Functional probe	Functionalization	Detection limit	Sensitivity (Detection range)	Transduction method	Deposition method	Electrode material Contact configuration	Substrate	Interference study	Ref.
					(100 nM ~ 1 mM)			**(30nm) (liquid, floating gate)**	**(borosilicate glass capillary)**	**monitoring**	
	MWCNT	PDMS	Non-covalent	25 µM	N/A (25 µM ~ 5 mM (Not linear))	Capacitive measurement	Mold injection and thermal curing	MWCNT	PDMS	Measured at 2.4kHz frequency	[202]
O_2	**MWCNT**	**Au NP**	**Non-covalent**	**0.1 ppm**	**N/A (0~ 50 ppm)**	**Cyclic voltammetry**	**Not provided**	**Glassy carbon electrode**	**Glassy carbon**	**Not provided**	[209]
Hydrogen peroxide	**MWCNT**	**nitrogen doped Co-CNTs over graphene sheets**	**Non covalent**	**100nM 3.4ppb**	**-0.85µA/ppm**	**Voltammetry, amperometry**	**Coating**	**Glassy carbon electrode**	**Glassy carbon electrode**	**No interference with uric acid, ascorbic acid and glucose**	[211]
	SWCNT	Phenyl capped aniline tetramer	Non covalent	<3ppm	1%/ppm (3ppm ~ 8 ppm) Nonlinear <1%/100ppm (48ppm ~ 1200 ppm)	Chemistor	Drop casting	Carbon ink	Glass	Not provided	[217]
Free chlorine	**MWCNT**	**Pristine**	**Non functionalized**	**<5ppb (ClO^-)**	**Logarithmic 39% /decade* (0.03~8 ppm)**	**Chemistor**	**Dielectrophoresis (aligned MWCNT)**	**Cr/Au**	**Glass**	**No information about selectivity, pH information not provided**	[215]
	MWCNT	**Epoxy EpoTek H77A**	**Non covalent**	**20 ppb (HClO)**	**0.15 µA/ppb (0.02~4 ppm)**	**Voltammetry**	**Paste poured into tube and thermally cured**	**Epoxy /MWCNT composite**	**Not provided (tube)**	**Validated in real water matrices (tap water and swimming pool)**	[218]

Analyte (Add. Analytes)	Type of CNT	Functional probe	Functionalization	Detection limit	Sensitivity (Detection range)	Transduction method	Deposition method	Electrode material Contact configuration	Substrate	Interference study	Ref.
	SWCNT	Phenyl capped aniline tetramer	Covalent	<60ppb	92 nA/decade (0.06~60 ppm (linear up to 6ppm))	Chemistor	Drop casting	Au	Glass	Non selective to different oxidants – list of oxidants not provided Regeneration possible	[79]
Sulfite	**MWCNT**	**Ferrocene**	**Non covalent (Physical immobilization)**	**0.1 µM**	**3.3 µA/µM (0.4 μM ~ 4 µM) 0.18 µA/µM (4 µM ~ 120 μM)**	**Differential Pulse Voltammetry**	**Paste mixture with graphite powder blended with paraffin oil**	**MWCNT paste, Copper wire**	**Glass tube**	**Not provided**	[120]
Sulfide	**MWCNT**	**Hematoxylin**	**Non covalent**	**0.2 µM**	**103 nA/ µM (0.5 µM ~ 150 µM)**	**Amperometry**	**Paste mixture of MWCNT, mineral oil and graphite powder**	**Carbon paste**	**Teflon tube**	**No interference with Sn2+, Co2+, Pb2+, Zn2+, Cu2+, Ni2+, Mn2+, Fe2+ and Fe3+**	[221]
	MWCNT	Pristine	Not functionalized	0.3 µM (CVD), 12.5 µM (ARC)	0.12 µA/µM (1.3 µM ~ 113 µM) (CVD), 0.005 µA/µM (12.5 µM ~ 87.5 µM) (ARC)	Hydrodynamic voltammetry	Drop casting	Glassy carbon electrode	Glassy carbon	Not provided	[222]
Bisphenol A	**SWCNT**	**βCD**	**Covalent**	**1.0 nM**	**1.3mA/mM 11nM – 19µM**	**Cyclic voltammetry**	**Drop casting**	**Glassy carbon electrode**	**Glassy carbon**	**No interference study, but tested on real plastic samples**	[229]

2.3.3.1 Discussion on transduction mode

There are five analytes for which different transduction modes may be compared: pH, Hg^{2+}, Cu^{2+}, Ca^{2+}, H_2O_2:

- for pH, FET and impedance spectroscopy reach the same performance, and are only slightly better than chemistor.
- for Cu^{2+}, the LOD achieved with FET is three times better than voltammetry
- for Hg^{2+}, the LOD achieved with voltammetry is three orders of magnitude better than with FET, the latter being two orders of magnitude better than with chemistor
- for H_2O_2, the LOD achieved with voltammetry is three orders of magnitude better than with chemistor
- for Ca^{2+}, the LOD achieved with FET is five orders of magnitude better than capacitive measurement (which can be seen as a derivative of impedance spectroscopy)

While electrochemical measurements have been more widely used than FET-based approaches (probably due to easier manufacturing), the latter reach comparable or even widely improved performances for 3 out of 4 analytes. Testing FET architectures on a wider range of analytes would thus be valuable, as FETs are expected to be easier to operate than electrochemical sensors in field conditions.

Regarding chemistors, they feature larger limits of detection than the two other types, but the comparison is only possible on 3 analytes (out of 15). Moreover, for 2 out of 3 of these analytes (pH and H_2O_2), the detection limits are still acceptable for the drink water application. Finally, for several analytes (Co^{2+} and Trinitrotoluene), ppt level detection limits are possible with chemistors. Considering chemistors are easier to fabricate then FET and to operate than electrochemical sensors, their extensive testing against other types of analytes would be useful as well.

2.3.3.2 Discussion on functionalization strategies

First, the comparison of limits of detection between functionalized and non-functionalized or COOH-functionalized CNTs is possible for 9 analytes out of 15. For lead(II), cadmium(II), mercury(II), arsenic(III), copper(II), the use of functionalization improves significantly (often by more than one order of magnitude) the limit of detection. Non-functionalized or COOH-functionalized CNT provide best (pH, free chlorine and Zinc(II)) or close to best (sulfide) performances for certain analytes (4 out 15).

This suggests the interest to systematically assess the performances of non-functionalized CNTs against functional ones (within the same device architecture), as they may be very sensitive. Moreover, while the literature often claims that pristine or COOH-CNTs do not have selectivity, one observes here that non-functionalized CNT sensors with excellent limit of detections may operate free from interferents as well [35], [69], [150] .

One may wonder whether the overall remarkably good performances of non-functionalized CNTs could be explained by an “effective” functionalization during the fabrication process. To clarify, CNT deposited by wet or paste process are dispersed in solvents or mixture whose molecules may remain (intentionally or not) on the CNTs sidewalls at the end of the process. Similarly, CNT synthesized in place by CVD may still carry leftover catalysts particles. The role of these by-products of fabrication is not addressed in the papers. A systematic study of the role of solvents and catalysts in the sensitivity to analytes in water could be valuable.

There are limited opportunities (5 analytes out of 15) to compare between covalent and non-covalent functionalization of CNTs, as non-covalent functionalization is featured in a large majority of references. However, for pH, free chlorine, Cu(II), Hg(II) and Pb(II), covalent and non-covalent functionalization strategies are both reported. Except for Pb(II), non-covalent functionalization provides better performance than covalent functionalization. However, this conclusion should be tampered by the fact that it is never the same active compound being tested by both covalent or non-covalent functionalization. For instance, in the case of lead(II) and cadmium(II), Bismuth is tested as an active compound of a lot of different functional probes, but all non-covalently functionalized. It would be very interesting to compare these results to a covalent functionalization strategy for Bismuth or a Bismuth derivative.

Going more specifically into the choice of functional probes, one can inventory in this review functional probes covering a wide range of size scale and featuring different levels of complexity. The literature includes primarily a large number of single-component functional probes, from monoatomic doping up to small molecules, then up to macromolecules and nanoparticles and finally up to polymer level.

Beyond these, composite probes composed of several functional building blocks are becoming very popular. Two-component strategies are fairly standardized now: a primary functional probe such as a polymer or a macromolecule is itself functionalized by a secondary probe (for instance PSS-Bismuth in [164]). Three (or more)-component

strategies are also appearing. For instance, in [173] PANI is functionalized with Bismuth, and the resulting two-component functional probe is used to functionalized graphene oxide sheets. As has been detailed in the previous sections, multi-component functional probes are thought to enhance the 3D structuration of the CNT layer, hence its adsorption capability and thus its sensitivity. It is worth mentioning than these three-component structures often include flagship bidimensional materials such as graphene oxide and graphene.

These observations are confirmed in Table 19 : Among the 12 analytes (and 12 references) where the best performance is achieved through functionalization, half of these are achieved through a multi-component strategy (4 papers on bi-component probes, 2 papers on 3-component probes). Moreover, 3 papers out of 12 includes graphene or graphene oxide and 3 papers out of 12 include a polymer (PANI or PSS) functionalized by a secondary probe.

2.4 Conclusion

Overall, there are so many parameters featuring in the design and operation of CNT based water quality sensors that a systematic comparison across all of these is not possible with the current extent of the literature. However, analyte by analyte, some key conclusions can be drawn regarding the best transduction mode and functional probe. To summarize, Figure 14 shows the general overview and comparison of 90 references based on CNT-based chemical sensors for water quality monitoring. A total of 20 analytes is covered, the most frequently investigated ones being H^+ (pH) and lead (with 18% of references each), then cadmium (14%) and nitrite (11%). Altogether, micronutrients and toxic metals cover 40% of all references.

Electrochemical sensors (73%) have been more investigated than chemistors (14%) or FETs (12%). Across all analytes, while electrochemical sensing with MWCNTs is the most frequently reported approach and allows to reach remarkable limit of detection (down to the ppt level), FET and chemistor approaches – which are much less frequently used - may also reach detection limits in the ppt range. In the rare instances where they are tested for the same analyte, FETs may perform as well or better than MWCNT electrodes, while chemistors usually perform worse than both FETs and electrochemical sensors. Overall, a more extensive evaluation of FET and chemistors for various analytes would be valuable.

A large variety of functional probes is reported. They cover the full-size scale from single atomic dopants to polymers and often couple 2 to 3 chemical building blocks. While these probes provide remarkable performances, especially the multi-component ones, there are – surprisingly - several analytes for which non-functionalized or COOH-functionalized CNTs provide better performances (pH, Zn(II), free chlorine). Non-functionalized or COOH-functionalized CNTs sensors are also reported to allow selectivity and to be resilient to interferents. These results suggest to systematically compare in new studies the performances of functionalized and non-functionalized CNTs.

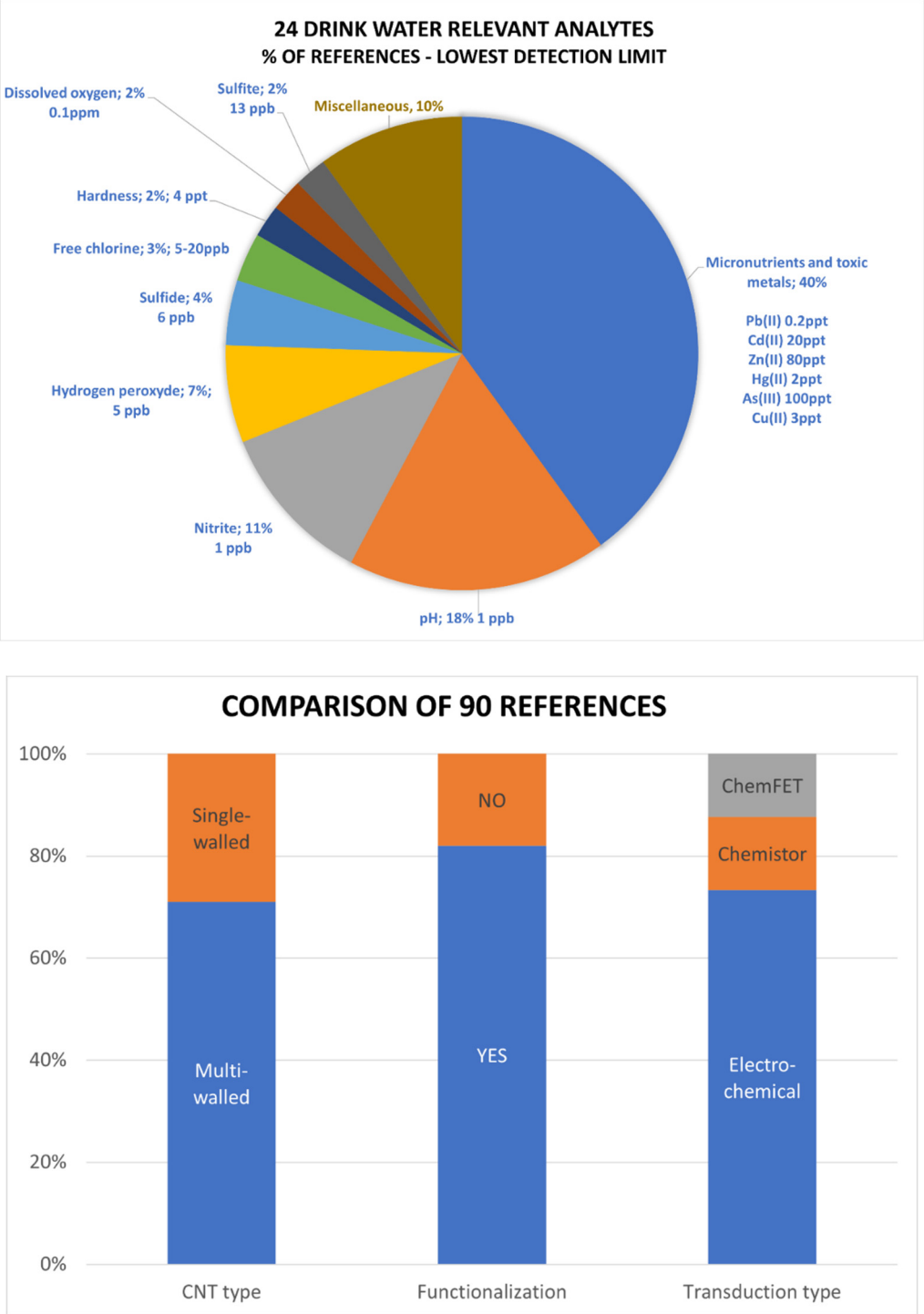

Figure 14. (top) 24 different drinking water-relevant analytes with their proportion and corresponding the lowest limit of detection (LOD) and (bottom) comparison of reported references on CNT-based chemical sensors for water quality monitoring based on their CNT type, functionalization, and transduction methods.

3 CNT-FET

In the previous chapter, we summarized the reported CNT-based chemical sensors in water and compared their sensing performances by CNT type, transduction methods, functionalization, type of analyte, detection range, LOD and selectivity. From the overview, while electrochemical measurements have been more widely used than FET-based approaches (probably due to easier manufacturing), the latter ones reach comparable or even improved performances for 3 out of the 4 analytes for which comparison is possible. Testing FET architectures on a wider range of analytes would thus be valuable, as FETs are expected to be easier to operate than electrochemical sensors in field conditions. For this reason, we focus in this thesis on CNT-FET as water quality sensors.

In the following section, we introduce CNT-FETs in more details, focusing on their operation as electronic devices. We discuss the CNT-FETs at general level first, then by comparison of the position of gate electrode, of the channel length and of the current injection methods. We also briefly discuss available modelling approaches for each type of CNT-FETs.

3.1 CNT-FET: General concept

Carbon nanotube field-effect transistors (CNT-FETs) were originally introduced as an alternative to the conventional silicon-based metal-oxide-semiconductor FETs (MOSFETs). They rely on using semiconducting CNTs instead of silicon as the channel of the transistor. This approach was motivated by the extraordinary electrical properties of CNTs, such as their high electrical conductivity up to 10^7 S/m and their tunable bandgap enabled by chirality control. As a semiconducting channel is required, only SWCNTs may be used, not MWCNTs. Therefore, we only focus on SWCNTs in this chapter. As described in the section 2.1.5, to fabricate CNT-FETs, CNT can be directly grown on the substrate between source and drain by a CVD method or can be deposited by a drop-casting, spray method or ink-jet printing of CNT dispersions.

In general, CNT-FET can be classified according to the following criteria: electrode geometry, CNT morphology, length of channel, current injection methods, carrier transport mode (ballistic or diffusive). Details are provided in the following sections.

3.2 Introduction to CNT-FET design

3.2.1 Electrode geometry

We introduced that there are four main types of device architecture for CNT-FET chemical sensors in section 2.2.3.2: bottom-gated, top-gated and, liquid-gated (also called electrolyte-gated – only suitable for use in electrically conducting environment) and hybrid structures (Figure 10). In this chapter, we detail bottom-gated and top-gated structures further, without limiting the discussion to only chemFET. To be noted, in case of hybrid structures, details were provided in section 2.2.3.2, hence are not repeated here.

3.2.1.1 Bottom-gated CNT-FET

Bottom-gated CNT-FETs have the simplest structure: the gate is embedded below the semiconducting layer with a separating dielectric layer of often considerable thickness (~100 nm or more). It has the drawback of requiring high gate voltage (usually several tens of Volts, due to the large contact resistance) for good electrical performances and for switching the devices on. In addition, use of the substrate as a gate implies that all devices are turned on simultaneously, precluding operation of all but the most basic electronic circuits.

Low gate voltage operation can be achieved by using very thin (~ 5 nm) dielectric layer with individual field-effect transistor gating, but it has a risk of leakage current in the off-state. Recently, Bachtold *et al.* [232] reported an improved bottom-gate structure with individual field-effect transistor gating. Those devices showed low gate voltage operation and featured the ability to switch on and off separately. Electrical performances (Ion, transconductance, subthreshold slope) can also be improved by reducing the contact resistance between the CNT and metal electrodes. The contact resistance, R_c, is the resistance between metal electrodes (Source and drain) and CNTs. Its magnitude is of the order of 1 MΩ per tube for conventional CNT-FET structure with deposition of CNTs on the substrate (Figure 15 (a)), and 10 ~100 kΩ per tube in case of the complicated structure with a CNT laying between electrodes and dielectric layer (Figure 15 (b)).

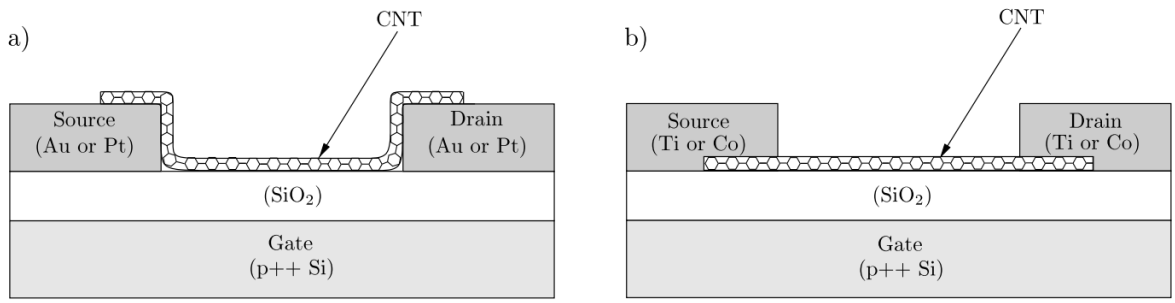

Figure 15. (a) Schematic of conventional CNT-FET structure with CNT laying on top of the metal electrodes (b) Improved CNT-FET structure with metal electrodes deposited upon the CNT, followed by annealing process to improve contact. Reproduced from [233]

The bottom-gated structures used in most previously published CNT-FET studies on sensors or digital circuits [33], [91], [234], have an open geometry, in which the CNT is exposed to air or in water. It is convenient for sensing applications, but presents an electrostatic disadvantage in that the gate insulator capacitance is smaller than that of other CNT-FETs by the lower dielectric constant and larger thickness of the insulating layer in order to prevent degradation from oxygen and water surrounding the CNT. Bottom-gated CNT-FETs generally show p-type behavior (hole conduction) due to the exposure of CNT to air or in water. Tuning their electrical properties (Threshold voltage

control, choice of p- or n-type behavior) requires doping or functionalization of CNTs [232].

3.2.1.2 Top-gated CNT-FET

In top-gated structures, the gate layer is located on top of the semiconducting channel. Therefore, CNTs are completely embedded within the gate insulator, offering notably higher subthreshold slope, higher transconductance and low hysteresis compared to bottom gate CNT-FETs [235]. These structures require lower operating gate voltage due to their lower contact resistance (10 to 100 kΩ). However, they are relatively little used for sensing application because the top gate isolates the sensitive channel from the environment.

Contrary to bottom-gated CNT-FETs, top-gated CNT-FETs are relatively easily tunable by additional processes. Derycke *et al.* reported that thermal treatment in an inert atmosphere can modify the metal–nanotube interface at the contacts, which leads to the *n*-type behavior of top-gated CNT-FETs [236].

An additional advantage of the top-gated structure is that with only slight modification, it can be made suitable for high-frequency operation, which is not possible with bottom-gated devices due to the large overlap capacitance between the gate, source, and drain.

3.2.2 CNTFET using single CNT, random network of CNT and partially aligned CNT

CNTFETs can also be classified into single CNT-based CNT-FETs (in short, single CNT-FET) and random network-based CNTFETs depending on the number of CNTs between source and drain electrodes.

3.2.2.1 Single CNT-FET

CNTFET can be formed out of a single semiconducting CNT between source and drain electrode. The distance between the source and drain (i.e. channel length) can be extremely short (~ 100 nm) or relatively longer (~ 1 μm). However, the channel length cannot be longer than the length of an individual CNT.

CNTFET based on single SWCNT have remarkable electrical performances [20] as individual SWCNTs have the ability to carry extremely high current density; their high aspect ratio with small radius can enhance an external electric field [237]. Moreover, electrical properties of single CNT-FETs are rather well predicted by modeling since the relationships between electronic properties of a single SWCNT and its morphological properties (length, diameter, chirality, defect density) can be derived.

However, the electrical and sensing performances of the device completely depend on the unique characteristics of each individual CNT, which always vary within a batch of CNT. As a result, one observes strong device-to-device variations in performances [238].

Moreover, single-CNT-based CNTFETs have the drawback of a complicated process: only a single semiconducting CNT should be positioned between source and drain electrodes, any overlap with other CNTs should be avoided. A frequently used process consists in placing a single CNT on pre-patterned electrodes [239], [240].

3.2.2.2 Random network CNT-FET

By contrast, carbon nanotubes can be randomly deposited or synthesized between source and drain and form a semi-conducting percolating network. Figure 16 shows a basic structure of the CNT-FET with a randomly percolated CNT network.

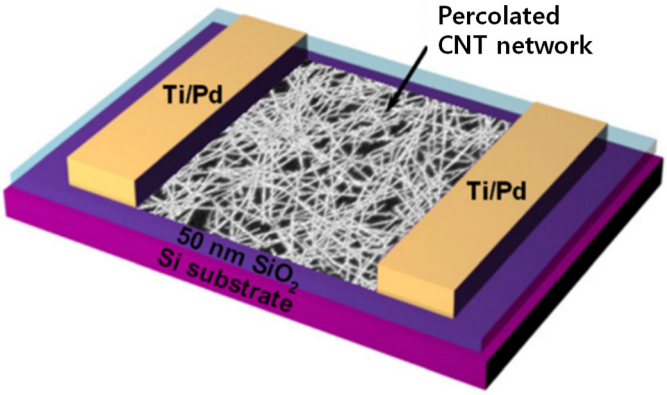

Figure 16. Basic structure of a CNT-FET with randomly percolated CNT network. Image taken from [241].

A percolating CNT network containing both semiconducting AND metallic CNTs may still behave as a semiconductor if there is no metallic path which short-circuit the device; this is possible for low density percolating network, that is, network close to the percolation threshold [242]–[244].

CNT networks for CNTFETs do not have to be random, they can be fully or partially aligned. This can be achieved by dielectrophoresis, between source and drain electrodes. Single CNTs [92] or bundles of CNTs [93] can be aligned by this process, which is discussed in section 2.1.5.

While there are usually easier to manufacture than single CNT-FET, electrical properties (I_{on}/I_{off} ratio, notably I_{off}) of random network CNT-FETs are generally worse, either because of the presence of some metallic (or almost metallic) paths or because of the effects of contacts along the semi-conducting paths.

The maximum current outputs is however larger due to the large numbers of SWCNTs. They have also higher effective sensing area. They also are more repeatable between devices because the network averages the properties of individual CNTs. Hence, they are more often used for sensing applications.

3.2.3 Short and long channel CNT-FET

CNT-FETs also can be sorted into two different groups according to the length of the semiconducting channel: short-channel CNTFET and long-channel CNTFET. Length of channel is tightly related to the transport mode for charge carrier: ballistic or diffusive.

3.2.3.1 Ballistic versus diffusive carrier transport

When the energy-carrying particles move inside a medium, the particles are scattered by impurities, defects or thermal fluctuations of ions. However, the particles can travel a certain distance without collision, thus conserving their momentum. This average distance is called mean free path. The mean free path can be increased by reducing the number of impurities in a crystal or by lowering the temperature in a system.

Ballistic transport describes operation of an electronic device where charge carriers are not (or negligibly) scattered over the length *L* of the device. In other words, the mean free path of the particles is (much) longer than the dimension of the medium. By contrast, diffusive transport is observed if the device size is longer than the mean free path of the particle. In this situation, carrier transport is dominantly determined by the scattering in the medium.

3.2.3.2 Short channel CNT-FET

Short channel CNT-FET is a type of CNT field-effect transistor with an extremely narrow channel length up to 1 µm. This type of CNT-FET generally operates in ballistic transport condition due to the channel length being shorter than the electron mean free path of CNTs (~ 1 µm) at room temperature [245], [246]. Figure 17 shows the basic structure of short channel CNT-FET.

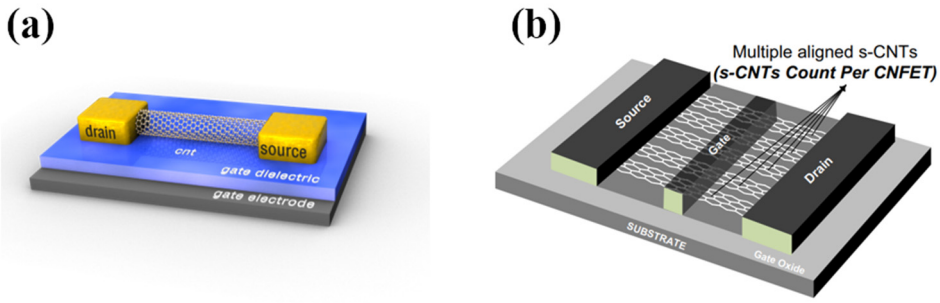

Figure 17. Schematic of short channel CNT-FET with (a) single SWCNT and (b) multiple aligned SWCNTs. Image taken from [234].

To fabricate a short channel CNT-FET, only semiconducting nanotubes should be deposited between metal electrodes since even a single metallic nanotube between source and drain would short-circuit the rest of the semiconducting CNTs. In case of unsorted SWCNTs (containing both metallic CNTs and semiconducting

CNTs) with low concentration, metallic CNTs can be selectively removed by a so-called breakdown process, which will be discussed in the next section. Short channel CNT-FETs may have very high on/off ratio up to ~10^7, which is higher than conventional MOSFETs. One of the drawbacks of short channel CNT-FETs is that they require very precise fabrication process to achieve a short channel [247]. They also have the generic drawbacks of single CNT FET.

Most devices are made out of single CNT, though it is possible to have devices made out of assemblies of CNTs, as long as each CNT connects both source and drain electrodes. In general, this is achieved by aligning CNTs. It can be down by directly growing them on quartz substrates (Figure 18) [248]–[250] or by dielectrophoresis [251]. The advantages of having multiple CNTs in parallel is to reduce contact resistance and increase On-current (I_{on}), device mobility [252] and device-to-device repeatability.

Franklin *et al.* (2010 [253]) introduced multiple-aligned CNT-FETs with a local-bottom-gate (LBG) configuration with high current density (more than 40 μA/ μm) and subthreshold slope of 70 mV/decade with very high on/off ratio of 10^5.

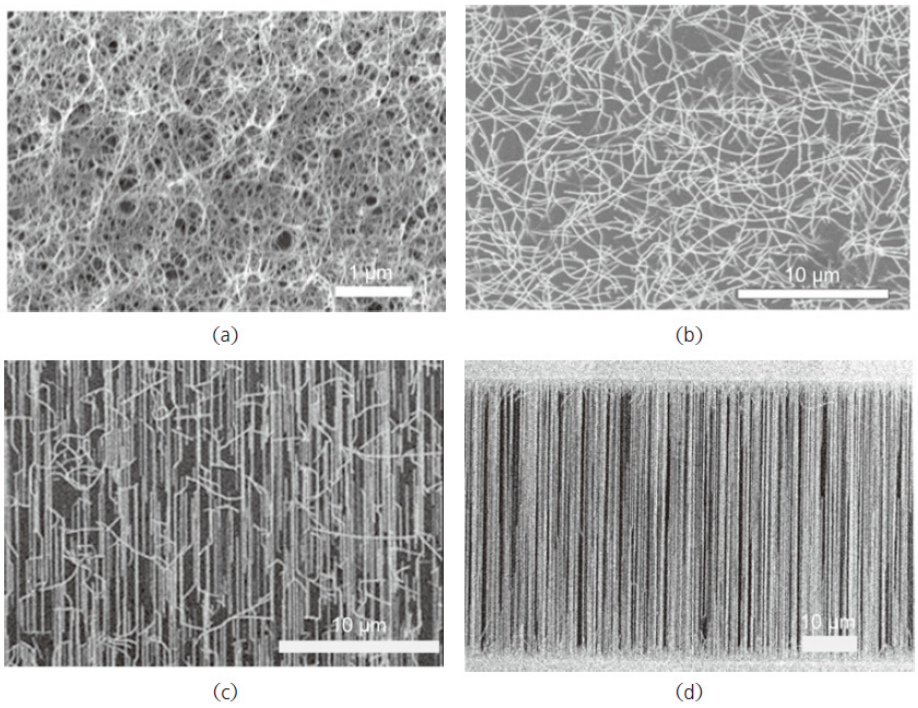

Figure 18. Scanning electron microscope (SEM) images of (a), (b) randomly grown SWCNTs by CVD method (c) partially aligned SWCNT grown on a single-crystalline quartz substrate (d) perfectly aligned SWCNT arrays grown with Fe catalysts on a quartz substrate. Image copyright [254].

3.2.3.3 Long channel CNT-FET

Long channel CNT-FET is a CNTET with a relatively longer channel distance (Longer than 1 µm). This type of CNT-FETs generally operates in diffusive transport condition since the channel length is longer than the mean free path of electrons in CNTs. Diffusive transport effect causes the on-current to decrease, due to increased scattering happening in the device compared to short channel CNT-FETs [255]. There has been reports of single CNT FET with long channel distance and thus operating in diffusive regime [256], but in general, long channel CNTFETs use randomly or quasi-randomly CNT network.

3.2.4 Electrical breakdown

In the previous sections, we mentioned that any metallic path between source and drain of the transistors can short-circuit the device and degrade the performance of the transistor. This is a significant issue because when unsorted (or imperfectly sorted) SWCNTs are deposited, the resulting CNT network is a random assembly of both metallic and semiconducting nanotubes. In-place grown SWCNT network also contain metallic SWCNT, as chirality control methods still yield some dispersion in chirality.

Since the presence of metallic SWCNTs is a major obstacle to achieve high performance transistors, many researchers have suggested the post-growth/deposition removal of metallic SWCNTs from substrates [73], [97], [257]–[261], among which the most widespread is electrical breakdown. A strong current is applied to the network. Semiconducting SWCNTs are placed in their OFF-regime by gate voltage control [97] so remain current-free. By contrast, the current keeps flowing through the metallic SWCNTs which have no OFF-state. They are thus destroyed by intense Joule heating. This method easily leads to a high I_{on}/I_{off} ratio for CNT-FETs by removing metallic percolating paths (Figure 19). It is worth mentioning that the burning of metallic CNTs paths may damage neighboring semi-conducting ones, especially with higher CNTs densities.

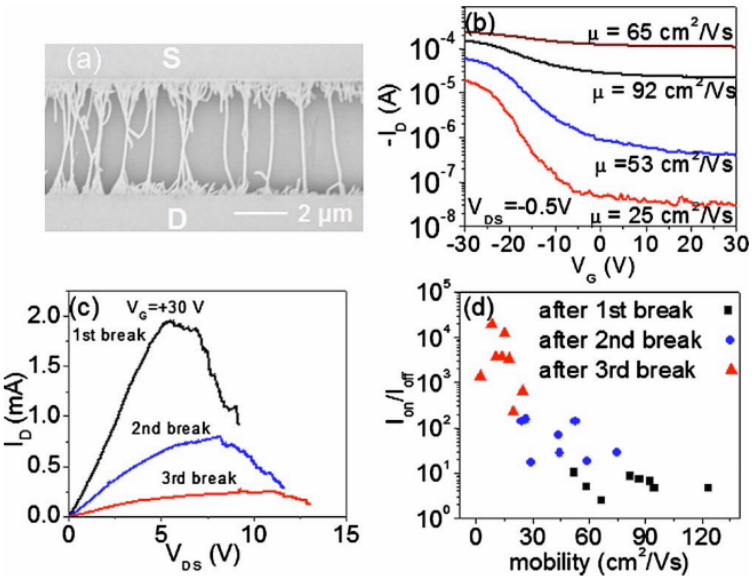

Figure 19. (a) SEM image of part of an aligned SWCNT device. (b) ID vs back gate voltage VG at constant V_{ds} of - 0.5 V after successive steps of electrical breakdown. (c) A representative plot of drain current (I_{ds}) vs source-drain voltage (V_{ds}) for three sequential breakdowns (first, second, and third break) (d) Plot of on-off ratios and corresponding mobility for several measured devices after each breakdown [92].

3.2.5 Current injection method and operating models for CNT-FET

There are two types of CNT-FETs differing by their current injection methods and the type of contacts between channel and electrodes; Schottky barrier CNT-FET and MOSFET-like CNT-FET [262]. Figure 20 shows a schematic of the two types of CNT-FET. The two following sections describe their operating models in the case of single CNT FET, while the third expands the conclusions to discuss the case of network of CNTs.

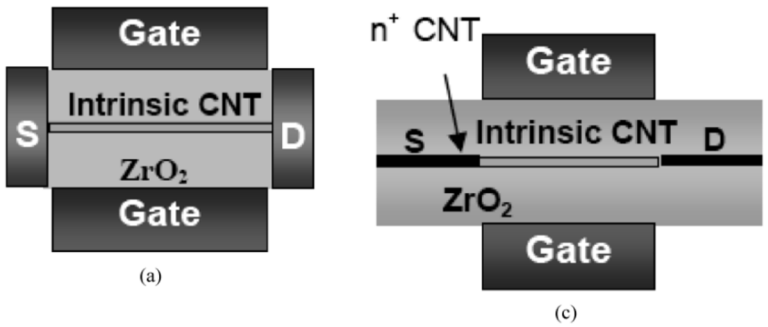

Figure 20. Two types of CNT-FETs. (left) A physical diagram of a Schottky barrier CNT-FET. (right) A physical diagram of a MOSFET-like CNT-FET. Image copyright from [262].

3.2.5.1 Schottky barrier CNT-FET

A Schottky barrier is a potential barrier created at the interface between a metal and a semiconductor. A Schottky barrier CNT-FET has Schottky contacts between semiconducting CNT channel and metallic electrodes [263]–[267]. A Schottky barrier CNT-FET relies on direct tunneling through the Schottky barrier formed at the source-channel junction [268]. Schottky barrier CNT-FETs are advantageous as they can have extremely small dimensions [269]. However, they exhibit strong ambipolar behavior since the Fermi level is at the middle of the bandgap: they have electron conduction at high range of negative gate voltage and hole conduction at high range of positive gate voltage. The gate voltage to reach minimum current defines the Dirac point. In semi-metal or zero-gap semiconductor, for example graphene, the Dirac point is the contact point between conduction and valence bands. Due to their ambipolar behavior, I_{on}/I_{off} ratio of Schottky barrier CNT-FETs is lower than that of MOSFET-like CNT-FETs.

Pourfath *et al.* reported that a double-gate electrode structure can suppress the ambipolar behavior of the

Schottky barrier CNT-FETs by separately controlling the carrier injection at source and drain electrodes [270].

However, if the gate oxide is thin enough, reducing the Schottky barrier height for electrons or holes to zero cannot suppress the ambipolar conduction since the thin oxide layer enables tunneling of carriers through the barrier regardless of its reduced Schottky barrier height, hence the transistor keeps its ambipolar behavior [271]. Hence, thickness of the gate oxide should also be thick enough to avoid the tunneling of carriers since the ambipolar conduction makes device worse due to its high I_{off}.

When the diameter of a CNT is large, its bandgap is smaller than that of small diameter CNTs, which reduces the Schottky barrier at source and drain electrodes. This enables easier tunneling hence significant ambipolar conduction (which in practice corresponds to a large leakage current). By contrast, large diameter CNT-FETs have high I_{on} due to their lower Schottky barriers [272].

In recent times, CNT-FETs with zero or slightly negative Schottky barriers have been developed by using an intrinsic CNT channel in contact with metals with high work function, which reduces the threshold voltage of devices [7].

Many researchers have studied the theoretical model of Schottky barrier CNT-FET [267], [273]. The drain current of Schottky barrier CNT-FET in ballistic regime can be expressed as

$$I_D = \frac{4ek_B}{h} \sum_{p=1}^{nb-sbbd} \left[\ln\left[1 + exp\frac{eV_s + \Phi_{SB}^{eff} - sbbd[p]}{k_B T}\right] - \ln\left[1 + exp\frac{eV_D + \Phi_{SB}^{eff} - sbbd[p]}{k_B T}\right]\right]$$

where

$$k_B = Boltzmann\ constant, h = Planck's\ constant, V_s = source\ voltage, V_D = drain\ voltage,$$
$$\Phi_{SB}^{eff} = effective\ Schottky\ barrier\ height, sbbd[p] = subband\ energy$$

Najari *et al.* demonstrated an equivalent circuit model for of Schottky barrier CNT-FETs [273] (Figure 21). They validated it on the current values found via Monte Carlo simulation by Nguyen *et al.* [274] and via experimental data (fabricated Schottky barrier CNT-FET with a single CNT with a diameter of 1.1 nm and a chirality of (14, 0)).

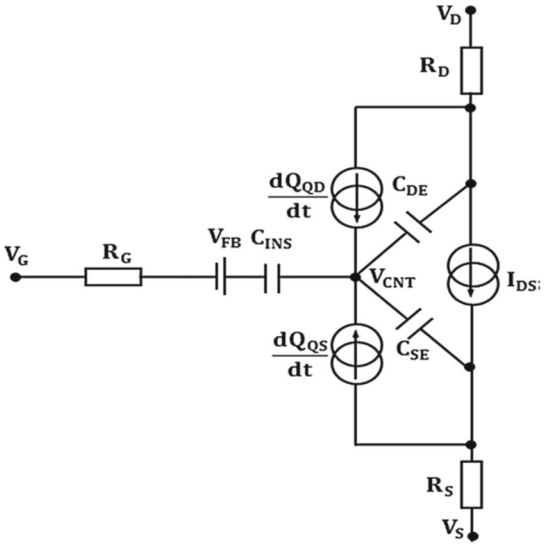

Figure 21. Schematic of the equivalent model of Schottky barrier CNT-FET. C_{INS} is the capacity of the gate oxide (which depends on the geometry and the dielectric constant of the insulator); V_{FB} is the voltage of flat bands, which takes into account the difference between the work function of the metal and the electron affinity of the nanotube; R_G is the access gate resistance; R_S and R_D are the access resistance of source and drain; C_{SE} and C_{DE} are the source and drain electrostatic capacitances. Copyright from [273].

3.2.5.2 MOSFET-like CNT-FET

MOSFET-like CNT-FETs have been widely studied with the prospect that CNT-based semiconducting channel could replace the conventional Si-based MOSFET with better electrical characteristics [275], [276]. A MOSFET-like CNT-FET has the same structure as a Si-based CNT-FET one except that the semiconducting CNT acts as the channel of the transistor. The most significant difference with Schottky barrier CNT-FET is that the MOSFET-like CNT-FETs have ohmic contacts between CNTs and metal electrodes instead of Schottky-barrier-controlled metal-CNT junction. Ohmic contacts are achieved by strong doping of the portion of the CNT in contact with the metallic electrodes. CNTs can be doped by various methods, either electrostatic interactions or chemically bonds [277], [278]. For the latter, notably covalent functionalization via electrochemical modification or fluorination [279] is often used.

Electrochemical modification of CNT is an efficient method for the covalent attachment of organic addends by the grafting of reduced aryl diazonium salts [280]. The electrochemical reaction is carried out in the acetonitrile solution with containing diazonium salt and an electrolyte (tetra-n-butylammonium tetrafluoroborate) at a certain potential of -1.0 V.

Fluorination takes a special place among the functionalization methods since it provides a high surface

concentration of functional groups without destructing the CNT structure [279]. Fluorination of CNT does not necessarily require solvent; it can be achieved by using gas carrying elemental fluorine, such as F_2 gas, CF_4 plasma, BrF_3 or XeF_2 vapor. During this process, a repulsive interaction of fluorine atoms de-bundle the CNTs and improves the CNT dispersion.

In MOSFET-like CNT-FETs, the barrier height is controlled by the (predetermined) doping of the CNT. The energy bands for low and high gate voltages and the potential barrier in the channel are shown in Figure 22. Only an increase of gate voltage turns on the MOSFET-like CNTFETs, because of the lowering of the barrier in the channel [16]. They can thus have unipolar characteristics, and generally have smaller leakage currents than Schottky barrier CNT-FETs.

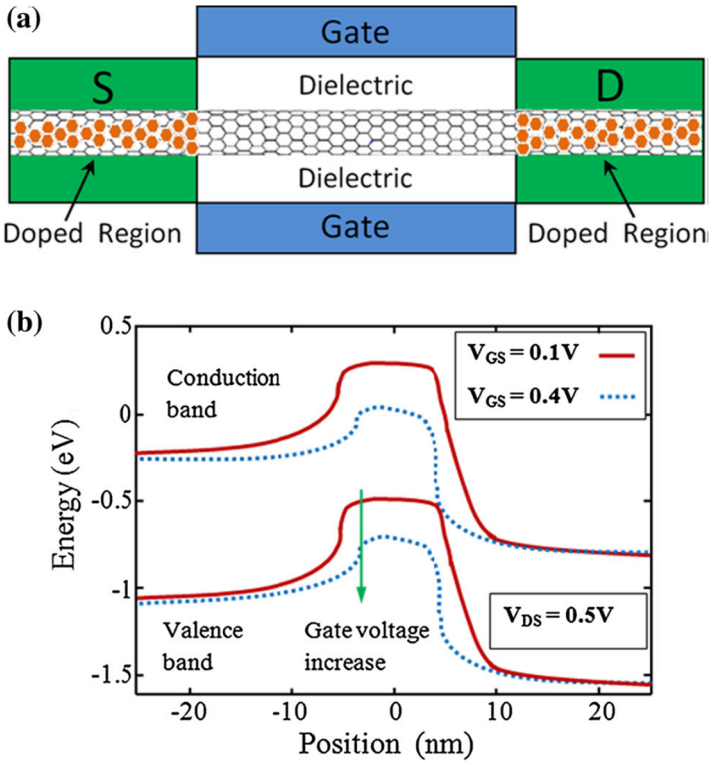

Figure 22. Energy bands for low and high gate voltages and the potential barrier in the channel of MOSFET-like CNTFET.

In [281], the drain current of a ballistic MOSFET-like CNT-FET is expressed as follows:

$$I_D = \frac{4qk_BT}{h}\left[\ln\left(1+exp\left(E_{F1}-U_{scf}\right)\right)-\ln\left(1+exp\left(E_{F2}-U_{scf}\right)\right)\right]$$

where k_B is the Boltzman constant, T is the operating temperature and h is the Plank's constant. The parameters E_{F1} and E_{F2} are the Fermi levels at the location of source and drain. The mobile charge in the CNT is derived from the local density of states at the top of the barrier, which is derived from the self-consistent potential at the top of the barrier, U_{scf}. The latter is derived by iterative (self-consistent) resolution of Poisson

equation in a two-dimensional model of CNT (one axis being the length of the CNT, the other its diameter) according to the compact model in Figure 23. A detailed description of the theoretical analysis procedure is given in Hashim *et al.* [276], who extended work by A. Rahman et al. [281].

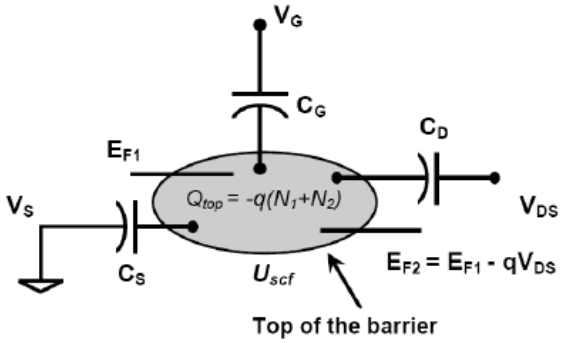

Figure 23. 2D MOSFET-like CNTFET model used for the simulation study in reference [276]

3.2.6 Theoretical approach of random network CNT-FETs

There are only a few theoretical and numerical models of random network CNT-FETs, because of the complexity to model the random morphology of the channel. A frequent approach consists in modeling the random CNT network by positioning each CNT at certain coordinates and accounting for parameters such as position and length of each CNT, and projected angle of CNT between source and drain. The coordinates can be predefined (for instance by an image of a CNT network) or drawn randomly. Some studies focus on modelling the property of a single realization of a random network, while (more frequently) others look into the average properties (Monte Carlo simulation) (Figure 24)

A Spice-based numerical simulation on random network CNT-FETs featuring a mixture of semiconducting and metallic CNTs as a two-dimensional random network channel is proposed in [282]. They choose the certain values of conductivity of on and off state semiconducting CNTs, metallic CNTs and contact resistance between the electrode and a CNT. And then, numerical simulations are performed varying the ratio between metallic and semiconducting CNTs, and the CNT density (CNTs/μm^2) to estimate the yield and characteristics of random network CNT-FETs. They demonstrated from the simulation that shortening the CNT length significantly increases the transistor yield even with high proportion of metallic CNTs (Semiconducting CNTs to metallic CNTs ratio as 3:1).

In [283], another spice-based simulation on random network CNT-FETs considering only the semiconducting CNTs is proposed. They calculate I_{on} and I_{off} with respect to CNT network density and proposed a simulation-based model demonstrating the relationship between average I_{on}/I_{off} ratio and the density of CNT network by using sigmoidal Boltzmann equation,

$$y = \frac{(A_1 - A_2)}{[1 + \exp(x - x_0)/\Delta x]} + A_2$$

where

$$y = percolation\ probability\ of\ CNT\ network, x = network\ density, A_1 = initial\ value\ of\ y$$

$$A_2 = final\ value\ of\ y, x_0 = center\ of\ the\ fuction, \Delta x = width\ of\ the\ function$$

Based on the spice-based simulation, off current linearly increases for all different channel lengths from 2 µm, 6 µm and 10 µm when the CNT network density increases. However, on current significantly decreases as channel length increases based on the simulation. The authors conclude that contact resistance between CNTs is dominant for on current since the number of CNT contacts also increases as channel length increases.

Seppälä *et al.* introduced an electrical transport model of percolating random networks of CNT bundles by estimating the resistance of different CNT bundle segments; (1) Only metallic percolation (2) Only semiconducting percolation (3) Both metallic and semiconducting percolation and (4) Only mixed percolation (Neither metallic nor semiconducting CNTs percolate separately).They demonstrated that CNTs in a bundle segment are more semi-conducting with high-density networks compared to corresponding CNT networks made out of well-isolated CNT by modelling two different scenarios; CNT bundle model and ordinary CNT network model [284].

Jang *et al.* reported on electrical percolation threshold of semiconducting SWCNT networks and electrical properties of CNT-FETs by varying the channel length and the CNT network density [283]. Ishida *et al.* estimated the yield of random network CNT-FETs by calculating the probability of open-circuit, short-circuit and switchable devices with respect to CNT length, channel length and density of unsorted SWCNTs [282].

Furthermore, in [244], Min-kyu *et al.* demonstrated a spice-based simulation of two-dimensional (2D) random network CNT-FET [285].They generated a finite 2D system with channel length and width, and randomly positioned CNTs with certain parameters; angles to the horizontal axis θ, center positions of each CNT (*x, y*) with a fixed CNT length of 1 µm (Figure 24).

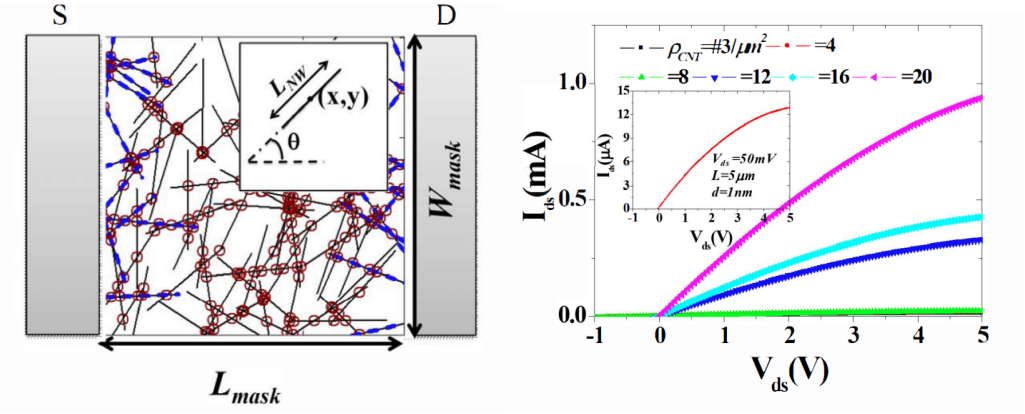

Figure 24. (left) Schematic of 2D random CNT network (right) Spice-simulated output characteristics [285].

3.3 Conclusion

In this chapter, we introduced the general concepts relevant to CNT-FET and compared different types of CNT-FETs according to their gate electrode geometry, their mode of charge transport (ballistic or diffusive), the number of CNTs in the channel (single CNT or assembly), the channel length and the current injection method. We also offer an example of the theoretical model of ballistic Schottky barrier CNT-FETs and MOSFET-like CNT-FETs before detailing the main modelling approaches for random network CNT-FETs.

Despite the remarkable electrical performances of single CNT FET, sensing performance are strongly dependent on the unique characteristics of each individual CNT, which causes sensitivity variation between each CNT FET device. In addition, they have a complicated fabrication process to separate an individual CNT from another and to position the CNT precisely between source and drain electrodes.

Henceforth, although their electrical performances are worse, devices based on random-network of SWCNTs are more often used for sensing applications: they have larger effective sensing area and can be fabricated with solution-based processes enabling mass production with reproducibility and low production cost. In addition, the electrical breakdown method can improve their electrical properties by selectively eliminating the metallic CNTs.

Therefore, in this dissertation, we mainly focus on the fabrication and characterization of random network CNT-FETs.

4 Fabrication & Characterization of CNT-FET

To fabricate a CNT-FET by ink-jet printing process, the transistor with proper scaling process and specific type of material for each layer is essential since a structure of the transistor directly determines the electrical properties of a device. These properties control the drain current modulation by the gate voltage, which affects the power consumption of the device.

In this chapter, we introduce the fabrication and characterization process of CNT-FETs from substrate preparation, ink-jet printing process, post-processing and electrical characterization process.

4.1 Substrate preparation

Our device is fabricated on a conventional silicon wafer. A standard design for CNTFET is selected from the literature and adapted to meet various design and fabrication requirements (see more details below) [137], [286], [287]. After adaptation, the cross section of final CNT-FET design is shown in Figure 25.

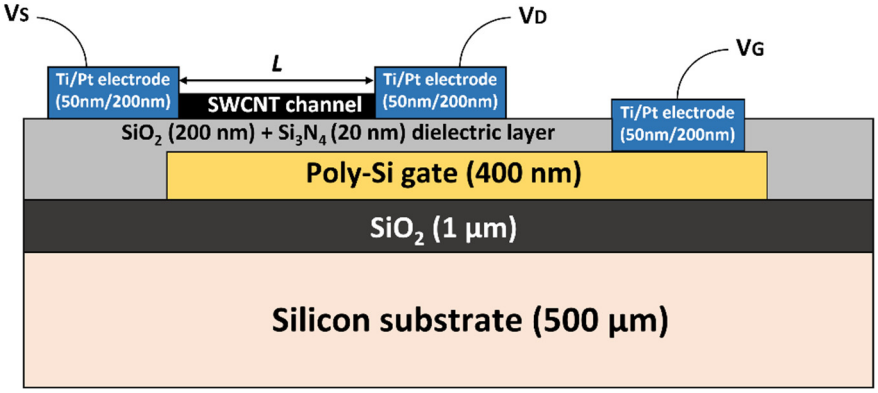

Figure 25. Schematic representation of a CNT-FET device. Vs: Source voltage, Vd: Drain voltage, V_G: Gate voltage, L: Channel length varying from 5 µm to 120 µm.

The fabrication process was proposed by Frédéric Marty, our contact person at ESIEE, the subcontractor cleanroom facility who fabricated the chips based on our design requirements. In turn, our design requirements were fine-tuned for a better technical feasibility at ESIEE (for instance regarding to thickness of SiN layer, thickness of metal electrodes…)

For the CNT-FET structure design, local bottom-gated (Not using the silicon substrate as back-gate) CNTFET structure is selected, as it allows maximum exposure of the CNT to water. As-fabricated chip and electrode design are presented in Figure 26. Each unit chip has 10 mm by 10 mm dimensions and includes 32 CNTFET devices (4 transistors each for 8 different channel lengths. The gate electrodes measure 1250 µm width with varying channel lengths while the source and drain electrodes measure 1100 µm by 250 µm. The spacing between source and drain electrodes defines the channel length, which varies from 5 µm to 120 µm. The

channel width can be controlled by the choice of the SWCNT deposition pattern during ink-jet printing so it is not included as a variable parameter in the layout.

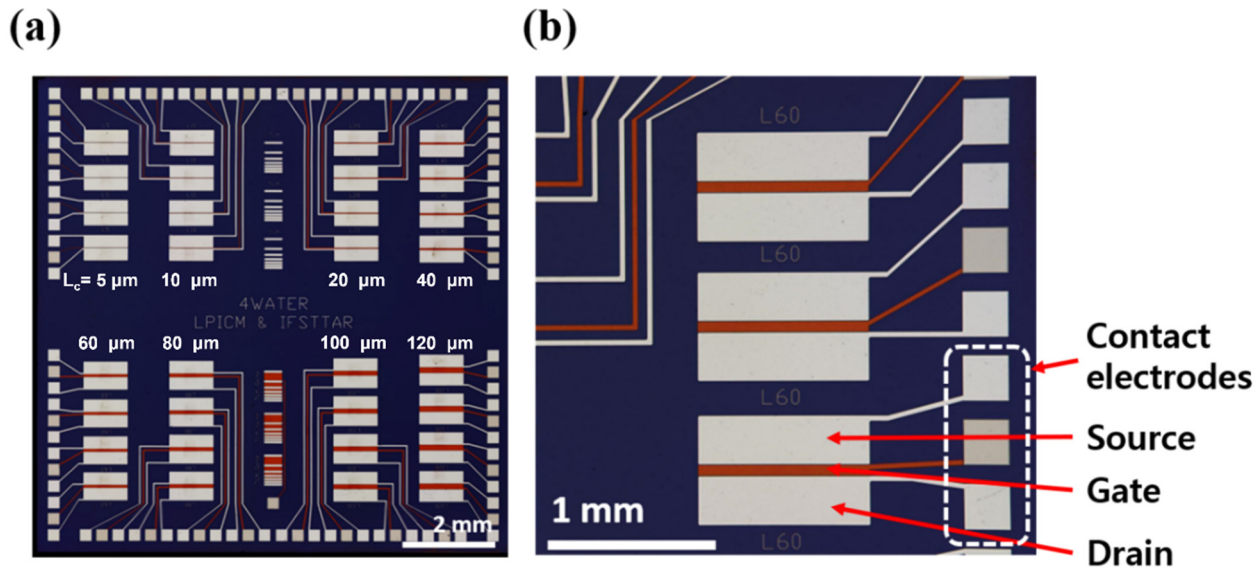

Figure 26. Fabricated chip (10 mm by 10 mm) with gate, source, drain for ink-jet printing process, and contact electrodes for wire-bonding on a printed circuit board (PCB). Channel length varies from 5 µm to 120 µm (From upper left to lower right).

The substrate is a 4-inch undoped silicon wafer with a thickness of 525 μm, which has a resistivity up to 20 Ohm·cm. The wafer is oxidized first to deposit a 1 µm of SiO_2 layer as an insulator. In the design shown in Figure 25, one can observe that there is another unneeded MOS structure in the device: between the poly-Si gate and the undoped silicon substrate. This unnecessary MOS structure may limit the precise operation of CNTFETs since there can be an effective gate voltage felt by the silicon substrate (floating voltage). In addition, there may be un unnecessary charge trapping effect between the SiO_2 layers (200 nm layer and 1 µm layer), which may cause hysteresis (such as what occurs on purpose in flash memory devices [288]). To reduce the voltage drop caused by the charge accumulation between poly-Si gate and silicon substrate, we define the thickness of the insulating layer to be 1 µm, which is much thicker than the dielectric layer between SWCNT channel and poly-Si gate.

Then 400 nm thickness of poly-Si layer is doped by an ion-implantation process with Boron at 40 keV, with a doping concentration of $5 \cdot 10^{15}$ at/cm^2. After another heating process at 1050 ºC for 30 min, the doping concentration increases up to $7 \cdot 10^{19}$ at/cm^2. During the doping process of poly-Si layer, a first mask level is required to pattern the gate electrode by photolithography.

In case of the insulating layer, we choose double insulating layer with Si_3N_4 layer on top of SiO_2 layer. Although silicon nitride is much more difficult to deposit as a thick layer than silicon to yield a thick a silicon

dioxide layer, a silicon nitride layer is essential for our water quality monitoring device since it has a significantly better diffusion barrier against water molecules and sodium ions than a silicon dioxide layer [40].

To evaluate the impact of the double layer on the FET operation, one calculates the oxide capacitance as

$$C_{ox} = \frac{\varepsilon_{ox}}{t_{ox}} (F/cm^2)$$

with the dielectric constant of the oxide ε_{ox}, and the thickness of the oxide t_{ox}.

In the case of a double insulating layer, the total capacitance (considering the insulating layers as series capacitors) is given by the following equation,

$$C_{tot} = \frac{1}{\frac{1}{C_{SiO_2}} + \frac{1}{C_{Si_3N_4}}}$$

where the capacitance of SiO_2 and Si_3N_4 can be defined as

$$C_{SiO_2} = \frac{\varepsilon_{SiO_2}}{t_{SiO_2}}, \qquad C_{Si_3N_4} = \frac{\varepsilon_{Si_3N_4}}{t_{Si_3N_4}} (F/cm^2)$$

Based on the literature and on fabrication constraints, we defined the thickness as 200-nm-thick SiO_2 layer and a 20-nm-thick Si_3N_4 layer [137], [287], [289]. The resulting dielectric capacitances were calculated to be:

$$C_{SiO_2} = 8.62 \times 10^{-9}\,, C_{Si_3N_4} = 3.31 \times 10^{-7}\,, C_{tot} = 8.41 \times 10^{-9} (F/cm^2)$$

For the metal source and drain electrodes, we deposit 50 nm of Ti as adhesion layer and 200 nm of Pt layer to serve as metallic contacts. Platinum is used instead of Gold since gold may react with sodium or potassium cyanide under alkaline conditions when oxygen is present to form soluble complexes [290]. The thickness of the adhesion layer and metal electrodes was proposed by the manufacturer.

We use a highly-doped poly-Si as gate material (and not Pt). The primary reason for this choice is that Pt cannot withstand the high temperature process needed to obtain the oxide layer on top of the gate electrode. Moreover, the threshold voltage fluctuations induced by random dopants are lower in poly-Si MOSFETs than in metal gate MOSFETs [291]. On the other hand, the work function of the poly-Si gate can be easily changed by controlling the type and level of doping.

The design of the chip was performed with a free and open-source 2D CAD software, LibreCAD. This software allows to design 2D multi-layers with different formats.

4.2 Ink formulation & Ink-jet printing process

In this chapter, we introduce the materials (Type of CNTs and solvents) used for ink fabrication. And then, we detail the optimization process for ink concentration and ink formulation parameters. The CNT functionalization process with conjugated polymer is also described. After the ink formulation process, we introduce the ink-jet printing process with optimized printing parameters.

4.2.1 Pristine CNT & Functionalized CNT ink fabrication

4.2.1.1 Optimized pristine CNT ink fabrication process

The CNT-ink fabrication process is adapted from our previous work [25]. This process was optimized to obtain high ON/OFF ratio transistors, as is detailed in supplementary information section 9.1. The resulting process is as follows: 1 mg of unsorted pristine single-walled carbon nanotube (HiPCo SWCNT, 95+ % purity, average diameter 0.8 ~ 1.2 nm, average length 100 ~ 1000 nm, 70 % semiconducting, Nanointegris^{TM}) is added in 100 ml of 1-methyl-2-pyrrolidinone (NMP, 99+ % purity, Sigma Aldrich), which corresponds to 0.001 wt %. This SWCNT/NMP mixture is sonicated by a high-power tip sonicator (Vibra-cell^{TM} ultrasonic liquid processor, Sonics^{TM}) with maximum power of 150 W, at 20 % power for 1 hour. Then, the remaining bundles are separated by centrifugation for 2 h at 10000 RCF and only the supernatant is used as a printable ink.

4.2.1.2 CNT ink functionalization with conjugated polymer

For CNT functionalization, we use the FF-UR conjugated polymer (Figure **27**) patented by our team for sensing application [106] and synthesized in house. The polymer is composed of a fluorene backbone. The fluorene moieties are functionalized either with two alkyl chains to enhance solubility and interaction strength with CNTs, or with two identical sensing moieties, a urea group NH-CO-NH between two phenyl groups. The capability of this polymer to functionalize non-covalently CNT is demonstrated by molecular dynamics in [292] while its sensing capabilities are analyzed by density functional theory with implicit solvent model in [293]. Briefly, the urea group is expected to complex anions through H-bonds (notably glyphosate, hypochlorous ions), while for cations, cation-pi interactions with the phenyl groups are enhanced through interaction with the oxygen of the urea, leading to a stronger interaction energy than with anions, notably for Mg^{2+} and Na^{+}.

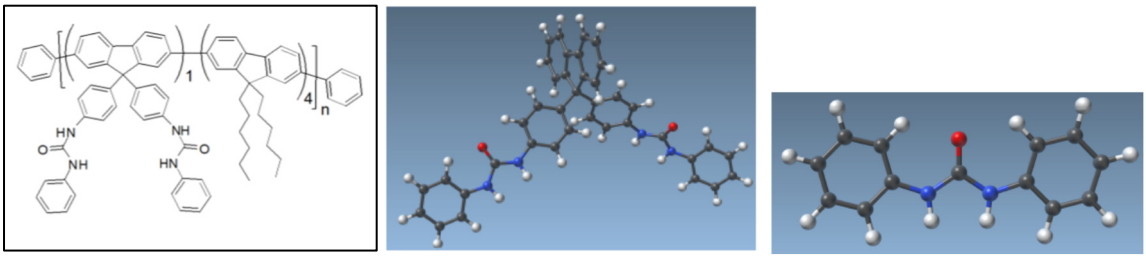

Figure 27. Left: Chemical structure of FF-UR polymer. Middle: Fluorene monomer carrying two urea-based sensing moieties (SAMSON software). Right: focus on the sensing moieties (SAMSON software.)

To functionalize CNT, FF-UR is first dissolved in NMP by magnetic agitation at an ambient temperature for 12 h with a concentration of 1.5 mg/100 ml, which corresponds to the target mass ratio between CNT and polymer of 1:1.5. Finally, the pristine CNT ink and the FF-UR solution are mixed together and then sonicated in a bath-type sonicator for 1 min at 25 ºC for non-covalent functionalization.

4.2.2 Ink-jet printing process

4.2.2.1 Introduction on ink-jet printing

Ink-jet printing is a direct fabrication technique based on solution process, which provides moderate control over the architecture, localization and thickness of patterns on a variety of substrates. Ink-jet printing process is widely used for the fabrication of conductive patterns, and also thin film transistors [22], solar cells [23], sensors [24]–[28], electrochemical energy storage devices [29], light-emitting devices [30], memory and magnetic devices [31], etc. Contrary to lithography or other conventional printing techniques, ink-jet printing process has great potential due to its simple, low cost and non-contact deposition method, which is suitable for mass production and large-scale production [21].

To understand the mechanism of the ink-jet printing process, piezoelectric effect should be discussed first since this effect is the key effect driving the piezo inkjet printing. Piezoelectric materials are used as actuator in various systems. The first piezoelectric ceramic was found in 1943 and the piezoelectric effect was detected by Roberts in 1947 [294]. Recently, lead zirconate titanate, which is called PZT, is the main conventional piezoelectric ceramic material and is broadly used in many products.

The piezoelectric effect can be explained as the generation of electric potential through certain faces of a crystal when mechanical pressure is applied to it. When the crystal is compressed, the ions in the cell are moved and this displacement of ions causes the electric polarization of the unit cell. This is called the piezoelectric effect. In contrast, if an external electric field is applied, the ions in the cell are moved by the electrostatic force, and the crystal structure undergoes a mechanical deformation. Such a mechanical deformation is called inverse piezoelectric effect.

Inkjet printing is based on the inverse-piezoelectric effect: ink is ejected by the pressure in the nozzle created by the dilatation of a piezoelectric material in the nozzle, caused by the applied voltage. The voltage level controls the volume of fluid which is ejected from the nozzle [295] and more generally affects the characteristics of droplets ejected from nozzles and, consequently, the quality of the patterns made by the droplets.

4.2.2.2 Ink-jet printer and printing parameters

For the inkjet printing process, we used the commercial product Dimatix Material Inkjet Printer DMP-2800 with DMC-11610 cartridges for high-resolution printing and reproducibility. Major components of the printer are shown in Figure 28.

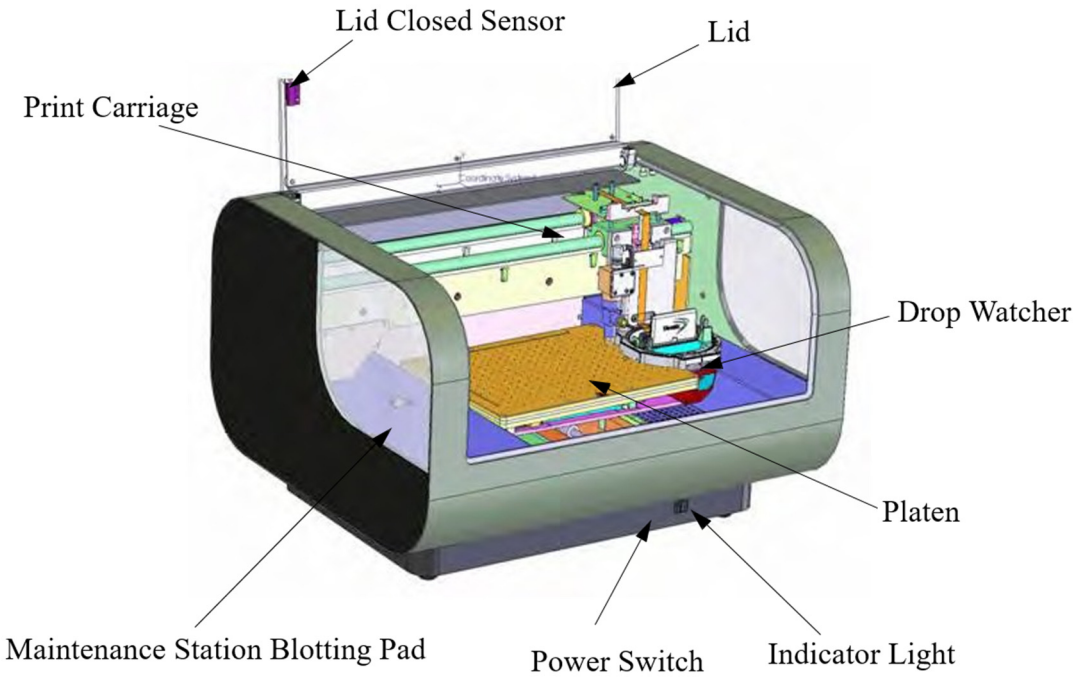

Figure 28. Major components of the inkjet printer. FUJIFILM, (2017), [ONLINE]. Available at:

http://www.fujifilmusa.com/products/industrial_inkjet_printheads/deposition-products/dmp-2800/

As-prepared pristine SWCNT ink is filled in a cartridge (DMP-11610, Fujifilm^{TM}) and the ink is printed with an industrial high-resolution ink-jet printer (DMP-2800, Fujifilm^{TM}). During the printing process, temperature of a cartridge is fixed at 20 ºC and temperature of a substrate is set to 50 ºC for homogeneous CNT deposition. In detail, 2 layers are printed between source and drain with 300 µm by 300 µm square pattern (25µm drop spacing) to create percolated CNT network as a semiconducting channel (Figure 30).

We choose the type of cartridge with a nozzle diameter of 21 µm, which corresponds to the volume per drop of approximately 10 pL. This nozzle diameter is large enough to have reduced risk of nozzle clogging (compared to cartridges with 1pL drop volume and 9 µm of nozzle diameter also available at Fujifilm) and enabled us to reach the uniform quality of each drop.

We already discussed in the previous section that the voltage of nozzles controls the volume of fluid ejected from the nozzles by the inverse piezoelectric effect. The pattern in time of the voltage is called waveform and should be adapted depending on the viscosity of the solvent [296].Figure 29 shows different examples of the driving waveform for drop-on-demand ink-jet printers.

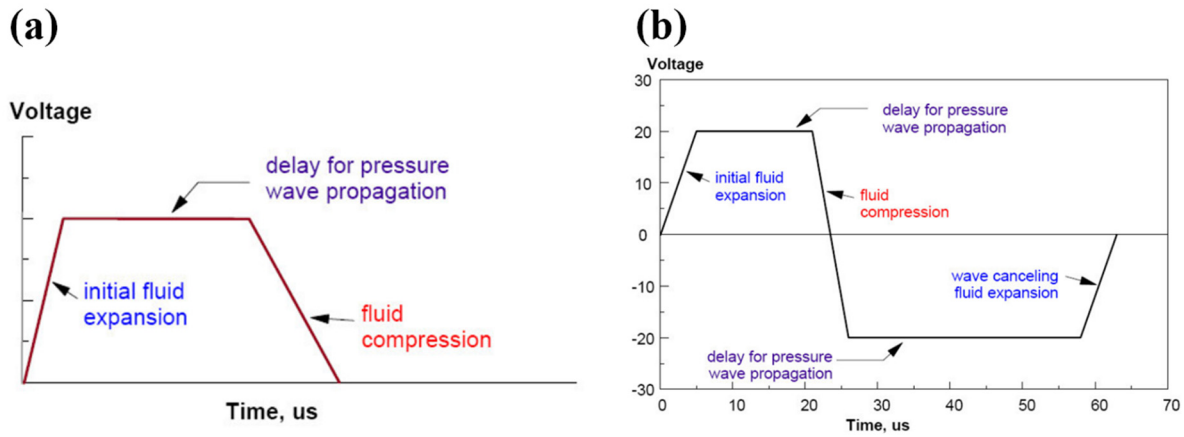

Figure 29. Different driving waveforms for drop-on-demand ink-jet printers. Image taken from [297].

The waveform shown in Figure 29 (a) has a simple trapzoidal waveform and monopolar jetting pulse. This waveform is suitable for solvents with low-viscosity around 1 cPs, such as water. In contrast, the waveform shown in Figure 29 (b) has a complex driving waveform with bipolar jetting pulse, which makes an additional delay and a canceling fluid expansion process. This waveform is optimized for high-viscosity solvents around 10 cPs. In our case, we choose the complex driving waveform despite of low viscosity of DCBZ or NMP (1.324 and 1.65 cp, respectively), since CNT-dispersed solvents showed more stable jetting by using this waveform.

The temperature of a substrate was fixed as 60 ºC to reduce a coffee-ring effect (Ring-like patterns with non-uniform surface thickness) and obtain a homogeneous deposition of nanotubes, and the temperature of a cartridge was fixed as 35 ºC. The drop spacing was set at 25 micrometers, corresponding to 5080 drops per inch (dpi). Though the cartridge has 16 nozzles available that can jet together, we only use a single nozzle at a time. We verify before printing that the preselected nozzle jets properly (e.g. vertical jetting without any unnecessary drop - i.e. satellite drop - or clogging) to reach a high-quality deposition. Figure 30 shows scanning electron microscope (SEM) image of ink-jet printed CNT random network between source and drain electrodes.

The same process is used for both pristine and functionalized CNT inks. In the rest, CNTFET using non-functionalized CNT are labelled p-CNTFET (p for pristine). CNTFET with functionalized CNT are labelled f-CNTFET.

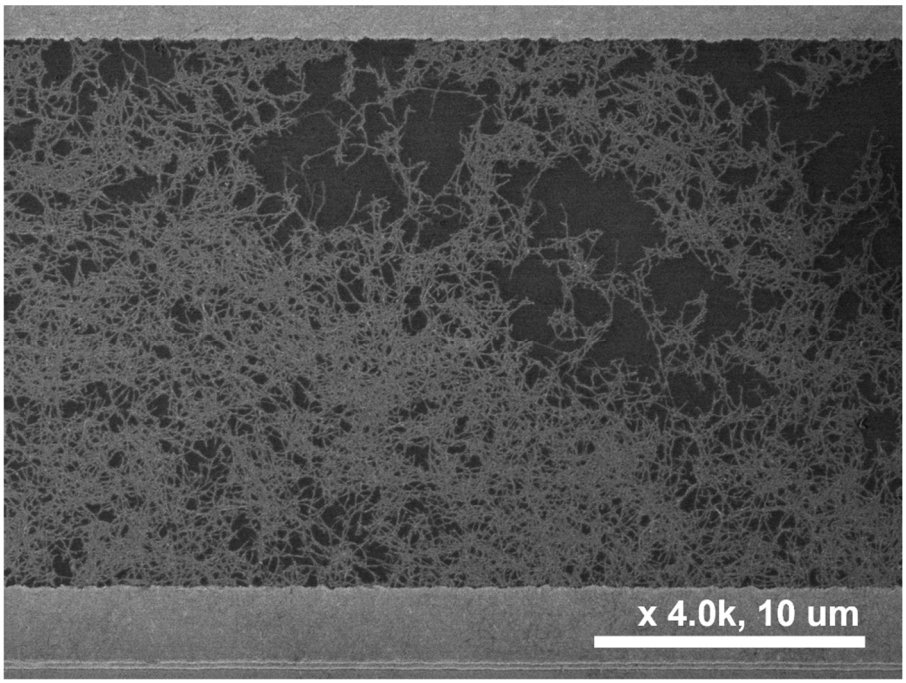

Figure 30. Scanning electron microscope (SEM) image of ink-jet printed CNT network on the Si_3N_4 dielectric layer (middle) between source and drain electrodes (top and bottom).

4.3 Post-processing steps

4.3.1 Curing process

After the ink-jet printing process, the as printed p-CNT-FETs are annealed at 160 ºC for 12 h to eliminate the remaining solvent. As-printed f-CNT FETs are annealed at 80 ºC for 24 h . The annealing temperature for f-CNT FET is lower than that for p-CNT FET to avoid any damage to the polymer by thermal degradation.

4.3.2 PMMA passivation

After the curing process, we deposit poly(methyl methacrylate)(PMMA) on the printed CNT-FETs by spin coating to passivate the printed CNTs and avoid any physical degradation or detachment of the CNT in aqueous solution. It is also known to improve CNTFET operating performances [298].

PMMA/toluene solution (PMMA: molecular weight 15 000 from Acros Organics; toluene: anhydrous at 99.8% from Sigma Aldrich) is prepared at a concentration of 5 mg/ml and spin coating is performed in two steps; 60 s with 1000 rpm and then 90 s with 3000 rpm.

To be noted, the PMMA layer needs to be porous for sensing application, hence a non-solvent induced phase separation process (NIPS) is performed. NIPS process is generally used to fabricate polymeric membranes with an asymmetric morphology. The NIPS method requires three components: polymer, solvent and non-

solvent. During the NIPS process, a polymer solution-based film is immersed in a non-solvent bath, which induces a phase separation of the film into a polymer-rich phase as the membrane matrix [299]. By contrast, a polymer-poor phase becomes the asymmetric membrane pores.

After the spin coating process, the chip is put in 5 % $CaCl_2$ solution as non-solvent for 1 minute to induce the phase separation of PMMA. Finally, as-NIPS processed chip is annealed at 80 ºC for 12 h. Schematic of NIPS process is shown in Figure **31**.

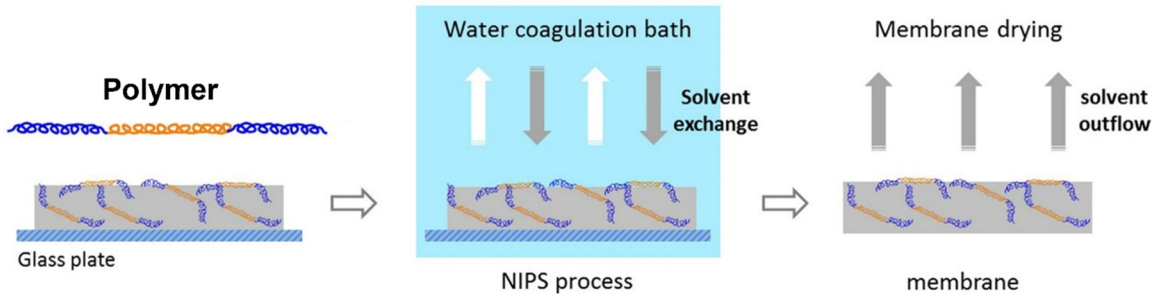

Figure 31. Example of a membrane preparation via NIPS process. Image reproduced from [299].

4.3.3 Wire-bonding & Electrode passivation process

After PMMA deposition via NIPS process (Figure **32** (a), PMMA passivated chips are wire-bonded on in-house designed PCBs (Figure **32** (b)) by a semi-automatic wire bonder (iBond 5000, Micro Point Pro™) for electrical characterization in air and water. Figure 33 shows the wire-bonded and passivated chip on a PCB which is ready to connect with the measurement device.

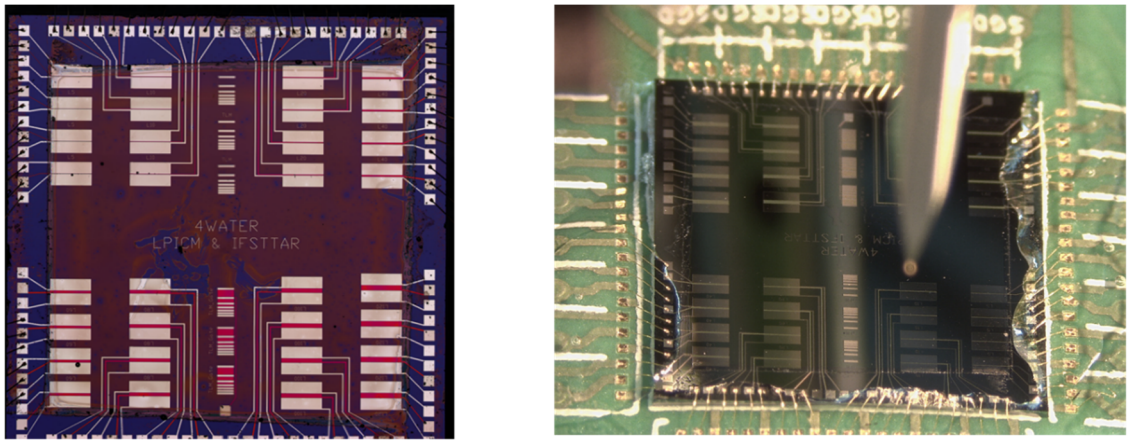

Figure 32. (a) Ink-jet printed CNT-FET device after PMMA deposition process (b) Wire bonding process and

passivation by UV glue.

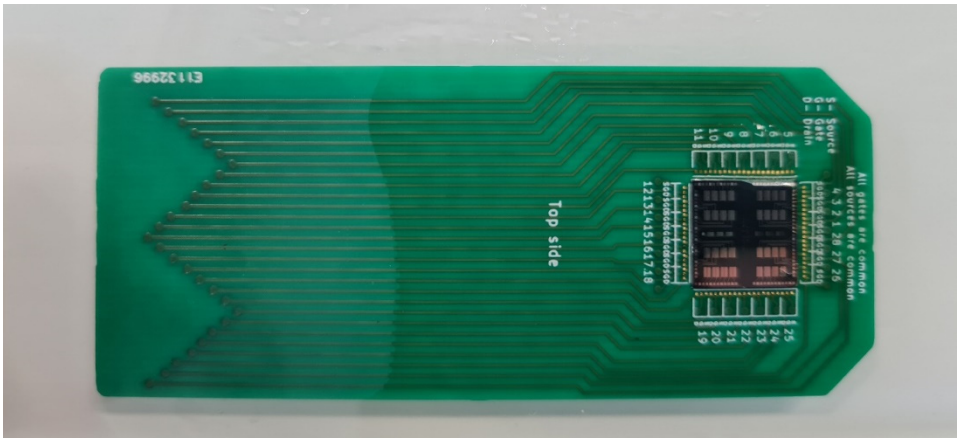

Figure 33. Image of a PCB with a CNT-FET device after wire bonding and passivation process.

4.4 Electrical characterization

4.4.1 Electrical characterization in an ambient condition

Before wirebonding, CNT-FETs are characterized under probe station using Keithley 4200A-SCS parametric analyzer, Tektronix™. Applied drain-to-source voltage (V_{ds}) is fixed at + 5 V and gate-to-source voltage (V_{gs}) is swept from + 60 V to - 60 V with an interval of 0.1 V, is kept at -60V for 5 to 10s, then is swept down continuously from - 60 V to + 60V with the same step. The acquisition time of each measurement is set to 1 s with a delay factor of 1.3 and a filter factor of 3 which are pre-defined parameters in the software. The high level of required gate voltage is expected from bottom-gated CNTFET structure in air [298].

In the rest, we denote I_{on} the current level at minimum voltage in air (-60V) and I_{off} its value at maximum voltage (+60V). Due to charging effects in the interval during the two sweeps, there might be two values of I_{off} at +60V, the first one (higher) being used for analysis.

4.4.2 Electrical characterization in an aqueous solution

For measurement in water, PCB-mounted chips are measured with a Keithley 2400 source measurement unit (Tektronix™). Applied drain and gate voltage are both limited from – 1 V to + 1 V to avoid water splitting [300]. Two types of measurements are carried out, source drain current measurements during gate voltage sweeps between -1V and +1V by step of 0.1 V at constant drain voltage of +0.8 V, and source drain current measurements at constant gate and drain voltage of + 0.8V (both optimized for maximal signal level and

stability in water, detailed information in section 5.2.4.1) with acquisition period of about 0.2s.

4.4.3 pH measurements in aqueous solution

The devices are tested in either 0.1 M of phosphate buffer (from pH 3 to pH 9) or borate buffer solutions (from pH 5 to pH 10). These two buffer solutions have stable pH even when small amounts of strong acid or base are added. Two different type of buffer solutions are tested and compared to verify whether the pH response of CNT-FETs is independent from the choice of buffer solution.

Phosphate buffer solutions are prepared as follows: in 900 mL of deionized water, $NaH_2PO_4 \cdot H_2O$ and NaH_2PO_4 is added in amount depending on the target pH (Table 20). Then NaOH (for increasing pH) or HCl (decreasing pH) is added while monitoring continuously the pH until the solution reaches the target pH value. Deionized water is then added to reach 1L total volume (with negligible impact on pH due to the high molarity of the buffer).

Borate buffer solutions are prepared as follows: in 900 mL, 6.2 g of Boric acid (Molecular weight: 62 g/mol) is added. Then progressive amounts of NaOH (for increasing pH) are added until the solution reaches the target pH value. Deionized water is then added to reach 1L total volume.

pH	**$Na_2HPO_4 \cdot 7H_2O$ (Sodium phosphate dibasic heptahydrate) (g)**	**$NaH_2PO_4 \cdot H_2O$ (Sodium phosphate monobasic monohydrate) (g)**	**Additional acid or base**
3	3.669	11.911	HCl until pH 3
4	3.669	11.911	HCl until pH 4
5	3.669	11.911	HCl until pH 5
6	3.669	11.911	
7	15.483	5.827	
8	15.483	5.827	NaOH until pH 8
9	15.483	5.827	NaOH until pH 9

Table 20. Detailed amount of Sodium phosphate dibasic heptahydrate and Sodium phosphate monobasic monohydrate for 0.1 M phosphate buffer solution.

For measurement, the device is placed in a beaker and connected to the electronic acquisition system. Magnetic agitation is not used to avoid electrical interferences. The pH is monitored continuously using pH meter ENV-40-pH, AtlasScientific™. The pH meter is recalibrated with commercial buffer solutions before each day of

measurement. For each pH step, the number of current measurement points at fixed gate and drain voltage is set at 3000. Each step lasts about 600 s. This duration was selected to enable stabilization of the current level for each pH value.

5 Results & discussions

5.1 Electrical characterization in air

In this section, we discuss the electrical characteristics of p-CNT FETs and f-CNT FETs in air before and after passivation by comparing their transfer curves, I_{on} (On-current), I_{off} (Off-current) and the I_{on}/I_{off} ratio of each device.

5.1.1 I-V Characterization and comparison between p-CNT FET and f-CNT FET before passivation

p-CNT FET and f-CNT FET are characterized by 4-point probe station to compare their electrical behavior. We measure their transfer curve from DC gate voltage ranging from – 60 V to + 60 V. To be noted, hysteresis and asymmetric current value at + 60 V are observed due to the charge trapping at the interface of CNTs in air [301]–[303]. Normalized (e.g. divided by I_{on}) transfer curves of p-CNT FETs (Figure 34 (a)) and f-CNT FETs (Figure 34 (b)) are displayed for 5 µm channels as an example.

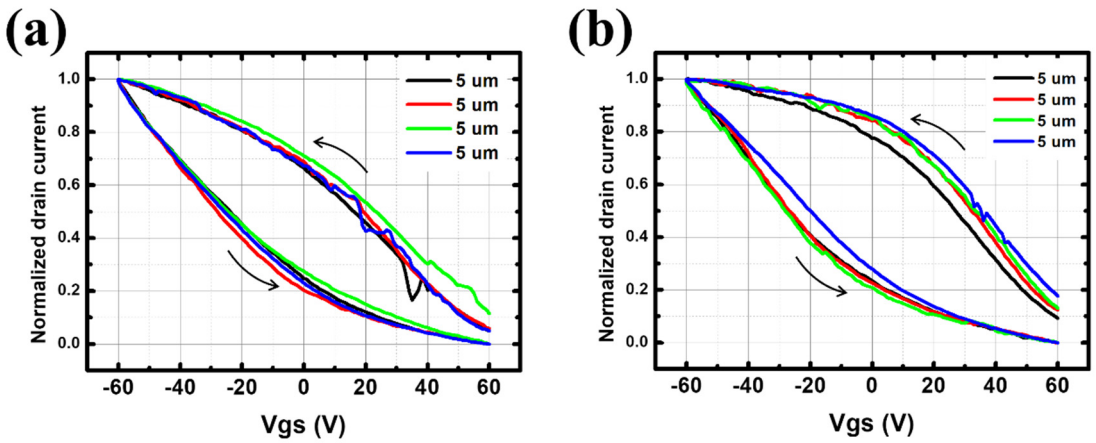

Figure 34. Normalized I-V transfer curves (e.g. I/I_{on}) of ink-jet printed (a) p-CNT FETs and (b) f-CNT FETs at Drain-Source voltage (V_{ds}) is + 5V in air. Four different transistors are shown for each type of FETs. Only 5 µm transistors are shown and each data is normalized. Solid line with an arrow indicates Gate-Source voltage (V_{gs}) sweeping direction. Each measurement starts from + 60 V.

The device-to-device reproducibility is quantified by calculating the average hysteresis of the transfer curves by type of devices, then by calculating the standard deviation over this average hysteresis. The hysteresis is defined here as the voltage difference between upward and downward sweep at current equal to $I_{on}/2$ (e.g. full width at half maximum). Results are expressed in Table 21: while the hysteresis is larger for f-CNTFET, the repeatability is better. The repeatability is also better for smaller channel length. For all types of devices, the hysteresis is large compared to the measurement range (-60V to +60V). It is attributed to the bottom-gated structure, as the CNT/insulator interface is exposed to humidity and surface defects are unpassivated, which results in strong charging effects. In the present structure, the SiO_2/Si_3N_4 interface may also contribute to the

hysteresis through the charging of interface defects [304], [305]

Type of CNT-FET	Channel length			
	5 µm		10 µm	
	Average	Standard deviation	Average	Standard deviation
p-CNT FET	44.9V	4.0V (8.9%)	27.3V	15.6V (57%)
f-CNT FET	57.3V	3.1V (5.4%)	63.0V	6.4V (10%)

Table 21. Average and standard deviation of hysteresis of p-CNT FETs and f-CNT FETs. Only 5 µm and 10 µm channel devices are considered.

Subthreshold slope is calculated to be 80 V/decade for p-CNT FET and 82 V/decade for f-CNT on average. To be noted, only the downward slope is considered for the subthreshold slope calculation (Lower curve from – 60 V to + 60 V). These values are relatively smaller than the literature for random assembly of unsorted CNT, for instance around 130 V/decade in [306] but it is not an issue for sensing applications: intermediate transistor performances are preferred, as too low values of I_{off} or too high values of the subthreshold slope are challenging to measure and interpret.

For a detailed comparison, we extracted the on-current (drain-source current when the transistor is in its conducting state) and the off-current (drain-source current when the transistor is in its insulating state) to calculate the I_{on}/I_{off} ratio of each transistor. As often reported [243], [254], [283], I_{on} and I_{off} values are found to be variable from device to device for both types of FETs.

Based on the I_{on}/I_{off} ratio of p-CNT FET and f-CNT FET as a function of channel length of the transistor (Figure 35), f-CNT FETs generally show higher on/off ratio, which indicates that the performance of the f-CNT FET is better than p-CNT FETs. And we observe an increasing trend of as a function of channel length in case of p-CNT-FETs over the full range of channel lengths, while f-CNT FETs shows the increasing trend only up to 40 µm channel length; from 60 µm the I_{on}/I_{off} ratio drops back to values close to the I_{on}/I_{off} of 5µm channel devices. It might be due to unreliable printing of the f-CNT ink for larger channel lengths.

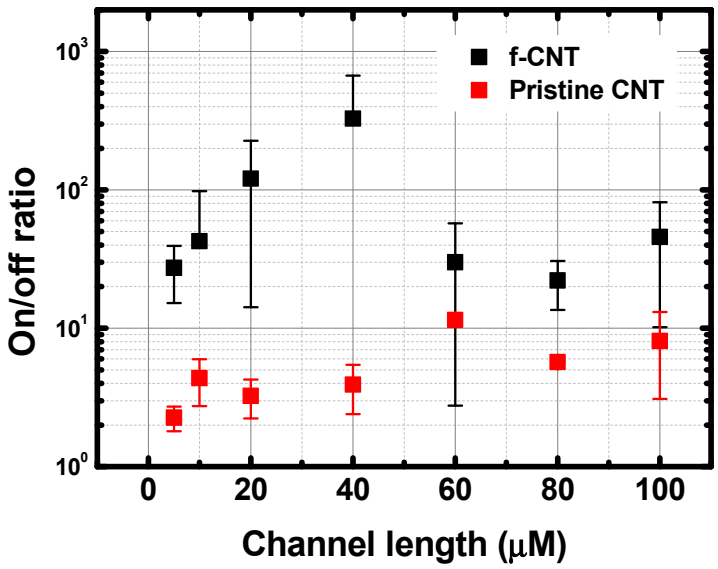

Figure 35. I_{on}/I_{off} ratio of p-CNT FET (Red square) and f-CNT FET (Black square) with respect to channel length from 5 μm to 120 μm before passivation.

5.1.2 Effect of PMMA passivation

Both p-CNT FETs and f-CNT FETs are passivated by PMMA primarily to protect the percolated CNT network from physical degradation in water. It has been reported that the passivation of CNT-FET by PMMA can enhance the performance of the transistor and reduce hysteresis [298].

We observe here at first glance a clear diminution of the I_{off} of the p-CNTFET and a reduction of the hysteresis and of the charging effet for the f-CNTFET (Figure 36).

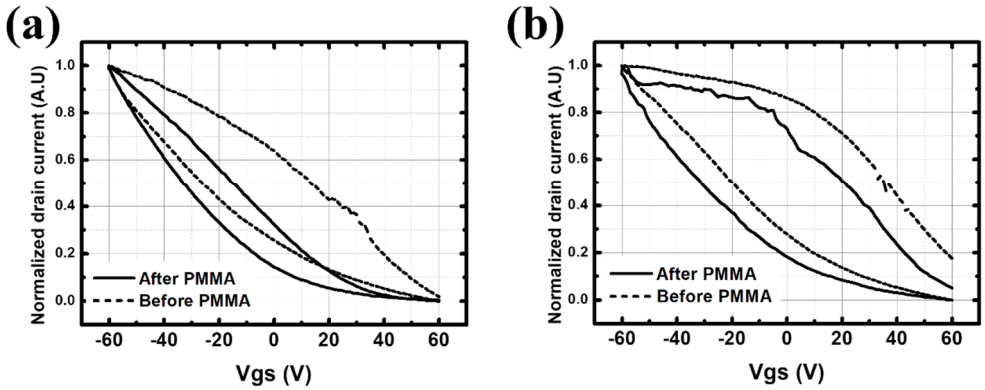

Figure 36. Normalized I-V transfer curve of (a) p-CNT-FET and (b) f-CNT FET before PMMA deposition (dotted line) and after PMMA deposition (sold line) in air.

More systematically, the I_{on} and I_{off} of p-CNT FETs and f-CNTFET with different channel lengths (from 5 µm to 100 µm for p-CNT FETs and only from 5 µm to 10 µm for f-CNT FETs due to the limit of device yield) are measured (Figure 37 and Figure 38). Overall, the effect of PMMA is relatively minor on the I_{on}, but decreases the I_{off} by 1 to 2 orders of magnitude.

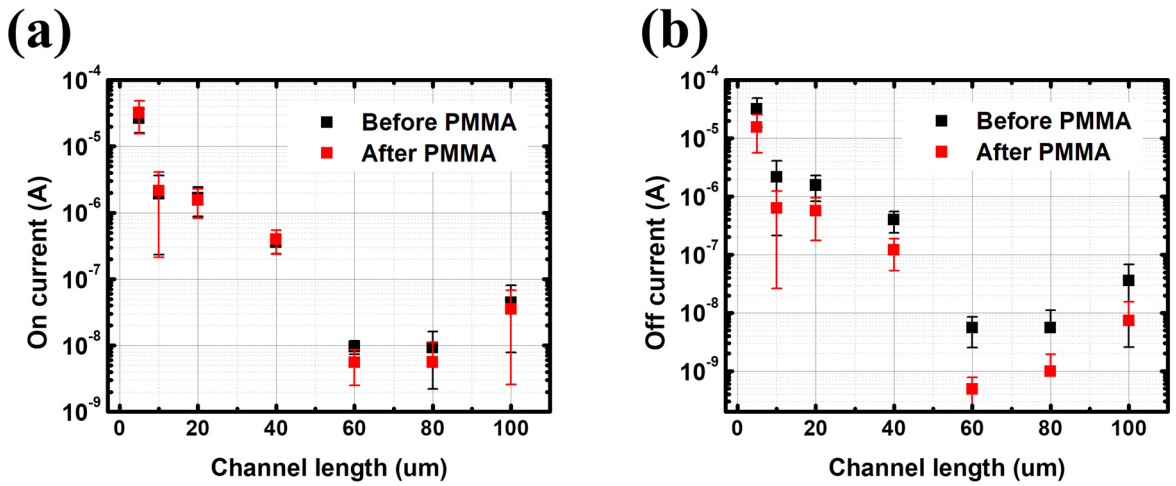

Figure 37. (a) Ion and (b) Ioff of p-CNT FETs before and after PMMA passivation with respect to channel length from 5 µm to 100 µm. On current is considered as drain current at – 60 V, off current is considered as drain current at + 60 V.

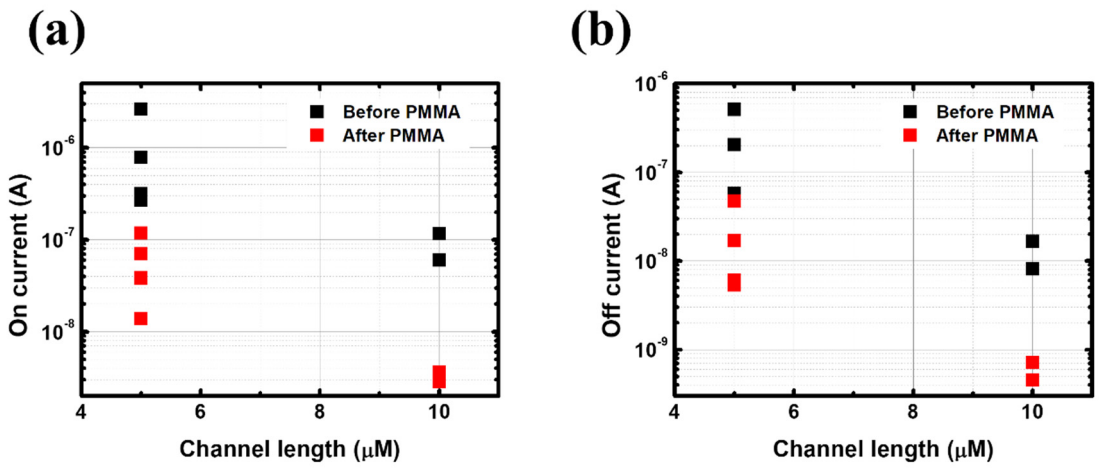

Figure 38. (a) I_{on} and (b) I_{off} of f-CNT FETs before and after PMMA passivation with respect to channel length from 5 µm to 10 µm. On current is considered as drain current at – 60 V, off current is considered as drain current at + 60 V.

It results in a significant increase of I_{on}/I_{off} ratio especially for larger channel lengths, reaching up to 2 orders of magnitude for p-CNTFET (Figure 39) and 1 order of magnitude (only 5 µm and 10 µm devices are considered) for f-CNTFET (Figure 40). To be noted, after passivation, the I_{on}/I_{off} ratio decreases from 5 µm to 10 µm channel devices for this batch, which is not following the usual channel length dependency. This may be due to a perturbation of the CNT network during the passivation process (spin coating of PMMA).

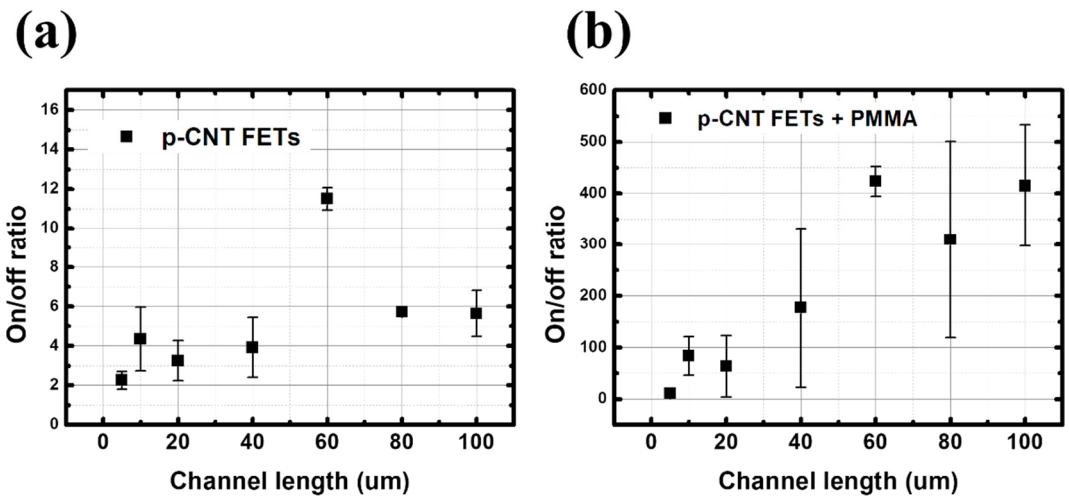

Figure 39. I_{on}/I_{off} ratio of p-CNT FETs (a) before and (b) after PMMA deposition with respect to channel length from 5 µm to 100 µm.

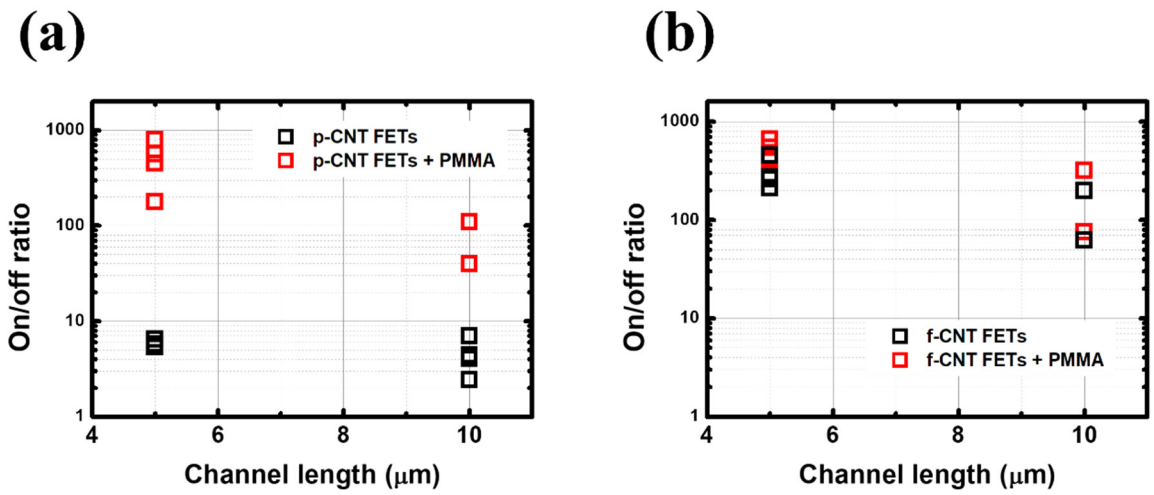

Figure 40. Ion/I_{off} ratio of (a) p-CNT FETs and (b) f-CNT FETs before and after PMMA passivation with channel length from 5 µm to 10 µm.

Finally, one also observes that the hysteresis decreases by 50 % (40 V to 20 V) for p-CNT FETs and by 10 %

(55 V to 50 V) for f-CNT FETs. The subthreshold slope increases by 15 % for both p-CNT FETs and f-CNT FETs with 5 µm channel length after PMMA passivation.

5.2 Electrical characterization in water

For characterization in water, 5µm-channel devices only are studied. This channel length is selected instead of 10µm because devices have good device-to-device reproducibility and have similar performances between p-CNTFET and f-CNTFET (I_{on}/I_{off}= 40~100 for p-CNTFET, 80~300 for f-CNTFET). To be noted, voltage levels are kept systematically between -1 V to + 1 V to avoid any water splitting issue in an aqueous solution.

5.2.1 Preliminary electrical characterization of CNT-FET in water

To verify the PMMA protected transistor can operate in water, we first put the device in deionized water and applied the fixed drain voltage (V_{ds}) as + 1 V, and sweeping gate voltage (V_{gs}) from – 1 V to + 1 V with 0.1 V step. As shown in Figure 41, a non-printed device tested as reference did not respond to the variation of gate voltage and shows flat curve (red solid line). However, the CNT-printed device shows definite drain current response as gate voltage varies from -1 V to + 1 V, with moderate I_{on}/I_{off} ratio around 300. Achieving such a I_{on}/I_{off} ratio in water (comparable to the value in air) with a much smaller gate voltage than in air is highly promising. It is not fully explained yet. One hypothesis is that water removes air as contact material to the CNT. The presence of air around the CNT is known to the degrade charge transport properties of CNTFET [302], [303], [307].

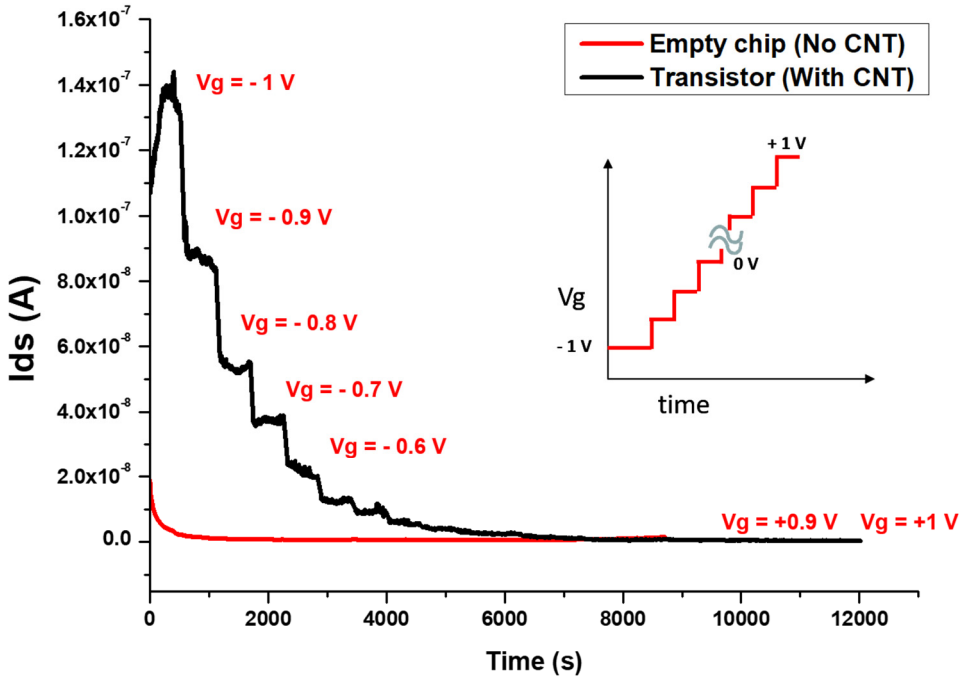

Figure 41. I-V transfer curves of p-CNT FET (Black solid line) and non-printed device (Red solid line) as reference. Drain voltage (V_{ds}) is fixed at 0.8 V.

5.2.2 Parameter optimization for CNTFET operation in aqueous solution

Optimization of measurement parameters was essential as preliminary trials showed frequent occurrences of current instabilities even when limiting applied gate voltage (V_{gs}) and drain voltage (V_{ds}) between -1 V to + 1 V to avoid water splitting issue as described in previous sections. Optimization was performed at pH 7 in phosphate buffer solution (PBS) at ambient temperature, which it is generally considered to be a reference condition.

First, we applied V_{gs} from -1V to + 1V which is the maximum voltage range in water, while fixing the V_{ds} at + 0.8V (Figure 42). To be noted, + 0.8 V is applied for V_{ds}, not + 1 V, to be further away from the water splitting voltage threshold. Instable drain current is observed at V_{gs} = -1 V, due to the non-stabilized measurement condition or high gate voltage which might give rise to the water splitting issue. Stable drain current is observed strating upward from V_{gs} = -0.8V.

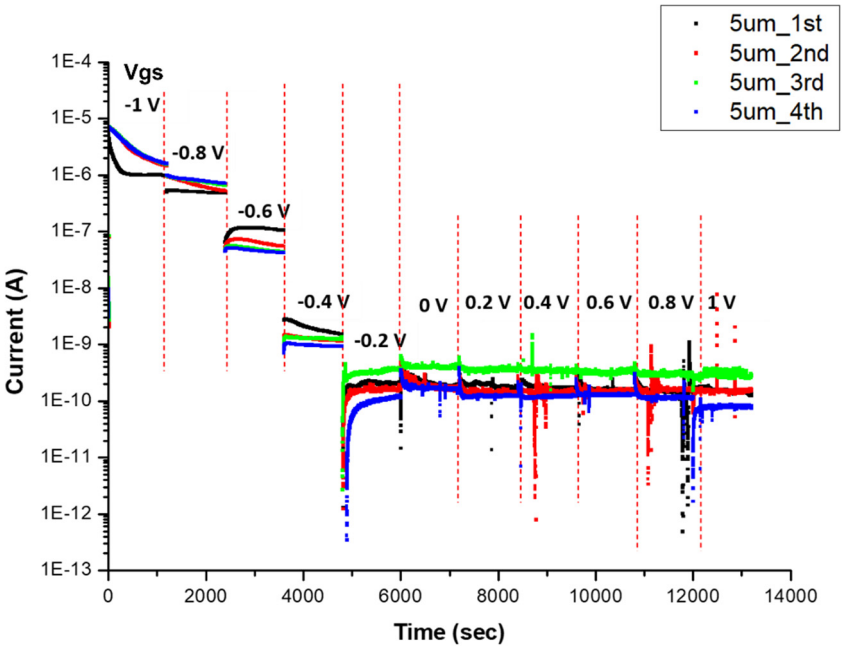

Figure 42. Real-time measured drain current of p-CNT FETs in logarithmic scale. 3000 points are measured for each V_{gs} value and measurement duration of each point is 0.2 seconds. Drain current is measured in pH 7 PBS and V_{ds} is fixed at + 0.8 V.

Different V_{ds} values are also tested from V_{ds} = +0.4 V to + 1V while sweeping the V_{gs} from – 1V to – 0.6 V (Figure 43). Drain current of p-CNT FET is significantly larger (~10^{-6} A) from V_{ds} = +0.6 V to V_{ds} = + 1 V. By contrast, below V_{ds} = +0.4 V the drain current ranges between 10^{-9} A and 10^{-10} A, which is the I_{off} of the p-CNT FET. Hence, the p-CNT FET is turned off when V_{ds} = + 0.4 V, even though V_{gs} is high enough to turn on the device.

Based on these results, the values for CNTFET operation V_{gs} = -0.8 V and V_{ds} = 0.8 V are selected. They allow for a moderate I_{on} without turning off the device.

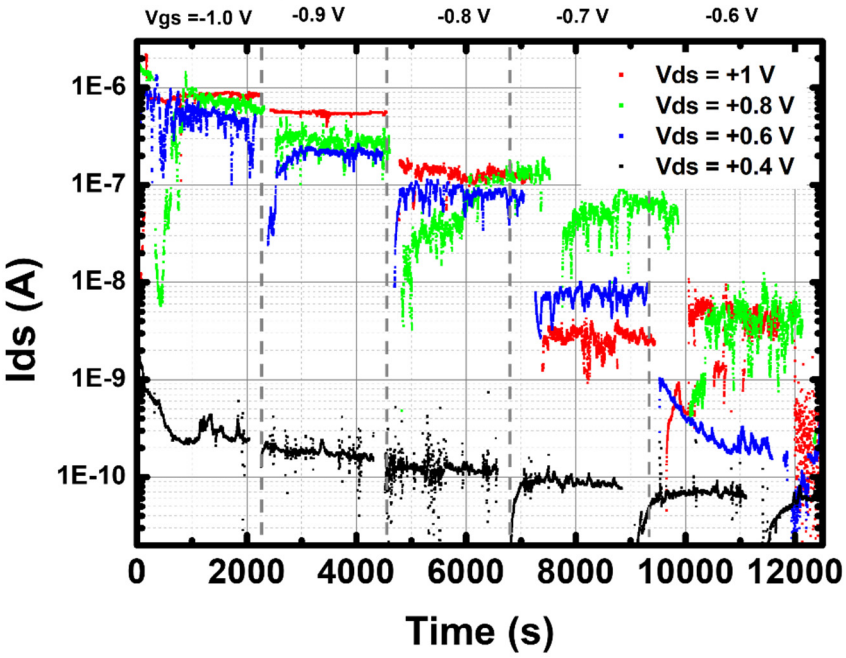

Figure 43. Real-time measured drain current of a p-CNT FET in logarithmic scale. 3000 points are measured for each V_{gs} value and measurement duration of each point is 0.2 seconds. V_{gs} is swept from -1 V to -0.6 V, and V_{ds} is swept from + 0.4 V to +1 V.

5.2.3 I-V characterization in water and comparison between p-CNT FETs and f-CNT FETs

Figure 44 shows a linear I-V transfer curve of 5 µm channel p-CNT FETs and f-CNT FETs at V_{ds} = + 0.8 V in pH 7 phosphate buffer solution (PBS). Compared to the I-V transfer curve in linear scale, logarithmic I-V transfer curves of p-CNT FET and f-CNT FET clearly show the I_{on}, I_{off}, and subthreshold slope of each transistor (Figure **45**). Pristine CNT FETs still show very good reproducibility and p-type behavior. One observes $I_{on} = 1.4 \cdot 10^{-6} \pm 3 \cdot 10^{-7}$A (20%) and $I_{off} = 1.6 \cdot 10^{-10} \pm 8 \cdot 10^{-11}$ A (50%) (Figure **45** (a)), which corresponds to a I_{on}/I_{off} ratio of ~10^4. In addition, they have threshold voltage (V_{th}) at ~ -0.5±0.04 V (20%) and subthreshold slope of ΔV_{gs} ~ 100 mV per decade (percentages after each value indicates the relative standard deviation – standard deviation divided by average). Threshold voltage, V_{th} is the minimum V_{gs} needed to create a conducting path between source and drain electrodes. This voltage is also called as pinch-off voltage. Many researchers have reported different methods to extract the V_{th} of a MOSFET [308]. In this dissertation, we use the linear extrapolation method to obtain the V_{th}. By comparison, in air, these devices have I_{on}/I_{off} ratio of ~10^2 and subthreshold slope of ~ 80 V per decade after PMMA deposition. As mentioned in the previous paragraph, this dramatic increase of performances may be due to an enhancement of charge transfer properties in water compared to that in air [302], [303].

By contrast, f-CNT FETs have $I_{on}=1.6\cdot10^{-7}\pm8\cdot10^{-8}$ A (50%), $I_{off}=2.3\cdot10^{-9}\pm9\cdot10^{-10}$ A (40%), V_{th} at ~ -0.65±0.08V (12%) and subthreshold slope of ΔV_{gs} ~ 200±50 mV (25%) per decade. (Figure **45** (b)). They have a larger device-to-device variability (with notably a strong outlier device) and feature larger subthreshold slope then p-CNT FETs.

Remarkably, 3 out of 4 f-CNT FETs show ambipolarity, with Dirac point at V_{Dirac} = ~ -0.1 V. This is not observed in air. At the Dirac point, f-CNT FETs have I_{Dirac} of 10^{-10} A at V_{gs} = -0.1 V, with I_{on} of 10^{-7} A. However, the I_{off} increases up to ~10^{-9} as V_{gs} increases to +1 V.

This behavior corresponds to an effective n-doping of the SWCNT functionalized by π-stacking by FF-UR [292] in the presence of PBS. Such effective doping is generally thought to result from a mixing of the energy states of the SWCNT and of functionalizing molecule (here) FF-UR, the energy levels of FF-UR (exposed to PBS) ending up within the bandgap of the (semi-conducting) SWCNTs [309]. The fact that this n-doping appears only in PBS, not in air, suggests a modification of the energy levels of FF-UR in the presence of PBS (compared to air), modification which was predicted in [293].

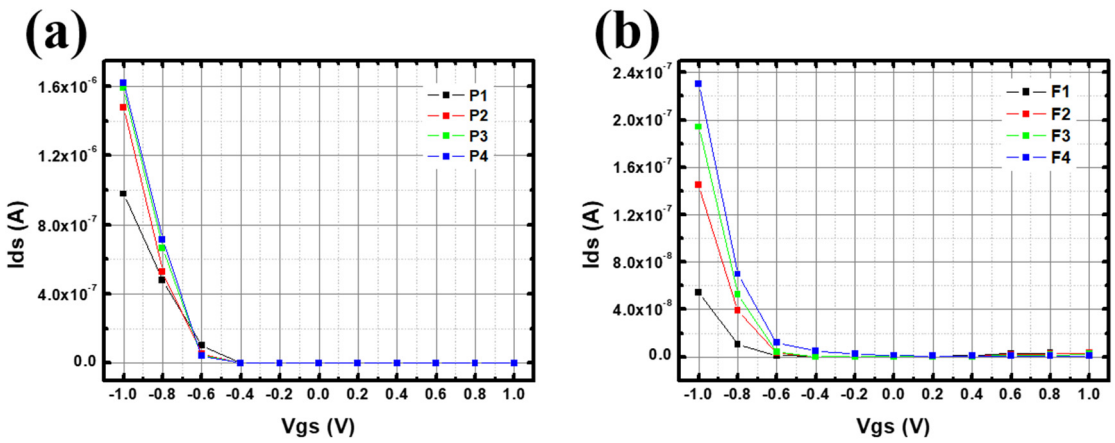

Figure 44. Linear I-V transfer curve of (a) p-CNT FETs and (b) f-CNT FETs in phosphate buffer solution (PBS) at pH 7. All transistors are 5 µm channel devices. V_{ds} is set to +0.8 V and V_{gs} is swapped from -1 V to + 1V.

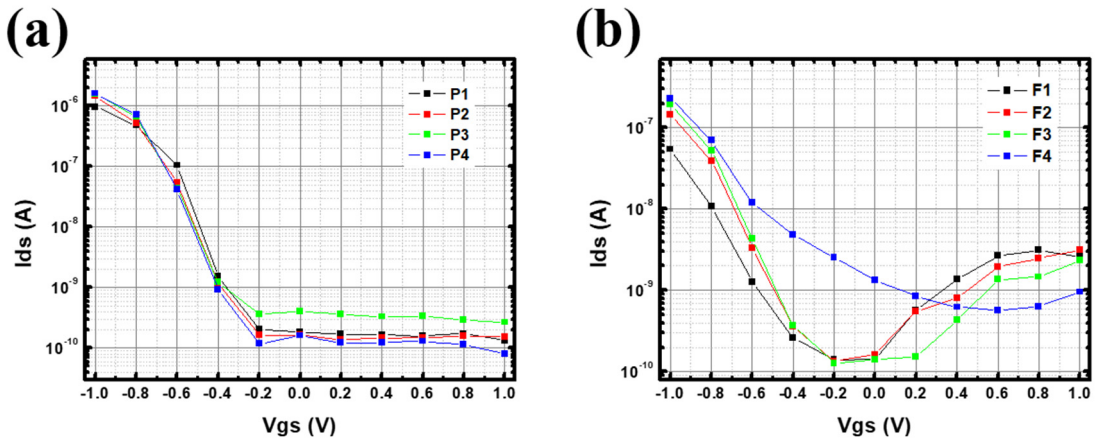

Figure 45. I-V transfer curve of (a) p-CNT FETs and (b) f-CNT FETs in phosphate buffer solution (PBS) at pH 7. All transistors are 5 µm channel devices. V_{ds} is set to +0.8 V and V_{gs} is swapped from -1 V to + 1V. Dirac point of f-CNT FET is observed at V_{gs} = - 0.1 V

5.2.4 CNT FET as pH sensor

In the previous chapter, we successfully observed the electrical behavior of ink-jet printed CNT-FETs in deionized water and pH 7 PBS. After the preliminary characterization of both p-CNT FETs and f-CNT FETs in aqueous solution, we moved forward to the study on pH response of both devices. We first optimized the measurement condition for pH sensitivity and compared their response to pH in two different types of buffer solutions, phosphate buffer solution (PBS) and borate buffer solution (BBS).

5.2.4.1 Real time response to pH steps

The pH response is measured for p-CNT FET and f-CNT FET in PBS with pH ranging from pH 3 to pH 9 then from pH 9 to pH 3. Figure **46** shows the real-time measured response of a 5 µm channel p-CNT FET.

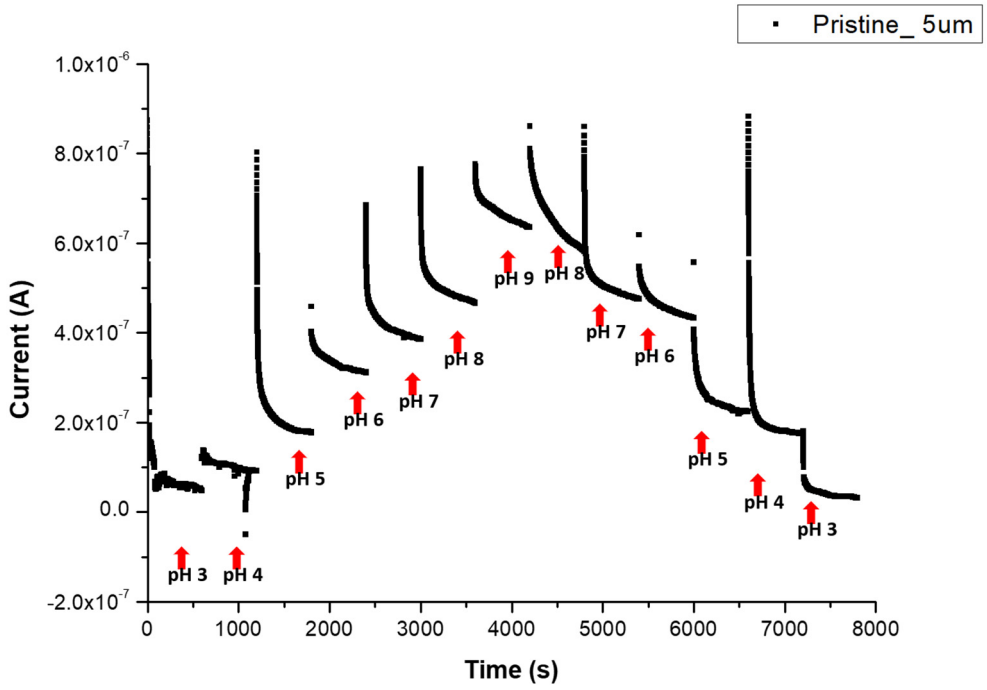

Figure 46. Real-time pH response measurement of p-CNT FET from pH 3 to pH 9 (Upward direction) and from pH 9 to pH 3 (Downward direction). V_{ds} is set to +0.8 V and V_{gs} is set to – 0.8 V.

We observe that the measured current stabilizes after hundreds of seconds for each step. To extract the current level as a function of pH, only the stabilized points should be taken into account. In practice, one averages the last 10% of each step, as detailed in Figure 47.

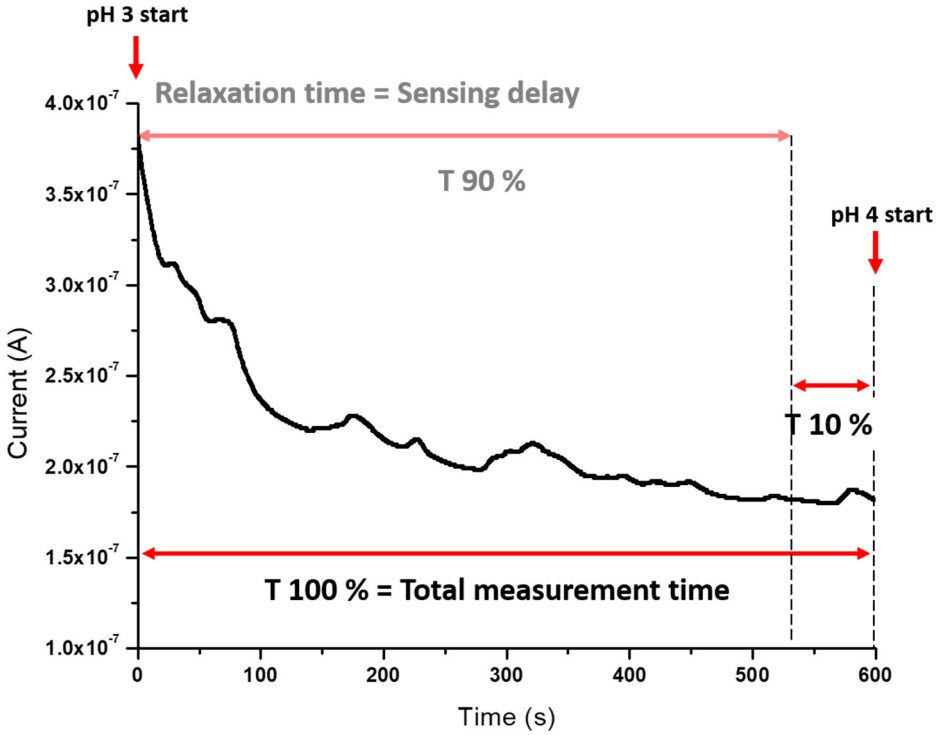

Figure 47. Data treatment process of the real-time measured current values at a given pH. Only 10 percent of measured points at each pH are averaged to obtain the stabilized current value for this pH.

5.2.4.2 pH response in phosphate buffer solution (PBS)

Figure 48 shows normalized current values of p-CNT FET and f-CNT FET from pH 3 to pH 9 based on the drain current at pH 7, with linear fitting lines. Pristine CNT FET shows linear pH response between pH 3 and pH 9 without hysteresis (Figure 48 (a)). The sensitivity is 26±2.2%/pH unit for upward pH and 21±2.1 % for downward pH direction; which corresponds to only 19% (relative) difference between upward and downward sensitivity.

By contrast, f-CNT FET has a much stronger, reversible pH response (368±164 % for upward, 368±44 % for downward), but only over the range from pH 7 to pH 9. The response from pH 3 to pH 7 is lower and less reversible than that of p-CNTFET. Table 22 shows the calculated current percentage variation per pH unit, which corresponds to the sensitivity of CNT-FETs.

It is worth mentioning that the choice of pH 7 as current reference amplifies the relative sensitivity of f-CNTFET compared to p-CNTFET because the f-CNTFET range starts only from pH 7 upward. Such large sensitivity of f-CNT FET from pH 7 to pH 9 is due to the limited current response of the device from pH 3 to pH 7, and the sensitivity is calculated based on the current value at pH 7.

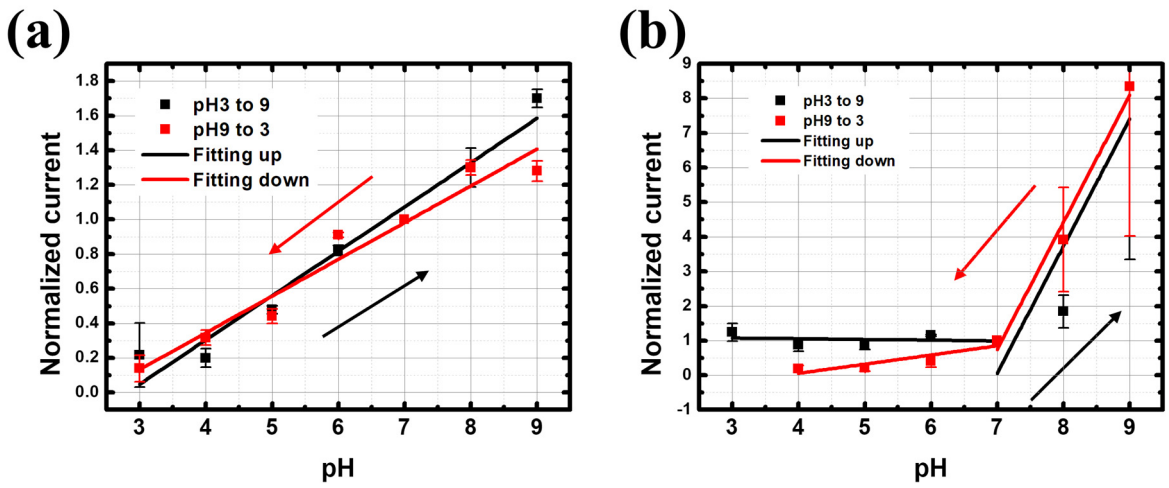

Figure 48. Normalized current values as a function of pH and linear fitting lines of (a) p-CNT FETs and (b) f-CNT FETs in phosphate buffer solutions (PBS) with increasing and decreasing pH from pH 3 to pH 9.

p-CNT FET			f-CNT FET		
Direction	**Sensitivity (%/ pH)**	**R^2**	**Direction**	**Sensitivity (%/ pH)**	**R^2**
Up (pH 3 → pH 9)	26±2.2	0.96	Up (pH 3 → pH 7)	-2±6	-0.28
			Up (pH 7 → pH 9)	368±164	0.67
Down (pH 9 → pH 3)	21±2.1	0.94	Down (pH 9 → pH 7)	368±44	0.97
			Down (pH 7 → pH 3)	26±9	0.71

Table 22. Calculated relative sensitivity of p-CNT FET and f-CNT FET from pH 3 to pH 9. The sensitivity of f-CNT FET is calculated in two different ranges, from pH 3 to pH 7 and from pH 7 to pH 9.

5.2.4.3 pH response in borate buffer solution (BBS)

The sensors are also tested in borate buffer solution (BBS) from pH 5 to pH 10 for comparison. Both p-CNT FET and f-CNT FET showed linear pH response in BBS, with a sensitivity of 56 %/pH for p-CNT FET and 96 %/pH for f-CNT FET (Figure 49 and Table 23). This result shows clearly that the composition of the pH buffer clearly impacts the pH sensing performances. The performances of f-CNTFET remains significantly better than that of p-CNTFET (+58 %), now with sensitivity over the full target range.

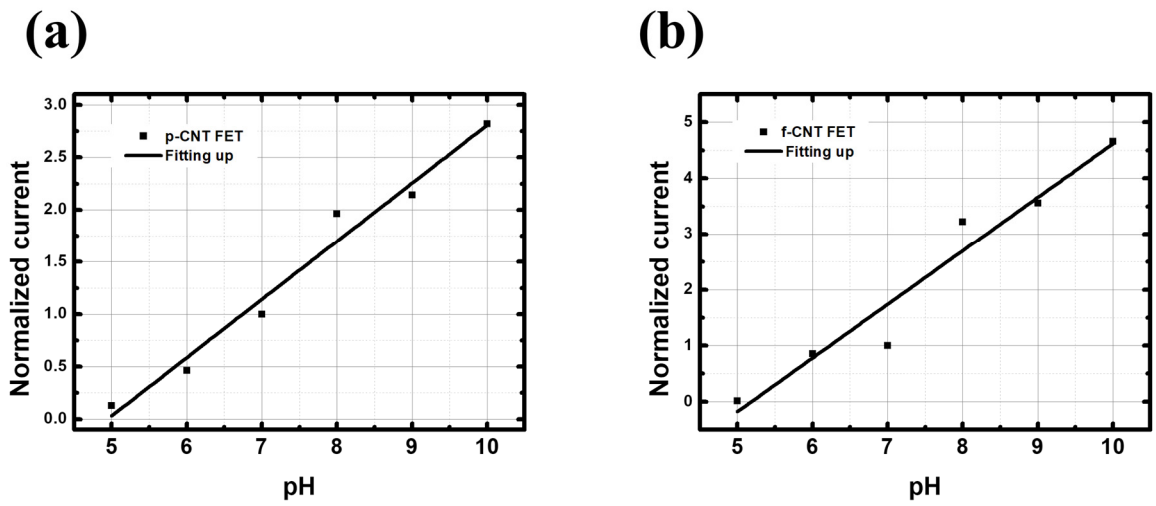

Figure 49. Normalized current values as a function of pH and linear fitting lines of (a) p-CNT FET and (b) f-CNT FET in borate buffer solution (BBS) based on the current at pH 7. Only single direction from pH 5 to pH 10 is measured. To be noted, pH range of BBS is limited from pH 5 to pH 10.

p-CNT FET			**f-CNT FET**		
Direction	**Sensitivity (%/ pH)**	**R^2**	**Direction**	**Sensitivity (%/ pH)**	**R^2**
Up (pH 5 → pH 10)	55.5	0.97	Up (pH 5 → pH 10)	95.9	0.94

Table 23. Calculated sensitivity of p-CNT FET and f-CNT FET from pH 5 to pH 10 in borate buffer solution (BBS).

5.2.4.4 Comparison to the state of the art

Table 24 reproduced from [19] provides a comparison with the state of the art. One observes that our p-CNTFET devices are comparable with other devices and f-CNTFET have dramatically improved performances. In PBS (most commonly used pH buffer in the literature), the relative sensitivity of p-CNTFET is the same as the best results in the literature (23%/pH unit with impedance spectroscopy on SWCNT-COOH coated on gold electrodes [80] and 23%/pH unit with dual-gated CNTFET with pristine CNT [33]). Relative sensitivity of p-CNTFET in BBS are considerably higher than the literature (by more than 2.5 times), but it might be due to the choice of buffer.

While in the literature, no other functionalization than COOH (naturally present of SWCNT sidewalls even

when non functionalized on-purpose) provides good performances does not improve sensitivity, we demonstrate here for the first-time strong improvement of pH sensitivity via SWCNT functionalization. This is observed both in PBS and BBS, even though the range in PBS is limited to pH 7 to 9.

Type of CNT	Functional probe	Functionalization	Detection range	Sensitivity	Relative Sensitivity*	Transduction method	CNT Deposition method	Electrode material Contact configuration	Substrate	Comments	Ref.
SWCNT	Polyaniline	Non covalent	pH 2.1~12.8	N/A	N/A	Chemistor	Drop-casting	Ti/Au	Si/SiO_2		[78]
SWCNT	Nafion	Non covalent	pH 1~12	N/A	3.5 %/pH	Chemistor	Screen printing	SWCNT	Polymide		[148]
MWCNT	Ni NP*	Non covalent	pH 2~10	N/A	5.0%/pH	Chemistor	Continuous pulling of super-aligned, CVD grown MWCNTs	MWCNT	PDMS		[149]
SWCNT	Pristine	Non functionalized	pH 1~11	34nS/pH (pH 1~6) 163nS/pH (pH 7~11)	3.4 %/pH (pH 1~6) 9.3%/pH (pH 7~11)	Chemistor	Spray-casting	Cr	Si/SiO_2		[86]
SWCNT	COOH	Covalent	pH 5~9	75Ω/pH	11%/pH	Chemistor	Dielectrophoresis (aligned CNTs)	Cr/Au	Si/SiO_2	Response time: 2s at pH 5, 24s at pH 9	[93]
SWCNT	Pristine	Non functionalized	pH 4~10	5.2kΩ/pH	14%/pH	Chemistor	Aerosol jet printing	Ag	Kapton		[88]
MWCNT	Pristine	Non functionalized	pH 5~9	63Ω/pH	18%/pH	Chemistor	Sucked by vacuum force	MWCNT	Filter paper		[89]
SWCNT	Malt extract agar	Non covalent	pH 3~5	N/A	N/A	FET (hybrid top gate)	Dip coating	Ti/Au (10/30 nm) contacts	Si/SiO_2(100nm)	Multiplexed detection of Fungus (A. niger, A. versicolor) and Yeast (S. cerevisiae)*	[82]
SWCNT	ETH500*, MDDA-Cl	Non covalent	pH 2~7.5	71nA/pH	7.5%/pH	FET (liquid gate)	Spray deposition	Aqueous electrolyte (gate) Cr/Au (5/50 nm)	Polymide (Kapton®)	Change from p-type to n-type transistor with the membrane layer	[37]
SWCNT	COOH	Covalent	pH 3~8	17nA/pH	8.2%/pH	FET (top gate)	N.P.	Cr/Au (30/50 nm) source & drain electrodes, Ag/AgCl for reference electrode	Glass/APS(50-200nm)/SWCNT /APS(500nm)/TopGate	CNT placement controlled by location of APS (modified to immobilize the CNTs)	[140]
SWCNT	Pristine	Non functionalized	pH 3.4~7.8	3.9μA/pH	13%/pH	FET (bottom gate)	Spin coating	Cr/Au (5/40 nm)	Si/SiO2(65nm)		[32]
SWCNT	Poly(1-aminoanthracene)	Non covalent	pH 3~11	FET 19μS/pH potentiometry 55 mV/pH	FET 14 %/pH potentiometry N/A	FET, potentiometry (liquid gate)	Dielectrophoresis (aligned CNTs)	Au contacts, Pt wire (Auxillary), Ag/AgCl electrode (Reference)	Si/SiO_2(300nm)	Multiplexed detection of Ca^{2+} and Na^{+}	[91]

Type of CNT	Functional probe	Functionalization	Detection range	Sensitivity	Relative Sensitivity*	Transduction method	CNT Deposition method	Electrode material Contact configuration	Substrate	Comments	Ref.
SWCNT	Pristine	Non functionalized	pH 3~10	7600mV/pH (Dual-gate mode) 59.5 mV/pH (single-gate mode potentiometry)	23%/pH (Dual-gate mode) N/A (single-gate mode potentiometry)	FET (double gate)	Spin coating	100 nm Ti contacts for source, drain and top gate	p-Si (substrate acting as bottom gate)		[33]
SWCNT	Polyaniline	Non covalent	pH 1~13	56 mV/pH	N/A	potentiometry	Spray casting	Polyvinyl chloride-coated steel wire	PVC	Highly selective against Li^+, Na^+, K^+	[85]
MWCNT	$COF_{THi\text{-}TFPB}$ *	Covalent	pH 1~12	54 mV/pH	N/A	Differential pulse voltammetry	Drop casting	Glassy carbon electrode	Glassy carbon	multiplexed detection of Ascorbic acid.	[147]
MWCNT	COOH	Covalent	pH 4~9	17Ω/pH (Au), 16Ω/pH (Al)	23%/pH (Au), 14 %/pH (Al)	Impedance spectroscopy	Dip coating	Au and Al interdigitated electrodes	Kapton®		[80]
SWCNT	Pristine	Non functionalized	pH 3~9 (PBS) pH 5~9 (BBS)	91.7 nA/pH (PBS) 0.37 µA/pH (BBS)	25.1 %/pH (PBS) 55.5 %/pH (BBS)	FET (bottom gate)	Ink-jet printing	Ti/Pt (50/ 200 nm)	Si/SiO_2(1000 nm)		**This paper**
SWCNT	FF-UR polymer	Non covalent	pH 7~ 9 (PBS) pH 5~9 (BBS)	2.8 nA/pH (pH 3~6 PBS) 65.1 nA/pH (pH 7~9 PBS) 0.21 µA/pH (BBS)	15.8 %/pH (pH 3~6 PBS) 372.9 %/pH (pH 7~9 PBS) 95.9 %/pH (BBS)	FET (bottom gate)	Ink-jet printing	Ti/Pt (50/ 200 nm)	Si/SiO_2(1000 nm)		**This paper**

Table 24. CNT-based pH sensors in water, sorted by transduction type then by relative sensitivity. Reproduced from [19].

5.2.4.5 Comparison between p CNT-FET and f CNT-FET

To investigate the reason for limited pH response range in case of f-CNT FETs, the I-V transfer curves of p-CNT FET and f-CNT FET is measured in PBS with different pH values, pH 10, pH 7, and pH 4 (Figure 50). As shown in the figure, it appears clearly that the effect of pH is to modulates the threshold voltage (V_{th}) for both p-CNT FET and f-CNT FET, the effect being intensified for f-CNTFET. Voltage threshold modulation is a known effect regarding the pH response of CNTFET [33]. It is also known that the level of doping amplifies this threshold voltage sensitivity to pH. As we have seen above, the functionalization with FF-UR in the presence of water results in effective n-doping [32], [310], and this explains the enhanced sensitivity of f-CNTET to pH.

The V_{th} dependence on pH of f-CNT FET is much stronger (~ 0.03 V/pH for p-CNT FET, ~ 0.1 V/pH for f-CNT FET), so that the current at fixed gate voltage varies strongly. However, for lower value of pH, the threshold voltage exceeds the gate voltage values of -0.8V used in Figure 50 (b) (here -0.9V at pH 4) so the device is in its off-state (where the current level has low sensitivity to gate voltage). It is worth mentioning that measuring at slightly lower gate voltage (-0.9V or -1V) could in theory increased the linear range for pH sensing for f-CNTFET devices, but preliminary tests showed higher instability of the current and longer response times at these voltage (probably due to early onset of water splitting), which made them impractical for further characterizations. The V_{th} dependence on pH is also observed in BBS, whereas p-CNT FET (Figure 51 (a)) and f-CNT FET (Figure 51 (b)) do not show significant difference.

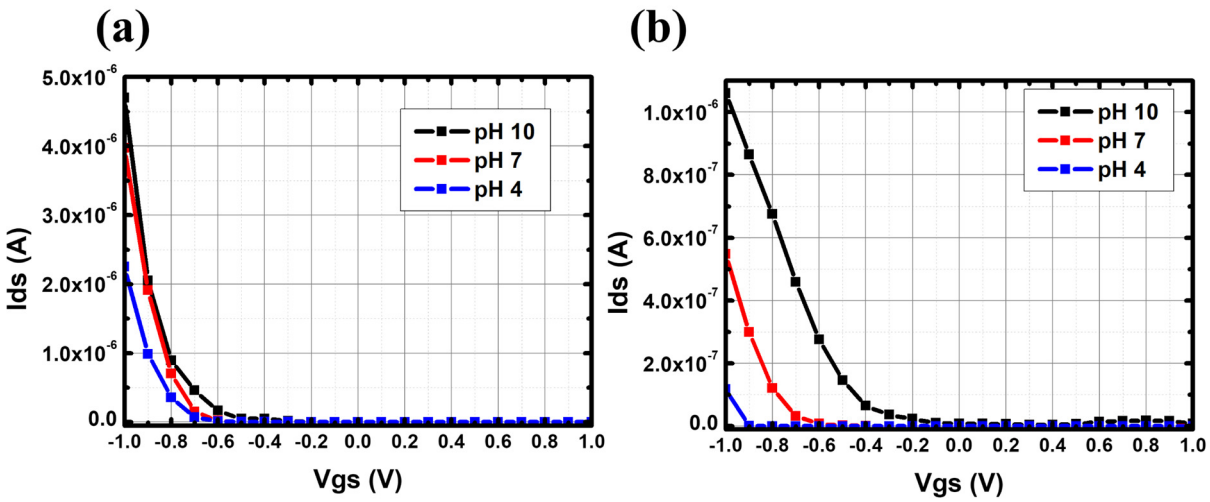

Figure 50. Linear I-V transfer curve of (a) p-CNT FETs and (b) f-CNT FETs in PBS with respect to different pH from pH 10 to pH 4. V_{ds} is fixed at + 0.8 V. Unstable current values from -0.8 V of p-CNT FET at pH 10 may be due to the excess voltage applied by the effective liquid gate effect.

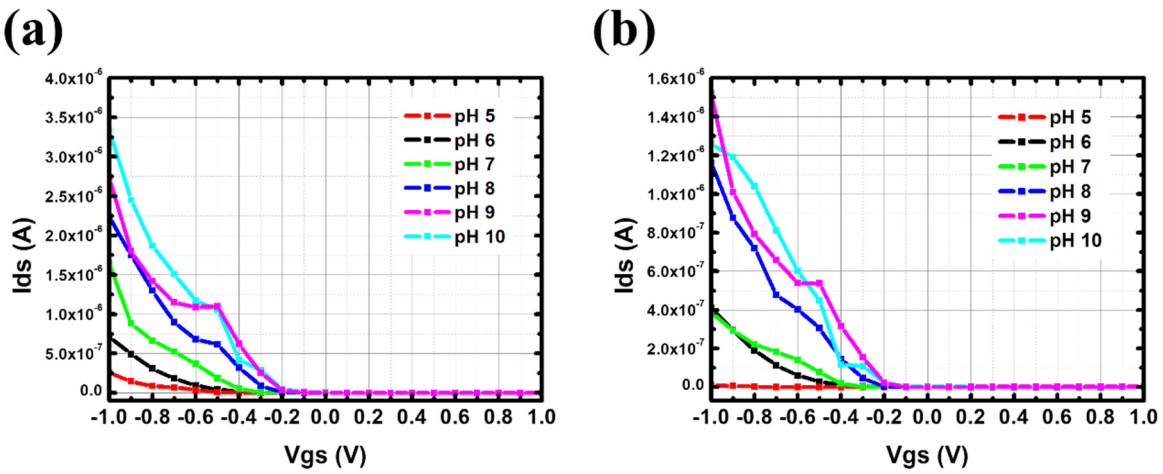

Figure 51. Linear I-V transfer curve of (a) p-CNT FETs and (b) f-CNT FETs in Borate buffer solution (BBS) with respect to different pH from pH 10 to pH 5. V_{ds} is fixed at + 0.8 V. To be noted, pH range of BBS is limited from pH 5 to pH 10.

5.2.4.6 Device reversibility

In terms of evaluation of the sensing device, durability and reversibility of the device is one of the important factors. Drain current of pristine CNT-FETs (p-CNT FETs) is measured in real-time to study the reversibility of CNT-FETs in a repeatedly varying pH condition in phosphate buffer solution (PBS) (Figure 52). As shown in the figure, p-CNT FETs respond to repetitive sweeping pH ranges (pH 9 to pH 6, pH 9 to pH 6) immediately for two consecutive days. In addition, the p-CNT FETs do not need additional reset or regeneration steps as pH sensors in consecutively reliable condition, whereas they need enough stabilization time to reach a constant drain current (several hundreds of seconds).

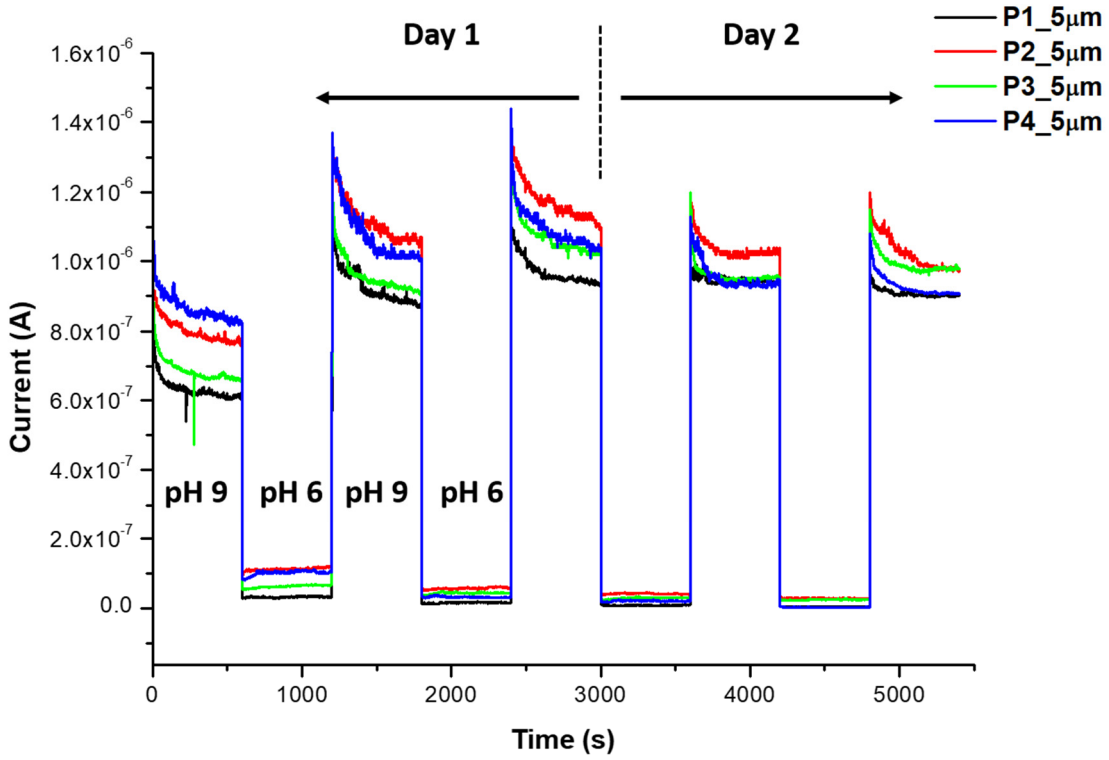

Figure 52. Real-time measured drain current of p-CNT FETs sweeping between pH 9 and pH 6 in PBS. Channel length of each device is 5 µm.

5.2.4.7 Lifetime study on conjugated polymer-CNT composite

As shown in the Figure 44 (b), we have apparently observed that f-CNT FETs show ambipolar behavior (Re-augmentation of the drain current after V_{gs}=-0.1 V up to V_{gs} = + 1 V) with Dirac point at V_{gs} ~-0.1 V. However, a degradation of this ambipolar behavior is observed over time, and this may be due to the physical degradation since CNT-FETs are stored in deionized water. Dirac point is clearly observed at V_{gs} = - 0.1 V for 3 out of 4 f-CNT FETs in Figure 53 (a), whereas the transistors partially lose their ambipolar behavior after 3 months of storage time (Figure 53 (b)). After 9 months in water, f-CNT totally lose their ambipolarity and Dirac point at V_{gs}=-0.1 is no longer observed (Figure 53 (c)). The results obviously show that the ambipolar behavior of f-CNT FETs is suppressed as the total storage time in water increases; I_{on}, I_{off} and I_{Dirac} increases. In addition, f-CNT FETs show same electrical characteristics as p-CNT FETs (p-type transistor-like behavior without ambipolarity) shown in Figure 54, it may suggest degradation of FF-UR after long exposition to water. This degradation can also explain the reason why p-CNT FETs and f-CNT FETs behaved identically without ambipolarity in BBS, which may be due to the degradation of FF-UR.

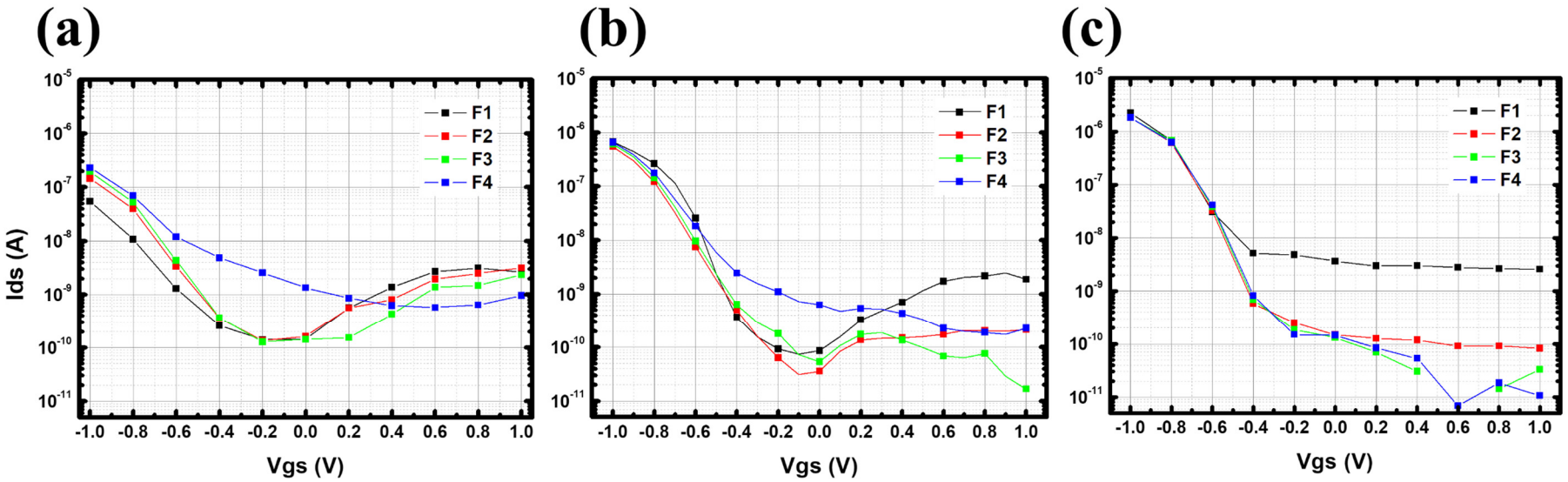

Figure 53. Logarithmic I-V transfer curve of f-CNT FETs in pH 7 phosphate buffer solution (PBS) after (a) 2 months (b) 3 months and (c) 9 months. All transistors are 5 µm channel devices. V_{ds} is set to +0.8 V and V_{gs} is swapped from -1 V to + 1V.

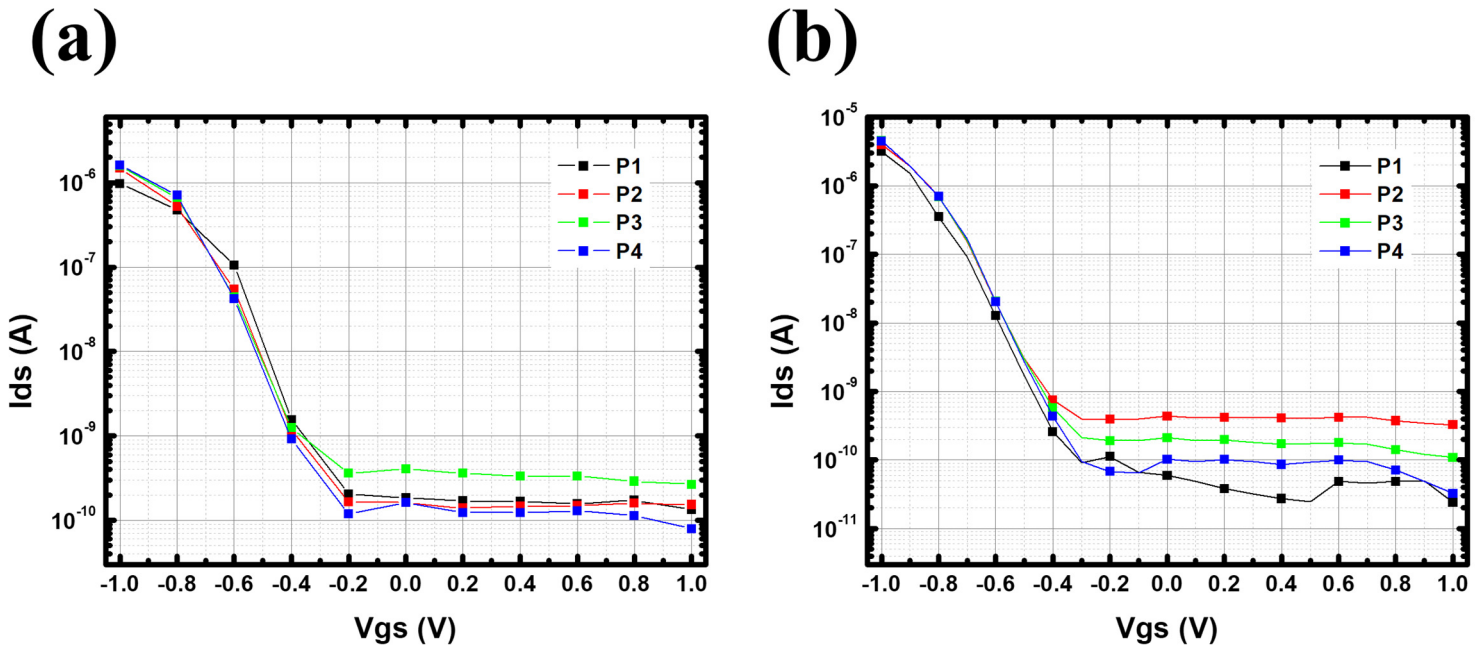

Figure 54. Logarithmic I-V transfer curve of p-CNT FETs in pH 7 phosphate buffer solution (PBS) after (a) 2 months and (b) 3 months. All transistors are 5 µm channel devices. V_{ds} is set to +0.8 V and V_{gs} is swapped from -1 V to + 1V.

5.2.4.8 Discussion on the possible mechanisms of sensing

To understand the sensing mechanism in PBS and BBS, the I-V transfer curves are measured at different pH (Figure 55 and Figure 56). Table 25 summarizes the behaviors of the curves, while Figure 57 compare $I_{on}/_{Off}$, V_{th} and subthreshold slopes in the different configurations.

Both in PBS and BBS, in p-CNTFET and f-CNTFET, it appears clearly that one of the effects of pH is to modulates the threshold voltage (V_{th}). This is a known effect of pH on CNTFET [33], which naturally explains the current sensitivity at gate voltage -0.8V discussed in the previous section. It also explains why the sensitivity of f-CNTFET in PBS is limited to pH 7 to 9, as below pH 7, the threshold voltage becomes lower than -0.8V (the transistor is in its OFF state). It is however not possible to operate the FET at lower gate voltage, as the current becomes less stable at gate voltage below -0.9V due to water splitting.

No significant ambipolarity is observed in BBS for p-CNTFET and f-CNTFET, while strong ambipolarity is observed for f-CNTFET only in PBS. It suggests that the n-doping effect caused by FF-UR is caused not directly by the pH, but by the phosphate ions in PBS. The strong n-doping in PBS explains the enhanced threshold voltage sensitivity to pH, as has been reported [32], [310]. The enhanced threshold voltage sensitivity to pH is also present in BBS but with no sign of n-doping, which suggests an additional effect of FF-UR in BBS still to be explained.

The subthreshold slope in CNTFET is related to the effective carrier mobility, which in SWCNT networks is controlled by the intrinsic mobility in the SWCNT and by the contact resistances. The subthreshold slope of p-CNT FETs tends to decrease with increasing pH in both PBS and BBS, whereas the subthreshold slope of f-CNT FETs generally increases with pH. This suggests that the pH impacts either carrier mobility or contact resistances in p- and f-CNT FETs. However, the mechanisms still remain uncertain.

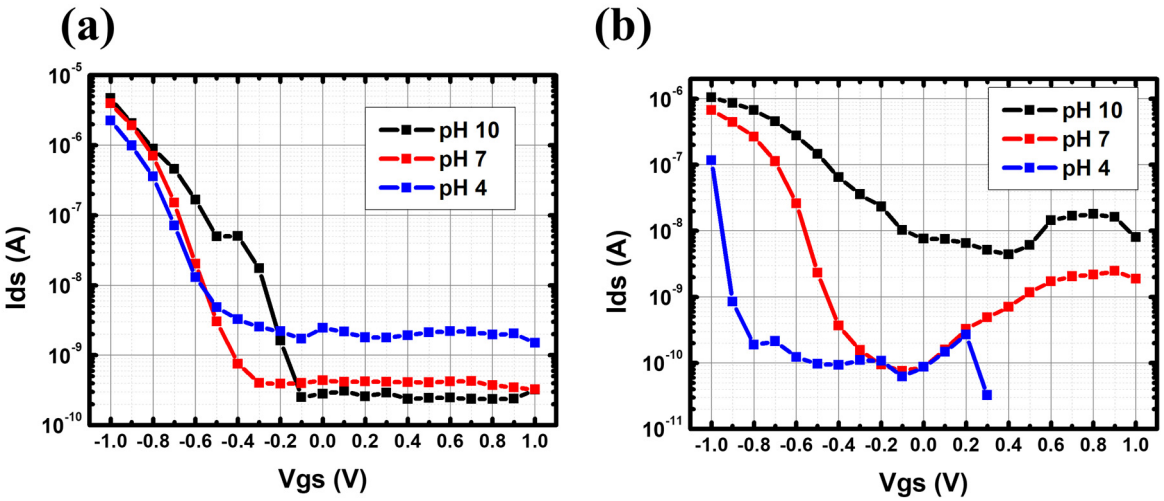

Figure 55. I-V transfer curve of (a) p-CNT FETs and (b) f-CNT FETs in PBS with respect to different pH from pH 10 to pH 4. V_{ds} is fixed at + 0.8 V.

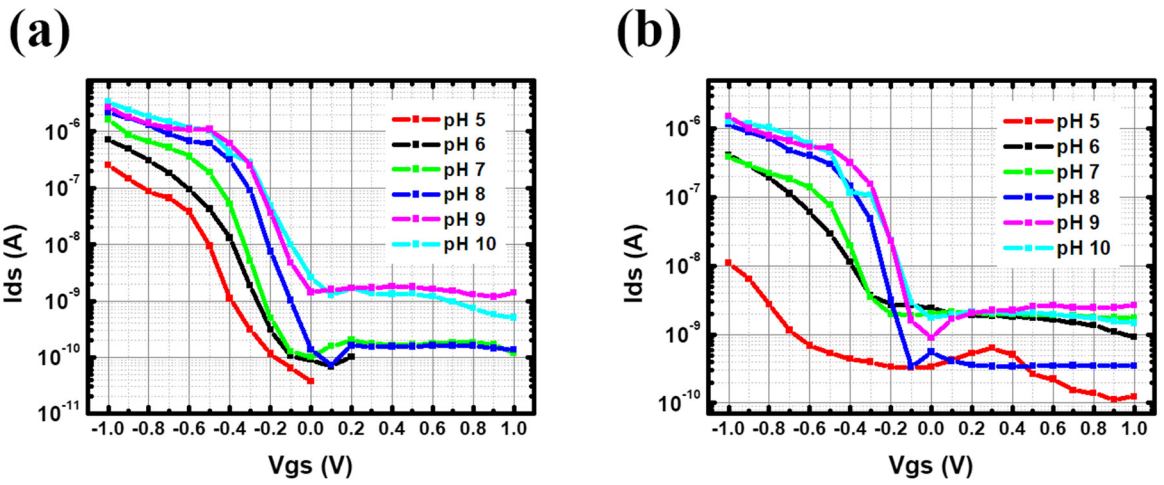

Figure 56. I-V transfer curve of (a) p-CNT FETs and (b) f-CNT FETs in BBS with respect to different pH from pH 10 to pH 4. V_{ds} is fixed at + 0.8 V.

Table 25. Summary of the I-V curves features as a function of pH in PBS and BBS for p-CNTFET and f-CNTFET

	p-CNTFET	f-CNTFET
PBS	I_{on} increases with pH, I_{off} decreases with pH I_{on}/I_{off} increases with pH V_{th} weakly increases with pH (~ 0.03 V/pH for p-CNT FET) Subthreshold slope decreases at pH 10 (ΔV_{gs} increases with pH) P-type, No ambipolarity	I_{on} increases with pH I_{off} increases with pH I_{on}/I_{off} increases with pH V_{th} strongly increases with pH (~ 0.1 V/pH for p-CNT FET) Subthreshold slope increases at pH 10 (ΔV_{gs} decreases with pH) Ambipolarity, strongest at pH 7 I_{Dirac} increases at pH 10 V_{Dirac} increases at pH 10
BBS	I_{on} increases with pH, I_{off} increases with pH I_{on}/I_{off} tends to increase with pH V_{th} increases with pH Subthreshold slope decreases with pH (ΔV_{gs} increases with pH) P-type (negligible ambipolarity at pH 6, 7 and 8)	I_{on} increases with pH, No trend on I_{off} I_{on}/I_{off} tends to increase with pH V_{th} increases with pH Subthreshold slope increases with pH (ΔV_{gs} decreases with pH) P-type (negligible ambipolarity at pH 5 and 9)

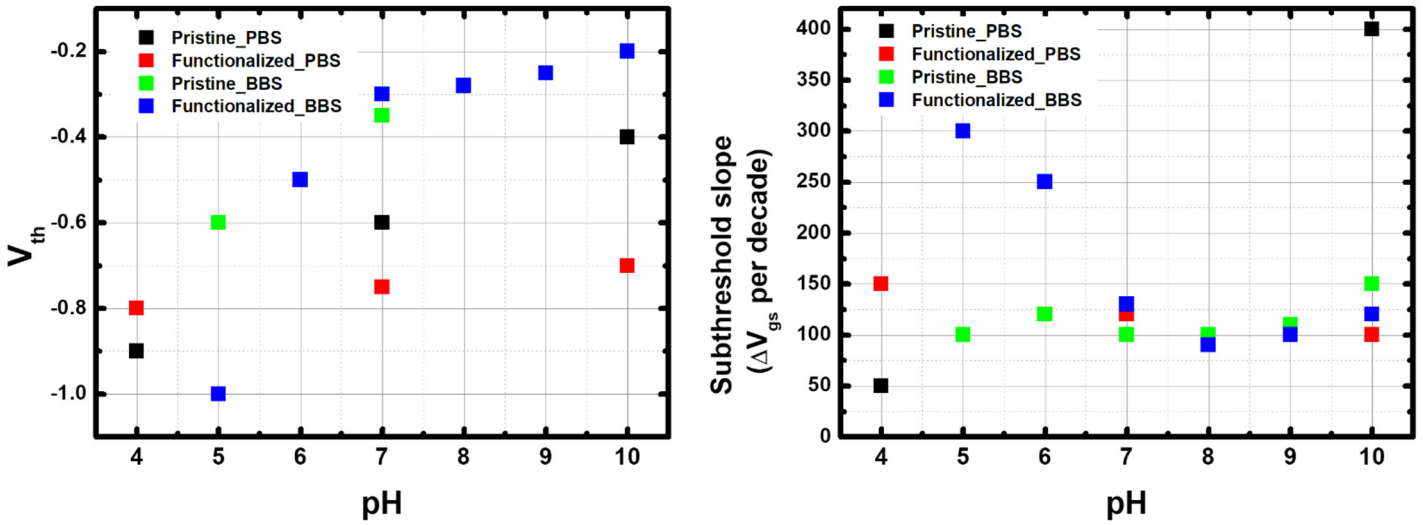

Figure 57. (Left) V_{th} and (Right) Subthreshold slope of p-CNT FETs and f-CNT FETs in different buffer solutions.

5.2.5 CNT-FET sensing for detection of other analytes

For the further study of CNT-FETs water quality monitoring sensors, we also tested both p-CNT FETs and f-CNT FETs with several different analytes in PBS at pH 7. Measurement parameters are the same for all analytes: V_{ds} is fixed at +0.8 V and V_{gs} is fixed at -0.8 V in the analysis. To be noted, we did not observe the ambipolarity of f-CNT FET during these studies.

5.2.5.1 Phosphate (PO_4^-) detection

In the previous section, we investigated the pH response of p-CNT FET and f-CNT FET in both phosphate buffer solution (PBS) and borate buffer solution (BBS). Based on the results, the ambipolar behavior of f-CNT FETs is observed only in PBS. In order to study the effect of weak salts in buffer solutions (phosphate ion in PBS and boric oxide ion in BBS, respectively), drain current of both p-CNT FETs and f-CNT FETs is measured with respect to different concentration of phosphate ion in BBS from 1 ppb to 100 ppm (Figure 58). To be noted, pH of each BBS with different phosphate concentration is stable as shown in Figure 59. In addition, both p-CNT FETs and f-CNT FETs have been exposed to water for 10 months, hence the conjugated polymer (FF-UR) may be degraded in case of f-CNT FETs. Neither p-CNT FETs (Figure 58 (a)) nor f-CNT FETs (Figure 58 (b)) show any significant response to phosphate ion.

Figure 60 shows the logarithmic I-V transfer curve of f-CNT FETs in pH 7 BBS, with respect to different concentration of phosphate ion from 0 to 100 ppm. Indeed, each f-CNT FETs do not show significant response to phosphate ion in BBS and remain their electrical behavior. Based on these results, we can conclude that the effect of phosphate ion in PBS is negligible.

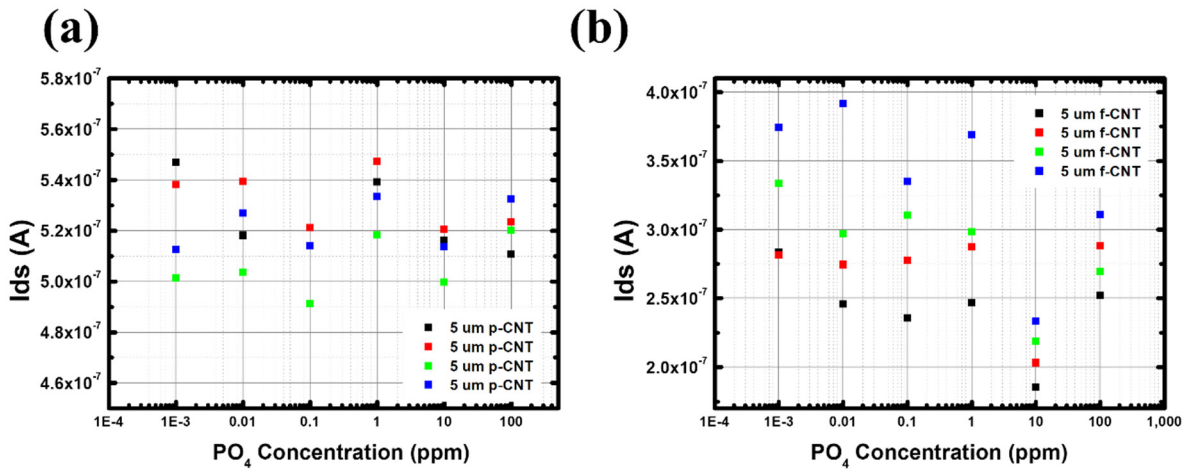

Figure 58. PO_4^- Response of (a) p-CNT FETs and (b) f-CNT FETs in Borate buffer solution (BBS) at pH 7. Each color shows different transistor with identical channel length of 5 µm.

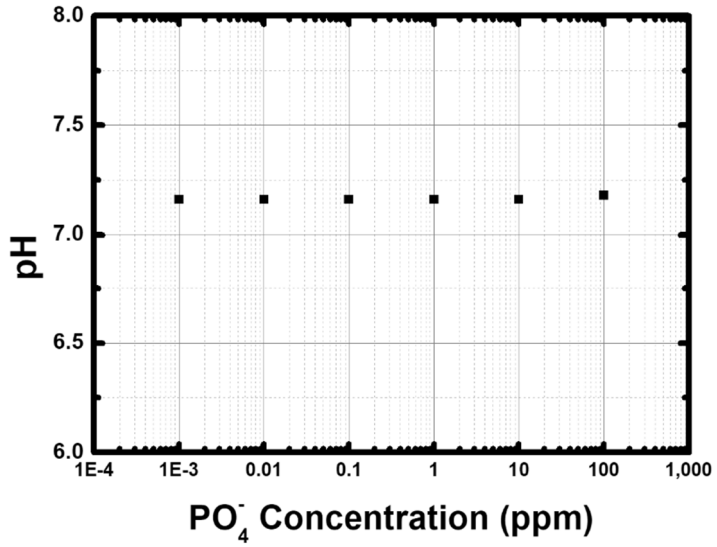

Figure 59. Measured pH values with respect to different PO_4^- concentration in Borate buffer solution (BBS) at pH 7.

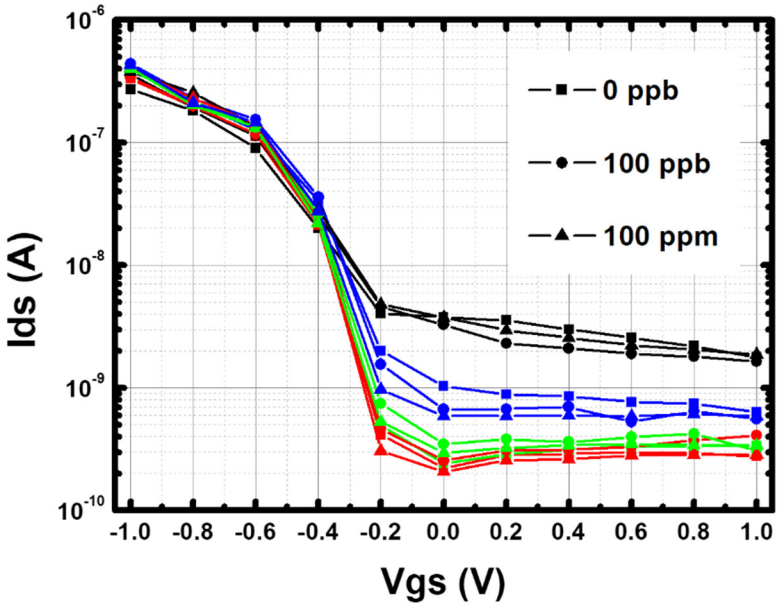

Figure 60. I-V transfer curve of f-CNT FETs at different phosphate ion concentration in borate buffer solution (BBS). Each symbol indicates the concentration of phosphate ion in BBS and each color indicates different p-CNT FETs with channel length of 5 μm.

5.2.5.2 Strong response to Mg^{2+} ($MgCl_2$)

For Mg^{2+} detection, we prepared two different solutions; 0.1 M phosphate buffer solution (PBS) and 0.1 M PBS containing 0.1 M concentration of $MgCl_2$. Both p-CNT FETs (Figure 61 (a)) and f-CNT FETs (Figure 61 (b)) respond to 0.1 M $MgCl_2$ with a strong decrease of drain current immediately after addition of $MgCl_2$ in PBS.

In order to investigate the $MgCl_2$ detection of CNT-FETs in details, borate buffer solutions (BBS) with different $MgCl_2$ concentration (0 M, 0.1 mM, 1 mM and 10 mM) are tested with p-CNT FETs (Figure 62). To be noted, BBS is used in this experiment since linear pH sensitivity of both p-CNT FETs and f-CNT FETs is observed, which may eliminate the risk of interference by phosphate ion in PBS. As shown in the figure, drain current of p-CNT FETs is saturated at low $MgCl_2$ concentration until 0.1 mM in BBS. The drain current decreases from 1 mM of $MgCl_2$ concentration to 10 mM. The result suggests that the limit of detection (LOD) of Mg^{2+} is around 0.1 mM, but the detailed sensitivity between 0.1 mM and 1 mM has not yet been studied. The differences between p-CNTFET and f-CNTFET were not investigated either.

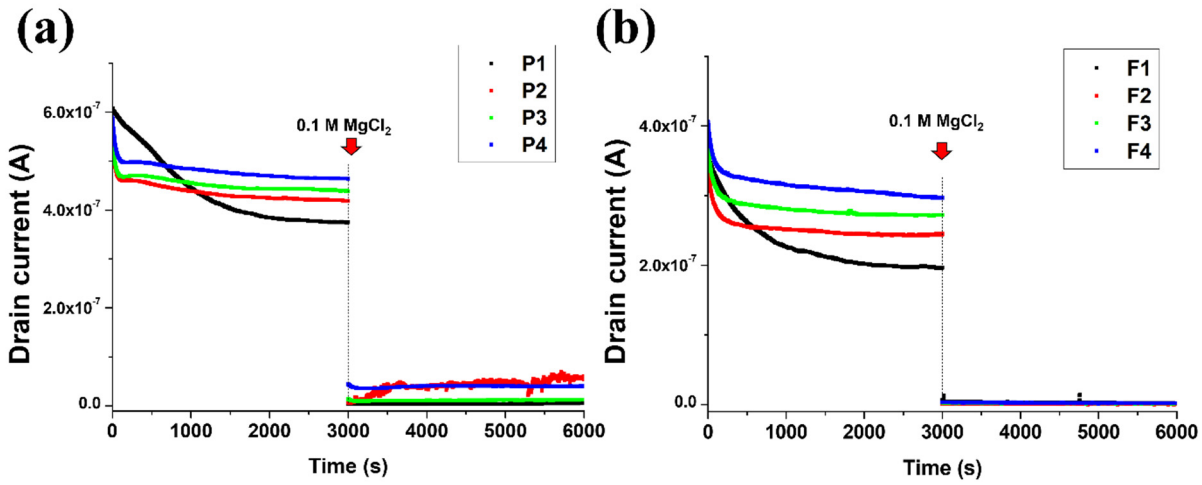

Figure 61. Response to 0.1 M $MgCl_2$ of (a) p-CNT FETs and (b) f-CNT FETs in phosphate buffer solution (PBS) at pH 7. Each color shows different transistors with identical channel length of 5 µm.

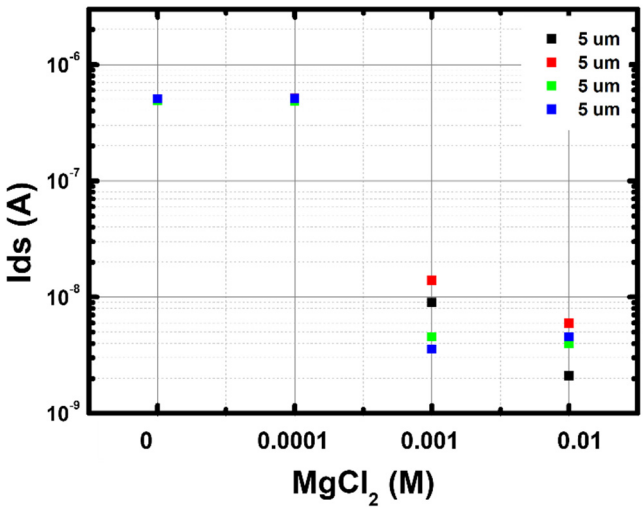

Figure 62. $MgCl_2$ Response of p-CNT FETs in Borate buffer solution (BBS) at pH 7. Each color shows different transistor with identical channel length of 5 µm.

5.2.5.3 Response to NH_4Cl, HNO_3 and KNO_3

We also studied the sensing response of p-CNTFET to several other analytes; NH_4Cl, HNO_3 and KNO_3. For these measurements, 5 ml of each solution is added in 100 ml of pH 7 phosphate buffer solution (PBS) with concentration of 0.1 M, respectively (Figure 63).

In the case of NH_4^+ (ammonium ion) detection (Figure 63 (a)), the drain current decreases when NH_4Cl solution is added in PBS, then a sharp upward peak current is detected after around 100 seconds. Finally, the current value stabilizes at a lower value than the initial current. It suggests a sensitivity to NH_4Cl

HNO_3 (Figure 63 (b)) and KNO_3 (Figure 63 (c)) are both tested for study the response to nitrate independently of the counter ion (K^+ or H^+). In PBS, the addition of H+ ions is not expected to impact the pH significantly. After an initial small peak, there is no significant response above noise level in the steady state for these two salts.

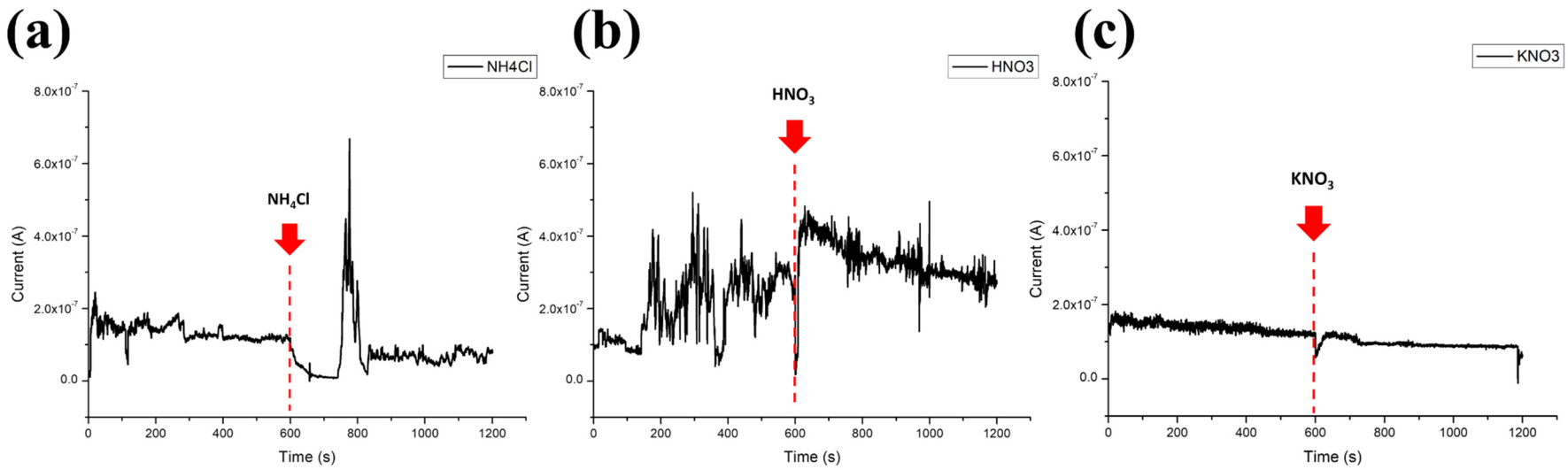

Figure 63. Real-time measured drain current of p-CNT FET with several different analytes; (a) Na_4Cl (b) HNO_3 and (c) KNO_3 in pH 7 phosphate buffer solution (PBS).

5.3 Conclusion

Pristine CNT-FETs responded to pH within linear and wide detection range from pH 3 to pH 9 without hysteresis, and also showed in phosphate buffer solution sensitivity comparable to the best previous results on CNT-based pH sensors. By contrast, f-CNT FET showed pH response with a narrow detection range from pH 7 to pH 9 but over 10 times larger sensitivity compared to p-CNT-FET. The detection range of f-CNT FET is relatively limited compared to p-CNT FET due to the high threshold voltage (Vth) below pH 7. p-CNT FET and f-CNT FET are also measured in borate buffer solution (BBS) to verify the effect of weak salts in different buffers. Contrary to the result from PBS, both p-CNT FET and f-CNT FET showed linear pH response from pH 5 to pH 9 in BBS due to the relatively weaker Vth modulation. This result may be due to the degradation of conjugated polymer (FF-UR) exposed in water.

The lifetime of both types of CNT-FETs stored in deionized water is remarkably long (More than 9 months with I_{on}/I_{off} ratio larger than ~10^3). While p-CNTFET keep their p-type behavior with only minor changes in I_{on} and I_{off}, f-CNT FETs progressively lose their ambipolar behavior over the course of the 9 months. This result confirms that the ambipolarity of the f-CNT FETs is induced by non-covalently functionalized polymer on the sidewall of CNTs, which is degrading over time in water.

The response of our CNTFET to other analytes (Phosphate, $MgCl_2$, NH_4Cl, KNO_3 and HNO_3) are also tested in buffer solution. Both p-CNT FETs and f-CNT FETs responded to $MgCl_2$ as Mg^{2+} ion with the limit of detection of around 0.1 mM; they both do not respond to phosphate. A small response is observed to NH4Cl with p-CNT-FET, while no significant response is observed for the other analytes.

6 General Conclusion

In this dissertation, we demonstrated the fabrication and characterization of CNT-based field-effect transistors as pH sensors by printing pristine CNTs or polymer-functionalized CNTs.

In terms of substrate preparation, we designed an unique transistor structure with double insulating layer consisting of Si_3N_4 and SiO_2 layer since Si_3N_4 layer has a significantly better diffusion barrier against water molecules and sodium ions than a SiO_2 layer.

We optimized the ink-jet printing process to improve the electrical characteristics (I_{on} and I_{off}) of the CNT-FETs. The initial ink formulation was 0.005 wt% of SWCNT in *o*-DCBZ. It yielded CNT-FET with I_{on}/I_{off} of less than 10. This formulation was optimized by changing the solvent from *o*-DCBZ to NMP, thus by passing the issue of the sono-chemical degradation of *o*-DCBZ. NMP-based CNT ink turned out to be more stable without agglomerates. In addition, CNT concentration in NMP was lowered to 0.001 wt%. The resulting formulation allowed to ink-jet print CNT-FETs with I_{on}/I_{off} ratio up to ~10^3.

After the optimized CNT ink fabrication and ink-jet printing process, we first characterized both p-CNT FETs and f-CNT FETs in ambient condition to study the electrical behavior of the devices in air. Large gate voltage (~ 60 V) was applied to turn on the transistor with small subthreshold slope but large hysteresis is observed, while relatively small drain voltage (~ 5V) is needed.

Comparison of electrical characteristics before and after PMMA passivation was also performed to investigate the effect of passivation process. PMMA passivation of CNT-FETs not only improved the electrical performance (Larger I_{on}, smaller I_{off}, Larger I_{on}/I_{off} ratio) of both p-CNT FETs and f-CNT FETs, but also increased the durability of the devices by preventing the physical loss of CNTs in water. However, the passivation process did not significantly reduce the hysteresis of CNT-FETs in the air.

Passivated p-CNT FETs showed high I_{on}/I_{off} ratio (~10^4) compared to other reported CNT-FETs in aqueous solution, with acceptable reproducibility of threshold voltage, I_{on} and I_{off} (respectively 20%, 18% and 43% standard relative deviation). By contrast, polymer-functionalized CNT-FETs showed clear ambipolar behavior; with I_{on}/I_{off} ratio (~10^3) at Dirac point (V_{gs} ~-0.1 V), and lower I_{on}/I_{off} ratio of ~10^2 compared to p-CNT FETs due to their ambipolar behavior. f-CNT FETs have lower reproducibility compared to p-CNT FETs. This ambipolarity of f-CNT FETs may be due to the non-covalent functionalization of CNT by π-stacking which leads to a superposition of the density of states of the CNT and of the energy level of the functionalization molecules.

In terms of pH sensitivity, our p-CNT FETs and f-CNT FETs both showed remarkable sensitivity to pH in PBS and BBS with significantly long lifetime. In general, p-CNT FETs showed linear and non-hysteresis detection, whereas f-CNT FETs showed very high sensitivity within narrow pH range. We also compared the electrical features (I_{on}, I_{off},

subthreshold slope and ambipolarity) of p-CNT FETs and f-CNT FETs in different buffer solutions in detail to investigate the effect of functionalization and type of buffer solution in terms of pH sensing. Several different analytes are also tested to investigate the selectivity of CNT-FET devices, while strong response to Mg^{2+} is only observed.

The main goal of this thesis is to fabricate a low-cost, reproducible and pH sensitive CNT-FET device by ink-jet printing process. Overall, the thesis achieved the goal and showed the promise of the technology, though a lot of work remain for future applications.

7 Perspectives

7.1 Further study on the detection of other analytes

In this work, we only preliminarily studied the sensing response to other analytes as PO_4^-, Mg^{2+}, Na_4Cl, HNO_3 and KNO_3. This work should be expanded, and there are still a large number of possible target analytes (i.e. micronutrients, heavy metals, nitrogen, disinfectants, sulfur, etc) to investigate. In addition, sensing response of p-CNT FETs and f-CNT FETs should be compared.

7.2 Interference study in detail

One of the most important factors in chemical sensors is selectivity without any interference by other analytes. CNTs are expected to have high sensitivity to target analyte due to large effective surface area. However, it has been reported that pristine CNT-based chemical sensors have limited selectivity to both gas- and liquid-phase sensing. Hence, f-CNT FETs may have advantages in terms of selectivity since the functionalizing molecules can be selected for their electron affinity to the certain analytes. Interference study with a quantitative comparison between p-CNT FETs and f-CNT FETs should be carried out.

7.3 Other materials and functionalization methods on CNT-FETs.

We functionalized the SWCNTs with as specific conjugated polymer by non-covalent functionalization process. However, there are other functional probes, and functionalization methods described in section 3.2.5.2. Different functionalization methods (i.e. top-coating) for CNT-FETs could be performed and characterized for selective sensing. In addition, other materials (i.e. imogolite) could also be functionalized on SWCNTs for selective sensing.

8 References

[1] D. Hinrichsen and H. Tacio, “The coming freshwater crisis is already here,” *Worldfile Discip. poluição Artig. introdução azizullah*, pp. 1–26, 2002.

[2] A. Solomon, Z. Ahmed, K. Biruktawit, D. Amare, A. Solomon, and Z. Endalew, “Bacteriological analysis of drinking water sources,” *African J. Microbiol. Res.*, vol. 5, no. 18, pp. 2638–2641, 2016.

[3] A. Aydin, “The microbiological and physico-chemical quality of groundwater in West Thrace, Turkey,” *Polish J. Environ. Stud.*, vol. 16, no. 3, pp. 377–383, 2007.

[4] E. Gyamfi *et al.*, “Chemical analysis of potable water samples from selected suburbs of Accra, Ghana,” *Proc. Int. Acad. Ecol. Environ. Sci.*, vol. 2, no. 2, pp. 118–127, Jan. 2012.

[5] R. M. Clark and J. A. Coyle, “Measuring and Modeling Variations in Distribution System Water Quality,” *J. Am. Water Works Assoc.*, 1990.

[6] J. Raich, “Review of sensors to monitor water quality,” *Eur. Ref. Netw. Crit. Infrastruct. Prot.*, no. December, 2013.

[7] P. Kruse, “Review on water quality sensors,” *J. Phys. D. Appl. Phys*, vol. 51, no. 20, p. aabb93, 2018.

[8] J. Bhardwaj, K. K. Gupta, and R. Gupta, “A review of emerging trends on water quality measurement sensors,” in *Proceedings - International Conference on Technologies for Sustainable Development, ICTSD 2015*, 2015.

[9] S. Mao, J. Chang, G. Zhou, and J. Chen, “Nanomaterial-enabled Rapid Detection of Water Contaminants,” *Small*, vol. 11, no. 40, pp. 5336–5359, 2015.

[10] R. Soni, M. Soni, and D. P. Shukla, “Emerging Techniques and Materials for Water Pollutants Detection,” in *Sensors in Water Pollutants Monitoring: Role of Material*, D. Pooja, P. Kumar, P. Singh, and S. Patil, Eds. Singapore: Springer Singapore, 2020, pp. 277–297.

[11] M. R. Willner and P. J. Vikesland, “Nanomaterial enabled sensors for environmental contaminants,” *J. Nanobiotechnology*, 2018.

[12] F. Arduini, J. Q. Calvo, G. Palleschi, D. Moscone, and A. Amine, “Bismuth-modified electrodes for lead detection,” *TrAC Trends Anal. Chem.*, vol. 29, no. 11, pp. 1295–1304, 2010.

[13] S. Yao, P. Swetha, and Y. Zhu, “Nanomaterial-Enabled Wearable Sensors for Healthcare,” *Adv. Healthc. Mater.*, vol. 7, no. 1, p. 1700889, 2018.

[14] J. Kong *et al.*, “Nanotube molecular wires as chemical sensors,” *Science (80-.).*, vol. 287, no. 5453, pp. 622–625, Jan. 2000.

[15] V. Schroeder, S. Savagatrup, M. He, S. Lin, and T. M. Swager, “Carbon Nanotube Chemical Sensors,” *Chem. Rev.*, vol. 119, no. 1, pp. 599–663, Jan. 2019.

[16] F. Arduini, S. Cinti, V. Scognamiglio, and D. Moscone, “13 - Nanomaterial-based sensors,” in *Handbook of Nanomaterials in Analytical Chemistry*, C. M. Hussain, Ed. Elsevier, 2020, pp. 329–359.

[17] M. S. Dresselhaus, “Science of Fullerenes and Carbon Nanotubes,” *Sci. Fullerenes Carbon Nanotub.*, 1996.

[18] L. Hu, D. S. Hecht, and G. Grüner, “Carbon Nanotube Thin Films: Fabrication, Properties, and Applications,” *Chem. Rev.*, vol. 110, no. 10, pp. 5790–5844, Oct. 2010.

[19] G. Cho, S. Assouzi, G. Zucchi, and B. Lebental, “Electrical and electrochemical sensors based on carbon nanotubes for the monitoring of chemicals in drink water - A review,” *Prog.*, 2021.

[20] M. P. Anantram and F. Léonard, “Physics of carbon nanotube electronic devices,” *Reports Prog. Phys.*, vol. 69, no. 3, pp. 507–561, 2006.

[21] A. Tyagi, K. Tripathi, and R. Gupta, “Recent progress on micro-scale energy storage devices and future aspects,” *J. Mater. Chem. A*, vol. 3, Sep. 2015.

[22] S. Chung, K. Cho, and T. Lee, “Recent Progress in Inkjet-Printed Thin-Film Transistors,” *Adv. Sci.*, vol. 6, no. 6, p. 1801445, Mar. 2019.

[23] S. K. Karunakaran *et al.*, “Recent progress in inkjet-printed solar cells,” *J. Mater. Chem. A*, vol. 7, no. 23, pp. 13873–13902, 2019.

[24] M. Singh, H. M. Haverinen, P. Dhagat, and G. E. Jabbour, “Inkjet printing-process and its applications,” *Adv. Mater.*, vol. 22, no. 6, pp. 673–685, 2010.

[25] F. Michelis *et al.*, “Highly reproducible, hysteresis-free, flexible strain sensors by inkjet printing of carbon nanotubes,” *Carbon N. Y.*, vol. 95, pp. 1020–1026, 2015.

[26] R. P. Tortorich, “Carbon Nanotube Inkjet Printing for Flexible Electronics and Chemical Sensor Applications,” 2014.

[27] T. Mustonen, *Inkjet printing of carbon nanotubes for electronic applications*. 2009.

[28] C. E. Rahm, F. Torres-Canas, P. Gupta, P. Poulin, and N. T. Alvarez, “Inkjet Printed Multi-walled Carbon Nanotube Sensor for the Detection of Lead in Drinking Water,” *Electroanalysis*, vol. 32, no. 7, pp. 1533–1545, 2020.

[29] M. Hilder, B. Winther-Jensen, and N. B. Clark, “Paper-based, printed zinc–air battery,” *J. Power*

Sources, vol. 194, no. 2, pp. 1135–1141, 2009.

[30] P. Yang, L. Zhang, D. J. Kang, R. Strahl, and T. Kraus, "High-Resolution Inkjet Printing of Quantum Dot Light-Emitting Microdiode Arrays," *Adv. Opt. Mater.*, vol. 8, no. 1, p. 1901429, Jan. 2020.

[31] B. Huber, P. B. Popp, M. Kaiser, A. Ruediger, and C. Schindler, "Fully inkjet printed flexible resistive memory," *Appl. Phys. Lett.*, vol. 110, no. 14, p. 143503, Apr. 2017.

[32] A. M. Münzer, K. Melzer, M. Heimgreiter, and G. Scarpa, "Random CNT network and regioregular poly(3-hexylthiophen) FETs for pH sensing applications: A comparison," *Biochim. Biophys. Acta - Gen. Subj.*, vol. 1830, no. 9, pp. 4353–4358, 2013.

[33] J. Y. Pyo and W. J. Cho, "High-sensitivity pH sensor using separative extended-gate field-effect transistors with single-walled carbon-nanotube networks," *Jpn. J. Appl. Phys.*, vol. 57, no. 4, 2018.

[34] M. Park, H. S. Kim, T. Kim, J. Kim, S. Seo, and B. Y. Lee, "Real-time monitoring of microbial activity using hydrogel-hybridized carbon nanotube transistors," *Sensors Actuators, B Chem.*, vol. 263, pp. 486–492, 2018.

[35] T. H. Kim, J. Lee, and S. Hong, "Highly selective environmental nanosensors based on anomalous response of carbon nanotube conductance to mercury ions," *J. Phys. Chem. C*, 2009.

[36] C. S. Lee, Y. Ju, J. Kim, and T. H. Kim, "Electrochemical functionalization of single-walled carbon nanotubes with amine-terminated dendrimers encapsulating Pt nanoparticles: Toward facile field-effect transistor-based sensing platforms," *Sensors Actuators, B Chem.*, vol. 275, no. June, pp. 367–372, 2018.

[37] S. Joshi *et al.*, "Ambient Processed, Water-Stable, Aqueous-Gated sub 1 V n-type Carbon Nanotube Field Effect Transistor," *Scientific Reports*, vol. 8, no. 1. 2018.

[38] P. R. Mudimela *et al.*, "Single-Walled Carbon Nanotube Network Field Effect Transistor as a Humidity Sensor," *J. Sensors*, vol. 2012, pp. 1–7, 2012.

[39] A. I. Chernov *et al.*, "Field Effect Transistor Based on Solely Semiconducting Single-Walled Carbon Nanotubes for the Detection of 2-Chlorophenol," *Phys. Status Solidi Basic Res.*, vol. 255, no. 1, pp. 1–5, 2018.

[40] H. O. Pierson, W. A. Publishing, and N. York, *Handbook of Chemical Vapor Deposition (CVD)*. 1999.

[41] D. S. Wuu *et al.*, "Water and oxygen permeation of silicon nitride films prepared by plasma-enhanced chemical vapor deposition," *Surf. Coatings Technol.*, vol. 198, no. 1-3 SPEC. ISS., pp. 114–117, 2005.

[42] C. Cazako *et al.*, “Hypothetic impact of chemical bonding on the moisture resistance of amorphous SixNyHz by plasma-enhanced chemical vapor deposition To cite this version : HAL Id : hal-02968666 T echnology Hypothetic impact of chemical bonding on the moisture resistance of,” pp. 0–6, 2020.

[43] Q. Zhang, “Carbon Nanotubes and Their Applications Carbon Nanotubes and Their Applications,” 2012.

[44] R. S. Ruoff, D. Qian, and W. K. Liu, “Mechanical properties of carbon nanotubes: Theoretical predictions and experimental measurements,” *Comptes Rendus Phys*, vol. 4, no. 9, pp. 993–1008, 2003.

[45] M. I. Katsnelson, *Graphene: Carbon in two dimensions*. Cambridge university press, 2012.

[46] R. Zhang, Y. Zhang, Q. Zhang, H. Xie, W. Qian, and F. Wei, “Growth of half-meter long carbon nanotubes based on Schulz-Flory distribution,” *ACS Nano*, 2013.

[47] R. Jasti, J. Bhattacharjee, J. B. Neaton, and C. R. Bertozzi, “Synthesis, characterization, and theory of [9]-, [12]-, and [18]cycloparaphenylene: carbon nanohoop structures,” *J. Am. Chem. Soc.*, vol. 130, no. 52, pp. 17646–17647, Dec. 2008.

[48] X. Wang *et al.*, “Fabrication of ultralong and electrically uniform single-walled carbon nanotubes on clean substrates,” *Nano Lett.*, 2009.

[49] P. A. Thrower and H. M. Cheng, “Growth of nanocarbons by catalysis and their applications,” *MRS Bull*, vol. 42, no. 11, pp. 790–793, 2017.

[50] T. J. Sisto, L. N. Zakharov, B. M. White, and R. Jasti, “Towards pi-extended cycloparaphenylenes as seeds for CNT growth: Investigating strain relieving ring-openings and rearrangements,” *Chem. Sci.*, vol. 7, no. 6, pp. 3681–3688, 2016.

[51] M. S. Dresselhaus, G. Dresselhaus, and R. Saito, “Physics of carbon nanotubes,” *Carbon N. Y.*, no. 33, pp. 883–891, 1995.

[52] J. W. Mintmire, B. I. Dunlap, and C. T. White, “Are fullerene tubules metallic?,” *Phys. Rev. Lett.*, vol. 68, no. 5, pp. 631–634, Feb. 1992.

[53] N. Hamada, S. Sawada, and A. Oshiyama, “New one-dimensional conductors: Graphitic microtubules,” *Phys. Rev. Lett.*, vol. 68, no. 10, pp. 1579–1581, Mar. 1992.

[54] J. M. Irudayaraj, *Biomedical Nanosensors*. Jenny Stanford Publishing, 2012.

[55] Y. T. Ong, A. L. Ahmad, S. Hussein, S. Zein, and S. H. Tan, “A review on carbon nanotubes in an

environmental protection and gree engineering perspective.," *Brazilian J Chem Engi*, 2010.

[56] P. M. Ajayan and T. W. Ebbesen, "Nanometre-size tubes of carbon, Reports Prog," *Phys*, 1997.

[57] Y. Zhang, Y. Bai, and B. Yan, "Functionalized carbon nanotubes for potential medicinal applications," *Drug Discov. Today*, vol. 15, no. 11–12, pp. 428–435, 2010.

[58] E. Abbasi *et al.*, "Dendrimers: Synthesis, applications, and properties," *Nanoscale Research Letters*. 2014.

[59] M. José-Yacamán, M. Miki-Yoshida, L. Rendón, and J. G. Santiesteban, "Catalytic growth of carbon microtubules with fullerene structure," *Appl. Phys. Lett.*, 1993.

[60] L. Chico, V. H. Crespi, L. X. Benedict, S. G. Louie, and M. L. Cohen, "Pure carbon nanoscale devices: Nanotube heterojunctions," *Phys. Rev. Lett.*, 1996.

[61] R. Hirlekar, M. Yamagar, H. Garse, and M. Vij, "CARBON NANOTUBES AND ITS APPLICATIONS: A REVIEW," *Asian J. Pharm. Clin. Res.*, 2009.

[62] P. X. Hou, S. Bai, Q. H. Yang, C. Liu, and H. M. Cheng, "Multi-step purification of carbon nanotubes," *Carbon N. Y.*, 2002.

[63] A. Thess *et al.*, "Crystalline ropes of metallic carbon nanotubes," *Science (80-.).*, vol. 273, no. 5274, pp. 483–487, 1996.

[64] M. L. Terranova, V. V. Sessa, and M. Rossi, "The World of Carbon Nanotubes: An Overview of CVD Growth Methodologies," *Chem. Vap. Depos.*, vol. 12, no. 6, pp. 315–325, Aug. 2006.

[65] A. L. Gorkina *et al.*, "Transparent and conductive hybrid graphene/carbon nanotube films," *Carbon N. Y.*, 2016.

[66] K. A. Williams, B. K. Pradhan, P. C. Eklund, M. K. Kostov, and M. W. Cole, "Raman Spectroscopic Investigation of H2, HD, and D2 Physisorption on Ropes of Single-Walled, Carbon Nanotubes," *Phys. Rev. Lett.*, vol. 88, no. 16, p. 165502, 2002.

[67] C. Journet *et al.*, "Large-scale production of single-walled carbon nanotubes by the electric-arc technique," *Nature*, vol. 388, no. 6644, pp. 756–758, 1997.

[68] S. Mohajeri, A. Dolati, and S. S. Rezaie, "Electrochemical sensors based on functionalized carbon nanotubes modified with platinum nanoparticles for the detection of sulfide ions in aqueous media," *J. Chem. Sci.*, vol. 131, no. 3, p. 21, 2019.

[69] A. Safavi, N. Maleki, and M. M. Doroodmand, "Fabrication of a selective mercury sensor based on the adsorption of cold vapor of mercury on carbon nanotubes: Determination of mercury in industrial

wastewater," *J. Hazard. Mater.*, vol. 173, no. 1–3, pp. 622–629, 2010.

[70] E. S. Forzani *et al.*, "Tuning the chemical selectivity of SWNT-FETs for detection of heavy-metal ions," *Small*, 2006.

[71] X. Zhou, F. Boey, and H. Zhang, "Controlled growth of single-walled carbon nanotubes on patterned substrates," *Chem. Soc. Rev.*, vol. 40, no. 11, pp. 5221–5231, 2011.

[72] R. Seidel *et al.*, "High-Current Nanotube Transistors," *Nano Lett.*, vol. 4, no. 5, pp. 831–834, May 2004.

[73] G. Zhang *et al.*, "Selective Etching of Metallic Carbon Nanotubes by Gas-Phase Reaction," *Science (80-.).*, vol. 314, no. 5801, pp. 974–977, 2006.

[74] Y. Y. Y. Zhang, Y. Y. Y. Zhang, X. Xian, J. Zhang, and Z. Liu, "Sorting out Semiconducting Single-Walled Carbon Nanotube Arrays by Preferential Destruction of Metallic Tubes Using Xenon-Lamp Irradiation," *J. Phys. Chem. C*, vol. 112, no. 10, pp. 3849–3856, Mar. 2008.

[75] Q. Zhao *et al.*, "Real-Time Observation of Carbon Nanotube Etching Process Using Polarized Optical Microscope," *Adv. Mater.*, vol. 29, no. 30, p. 1701959, Aug. 2017.

[76] T. Chen *et al.*, "Highly enhanced gas sensing in single-walled carbon nanotube-based thin-film transistor sensors by ultraviolet light irradiation," *Nanoscale Res. Lett.*, vol. 7, no. 1, p. 644, 2012.

[77] T. Lei, I. Pochorovski, and Z. Bao, "Separation of Semiconducting Carbon Nanotubes for Flexible and Stretchable Electronics Using Polymer Removable Method," *Acc. Chem. Res.*, vol. 50, no. 4, pp. 1096–1104, Apr. 2017.

[78] Y. Liao *et al.*, "Carbon nanotube/polyaniline composite nanofibers: Facile synthesis and chemosensors," *Nano Lett.*, vol. 11, no. 3, pp. 954–959, Mar. 2011.

[79] L. Hsu, P. R. Selvaganapathy, E. Houqe, and P. Kruse, "A carbon nanotube based resettable sensor for measuring free chlorine in drinking water," in *Proceedings of IEEE Sensors*, 2014.

[80] G. Stojanović *et al.*, "Flexible sensors based on two conductive electrodes and MWCNTs coating for efficient pH value measurement," *J. Alloys Compd.*, vol. 794, pp. 76–83, Jul. 2019.

[81] L. Wei *et al.*, "Highly sensitive detection of trinitrotoluene in water by chemiresistive sensor based on noncovalently amino functionalized single-walled carbon nanotube," *Sensors Actuators, B Chem.*, 2014.

[82] M. Park *et al.*, "Real-time monitoring of microbial activity using hydrogel-hybridized carbon nanotube transistors," *Sensors Actuators, B Chem.*, vol. 263, pp. 486–492, 2018.

[83] R. Tortorich and J.-W. J.-W. Choi, “Inkjet Printing of Carbon Nanotubes,” *Nanomaterials*, vol. 3, no. 3, pp. 453–468, Jul. 2013.

[84] S. Kholghi Eshkalak, A. Chinnappan, W. A. D. M. Jayathilaka, M. Khatibzadeh, E. Kowsari, and S. Ramakrishna, “A review on inkjet printing of CNT composites for smart applications,” *Appl. Mater. Today*, vol. 9, pp. 372–386, 2017.

[85] M. Kaempgen and S. Roth, “Transparent and flexible carbon nanotube/polyaniline pH sensors,” *J. Electroanal. Chem.*, vol. 586, no. 1, pp. 72–76, 2005.

[86] J.-H. Kwon, K.-S. Lee, Y.-H. Lee, and B.-K. Ju, “Single-Wall Carbon Nanotube-Based pH Sensor Fabricated by the Spray Method,” *Electrochem. Solid-State Lett.*, vol. 9, no. 9, p. H85, 2006.

[87] P. Gou, N. D. Kraut, I. M. Feigel, and A. Star, “Rigid versus flexible ligands on carbon nanotubes for the enhanced sensitivity of cobalt ions,” *Macromolecules*, 2013.

[88] G. L. Goh, S. Agarwala, Y. J. Tan, and W. Y. Yeong, “A low cost and flexible carbon nanotube pH sensor fabricated using aerosol jet technology for live cell applications,” *Sensors Actuators, B Chem.*, vol. 260, pp. 227–235, 2018.

[89] K. F. Lei, K. F. Lee, and S. I. Yang, “Fabrication of carbon nanotube-based pH sensor for paper-based microfluidics,” *Microelectron. Eng.*, vol. 100, pp. 1–5, 2012.

[90] J. Zhao, A. Hashmi, J. Xu, and W. Xue, “A compact lab-on-a-chip nanosensor for glycerol detection,” *Appl. Phys. Lett.*, vol. 100, no. 24, 2012.

[91] P. Gou *et al.*, “Carbon nanotube chemiresistor for wireless pH sensing,” *Sci. Rep.*, 2014.

[92] P. Stokes and S. I. Khondaker, “Directed assembly of solution processed single-walled carbon nanotubes via dielectrophoresis: From aligned array to individual nanotube devices,” *J. Vac. Sci. Technol. B, Nanotechnol. Microelectron. Mater. Process. Meas. Phenom.*, vol. 28, no. 6, p. C6B7-C6B12, 2010.

[93] P. Li, C. M. Martin, K. K. Yeung, and W. Xue, “Dielectrophoresis aligned single-walled carbon nanotubes as pH sensors,” *Biosensors*, vol. 1, no. 1, pp. 23–35, 2011.

[94] S. Blatt, “Dielectrophoresis of single-walled carbon nanotubes,” *Wissenschaftliche Berichte FZKA*, vol. 7431, no. August, 2008.

[95] R. Krupke, F. Hennrich, H. B. Weber, M. M. Kappes, and H. v. Löhneysen, “Simultaneous Deposition of Metallic Bundles of Single-walled Carbon Nanotubes Using Ac-dielectrophoresis,” *Nano Lett.*, vol. 3, no. 8, pp. 1019–1023, Aug. 2003.

[96] D. Jung, D. Kim, K. H. Lee, L. J. Overzet, and G. S. Lee, "Transparent film heaters using multi-walled carbon nanotube sheets," *Sensors Actuators, A Phys.*, vol. 199, pp. 176–180, 2013.

[97] P. G. Collins, M. S. Arnold, and P. Avouris, "Engineering carbon nanotubes and nanotube circuits using electrical breakdown," *Science (80-.).*, vol. 292, no. 5517, pp. 706–709, 2001.

[98] T. Zhang, S. Mubeen, N. V. Myung, and M. A. Deshusses, "Recent progress in carbon nanotube-based gas sensors," *Nanotechnology*, vol. 19, no. 33, p. 332001, 2008.

[99] A. M. Andringa, J. R. Meijboom, E. C. P. Smits, S. G. J. Mathijssen, P. W. M. Blom, and D. M. De Leeuw, "Gate-bias controlled charge trapping as a mechanism for NO2 detection with field-effect transistors," *Adv. Funct. Mater.*, vol. 21, no. 1, pp. 100–107, 2011.

[100] S. Banerjee, T. Hemraj-Benny, and S. S. Wong, "Covalent surface chemistry of single-walled carbon nanotubes," *Advanced Materials*. 2005.

[101] D. A. Britz and A. N. Khlobystov, "Noncovalent interactions of molecules with single walled carbon nanotubes," *Chemical Society Reviews*. 2006.

[102] P. Bondavalli, L. Gorintin, G. Feugnet, G. Lehoucq, and D. Pribat, "Selective gas detection using CNTFET arrays fabricated using air-brush technique, with different metal as electrodes," *Sensors Actuators, B Chem*, vol. 202, pp. 1290–1297, 2014.

[103] B. Cardenas-Benitez, I. Djordjevic, S. Hosseini, M. J. Madou, and S. O. Martinez-Chapa, "Review—Covalent Functionalization of Carbon Nanomaterials for Biosensor Applications: An Update," *J. Electrochem. Soc.*, vol. 165, no. 3, pp. B103–B117, 2018.

[104] Y. Zhou, Y. Fang, and R. P. Ramasamy, "Non-covalent functionalization of carbon nanotubes for electrochemical biosensor development," *Sensors (Switzerland)*, vol. 19, no. 2, 2019.

[105] F. Toshimitsu and N. Nakashima, "Semiconducting single-walled carbon nanotubes sorting with a removable solubilizer based on dynamic supramolecular coordination chemistry," *Nat. Commun.*, vol. 5, pp. 1–9, 2015.

[106] G. Zucchi *et al.*, "Chemical sensors based on carbon nanotubes functionalised by conjugated polymers for analysis in aqueous medium," *World Pat. Appl. WO2018189479A1*, 2018.

[107] S. Gómez, N. M. Rendtorff, E. F. Aglietti, Y. Sakka, and G. Suárez, "Surface modification of multiwall carbon nanotubes by sulfonitric treatment," *Appl. Surf. Sci.*, vol. 379, pp. 264–269, Aug. 2016.

[108] H. Gong, S.-T. Kim, J. D. Lee, and S. Yim, "Simple quantification of surface carboxylic acids on chemically oxidized multi-walled carbon nanotubes," *Appl. Surf. Sci.*, vol. 266, pp. 219–224, Feb.

2013.

[109] K. A. Wepasnick, B. A. Smith, K. E. Schrote, H. K. Wilson, S. R. Diegelmann, and D. H. Fairbrother, "Surface and structural characterization of multi-walled carbon nanotubes following different oxidative treatments," *Carbon N. Y.*, vol. 49, no. 1, pp. 24–36, Jan. 2011.

[110] P. J. Vikesland and K. R. Wigginton, "Nanomaterial enabled biosensors for pathogen monitoring - A review," *Environ. Sci. Technol.*, vol. 44, no. 10, pp. 3656–3669, 2010.

[111] "Allen J. Bard and Larry R. Faulkner, Electrochemical Methods: Fundamentals and Applications, New York: Wiley, 2001, 2nd ed.," *Russ. J. Electrochem.*, vol. 38, no. 12, pp. 1364–1365, 2002.

[112] E. Bakker and E. Pretsch, "Potentiometric sensors for trace-level analysis," *Trends Anal. Chem*, vol. 24, no. 2, pp. 199–207, 2006.

[113] G. Hanrahan, D. G. Patil, and J. Wang, "Electrochemical sensors for environmental monitoring: Design, development and applications," *J. Environ. Monit.*, vol. 6, no. 8, pp. 657–664, 2004.

[114] F. R. Simões and M. G. Xavier, "6 - Electrochemical Sensors," in *Micro and Nano Technologies*, A. L. Da Róz, M. Ferreira, F. de Lima Leite, and O. N. B. T.-N. and its A. Oliveira, Eds. William Andrew Publishing, 2017, pp. 155–178.

[115] G. March, T. D. Nguyen, and B. Piro, "Modified electrodes used for electrochemical detection of metal ions in environmental analysis," *Biosensors*, vol. 5, no. 2, pp. 241–275, 2015.

[116] H. Zhou, W. Yang, and C. Sun, "Amperometric sulfite sensor based on multiwalled carbon nanotubes/ferrocene-branched chitosan composites," *Talanta*, vol. 77, no. 1, pp. 366–371, 2008.

[117] X. Gao, W. Wei, L. Yang, and M. Guo, "Carbon nanotubes/poly(1,2-diaminobenzene) nanoporous composite film electrode prepared by multipulse potentiostatic electropolymerisation and its application to determination of trace heavy metal ions," *Electroanalysis*, vol. 18, no. 5, pp. 485–492, 2006.

[118] M. U. Farid, N. K. Khanzada, and A. K. An, "Understanding fouling dynamics on functionalized CNT-based membranes: Mechanisms and reversibility," *Desalination*, vol. 456, pp. 74–84, 2019.

[119] C. Hu and S. Hu, "Carbon Nanotube-Based Electrochemical Sensors: Principles and Applications in Biomedical Systems," *J. Sensors*, vol. 2009, p. 187615, 2009.

[120] H. Karimi-Maleh, A. A. Ensafi, H. Beitollahi, V. Nasiri, M. A. Khalilzadeh, and P. Biparva, "Electrocatalytic determination of sulfite using a modified carbon nanotubes paste electrode: Application for determination of sulfite in real samples," *Ionics (Kiel*, vol. 18, no. 7, pp. 687–694, Jul. 2012.

[121] H. Khani, M. K. Rofouei, P. Arab, V. K. Gupta, and Z. Vafaei, "Multi-walled carbon nanotubes-ionic liquid-carbon paste electrode as a super selectivity sensor: Application to potentiometric monitoring of mercury ion(II)," *J. Hazard. Mater.*, vol. 183, no. 1, pp. 402–409, 2010.

[122] Y. Yan, M. Zhang, L. Su, S. Xiong, and L. Mao, "Electrochemistry and Electroanalytical Applications of Carbon Nanotubes: A Review," *Anal. Sci.*, vol. 21, pp. 1383–1393, Jan. 2006.

[123] Y. He, W. Chen, C. Gao, J. Zhou, X. Li, and E. Xie, "An overview of carbon materials for flexible electrochemical capacitors," *Nanoscale*, vol. 5, no. 19, pp. 8799–8820, 2013.

[124] J. Zhang *et al.*, "Effect of Chemical Oxidation on the Structure of Single-Walled Carbon Nanotubes," *J. Phys. Chem. B*, vol. 107, no. 16, pp. 3712–3718, Apr. 2003.

[125] H. Luo, Z. Shi, N. Li, Z. Gu, and Q. Zhuang, "Investigation of the Electrochemical and Electrocatalytic Behavior of Single-Wall Carbon Nanotube Film on a Glassy Carbon Electrode," *Anal. Chem.*, vol. 73, no. 5, pp. 915–920, Mar. 2001.

[126] L. J. van der PAUW, "A method of measuring specific resistivity and Hall effect of discs of arbitrary shape," in *Semiconductor Devices: Pioneering Papers*, vol. 13, no. 1, WORLD SCIENTIFIC, 1991, pp. 174–182.

[127] R. Tang, Y. Shi, Z. Hou, and L. Wei, "Carbon nanotube-based chemiresistive sensors," *Sensors (switzerl.*, vol. 17, no. 4, 2017.

[128] M. Meyyappan, "Carbon Nanotube-Based Chemical Sensors," *Small*, vol. 12, no. 16, pp. 2118–2129, Apr. 2016.

[129] D. Jung, M. Han, and G. S. Lee, "Gas sensor using a multi-walled carbon nanotube sheet to detect hydrogen molecules," *Sensors Actuators, A Phys.*, vol. 211, no. 2, pp. 51–54, 2014.

[130] J. Li, L. YJ, Q. Ye, L. Delzeit, and M. Meyyappan, "A gas sensor array using carbon nanotubes and microfabrication technology, Electrochem," *Electrochem. Solid State Lett.*, vol. 8, no. 11, pp. 100–102, 2005.

[131] A. Naderi and B. A. Tahne, "Review—Methods in Improving the Performance of Carbon Nanotube Field Effect Transistors," *ECS J. Solid State Sci. Technol.*, vol. 5, no. 12, pp. M131–M140, 2016.

[132] N. Valed Karimi and Y. Pourasad, "Investigating the effect of some parameters of the channel on the characteristics of tunneling carbon nanotube field-effect transistor," *Int. Nano Lett.*, vol. 6, no. 4, pp. 215–221, 2016.

[133] S.-A. S.-A. Imam, N. Kalam, and S. Abdullah, "Comparative Analysis of Control Coefficients on the Performance of CNTFET Under Different Parameters," *Int. J. Nanosci*, vol. 15, no. 03, p. 1640005,

2016.

[134] R. Saito, M. Fujita, G. Dresselhaus, and M. S. Dresselhaus, “Electronic structure of chiral graphene tubules,” *Appl. Phys. Lett*, vol. 60, no. 18, pp. 2204–2206, 1992.

[135] G. Ruiz-Soria *et al.*, “Revealing the adsorption mechanisms of nitroxides on ultrapure, metallicity-sorted carbon nanotubes,” *ACS Nano*, vol. 8, no. 2, pp. 1375–1383, 2014.

[136] W. Liu, K. Chikkadi, S. W. Lee, C. Hierold, and M. Haluska, “Improving non-suspended carbon nanotube FET performance by using an alumina protective layer,” *Sensors Actuators, B Chem*, vol. 198, pp. 479–486, 2014.

[137] S. N. Barman, M. C. Lemieux, J. Baek, R. Rivera, and Z. Bao, “Effects of dispersion conditions of single-walled carbon nanotubes on the electrical characteristics of thin film network transistors,” *ACS Appl. Mater. Interfaces*, vol. 2, no. 9, pp. 2672–2678, 2010.

[138] J. Guo, A. Javey, H. Dai, S. Datta, and M. Lundstrom, “Predicted Performance Advantages of Carbon Nanotube Transistors with Doped Nanotubes as Source / Drain,” *Sci. AAAS*, no. Sep., pp. 1–18, 2003.

[139] N. Pimparkar, C. Kocabas, S. J. Kang, J. Rogers, and M. A. Alam, “Limits of performance gain of aligned CNT over randomized network: Theoretical predictions and experimental validation,” *IEEE Electron Device Lett.*, vol. 28, no. 7, pp. 593–595, 2007.

[140] S. Takeda *et al.*, “A pH sensor based on electric properties of nanotubes on a glass substrate,” *Nanoscale Res. Lett.*, vol. 2, no. 4, pp. 207–212, 2007.

[141] N. H. Lee, S. H. Nahm, and I. S. Choi, “Real-time monitoring of a botulinum neurotoxin using all-carbon nanotube-based field-effect transistor devices,” *Sensors (Switzerland)*, vol. 18, no. 12, pp. 1–12, 2018.

[142] A. Boyd, I. Dube, G. Fedorov, M. Paranjape, and P. Barbara, “Gas sensing mechanism of carbon nanotubes: From single tubes to high-density networks,” *Carbon N. Y.*, vol. 69, pp. 417–423, 2014.

[143] R. Benda, E. Cancès, B. Lebental, and B. L. R. Benda E. Cancès, “Effective resistance of random percolating networks of stick nanowires: Functional dependence on elementary physical parameters,” *J. Appl. Phys*, vol. 126, no. 4, p. 44306, Jul. 2019.

[144] J. S. Noori, J. Mortensen, and A. Geto, “Recent Development on the Electrochemical Detection of Selected Pesticides: A Focused Review,” *Sensors (Basel).*, vol. 20, no. 8, p. 2221, Apr. 2020.

[145] A. K. Covington, R. G. Bates, and R. A. Durst, “Definition of pH scales, standard reference values, measurement of pH and related terminology (Recommendations 1984),” *Pure Appl. Chem.*, vol. 57, no. 3, pp. 531–542, Nov. 2007.

[146] World Health Organization, “pH in Drinking-water Background document for development of,” *WHO Guidel. Drink. Qual.*, 1996.

[147] L. Wang, Y. Xie, Y. Yang, H. Liang, L. Wang, and Y. Song, “Electroactive Covalent Organic Frameworks/Carbon Nanotubes Composites for Electrochemical Sensing,” *ACS Appl. Nano Mater*, 2020.

[148] J. Y. Jeon, B. C. Kang, and T. J. Ha, “Flexible pH sensors based on printed nanocomposites of single-wall carbon nanotubes and Nafion,” *Appl. Surf. Sci.*, vol. 514, p. 145956, Jun. 2020.

[149] D. Jung, M. Han, and G. S. Lee, “pH-sensing characteristics of multi-walled carbon nanotube sheet,” *Mater. Lett.*, vol. 122, pp. 281–284, 2014.

[150] D. Zhao, X. Guo, T. Wang, N. Alvarez, V. N. Shanov, and W. R. Heineman, “Simultaneous Detection of Heavy Metals by Anodic Stripping Voltammetry Using Carbon Nanotube Thread,” *Electroanalysis*, vol. 26, no. 3, pp. 488–496, Mar. 2014.

[151] C. R. T. Tarley, V. S. Santos, B. E. L. Baêta, A. C. Pereira, and L. T. Kubota, “Simultaneous determination of zinc, cadmium and lead in environmental water samples by potentiometric stripping analysis (PSA) using multiwalled carbon nanotube electrode,” *J. Hazard. Mater.*, vol. 169, no. 1–3, pp. 256–262, 2009.

[152] N. E. Eltayeb and A. Khan, “Design and Preparation of a New and Novel Nanocomposite with CNTs and Its Sensor Applications,” *J. Mater. Res. Technol.*, vol. 8, no. 2, pp. 2238–2246, 2019.

[153] H. Xu, L. Zeng, S. Xing, Y. Xian, G. Shi, and L. Jin, “Ultrasensitive voltammetric detection of trace lead(II) and cadmium(II) using MWCNTs-nafion/bismuth composite electrodes,” *Electroanalysis*, vol. 20, no. 24, pp. 2655–2662, 2008.

[154] Q. Wan, F. Yu, L. Zhu, X. Wang, and N. Yang, “Bucky-gel coated glassy carbon electrodes, for voltammetric detection of femtomolar leveled lead ions,” *Talanta*, vol. 82, no. 5, pp. 1820–1825, 2010.

[155] J. Morton, N. Havens, A. Mugweru, and A. K. Wanekaya, “Detection of trace heavy metal ions using carbon nanotube modified electrodes,” *Electroanalysis*, 2009.

[156] L. Wang, X. Wang, G. Shi, C. Peng, and Y. Ding, “Thiacalixarene covalently functionalized multiwalled carbon nanotubes as chemically modified electrode material for detection of ultratrace Pb 2+ ions,” *Anal. Chem.*, vol. 84, no. 24, pp. 10560–10567, Dec. 2012.

[157] F. Zhang, Y. Sun, D. Tian, W. S. Shin, J. S. Kim, and H. Li, “Selective molecular recognition on calixarene-functionalized 3D surfaces,” *Chem. Commun.*, 2016.

[158] T. Fukushima *et al.*, “Molecular ordering of organic molten salts triggered by single-walled carbon nanotubes.,” *Science*, vol. 300, no. 5628, pp. 2072–2074, 2003.

[159] T. Le Hai *et al.*, “Multiwall carbon nanotube modified by antimony oxide (Sb2O3/MWCNTs) paste electrode for the simultaneous electrochemical detection of cadmium and lead ions,” *Microchem. J.*, vol. 153, p. 104456, 2020.

[160] J. Wang, “Stripping Analysis at Bismuth Electrodes: A Review,” *Electroanalysis*, vol. 17, no. 15-16, pp. 1341–1346, Aug. 2005.

[161] U. Injang, P. Noyrod, W. Siangproh, W. Dungchai, S. Motomizu, and O. Chailapakul, “Determination of trace heavy metals in herbs by sequential injection analysis-anodic stripping voltammetry using screen-printed carbon nanotubes electrodes,” *Anal. Chim. Acta*, vol. 668, no. 1, pp. 54–60, 2010.

[162] G. H. Hwang, W. K. Han, J. S. Park, and S. G. Kang, “Determination of trace metals by anodic stripping voltammetry using a bismuth-modified carbon nanotube electrode,” *Talanta*, vol. 76, no. 2, pp. 301–308, 2008.

[163] A. Ivaska and W. W. Kubiak, “Application of sequential injection analysis to anodic stripping voltammetry,” *Talanta*, vol. 44, no. 4, pp. 713–723, 1997.

[164] X. Jia, J. Li, and E. Wang, “High-sensitivity determination of Lead(II) and Cadmium(II) based on the CNTs-PSS/Bi composite film electrode,” *Electroanalysis*, vol. 22, no. 15, pp. 1682–1687, 2010.

[165] G. Liu, Y. Lin, Y. Tu, and Z. Ren, “Ultrasensitive voltammetric detection of trace heavy metal ions using carbon nanotube nanoelectrode array,” *Analyst*, vol. 130, no. 7, pp. 1098–1101, 2005.

[166] Z. Xu *et al.*, “A sensitive electrochemical sensor for simultaneous voltammetric sensing of cadmium and lead based on Fe3O4/multiwalled carbon nanotube/laser scribed graphene composites functionalized with chitosan modified electrode,” *Mater. Chem. Phys.*, vol. 238, p. 121877, 2019.

[167] L. Oularbi, M. Turmine, and M. El Rhazi, “Preparation of novel nanocomposite consisting of bismuth particles, polypyrrole and multi-walled carbon nanotubes for simultaneous voltammetric determination of cadmium(II) and lead(II),” *Synth. Met.*, vol. 253, pp. 1–8, 2019.

[168] X. Xuan and J. Y. Park, “A miniaturized and flexible cadmium and lead ion detection sensor based on micro-patterned reduced graphene oxide/carbon nanotube/bismuth composite electrodes,” *Sensors Actuators B Chem.*, vol. 255, pp. 1220–1227, 2018.

[169] S. Mohammadi, M. A. Taher, H. Beitollahi, and M. Naghizadeh, “Sensitive voltammetric determination of cadmium at a carbon nanotubes/Fe3O4/eggshell composites modified carbon paste

electrode," *Environ. Nanotechnology, Monit. Manag.*, vol. 12, p. 100241, 2019.

[170] S. Li, D. Guérin, and K. Lmimouni, "Improving performance of OFET by tuning occurrence of charge transport based on pentacene interaction with SAM functionalized contacts," *Microelectron. Eng.*, vol. 195, no. July 2017, pp. 62–67, 2018.

[171] M. Bassyouni, A. E. Mansi, A. Elgabry, B. A. Ibrahim, O. A. Kassem, and R. Alhebeshy, "Utilization of carbon nanotubes in removal of heavy metals from wastewater: a review of the CNTs' potential and current challenges," *Appl. Phys. A*, vol. 126, no. 1, p. 38, 2019.

[172] J. Wei, D. Yang, H. Chen, Y. Gao, and H. Li, "Stripping voltammetric determination of mercury(II) based on SWCNT-PhSH modified gold electrode," *Sensors Actuators B Chem.*, vol. 190, pp. 968–974, 2014.

[173] Q. Bao *et al.*, "Electrochemical performance of a three-layer electrode based on Bi nanoparticles, multi-walled carbon nanotube composites for simultaneous Hg(II) and Cu(II) detection," *Chinese Chem. Lett.*, vol. 31, no. 2019, pp. 2752–2756, Oct. 2020.

[174] H. Xu, L. Zeng, S. Xing, G. Shi, Y. Xian, and L. Jin, "Microwave-radiated synthesis of gold nanoparticles/carbon nanotubes composites and its application to voltammetric detection of trace mercury(II)," *Electrochem. commun.*, vol. 10, no. 12, pp. 1839–1843, 2008.

[175] W. Deng *et al.*, "Square wave voltammetric determination of Hg(II) using thiol functionalized chitosan-multiwalled carbon nanotubes nanocomposite film electrode," *Microchim. Acta*, vol. 169, no. 3, pp. 367–373, 2010.

[176] M. H. Mashhadizadeh, S. Ramezani, and M. K. Rofouei, "Development of a novel MWCNTs-triazene-modified carbon paste electrode for potentiometric assessment of Hg(II) in the aquatic environments," *Mater. Sci. Eng. C*, vol. 47, pp. 273–280, 2015.

[177] A. Profumo *et al.*, "Multiwalled Carbon Nanotube Chemically Modified Gold Electrode for Inorganic As Speciation and Bi(III) Determination," *Anal. Chem.*, vol. 78, no. 12, pp. 4194–4199, Jun. 2006.

[178] N. Daud, N. A. Yusof, T. W. Tee, and A. H. Abdullah, "Electrochemical sensor for As(III) utilizing CNTs/Leucine/Nafion modified electrode," *Int. J. Electrochem. Sci.*, vol. 7, no. 1, pp. 175–185, 2012.

[179] S. Kempahanumakkagari, A. Deep, K.-H. Kim, S. Kumar Kailasa, and H.-O. Yoon, "Nanomaterial-based electrochemical sensors for arsenic - A review," *Biosens. Bioelectron.*, vol. 95, pp. 106–116, 2017.

[180] L. Xiao, G. G. Wildgoose, and R. G. Compton, "Sensitive electrochemical detection of arsenic (III) using gold nanoparticle modified carbon nanotubes via anodic stripping voltammetry," *Anal. Chim.*

Acta, vol. 620, no. 1–2, pp. 44–49, 2008.

[181] S. H. Shin and H. G. Hong, "Anodic stripping voltammetric detection of arsenic(III) at platinum-iron(III) nanoparticle modified carbon nanotube on glassy carbon electrode," *Bull. Korean Chem. Soc.*, vol. 31, no. 11, pp. 3077–3083, 2010.

[182] A. Buffa and D. Mandler, "Arsenic(III) detection in water by flow-through carbon nanotube membrane decorated by gold nanoparticles," *Electrochim. Acta*, vol. 318, pp. 496–503, Sep. 2019.

[183] V. Izadkhah, A. Farmany, and S. S. Mortazavi, "Voltammetric determination of copper in water samples using a Schiff base/carbon nanotube-modified carbon paste electrode," *J. Ind. Eng. Chem.*, vol. 21, pp. 994–996, 2015.

[184] H. Zhao *et al.*, "Poly(2-amino-4-thiazoleacetic acid)/multiwalled carbon nanotubes modified glassy carbon electrodes for the electrochemical detection of copper(II)," *Electrochim. Acta*, vol. 55, no. 7, pp. 2518–2521, 2010.

[185] S. E. Cabaniss, "Forward Modeling of Metal Complexation by NOM: II. Prediction of Binding Site Properties," *Environ. Sci. Technol.*, vol. 45, no. 8, pp. 3202–3209, Apr. 2011.

[186] D. Qin, X. Mamat, Y. Li, X. Hu, H. Cheng, and G. Hu, "A composite with botryoidal texture prepared from nitrogen-doped carbon spheres and carbon nanotubes for voltammetric sensing of copper(II)," *Microchem. J.*, vol. 153, p. 104299, 2020.

[187] S. Wang, J. Li, Y. Qiu, X. Zhuang, X. Wu, and J. Jiang, "Facile synthesis of oxidized multi-walled carbon nanotubes functionalized with 5-sulfosalicylic acid/MoS2 nanosheets nanocomposites for electrochemical detection of copper ions," *Appl. Surf. Sci.*, vol. 487, pp. 766–772, 2019.

[188] P. Li, L. Sun, M. Li, B. Yang, H. Li, and C. Li, " Simultaneous Determination of Small Biomolecules and Nitrite Using an Au/TiO 2 /Carbon Nanotube Composite-Modified Electrode ," *J. Electrochem. Soc.*, vol. 163, no. 13, pp. B567–B572, 2016.

[189] Z. Zhao *et al.*, "Synthesis and electrochemical properties of Co3O4-rGO/CNTs composites towards highly sensitive nitrite detection," *Appl. Surf. Sci.*, vol. 485, pp. 274–282, Aug. 2019.

[190] F. Hu, S. Chen, C. Wang, R. Yuan, D. Yuan, and C. Wang, "Study on the application of reduced graphene oxide and multiwall carbon nanotubes hybrid materials for simultaneous determination of catechol, hydroquinone, p-cresol and nitrite," *Anal. Chim. Acta*, vol. 724, pp. 40–46, 2012.

[191] M. Thamae and T. Nyokong, "Cobalt(II) porphyrazine catalysed reduction of nitrite," *J. Electroanal. Chem.*, vol. 470, no. 2, pp. 126–135, 1999.

[192] M. Xu *et al.*, "An electro-active amphiphilic copolymer to functionalize carbon nanotubes for highly

sensitive determination of nitrite in water," *Colloids Surfaces A Physicochem. Eng. Asp.*, vol. 576, pp. 123–129, 2019.

[193] A. Azadbakht, A. R. Abbasi, Z. Derikvand, and S. Amraei, "Immobilized organoruthenium(II) complexes onto polyethyleneimine-wrapped carbon nanotubes/in situ formed gold nanoparticles as a novel electrochemical sensing platform," *Mater. Sci. Eng. C*, vol. 48, pp. 270–278, 2015.

[194] X. H. Pham *et al.*, "Electrochemical detection of nitrite using urchin-like palladium nanostructures on carbon nanotube thin film electrodes," *Sensors Actuators, B Chem*, vol. 193, pp. 815–822, 2014.

[195] W. Wu *et al.*, "Sensing nitrite with a glassy carbon electrode modified with a three-dimensional network consisting of Ni7S6 and multi-walled carbon nanotubes," *Microchim. Acta*, vol. 183, no. 12, pp. 3159–3166, 2016.

[196] D. Rao, Q. Sheng, and J. Zheng, "Self-assembly preparation of gold nanoparticle decorated 1-pyrenemethylamine functionalized graphene oxide–carbon nanotube composites for highly sensitive detection of nitrite," *Anal. Methods*, vol. 8, no. 24, pp. 4926–4933, 2016.

[197] A. Salimi, A. Noorbakhash, and F. S. Karonian, "Amperometric detection of nitrite, iodate and periodate on glassy carbon electrode modified with thionin and multi-wall carbon nanotubes," *Int. J. Electrochem. Sci.*, vol. 1, no. 8, pp. 435–446, 2006.

[198] N. Hui *et al.*, "Electrodeposited Conducting Polyaniline Nanowire Arrays Aligned on Carbon Nanotubes Network for High Performance Supercapacitors and Sensors," *Electrochim. Acta*, vol. 199, pp. 234–241, 2016.

[199] T. M. Lerga and C. K. O'Sullivan, "Rapid determination of total hardness in water using fluorescent molecular aptamer beacon," *Anal. Chim. Acta*, vol. 610, no. 1, pp. 105–111, 2008.

[200] K. R. Gee, K. A. Brown, W.-N. U. Chen, J. Bishop-Stewart, D. Gray, and I. Johnson, "Chemical and physiological characterization of fluo-4 Ca2+-indicator dyes," *Cell Calcium*, vol. 27, no. 2, pp. 97–106, 2000.

[201] D. Son *et al.*, "Nanoneedle transistor-based sensors for the selective detection of intracellular calcium ions," *ACS Nano*, vol. 5, no. 5, pp. 3888–3895, 2011.

[202] F. Akhter, A. Nag, M. E. E. Alahi, H. Liu, and S. C. Mukhopadhyay, "Electrochemical detection of calcium and magnesium in water bodies," *Sensors Actuators, A Phys.*, vol. 305, p. 111949, 2020.

[203] P. J. Mulholland, J. N. Houser, and K. O. Maloney, "Stream diurnal dissolved oxygen profiles as indicators of in-stream metabolism and disturbance effects: Fort Benning as a case study," *Ecol. Indic.*, 2005.

[204] E. Sánchez *et al.*, "Use of the water quality index and dissolved oxygen deficit as simple indicators of watersheds pollution," *Ecol. Indic.*, vol. 7, no. 2, pp. 315–328, 2007.

[205] P. G. Collins, "Extreme Oxygen Sensitivity of Electronic Properties of Carbon Nanotubes," *Science (80-.).*, 2002.

[206] K. R. Moonoosawmy and P. Kruse, "Cause and consequence of carbon nanotube doping in water and aqueous media," *J. Am. Chem. Soc.*, 2010.

[207] J. S. Ye *et al.*, "Application of multi-walled carbon nanotubes functionalized with hemin for oxygen detection in neutral solution," *J. Electroanal. Chem.*, vol. 562, no. 2, pp. 241–246, 2004.

[208] C. Shi and F. C. Anson, "Catalytic pathways for the electroreduction of oxygen by iron tetrakis(4-N-methylpyridyl)porphyrin or iron tetraphenylporphyrin adsorbed on edge plane pyrolytic graphite electrodes," *Inorg. Chem.*, vol. 29, no. 21, pp. 4298–4305, Oct. 1990.

[209] T. H. Tsai, C. Y. Yang, and S. M. Chen, "Development of a dissolved oxygen sensor for commercial applications," *Int. J. Electrochem. Sci.*, vol. 8, no. 4, pp. 5250–5261, 2013.

[210] M. Sosna, G. Denuault, R. W. Pascal, R. D. Prien, and M. Mowlem, "Development of a reliable microelectrode dissolved oxygen sensor," *Sensors Actuators B Chem.*, vol. 123, no. 1, pp. 344–351, 2007.

[211] J. Balamurugan, T. D. Thanh, G. Karthikeyan, N. H. Kim, and J. H. Lee, "A novel hierarchical 3D N-Co-CNT@NG nanocomposite electrode for non-enzymatic glucose and hydrogen peroxide sensing applications," *Biosens. Bioelectron.*, vol. 89, no. August 2016, pp. 970–977, 2017.

[212] W. Zhang, G. Wang, X. Zhang, and B. Fang, "Amperometric detection of hydrogen peroxide using glassy carbon electrodes modified with chromium hexacyanoferrate/single-walled carbon nanotube nanocomposites," *Electroanalysis*, vol. 21, no. 2, pp. 179–183, 2009.

[213] S. T. R. Naqvi *et al.*, "Electrochemical Sensing of Ascorbic Acid, Hydrogen Peroxide and Glucose by Bimetallic (Fe, Ni)−CNTs Composite Modified Electrode," *Electroanalysis*, vol. 31, no. 5, pp. 851–857, 2019.

[214] S. K. Annamalai, B. Palani, and K. Chandrasekara Pillai, "Highly stable and redox active nano copper species stabilized functionalized-multiwalled carbon nanotube/chitosan modified electrode for efficient hydrogen peroxide detection," *Colloids Surfaces A Physicochem. Eng. Asp.*, vol. 395, pp. 207–216, 2012.

[215] L. Yang, M. Li, Y. Qu, Z. Dong, and W. J. Li, "Carbon nanotube-sensor-integrated microfluidic platform for real-time chemical concentration detection," *Electrophoresis*, vol. 30, no. 18, pp. 3198–

3205, Sep. 2009.

[216] J. Wang and M. Musameh, “Carbon nanotube screen-printed electrochemical sensors.,” *Analyst*, vol. 129, no. 1, pp. 1–2, 2004.

[217] V. Patel, P. Kruse, and P. R. Selvaganapathy, “Hydrogen peroxide chemiresistive detection platform with wide range of detection,” in *2019 IEEE SENSORS*, 2019, vol. 2019-Octob, pp. 1–4.

[218] R. Olivé-Monllau, A. Pereira, J. Bartrolí, M. Baeza, and F. Céspedes, “Highly sensitive CNT composite amperometric sensors integrated in an automated flow system for the determination of free chlorine in waters,” *Talanta*, vol. 81, no. 4–5, pp. 1593–1598, 2010.

[219] A. Isaac, J. Davis, C. Livingstone, A. J. Wain, and R. G. Compton, “Electroanalytical methods for the determination of sulfite in food and beverages,” *TrAC - Trends Anal. Chem.*, vol. 25, no. 6, pp. 589–598, 2006.

[220] J. B. Raoof, R. Ojani, and H. Karimi-maleh, “Electrocatalytic Determination of Sulfite at the Surface of a New Ferrocene Derivative-Modified Carbon Paste Electrode,” *Int. J. Electrochem. Sci.*, vol. 2, pp. 257–269, Jan. 2007.

[221] L. Vu and L. Cervenka, “Determination of Sulfide by Hematoxylin Multiwalled Carbon Nanotubes Modified Carbon Paste Electrode,” *Electroanalysis*, vol. 25, pp. 1967–1973, Aug. 2013.

[222] N. S. Lawrence, R. P. Deo, and J. Wang, “Electrochemical determination of hydrogen sulfide at carbon nanotube modified electrodes,” *Anal. Chim. Acta*, vol. 517, no. 1–2, pp. 131–137, 2004.

[223] M. Shamsipur, M. Roushani, S. M. Pourmortazavi, and N. Shahabadi, “Amperometric determination of sulfide ion by glassy carbon electrode modified with multiwall carbon nanotubes and copper (II) phenanthroline complex,” *Cent. Eur. J. Chem.*, vol. 12, pp. 1091–1099, May 2014.

[224] E. Perales *et al.*, “Comparative ecotoxicity study of glycerol-biobased solvents,” *Environ. Chem.*, vol. 14, no. 6, pp. 370–377, 2017.

[225] Y. Cheng *et al.*, “Rapid amperometric detection of coliforms based on MWNTs/Nafion composite film modified glass carbon electrode,” *Talanta*, vol. 75, no. 1, pp. 167–171, 2008.

[226] M. M. Khalil, A. A. Farghali, W. M. A. E. Rouby, I. H. Abd-Elgawad, W. M. A. El Rouby, and I. H. Abd-Elgawad, “Preparation and characterization of novel MWCNTs/Fe-Co doped TNTs nanocomposite for potentiometric determination of sulpiride in real water samples, Sci,” *Rep*, vol. 10, no. 1, pp. 1–9, 2020.

[227] M. Y. Ali, A. U. Alam, and M. M. R. Howlader, “Fabrication of highly sensitive bisphenol a electrochemical sensor amplified with chemically modified multiwall carbon nanotubes and β-

cyclodextrin," *Sensors Actuators, B Chem.*, vol. 320, no. March, p. 128319, 2020.

[228] T. Zhou *et al.*, "Electrochemical determination of tetrabromobisphenol A in water samples based on a carbon nanotubes@zeolitic imidazole framework-67 modified electrode," *RSC Adv*, vol. 10, no. 4, pp. 2123–2132, 2020.

[229] Y. Gao, Y. Cao, D. Yang, X. Luo, Y. Tang, and H. Li, "Sensitivity and selectivity determination of bisphenol A using SWCNT–CD conjugate modified glassy carbon electrode," *J. Hazard. Mater.*, vol. 199–200, pp. 111–118, 2012.

[230] S. Dey, F. Bano, and A. Malik, "1 - Pharmaceuticals and personal care product (PPCP) contamination—a global discharge inventory," in *Pharmaceuticals and Personal Care Products: Waste Management and Treatment Technology*, M. N. V. Prasad, M. Vithanage, and A. Kapley, Eds. Butterworth-Heinemann, 2019, pp. 1–26.

[231] N. Anzar, R. Hasan, M. Tyagi, N. Yadav, and J. Narang, "Carbon nanotube - A review on Synthesis, Properties and plethora of applications in the field of biomedical science," *Sensors Int.*, vol. 1, p. 100003, 2020.

[232] A. Bachtold, P. Hadley, T. Nakanishi, and C. Dekker, "Logic circuits with carbon nanotube transistors," *Science (80-.).*, vol. 294, no. 5545, pp. 1317–1320, 2001.

[233] M. Pourfath, H. Kosina, and S. Selberherr, "Numerical study of quantum transport in carbon nanotube transistors," *Math. Comput. Simul.*, 2008.

[234] F. Saeedi, B. Ghavami, and M. Raji, "A fast method for process reliability analysis of CNFET-based digital integrated circuits," *J. Comput. Electron.*, 2018.

[235] M. H. Yang *et al.*, "Advantages of top-gate, high-k dielectric carbon nanotube field-effect transistors," *Physics (College. Park. Md).*, vol. 88, pp. 113507–113508, 2006.

[236] S. J. Wind, J. Appenzeller, R. Martel, V. Derycke, and P. Avouris, "Vertical scaling of carbon nanotube field-effect transistors using top gate electrodes," *Appl. Phys. Lett.*, vol. 80, no. 20, pp. 3817–3819, 2002.

[237] P. Yaghoobi and A. Nojeh, "Electron Emission from Carbon Nanotubes," *Mod. Phys. Lett. B - MOD PHYS LETT B*, vol. 21, pp. 1807–1830, Nov. 2007.

[238] P. L. Neumann *et al.*, "Different sensing mechanisms in single wire and mat carbon nanotubes chemical sensors," *Appl. Phys. A Mater. Sci. Process.*, vol. 117, no. 4, pp. 2107–2113, 2014.

[239] T. Mizutani and Y. Ohno, "Fabrication and characterization of carbon nanotube FETs," p. 28, 2005.

[240] V. Derycke, R. Martel, J. Appenzeller, and P. Avouris, “Carbon Nanotube Inter- and Intramolecular Logic Gates,” *Nano Lett.*, vol. 1, no. 9, pp. 453–456, 2001.

[241] Y. Che, H. Chen, H. Gui, J. Liu, B. Liu, and C. Zhou, “Review of carbon nanotube nanoelectronics and macroelectronics,” vol. 073001.

[242] G. S. F. P. N. H. J. L. J. M. G. T. K. K. H. J. M. T. P. H. H. S. P. M. A. R. V. Eduardo Gracia-Espino, “Electrical transport and field-effect transistors using inkjet-printed SWCNT films having different functional side groups,” *ACS Nano*, vol. 4, no. 6, pp. 3318–3324, 2010.

[243] L. Gorintin, P. Bondavalli, P. Legagneux, and D. Pribat, “High performances CNTFETs achieved using CNT networks for selective gas sensing,” *Carbon Nanotub. Graphene, Assoc. Devices II*, vol. 7399, p. 739909, 2009.

[244] J. Heitz, Y. Leroy, L. Hébrard, and C. Lallement, “Theoretical characterization of the topology of connected carbon nanotubes in random networks,” *Nanotechnology*, vol. 22, no. 34, p. 345703, 2011.

[245] M. S. Purewal, B. H. Hong, A. Ravi, B. Chandra, J. Hone, and P. Kim, “Scaling of resistance and electron mean free path of single-walled carbon nanotubes,” *Phys. Rev. Lett.*, vol. 98, no. 18, pp. 2–5, 2007.

[246] M. Purewal, “Electron transport in single-walled carbon nanotubes,” Jan. 2008.

[247] S. A. McGill, S. G. Rao, P. Manandhar, P. Xiong, and S. Hong, “High-performance, hysteresis-free carbon nanotube field-effect transistors via directed assembly,” *Appl. Phys. Lett.*, vol. 89, no. 16, pp. 87–90, 2006.

[248] N. Patil *et al.*, “Wafer-scale growth and transfer of aligned single-walled carbon nanotubes,” *IEEE Trans. Nanotechnol.*, vol. 8, no. 4, 2009.

[249] C. Kocabas, S. J. Kang, T. Ozel, M. Shim, and J. A. Rogers, “Improved synthesis of aligned arrays of single-walled carbon nanotubes and their implementation in thin film type transistors,” *J. Phys. Chem. C*, vol. 111, no. 48, 2007.

[250] S. J. Kang *et al.*, “High-performance electronics using dense, perfectly aligned arrays of single-walled carbon nanotubes,” *Nat. Nanotechnol.*, vol. 2, no. 4, 2007.

[251] M. Schröter, M. Claus, P. Sakalas, M. Haferlach, and D. Wang, “Carbon nanotube FET technology for radio-frequency electronics: State-of-The-Art overview,” *IEEE J. Electron Devices Soc.*, vol. 1, no. 1, pp. 9–20, 2013.

[252] Y. Gao, Y. Deng, Z. Liao, and M. Zhang, “Aligned carbon nanotube field effect transistors by repeated compression-expansion cycles in Langmuir-Blodgett,” in *2017 IEEE 17th International*

Conference on Nanotechnology (IEEE-NANO), 2017, pp. 731–734.

[253] A. D. Franklin, A. Lin, H. S. P. Wong, and Z. Chen, "Current scaling in aligned carbon nanotube array transistors with local bottom gating," *IEEE Electron Device Lett.*, vol. 31, no. 7, pp. 644–646, 2010.

[254] Q. Cao and J. A. Rogers, "Random networks and aligned arrays of single-walled carbon nanotubes for electronic device applications," *Nano Res.*, vol. 1, no. 4, pp. 259–272, 2008.

[255] Rahmat bin Sanudin and R. Sanudin, "Characterisation of ballistic carbon nanotube field-effect transistor," no. May, p. 114, Aug. 2021.

[256] Z. Y. Zhang, S. Wang, and L. M. Peng, "High-performance doping-free carbon-nanotube-based CMOS devices and integrated circuits," *Chinese Sci. Bull.*, vol. 57, no. 2–3, pp. 135–148, 2012.

[257] M. M. Shulaker *et al.*, "Carbon nanotube computer," *Nature*, vol. 501, no. 7468, pp. 526–530, 2013.

[258] K. Otsuka, T. Inoue, S. Chiashi, and S. Maruyama, "Selective removal of metallic single-walled carbon nanotubes in full length by organic film-assisted electrical breakdown," *Nanoscale*, vol. 6, no. 15, pp. 8831–8835, 2014.

[259] M. P. Gupta, A. Behnam, F. Lian, D. Estrada, E. Pop, and S. Kumar, "High field breakdown characteristics of carbon nanotube thin film transistors," *Nanotechnology*, vol. 24, no. 40, 2013.

[260] T. Ma and Y. Liu, "Study on breakdown to nano TFT loaded by GPa order mechanical stress," *Microsyst. Technol.*, vol. 22, no. 8, pp. 2151–2157, 2016.

[261] J. Li, A. D. Franklin, and J. Liu, "Gate-Free Electrical Breakdown of Metallic Pathways in Single-Walled Carbon Nanotube Crossbar Networks," *Nano Lett.*, vol. 15, no. 9, pp. 6058–6065, 2015.

[262] A. Raychowdhury, S. Mukhopadhyay, and K. Roy, "A circuit-compatible model of ballistic carbon nanotube field-effect transistors," *IEEE Trans. Comput. Des. Integr. Circuits Syst.*, vol. 23, no. 10, pp. 1411–1420, 2004.

[263] H. P. Wong, J. Appenzeller, V. Derycke, R. Martel, S. Wind, and P. Avouris, "Carbon Nanotube Field Effect Transistors – Fabrication, Device Physics, and Circuit Implications," *2003 IEEE Int. Solid-State Circuits Conf.*, 2003.

[264] J. Appenzeller, J. Knoch, M. Radosavljevi\ifmmode \acutec\else ć\fi, and P. Avouris, "Multimode Transport in Schottky-Barrier Carbon-Nanotube Field-Effect Transistors," *Phys. Rev. Lett.*, vol. 92, no. 22, p. 226802, 2004.

[265] M. Radosavljević, S. Heinze, J. Tersoff, and P. Avouris, "Drain voltage scaling in carbon nanotube

transistors," *Appl. Phys. Lett.*, vol. 83, no. 12, pp. 2435–2437, Sep. 2003.

[266] A. Javey *et al.*, "Self-Aligned Ballistic Molecular Transistors and Electrically Parallel Nanotube Arrays," *Nano Lett.*, vol. 4, no. 7, pp. 1319–1322, Jul. 2004.

[267] A. Diabi, A. Hocini, S. Mouetsi, and D. Khedrouche, "Modeling and performance analysis of Schottky barrier carbon nanotube field effect transistor SB-CNTFET," *J. Comput. Electron.*, vol. 16, no. 3, pp. 593–600, 2017.

[268] J. Guo, S. Datta, and M. Lundstrom, "A numerical study of scaling issues for Schottky-barrier carbon nanotube transistors," *IEEE Trans. Electron Devices*, vol. 51, no. 2, pp. 172–177, 2004.

[269] J. R. Tucker, C. Wang, and P. S. Carney, "Silicon field-effect transistor based on quantum tunneling," *Appl. Phys. Lett.*, vol. 65, no. 5, pp. 618–620, 1994.

[270] M. Pourfath *et al.*, "Improving the ambipolar behavior of schottky barrier carbon nanotube field effect transistors," *ESSCIRC 2004 - Proc. 34th Eur. Solid-State Device Res. Conf.*, no. May 2014, pp. 429–432, 2004.

[271] P. Reena Monica and V. T. Sreedevi, "Suppression of ambipolar conduction in Schottky barrier carbon nanotube field effect transistors: Modeling, optimization using particle swarm intelligence, and fabrication," *C. - Comput. Model. Eng. Sci.*, vol. 119, no. 3, pp. 577–591, 2019.

[272] S. Heinze, J. Tersoff, and P. Avouris, "Carbon nanotube electronics and optoelectronics," *Lect. Notes Phys.*, vol. 680, no. July 2014, pp. 381–409, 2006.

[273] M. Najari, S. Frégonèse, C. Maneux, H. Mnif, N. Masmoudi, and T. Zimmer, "Schottky barrier carbon nanotube transistor: Compact modeling, scaling study, and circuit design applications," *IEEE Trans. Electron Devices*, vol. 58, no. 1, pp. 195–205, 2011.

[274] H. N. Nguyen, S. Retailleau, D. Querlioz, A. Bournel, and P. Dollfus, "Monte Carlo study of ambipolar transport and quantum effects in carbon nanotube transistors," in *International Conference on Simulation of Semiconductor Processes and Devices, SISPAD*, 2009.

[275] V. Prasad and D. Das, "A Review on MOSFET-Like CNTFETs," *Sci. Technol. J.*, vol. 4, no. 2, pp. 124–129, 2016.

[276] A. M. Hashim, H. H. Ping, and C. Y. Pin, "Characterization of MOSFET-like carbon nanotube field effect transistor," *AIP Conf. Proc.*, vol. 1217, no. March, pp. 11–18, 2010.

[277] Y. M. Lin, J. Appenzeller, J. Knoch, and P. Avouris, "High-performance carbon nanotube field-effect transistor with tunable polarities," *IEEE Trans. Nanotechnol.*, vol. 4, no. 5, 2005.

[278] A. Javey, R. Tu, D. B. Farmer, J. Guo, R. G. Gordon, and H. Dai, "High performance n-type carbon nanotube field-effect transistors with chemically doped contacts," *Nano Letters*, vol. 5, no. 2. 2005.

[279] W. Chen, *Doped Nanomaterials and Nanodevices: Luminescence and applications*. American Scientific Publishers, 2010.

[280] J. L. Bahr, J. Yang, D. V Kosynkin, M. J. Bronikowski, R. E. Smalley, and J. M. Tour, "Functionalization of Carbon Nanotubes by Electrochemical Reduction of Aryl Diazonium Salts: A Bucky Paper Electrode," *J. Am. Chem. Soc.*, vol. 123, no. 27, pp. 6536–6542, Jul. 2001.

[281] A. Rahman, J. Guo, S. Datta, and M. . Lundstrom, "Theory of ballistic nanotransistors," *Electron Devices, IEEE Trans.*, vol. 50, pp. 1853–1864, Oct. 2003.

[282] M. Ishida and F. Nihey, "Estimating the yield and characteristics of random network carbon nanotube transistors," *Appl. Phys. Lett.*, vol. 92, no. 16, pp. 2006–2009, 2008.

[283] H.-K. Jang, J. E. Jin, J. H. Choi, P.-S. Kang, D.-H. Kim, and G. T. Kim, "Electrical percolation thresholds of semiconducting single-walled carbon nanotube networks in field-effect transistors," *Phys. Chem. Chem. Phys.*, vol. 17, no. 10, pp. 6874–6880, 2015.

[284] S. Seppälä, E. Häkkinen, M. J. Alava, V. Ermolov, and E. T. Seppälä, "Electrical transport properties of percolating random networks of carbon nanotube bundles," *Epl*, vol. 91, no. 4, 2010.

[285] J. Min-kyu, M. Mouis, G. Kim, U. J. Kim, and G. Ghibaudo, "Simulation Methodology for 2D random network of CNTs field-effect transistors," pp. 197–200.

[286] T. Takenobu *et al.*, "Ink-jet printing of carbon nanotube thin-film transistors on flexible plastic substrates," *Appl. Phys. Express*, vol. 2, no. 2, 2009.

[287] H. K. Jang, J. H. Choi, D. H. Kim, and G. T. Kim, "On/off ratio enhancement in single-walled carbon nanotube field-effect transistor by controlling network density via sonication," *Appl. Surf. Sci.*, vol. 444, pp. 442–447, 2018.

[288] C. Y. Lu, K. Y. Hsieh, and R. Liu, "Future challenges of flash memory technologies," *Microelectron. Eng.*, vol. 86, no. 3, pp. 283–286, Mar. 2009.

[289] P. Beecher *et al.*, "Ink-jet printing of carbon nanotube thin film transistors," *J. Appl. Phys.*, vol. 102, no. 4, pp. 1–7, 2007.

[290] J. F. Emery and G. W. Leddicottte, "The Radiochemistry of Gold," *Nucl. Sci. Ser.*, p. 40, 1961.

[291] A. Asenov and S. Saini, "Polysilicon gate enhancement of the random dopant induced threshold voltage fluctuations in sub-100 nm MOSFET's with ultrathin gate oxide," *IEEE Trans. Electron*

Devices, vol. 47, no. 4, 2000.

[292] R. Benda, G. Zucchi, E. Cancès, and B. Lebental, "Insights into the π – π interaction driven non-covalent functionalization of carbon nanotubes of various diameters by conjugated fluorene and carbazole copolymers," *J. Chem. Phys.*, vol. 152, no. 6, p. 64708, Feb. 2020.

[293] R. Benda, T. Vezin, G. Zucchi, E. Cancès, and B. Lebental, "Prediction of the interaction strength of an urea-based probe towards ions in water by means of DFT/PCM calculations," Springer Verlag, 2021.

[294] S. Roberts, "Dielectric and piezoelectric properties of barium titanate," *Phys. Rev.*, 1947.

[295] H. Wijshoff, "The dynamics of the piezo inkjet printhead operation $," *Phys. Rep.*, vol. 491, no. 4–5, pp. 77–177, 2010.

[296] S. Jung, "Fluid characterisation and drop impact in inkjet printing for organic semiconductor devices," no. April, p. 168, 2011.

[297] M. Mcdonald, "39 . 3 : Manufacture of Flat Panel Displays Using Piezoelectric Drop-On-Demand Ink Jet Ink Jet Attributes for FPD Printing 10 pl ~ 30 um 10 um clearance Ink jet optimization," pp. 1186–1189, 2003.

[298] L. Rispal, T. Tschischke, H. Yang, and U. Schwalke, "Polymethyl methacrylate passivation of carbon nanotube field-effect transistors: Novel self-aligned process and effect on device transfer characteristic hysteresis," *Jpn. J. Appl. Phys.*, vol. 47, no. 4 PART 2, pp. 3287–3291, 2008.

[299] E. Folgado, V. Ladmiral, and M. Semsarilar, "Towards permanent hydrophilic PVDF membranes. Amphiphilic PVDF-b-PEG-b-PVDF triblock copolymer as membrane additive," *Eur. Polym. J.*, vol. 131, p. 109708, May 2020.

[300] X. Li *et al.*, "Water Splitting: From Electrode to Green Energy System," *Nano-Micro Lett.*, vol. 12, no. 1, p. 131, 2020.

[301] H. Yoo *et al.*, "Balancing Hole and Electron Conduction in Ambipolar Split-Gate Thin-Film Transistors," *Sci. Rep.*, vol. 7, Jul. 2017.

[302] R. Di Pietro, D. Fazzi, T. B. Kehoe, and H. Sirringhaus, "Spectroscopic investigation of oxygen- and water-induced electron trapping and charge transport instabilities in n-type polymer semiconductors," *J. Am. Chem. Soc.*, vol. 134, no. 36, 2012.

[303] R. Di Pietro and H. Sirringhaus, "High resolution optical spectroscopy of air-induced electrical instabilities in n-type polymer semiconductors," *Adv. Mater.*, vol. 24, no. 25, 2012.

[304] W. Kim, A. Javey, O. Vermesh, Q. Wang, Y. Li, and H. Dai, "Hysteresis caused by water molecules in carbon nanotube field-effect transistors," *Nano Lett.*, vol. 3, no. 2, pp. 193–198, 2003.

[305] R. S. Park *et al.*, "Hysteresis in Carbon Nanotube Transistors: Measurement and Analysis of Trap Density, Energy Level, and Spatial Distribution," *ACS Nano*, vol. 10, no. 4, pp. 4599–4608, 2016.

[306] B. Liu, M. A. McCarthy, and A. G. Rinzler, "Non-Volatile Organic Memory Elements Based on Carbon-Nanotube-Enabled Vertical Field-Effect Transistors," *Adv. Funct. Mater.*, vol. 20, no. 20, pp. 3440–3445, 2010.

[307] G. Lu *et al.*, "Moderate doping leads to high performance of semiconductor/insulator polymer blend transistors," *Nat. Commun.*, vol. 4, 2013.

[308] A. Ortiz-Conde, F. J. García Sánchez, J. J. Liou, A. Cerdeira, M. Estrada, and Y. Yue, "A review of recent MOSFET threshold voltage extraction methods," *Microelectron. Reliab.*, vol. 42, no. 4–5, pp. 583–596, Apr. 2002.

[309] F. Tournus, S. Latil, M. I. Heggie, and J.-C. Charlier, "pi-stacking interaction between carbon nanotubes and organic molecules," *Phys. Rev. B*, vol. 72, no. 7, p. 75431, 2005.

[310] H. Wang *et al.*, "Tuning the threshold voltage of carbon nanotube transistors by n-type molecular doping for robust and flexible complementary circuits," *Proc. Natl. Acad. Sci. U. S. A.*, vol. 111, no. 13, pp. 4776–4781, 2014.

[311] B. Liu *et al.*, "Dispersion of Single-Walled Carbon Nanotubes in Organic Solvents DMAC," *Adv. Funct. Mater.*, pp. 841–852, 2018.

[312] Q. Cheng, S. Debnath, E. Gregan, and H. J. Byrne, "Effects of chlorinated aromatic solvents on the dispersion of HiPco SWNTs," *Phys. Status Solidi Basic Res.*, vol. 245, no. 10, pp. 1947–1950, 2008.

[313] S. Niyogi *et al.*, "Ultrasonic dispersions of single-walled carbon nanotubes," *J. Phys. Chem. B*, vol. 107, no. 34, pp. 8799–8804, 2003.

[314] M. J. Ganter, B. J. Landi, J. J. Worman, C. M. Schauerman, C. D. Cress, and R. P. Raffaelle, "Variation of single wall carbon nanotube dispersion properties with alkyl amide and halogenated aromatic solvents," *Mater. Chem. Phys.*, vol. 116, no. 1, pp. 235–241, 2009.

[315] H. C. Yau, M. K. Bayazit, J. H. G. Steinke, and M. S. P. Shaffer, "Sonochemical degradation of N-methylpyrrolidone and its influence on single walled carbon nanotube dispersion," *Chem. Commun.*, vol. 51, no. 93, pp. 16621–16624, 2015.

[316] S. D. Bergin *et al.*, "Towards solutions of single-walled carbon nanotubes in common solvents," *Adv. Mater.*, vol. 20, no. 10, pp. 1876–1881, 2008.

9 Supplementary information

9.1 Ink optimization process

The historical process in the team had MWCNT concentration at 0.005 wt% in *o*-dichlorobenzene. The final process after optimization has SWCNT concentration of 0.001wt% in NMP. The following section highlights the process toward achieving the optimized ink formulation described in the section 4.2.1.1.

- From MWCNT to SWCNT at 0.005 wt%

Replacing MWCNT by SWCNT in the historical process (*o*-DCBZ at 0.005wt%) did not feature specific process challenge. However, it yielded high SWCNT density per unit area after deposition (Figure S 1), so the resulting networks were revealed not to have semi-conducting properties.

- From 0.005wt% to 0.001 wt%

Therefore, we decreased the concentration down to 0.001 wt % of SWCNT/*o*-DCBZ solution and we achieved sparse SWCNTs network (Figure S 2) between source and drain after deposition (with semi-conducting characteristics, as shown in Figure S 3). To be noted, we did not simply dilute the SWCNT/*o*-DCBZ ink from 0.005 wt % (5 mg SWCNTs/ 80 ml *o*-DCBZ) to 0.001 wt %, but we initially prepared from 0.001 wt % (1 mg SWCNTs/ 80 ml *o*-DCBZ) during ink fabrication process. The challenge of the "simple" dilution method is that it causes instability in the ink (agglomeration of CNTs). A lot of work has gone toward optimizing the dilution approach to remove such instability (See section 9.1).

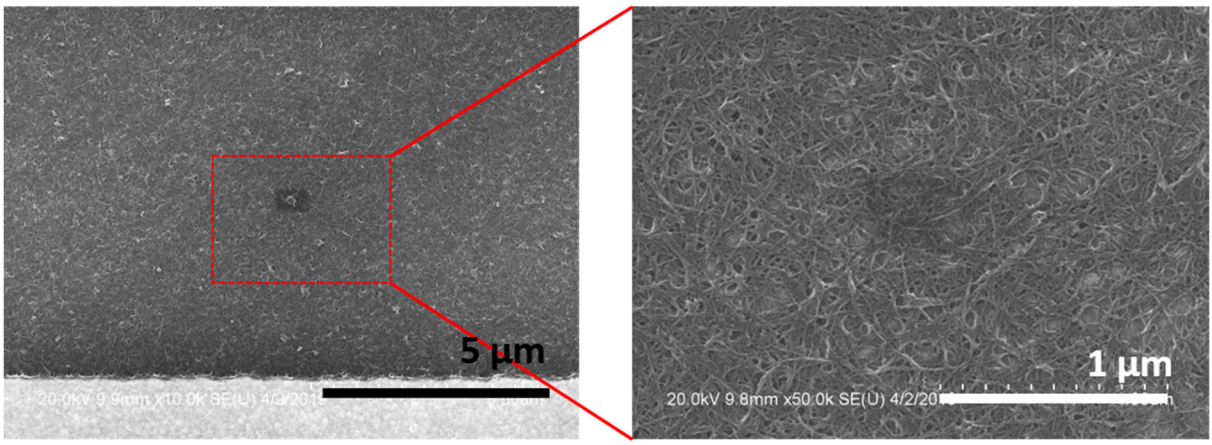

Figure S 1. SEM images of percolated SWCNT network between metal electrodes. Concentration of the ink is 0.005 wt %.

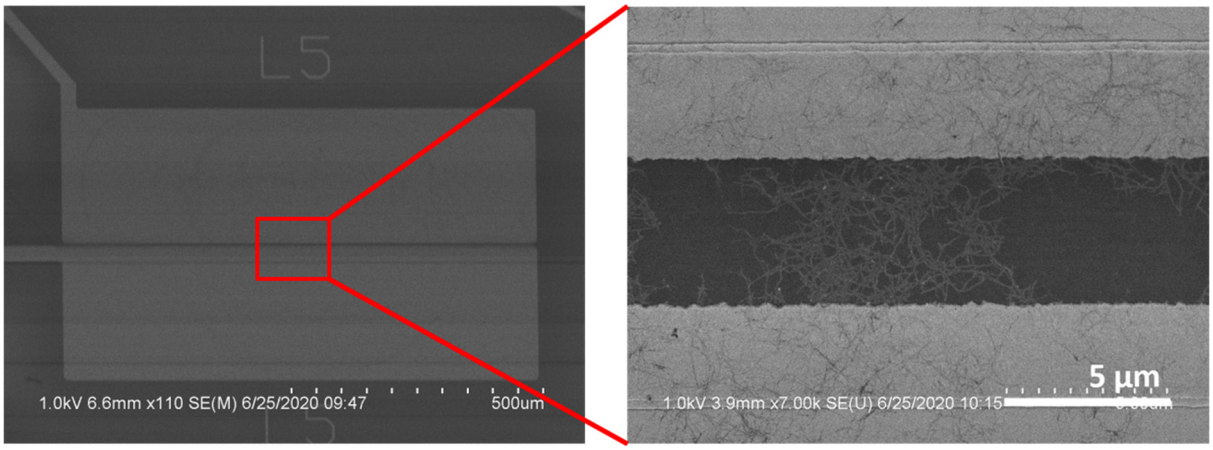

Figure S 2. SEM images of percolated SWCNT network between metal electrodes. Concentration of the ink is 0.001 wt %.

Initially, we printed 3 layers of 300 um by 300 um square-like pattern with 0.005 wt % SWCNT ink, and then we obtained relatively low on-off ratio (below 10) with DC gate voltage sweeping from – 50 V to 50 V. 1 or 2 layers of printing had insufficient amount of CNTs to have percolated random CNT network between metal electrodes and were not in general measurable (except for outlier devices).

By contrast, we printed the same pattern with 0.001 wt % SWCNT ink but only 2 layers. This led to obtain an on-off ratio up to 10^3, which is dramatically higher than the previous results and in the proper range of magnitude for sensing applications [32], [33] (Figure S 3).

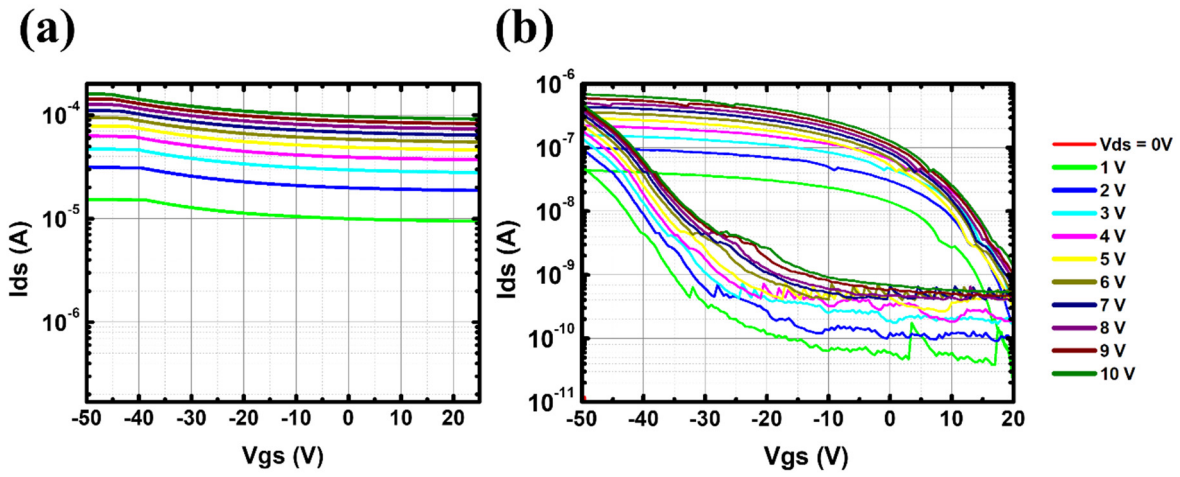

Figure S 3. Transfer curves of CNT-FETs with different density with respect to drain voltage from 0 V to 10 V; (a) 0.005 wt % ink concentration (b) 0.001 wt % ink concentration of CNT/*o*-DCBZ. Channel length of the tested device is 60 µm. Each transfer curve is measured in air.

- Ink formulation optimization (DCBZ towards NMP)

Dichlorobenzene (DCBZ) has been known as a good solvent for CNT dispersion. However, many researchers reported that high power tip sonication process with aromatic solvents (among which DCBZ) creates unexpected polymerization yielding a so-called sono-polymer by the sono-chemical degradation [311]–[314]. We also observed for ourselves the occurence of sono-polymer with DCBZ (Figure S 4). As shown in the figure, transparency of *o*-DCBZ (1,2-DCBZ) decreases after 30 min of sonication process.

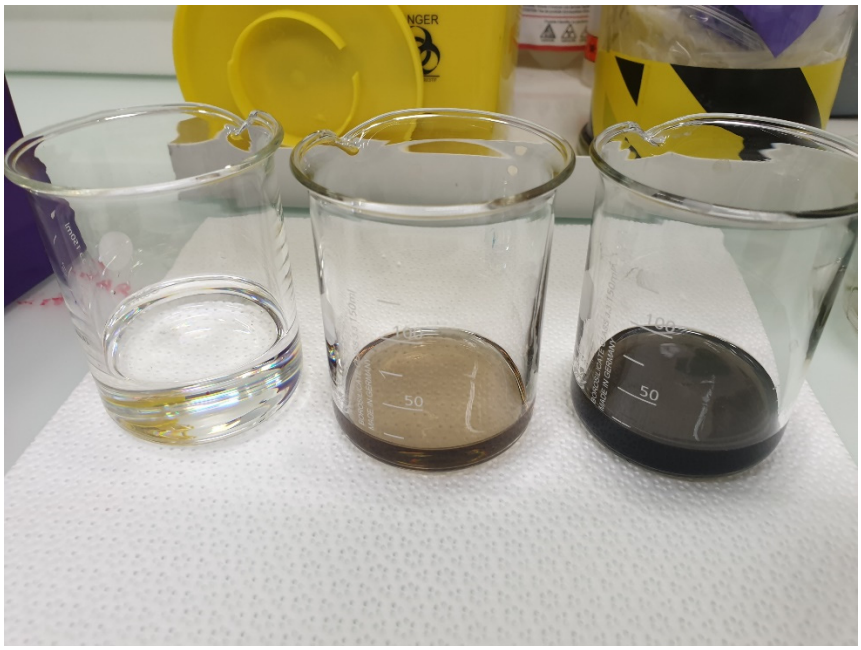

Figure S 4. Image of pure *o*-DCBZ (left), *o*-DCBZ after 30 min of sonication process (middle) and CNT dispersed in DCBZ after the identical sonication process (right).

In order to study the sono-chemical degradation by sonication process in detail, comparison of several different solvent is followed. Figure S 5 shows the absorption spectrum of three different pure solvents without CNTs ; *o*-DCBZ (1,2-DCBZ), NMP (1-methyl-2-pyrrolidinone) and DMF (Dimethylformamide), with different sonication time from 5 min to 30 min. Notably, absorbance of *o*-DCBZ (Figure S 5 (a)) dramatically increases as sonication time increases in entire wavelength range, whereas NMP (Figure S 5 (b)) and DMF (Figure S 5 (c)) do not show significant difference in terms of absorbance as sonication time increases. In fact, NMP has been also known as a good CNT-dispersing solvent [315], [316]. Therefore, we changed the CNT dispersing solvent from *o*-DCBZ to NMP to prevent this sono-chemical degradation.

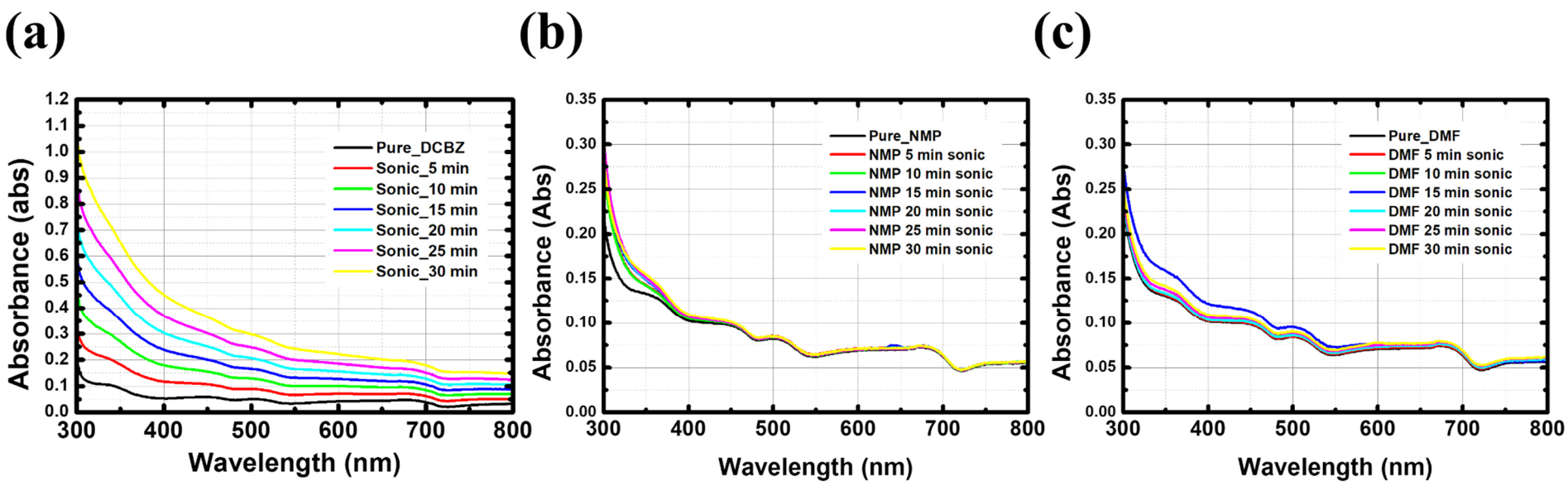

Figure S 5. Absorption spectrums of different solvents with different sonication time; (a) *o*-DCBZ, (b) NMP and (c) DMF. Each solvent is sonicated in a high-power tip sonicator

9.2 Résumé de la thèse en Français

Au cours des dernières décennies, la croissance démographique rapide et l'utilisation non durable de l'eau dans l'agriculture et l'industrie ont provoqué un stress hydrique dans le monde entier. Alors que la demande en eau douce augmente, sa qualité diminue.

Les chercheurs s'intéressent aux capteurs de qualité de l'eau, souvent à base de nanomatériaux pour réduire le coût, augmenter la sensibilité et la sélectivité.

Parmi divers nanomatériaux, les capteurs à nanotubes de carbone (CNT) ont été largement proposés pour la détection chimique dans l'eau en raison de leurs propriétés physiques, chimiques et électriques remarquables. Cependant, il n'y a pas de revue qui compare quantitativement leurs performances de détection en se concentrant sur les capteurs chimiques à base de CNT pour la surveillance de la qualité de l'eau.

Nous passons ainsi en revue l'état de l'art des capteurs CNT dans l'eau à travers 90 références et 20 analytes que les capteurs électrochimiques à base de nanotubes de carbone, les chimistes et les transistors à effet de champ (chemFET) peuvent répondre à ces besoins.

Sur la base de cette revue, le potentiel du transistor à effet de champ à base de nanotubes de carbone (CNT-FET) semble aussi prometteur pour une limite de détection extrêmement basse que les capteurs électrochimiques.

Parmi les CNT-FET, diverses options de conception, de fabrication et de mécanismes de fonctionnement sont disponibles. Dans cette thèse, nous nous concentrons sur les options de conception/fabrication suivantes ; Conception à grille inférieure, fabriquée par impression à jet d'encre de nanotubes de carbone à paroi unique non triés (SWCNT) dispersés dans de la 1-méthyl-2-pyrrolidinone (NMP)).

Nous présentons et comparons également le CNT-FET vierge (p-CNT FET) et le CNT-FET fonctionnalisé de manière non covalente (f-CNT FET) avec un polymère conjugué. Notre polymère conjugué développé sur mesure (FF-UR) est basé sur une chaîne fluorène portant deux fragments de détection identiques, un groupe urée NH-CO-NH entre deux groupes phényle.

Le poly(méthacrylate de méthyle) (PMMA) est déposé sur le réseau aléatoire CNT imprimé par jet d'encre par un procédé de séparation de phase induite par non-solvant (NIPS). La couche de PMMA passive non seulement le réseau CNT en empêchant la dégradation physique dans l'eau, mais augmente également les performances électriques des transistors dans l'air.

Notamment, le rapport I_{on}/I_{off} des transistors est passé de ~10 à ~10^3 selon la longueur du canal, après passivation du PMMA. Après avoir développé un protocole de caractérisation pour le CNT-FET dans l'eau, nous démontrons une sensibilité élevée au pH avec les deux types de FET (p- et f -) en solution tampon phosphate et borate. Un comportement général de type p est observé dans le cas du FET p-CNT, alors qu'une

ambipolarité est observée dans le cas du FET f-CNT. Le CNT-FET fonctionnalisé par un polymère montre un comportement ambipolaire avec le point de Dirac à la tension de grille de -0,1 V, ce qui n'est pas observé dans le p-CNT FET.

Le p-CNT FET montre une sensibilité au pH de 25,1 % par pH entre pH 3 et pH 9 dans le PBS, tandis que le f-CNT FET montre une sensibilité au pH significativement plus élevée de 327,9 %/unité de pH mais dans une plage de détection limitée de pH 7 à pH 9 dans le PBS. La sensibilité au pH mesurée dans le PBS est supérieure à celle d'autres capteurs chimiques CNT signalés pour la détection du pH. Cette sensibilité élevée est également observée dans la solution tampon borate (BBS). L'effet du pH est de modifier la tension de seuil du FET, qui s'observe plus fortement sur le f-CNT FET du fait de la fonctionnalisation. Cependant, sur f-CNT FET, en dessous de pH 7, la tension de seuil devient trop proche de la tension limite (~ -1 V) pour l'utilisation de FET dans l'eau, ce qui explique la faible sensibilité en dessous de pH 7.

Les dispositifs tels que fabriqués présentent une réversibilité remarquable et une durée de vie de plus de 10 mois dans l'eau. Cependant, le comportement ambipolaire du f-CNT FET est partiellement supprimé après 90 jours et est totalement dégradé après 270 jours dans l'eau ; tandis que les caractéristiques électriques du p-CNT FET restent presque inchangées. Ceci suggère une dégradation du polymère avec le temps, dont les mécanismes n'ont pas encore été étudiés. La réponse du CNT-FET à d'autres analytes a également été testée en solution tampon phosphate.

Le p-CNT FET et le f-CNT FET répondent de la même manière au Mg^{2+} dans une solution de $MgCl_2$, alors qu'aucune réponse significative n'est observée dans le cas de NaCl, KNO_3 et HNO_3. Nous nous attendons à ce que ces CNT-FET puissent être appliqués à l'avenir en tant que capteurs de pH hautement sensibles et peu coûteux. De plus, des études détaillées sur d'autres analytes proposeront une perspective pour développer la sélectivité des dispositifs.

ECOLE DOCTORALE

Titre : Transistor à Nanotubes de Carbone imprimés par jet d'encre pour la surveillance de la qualité de l'eau

Mots clés : Nanotube de carbone, Qualité de l'eau, Capteur chimique, Transistor à effet de champ, Nanomatériaux, Capteur de pH, Impression jet d'encre

Résumé: Parmi divers nanomatériaux, les capteurs de la qualité de l'eau à nanotubes de carbone (CNT) ont été largement proposés pour la détection chimique dans l'eau en raison de leurs propriétés physiques, chimiques et électriques remarquables.
Dans cette thèse, nous nous concentrons sur les options de conception/fabrication du CNT-FET suivantes ; Conception à grille inférieure, fabriquée par impression à jet d'encre de nanotubes de carbone à paroi unique non triés (SWCNT) dispersés dans de la 1-méthyl-2-pyrrolidinone (NMP)). Nous présentons et comparons également le CNT-FET vierge (p-CNT FET) et le CNT-FET fonctionnalisé de manière non covalente (f-CNT FET) avec un polymère conjugué.
Le poly(méthacrylate de méthyle) (PMMA) est déposé sur le réseau aléatoire CNT. La couche de PMMA passive non seulement le réseau CNT, mais augmente également les performances électriques des transistors dans l'air.
Après avoir développé un protocole de caractérisation pour le CNT-FET dans l'eau, nous démontrons une sensibilité élevée au pH avec les
deux types de FET (p- et f -) en solution tampon phosphate et borate. La sensibilité au pH mesurée dans est supérieure à celle d'autres capteurs chimiques CNT signalés pour la détection du pH.
Un comportement général de type p est observé dans le cas du p-CNT FET, alors qu'une ambipolarité est observée dans le cas du f-CNT FET. Le CNT-FET fonctionnalisé par un polymère montre un comportement ambipolaire avec le point de Dirac à la tension de grille de -0,1 V, ce qui n'est pas observé dans le p-CNT FET. Le comportement ambipolaire du f-CNT FET est partiellement supprimé après 90 jours et est totalement dégradé après 270 jours dans l'eau ; tandis que les caractéristiques électriques du p-CNT FET restent presque inchangées. La réponse du CNT-FET à d'autres analytes a également été testée en solution tampon phosphate.
Nous nous attendons à ce que ces CNT-FET puissent être appliqués à l'avenir en tant que capteurs de pH hautement sensibles et peu coûteux. De plus, des études détaillées sur d'autres analytes proposeront une perspective pour développer la sélectivité des dispositifs.

Title : Ink-jet printed carbon nanotube-based transistors as water quality sensors

Keywords : Carbon nanotubes, Water quality, Chemical sensor, Field effect transistor, Nanomaterials, pH sensor, Ink-jet printing

Abstract: Among various nanomaterials integrated to water quality sensors to reduce cost and increase sensitivity and selectivity, carbon nanotube (CNT) based sensors are very promising due to their remarkable physical, chemical and electrical properties.
In this dissertation, bottom-gated CNT-FET is fabricated by ink-jet printing unsorted single-walled carbon nanotubes (SWCNTs) dispersed in 1-methyl-2-pyrrolidinone (NMP)). The SWCNTs are either non functionalized (p-CNT FET) or functionalized non covalently with a custom-developed conjugated polymer.
The CNT-FETs are then passivated with porous PMMA to prevent CNT loss in water. The PMMA layer also improves the I_{on}/I_{off} of the transistors in air.
After developing a characterization protocol for CNT-FET in water, we demonstrate high pH sensitivity with both FET types (p- and f-) in phosphate and borate buffer solution.
Measured pH sensitivity is higher than that from other reported CNT-based pH sensors.
p-type behavior is observed in the case of p-CNT FETs, whereas ambipolarity is observed in the case of f-CNT FETs, with the Dirac point at the gate voltage of -0.1 V. The ambipolar behavior of f-CNT FETs is partially suppressed after 90 days and is totally degraded after 270 days in water; while the electrical characteristics of the p-CNT FET remains almost unchanged.
The response of the CNT-FETs to other analytes has also been tested in phosphate buffer solution. We expect that these CNT-FETs can be applied as highly sensitive, low-cost pH sensors in the future. Furthermore, detailed studies on other analytes will propose a perspective to develop the selectivity of the devices.

Institut Polytechnique de Paris

91120 Palaiseau, France